

Archive ouverte UNIGE

https://archive-ouverte.unige.ch

Thèse 2010

Open Access

This version of the publication is provided by the author(s) and made available in accordance with the copyright holder(s).

Impacts of a warmer climate on the deep Lake Geneva temperature profiles

Perroud, Marjorie

How to cite

PERROUD, Marjorie. Impacts of a warmer climate on the deep Lake Geneva temperature profiles. Doctoral Thesis, 2010. doi: 10.13097/archive-ouverte/unige:16827

This publication URL: https://archive-ouverte.unige.ch/unige:16827

Publication DOI: <u>10.13097/archive-ouverte/unige:16827</u>

© This document is protected by copyright. Please refer to copyright holder(s) for terms of use.

Impacts of a Warmer Climate on the Deep Lake Geneva Temperature Profiles

THÈSE

présentée à la Faculté des Sciences de l'Université de Genève pour obtenir le grade de Docteur ès Sciences, mention interdisciplinaire

> par Marjorie PERROUD de Attalens (FR)

> > Thèse N° 4188

GENÈVE Atelier d'impression ReproMail 2010 La Faculté des sciences, sur le préavis de Messieurs M. BENISTON, professeur ordinaire et directeur de thèse (Institut des Sciences de l'Environnement), S. GOYETTE, docteur (Section de physique), et B, WEHRLI, professeur (Eidgenössische Technische Hochschule Zürich – Intitut für Biogeochemie und Schadstoffdynamik – Zürich, Suisse), autorise l'impression de la présente thèse, sans exprimer d'opinion sur les propositions qui y sont énoncées.

Genève, le 2 mars 2010

Thèse - 4188 -

Le Doyen, Jean-Marc TRISCONE

Remerciements

Je tiens à remercier en tout premier lieu Martin Beniston, directeur de cette thèse, pour m'avoir proposé ce sujet excitant, puis guidé et conseillé tout au long de mes recherches. Il a eu la patience de relire et d'affiner mes textes rédigés en anglais. Il m'a encouragé à aller à la rencontre d'autres scientifiques et m'a offert l'opportunité d'aller présenter mes recherches dans de nombreuses conférences. Je n'oublierai jamais cet instant particulier où il m'a annoncé que le groupe "Climat "allait se déplacer vers Genève! Merci de m'avoir donné la chance de réaliser cette merveilleuse expérience académique.

J'exprime ma plus grande reconnaissance à Stéphane Goyette, maître d'enseignement et de recherche, pour son aide inconditionnelle dans toutes les étapes de cette thèse. Par ses exigences, il m'a appris le travail et la rigueur du scientifique, ainsi que les bases de la rédaction d'articles. Il a toujours partagé, avec grand enthousiasme, ses connaissances théoriques de l'atmosphère et de la modélisation. Sa porte était toujours ouverte pour des discussions ainsi que pour répondre à mes questions, jusque tard le soir. Stéphane est à la base de l'aboutissement de cette thèse.

Je remercie également René Laprise et Bernhard Wehrli d'avoir accepté de faire partie de mon jury de thèse et pour avoir contribuer à la critique de ce manuscrit.

Merci à tous mes collègues de bureau, Bastienne Uhlmann, Christophe Etienne, Diana Forster, Margot Hill et Nicole Gallina, pour les échanges de compétences que nous avons eu et surtout pour la bonne ambiance qu'il y a toujours régné. Un immense remerciement tout particulièrement à Margot pour la relecture méticuleuse de mes travaux en anglais et du temps qu'elle y a consacré, de même qu'à Nicole pour m'avoir transmis quelques de ces connaissances du monde biologique. Sans Christophe, ma vie extra-professionnelle à Genève n'aurait pas été ce qu'elle a été. Je tiens à saluer également toutes les personnes de l'institut des Sciences de l'Environnement que j'ai côtoyées et avec qui j'ai eu le plaisir de partager des moments privilégiés, de convivialité et de détente.

Je souhaite remercier Marc qui m'a encouragé, aidé à avancer et à ne pas lâcher prise dans les moments plus difficiles. Les petites attentions et les corvées qu'il a assumées pour que je puisse travailler dans les meilleures conditions sont des gestes inestimables.

Une pensée pour mes amis de longue date, Aline, Florence, Francine, Martine, Sophie M., Jean-Maurice et José. Leurs messages d'encouragement étaient d'une grande valeur. Je me dois de remercier également mon amie Sophie H. qui, par un parcours similaire, m'a donné des pistes de réflexion et prodigué d'utiles conseils.

Je ne pourrais terminer sans remercier mes parents que j'ai toujours eus à mes côtés. Ils m'ont encouragé dans mes choix et m'ont aidé à atteindre les buts que je me fixais. Au-delà de ça, ils m'ont transmis un bien précieux, la persévérance.

Résumé

Les premiers signes du réchauffement climatique commencent à se faire ressentir un peu partout dans le monde, gagnant progressivement les milieux lacustres également. Ces changements, bien que pour l'instant encore relativement mineurs, pourraient avoir de sévères conséquences sur les écosystèmes si cette tendance allait se confirmer. En effet, une augmentation moyenne des températures de 1.5 °C à 2.5 °C pourraient induire des changements dans la structure et la fonction des écosystèmes, de même que modifier les interactions écologiques entre les espèces et leur répartitions géographiques (Fischlin *et al.* 2007). Afin d'évaluer l'évolution du climat régional et quantifier les impacts potentiels que ce dernier peut avoir sur l'écosystème aquatique, il est nécessaire de recourir aux prédictions issues des résultats de modèles de circulation générale (GCM) ou de modèles régionaux du climat (RCM). Malgré les incertitudes liées à l'évolution des émissions des gaz à effets de serre, les modèles s'accordent à dire que le réchauffement va se poursuivre dans les décennies à venir (Christensen *et al.* 2007). En Europe, on projette des augmentations de 1 à 5.5 °C pour la période 2070-2099 par rapport à la période de référence (1961-1990), soit au climat actuel (Alcamo *et al.* 2007).

Cette étude se concentre sur les impacts d'une augmentation de la concentration de CO_2 atmosphérique sur le lac Léman, un lac monomictique chaud et profond (309 m) dans lequel les effets d'un climat plus doux se sont déjà fait ressentir (Lazzarotto *et al.* 2004). Ayant pour objectif d'étudier l'évolution thermique du lac sur le long terme, cette étude a d'abord voulu évaluer la capacité de modèles de lac, alimentés par des observations atmosphériques, à reproduire ses conditions en son point le plus profond. Etant donné l'efficacité des modèles de lac à une dimension (1D) pour des applications climatologiques (en termes de temps de calcul), quatre d'entre eux ont été retenus et testés pour les besoins de cette étude. On trouve un modèle de diffusion turbulente, soit le 'modèle de Hostetler', un modèle lagrangien, le Dynamic Reservoir Simulation Model, 'DYRESM', un modèle de diffusion-dissipation de la turbulence, le k- ε modèle 'SIMSTRAT', et un modèle basé sur le concept de la ressemblance (forme attendue) de la courbe de température en fonction de la profondeur, le modèle 'Freshwater Lake', soit 'FLake'.

Sur la base de ses bonnes performances, le modèle de lac numérique SIMSTRAT (Goudsmit *et al.* 2002) a été sélectionné pour simuler les profils thermiques du Lac Léman. Afin de connaître de quelle manière ce dernier va être affecté par des changements du climat d'ici la fin du 21^{ème} siècle, on a eu recours à deux différentes méthodes.

Dans la première, les observations collectées pendant la période de référence ont été utilisées pour tourner SIMSTRAT, avant d'être perturbées en fonction des changements diagnostiqués dans les sorties du RCM HIRHAM entre un climat futur et actuel. Ces sorties de modèle sont issues du projet EU-Prudence (Christensen *et al.* 1998), pour le scénario de l'IPCC A2 (Nakicenovic *et al.* 2000). Cependant, plutôt que d'ajouter une différence moyenne (par exemple de température) aux observations, notre méthode propose d'appliquer un certain nombre de perturbations à une même variable ce, afin de mieux prendre en compte la variabilité du changement d'une variable.

Dans la seconde, un modèle atmosphérique à colonne unique (SCM), nommée FIZC, est couplé au modèle de lac SIMSTRAT. Les intrants nécessaires pour tourner FIZC sont fournis par les champs générés par le GCM canadien de seconde génération (McFarlane *et al.* 1992). Le modèle couplé FIZC-SIMSTRAT est ensuite employé pour simuler les changements dans les propriétés thermiques du Lac Léman en réponse à un climat plus chaud. Le climat futur est le résultat d'un doublement de la concentration en CO₂ par rapport à une simulation de contrôle (1 X CO2). En comparaison avec la première méthode où les flux de la surface du lac ne peuvent pas modifier l'état de l'atmosphère, cette technique couplée a l'avantage de prendre en compte les rétroactions mutuelles entre le lac et l'atmosphère.

Dans chaque expérience, on note que les augmentations de CO₂ atmosphérique mènent à des changements significatifs des composantes du budget d'énergie à la surface du lac. Bien que les conclusions de ces deux expériences soient similaires en termes de réponse du lac au réchauffement global, les flux de chaleur qui gouvernent le modèle de lac divergent de manière significative à certaines périodes. Ces différences peuvent être dues à l'inclusion des mécanismes de rétroaction du lac dans le modèle de climat, mais aussi aux modèles de climat et aux spécifications de la modélisation utilisés pour simuler un climat futur.

Quoi qu'il en soit, dû à l'augmentation des températures de l'air et de la surface du lac, de plus fortes valeurs de rayonnement infrarouge entrant et sortant sont diagnostiquées à la surface du lac, résultant en un bilan positif pour le lac. Les changements de flux de chaleur sensible ont pour effet de réchauffer le lac. Inversement, une réduction de l'humidité relative combinée à de plus hautes températures de l'air augmente le déficit en vapeur d'eau à l'interface air-eau, et refroidit le lac. Au contraire de l'expérience unidirectionnelle, l'expérience couplée, développée pour prendre en compte les rétroactions entre la surface du lac et l'atmosphère, s'est révélée sensible aux variations d'humidité dans la colonne atmosphérique et à la formation de nuages. Elle est alors en mesure d'influencer les flux radiatifs solaires et infrarouges.

Dans les deux expériences, l'analyse de sensibilité du lac aux changements de la teneur de l'atmosphère en CO₂ a montré que toute la colonne d'eau pourrait se réchauffer, jusqu'à un maximum de 3.83 °C (août) et 4.20 °C (juillet) dans l'épilimnion et de 2.33 °C (mars) et 2.25 °C (mars) dans l'hypolimnion, respectivement. L'évolution des températures mensuelles de l'épilimnion suit celle des températures de l'air, sans qu'il n'y ait aucun retard dans les maxima et minima de températures dans le lac. Etant donné que le réchauffement des couches de surface est supérieur à celui des couches plus profondes de la colonne d'eau, le métalimnion se révèle plus fortement stratifié. Réduisant ainsi les échanges de chaleur épihypolimniques par rapport au régime actuel. De même, cette plus forte stabilité a pour effet d'affaiblir le mélange induit par le stress du vent en surface à la fin de l'été, retardant ainsi l'érosion de la stratification. Un allongement de la période où le lac est stratifié (3 semaines) est également simulé dans les 2 expériences, avec des changements dus autant à une mise en place plus précoce qu'à une plus longue durée de la stratification. Le raccourcissement de la période où le lac est peu stratifié devrait réduire la fréquence des brassages complets du lac. Néanmoins, les augmentations de température, similaires dans toute la colonne en février et mars, ou en mars uniquement (selon la méthode), laissent penser que des renversements pourraient toujours avoir lieu occasionnellement.

Resume

Lake thermal response to recent atmospheric warming reveals the first signs of observed change in many regions. These changes may become problematic, as an increase in mean temperature of 1.5 to 2.5 °C may induce changes in ecosystem structure and function as well as ecological interactions between species and their geographical ranges (Fischlin *et al.* 2007). To assess regional climate evolution and quantify potential impacts on this aquatic ecosystem, Regional Climate models (RCMs) or General Circulation Models (GCMs), forced by climate change scenarios are required. Despite uncertainties concerning future greenhouse gas emissions, the models indicate that there is considerably strong evidence to confirm this warming over the coming decades (Christensen *et al.* 2007). In Europe, an increase of 1 to 5.5 °C is expected in the 2070 - 2099 timeframe compared to the baseline, or "current", (1961 - 1990) climate (Alcamo *et al.* 2007).

This project studies the impact of an increase in atmospheric CO_2 concentration on Lake Geneva, a warm and deep monomictic lake (309 m) within which the effects of warmer meteorological conditions have recently been observed (Lazzarotto *et al.* 2006). With the purpose of examining the long term thermal evolution of Lake Geneva, this study first aimed at evaluating the ability of lake models, driven by atmospheric observations, to reproduce the thermal characteristics of its deep segment. Because of their computational efficiency for climatological applications, one-dimensional (1D) lake models have been chosen for the purpose of this study. The four models tested include an eddy-diffusive lake model, the Hostetler model; a Lagrangian model, the one-dimensional Dynamic Reservoir Simulation Model 'DYRESM'; a k- ε turbulence model, 'SIMSTRAT'; and finally, a model based on the concept of self-similarity (assumed shape) of the temperature-depth curve, the Freshwater Lake model 'FLake'.

Based on the good performance of the numerical lake model SIMSTRAT (Goudsmit *et al.* 2002), it has been chosen to simulate water temperature profiles of the lake. To explore how Lake Geneva might be affected by changes in climatic conditions by the end of the 21st century, two different techniques were applied.

In the first method, observed meteorological data, collected during the reference period, were used to drive SIMSTRAT, before being perturbed using changes diagnosed in the outputs of the HIRHAM RCM for a future and current climate. These results were produced in the context of the EU-Prudence project (Christensen *et al.* 1998) under the IPCC A2 scenario (Nakicenovic *et al.* 2000). However, rather than just adjusting the observation by a difference between period-average results (for instance a monthly temperature change), our method proposes providing a number of perturbations for the same variable to take into better account its variability.

In the second method, a single column atmospheric model (SCM) called FIZC was interfaced with the lake model SIMSTRAT. Inputs required to run FIZC were provided by fields generated through the second-generation Canadian GCM, GCMii (McFarlane *et al.* 1992). The coupled FIZC- SIMSTRAT model was then used to simulate changes in Lake Geneva water temperature profiles, in response to global warming following a doubling in atmospheric CO₂ concentrations compared to a "control" 1 x CO₂ simulation. Compared to

the first method where flux from the water surface could not lead to changes in the atmosphere, the main challenge of this method was to control the feedbacks between the lake surface and the atmosphere.

In each experiment, increasing CO₂ concentrations in the atmosphere produced significant changes in the components of the energy budget at the lake surface. Although both experiments provided similar conclusions on Lake Geneva's response to global warming, heat fluxes driving the lake model proved to diverge significantly at some time. These differences may be due to the inclusion of lake feedback mechanisms in climate models, and to the climate models and modelling assumptions used to provide the future climate (Hingray et al. 2007).

However, due to the increase in air and surface water temperature, higher values of downward and upward infrared radiation were diagnosed at the lake surface, resulting in a positive balance for the lake. Additionally, changes in sensible heat flux had a warming effect on the lake. While on the contrary a combined increase in air temperature and decrease in relative humidity enhanced the water vapour deficit at the air-water interface, inducing a cooling effect in the lake. Unlike the one-way experiment, the coupled experiment, developed to include feedbacks between the lake surface and the atmosphere, showed sensitivity to the moisture variations in the atmospheric column and to cloud formation which had an influence both on the downward solar as well as on longwave radiative fluxes.

In both experiments, the lake sensitivity analysis to changes in greenhouse gases showed a warming of the whole column, of a maximum of 3.83°C (August) and 4.20°C (July) in the epilimnion, and of 2.33°C (March) and 2.25°C (March) in the hypolimnion, respectively. The evolution of monthly epilimnic temperatures correlate with that of the air temperatures without any delay in the timing of maxima and minima. Due to a higher warming in the upper layers compared to the lower layers of the water column, the metalimnion proved to be more strongly stratified. Epi-hypolimnic heat exchanges are thus reduced compared to today's regime. Moreover, the stronger stability of the water column reduces mixing caused by wind stress at the end of summer and hence delays the stratification decay. An increase in the period of stratification (3 weeks) was also simulated in both experiments, with changes almost equally due to an earlier onset than to a longer duration of the stratification. The shorter duration of the weakly stratified period should reduce the frequency of complete mixing. However, a similar increase in water temperatures through the whole column in both February and March or February alone (method dependant) suggests that overturns might still occasionally occur.

Content

Remerc	elements	
Résumé	ś	iii
Resume	ə	v
Content	t	vii
Overall	introduction	1
0.1 1	Thermal structure of warm monomictic lakes	3
0.2 L	_ake model	4
0.3.1 (0.3.2 0.3.3	Climate models	
Simulat one-dim	ion of multi-annual profiles in deep Lake Geneva: a comparison of nensional lake models	
	ntroduction	
1.2.1 1.2.2	Model descriptions	15 17
1.3.1	Experimental setup Model calibrations and wind-speed adjustment	21

	Results	
1.4.1		
1.4.2	•	_
1.4.3 1.4.4		
	Additional assessments	
1.4.3	Additional assessments	32
1.5	Discussion	35
1.6	Acknowledgments	37
1.7	Appendix	38
1.8	Reference	44
Chapte	er 2	49
-	s of a warmer climate on Lake Geneva water temperature profiles	
2.1	Introduction	50
2.2	Material and methods	51
2.2.1	Study site and lake data	51
2.2.2		
2.2.3		
	2.2.3.1 Current data set	
	2.2.3.2 Data set perturbed using the decile method	
2.2.4	Experimental setup	61
2.3	Results	63
2.3.1	Projected Lake water temperature changes using the decile method	63
2.3.2		
2.3.3		
2.3.4		
2.3.5	, and the second se	
2.3.6	The decile method with a linear increase vs a constant Δ	68
2.4	Discussion	69
2.5	Conclusion	73
2.6	Acknowledgments	74
2.7	Appendix	75
2 8	References	77

Chapte	er 3	83
	cing a one-dimensional lake model with a single-column atmospheric model: ation to the deep Lake Geneva, Switzerland	
3.1	Introduction	84
3.2	Methodology	85
3.2.1		85
3.2.2	11	
3.2.3	3 3	
3.2.4		
3.2.5	3 1	
3.2.6 3.2.7		
3.2.7	Coupling Fize with Simstrat take model	90
3.3	Data and experimental setup	91
3.4	Results	
3.4.1		
3.4.2		
3.4.3	,	
3.4.4		
3.4.5	,	
3.4.6		
3.4.7	,	
3.5	Discussion and concluding remarks	109
3.6	Acknowledgements	111
3.7	References	112
•	er 4	115
Therm	al response of the deep Swiss Lake Geneva under a 2 x ${ m CO_2}$ global climate e	
4.1	Introduction	116
4.2	The coupled model	117
4.3	Comparison of FIZC and GCMii simulated variables over land	120
4.4	Application of the coupled FIZC-SIMSTRAT to the deep Lake Geneva	124
4.4.1		
4.4.2		
4.4.3	Simulated lake thermal profiles under a 2 X CO ₂ climate warming scenario	130
4.5	Discussion	134
4.6	Conclusion	137

4.7	Acknowledgments	139
4.8	References	140
Conc	clusion	147
Refe	erences	

Overall introduction

Regional climate is a dominant factor controlling the evolution of the thermal structure and water movements in lakes. Inter- and intra- annual variations of thermal and dynamic properties in lakes are thus strongly dependent on meteorological conditions and may in turn affect the distribution of nutrients, and other chemical properties (Wetzel 2001). Annual variations of these entities are not an issue and are part of the natural process that may be observed in lakes. However, significant shifts from these natural variations may be severely detrimental for ecosystem functioning, affecting lake biodiversity and more specifically water quality and drinking-water supply.

The interest in assessing lake response to global warming comes from first signs of changes observed in many parts of the world as a result of the very rapid atmospheric warming, considered to be the most rapid of the last 10'000 years (Alcamo et al. 2007). There is every reason to believe that this trend will continue over coming decades and therefore affect the thermal structure of lakes and their ecosystems. Indeed, the increase in global mean surface temperature in the range of 1.8°C to 6.4°C projected by the Intergovernmental Panel on Climate Change (IPCC) by the end of the 21st century suggests that severe impacts may be expected (Meehl et al. 2007). Lakes studies can therefore no longer be confined only to monitoring and understanding internal physical processes and ecosystem functioning. There is a need to investigate changes in the thermal structure of lakes and possible indirect effects on aquatic ecosystems and water resources to this warming. Prior studies based on observed or simulated trends in lakes in a changing environment revealed that a further increase in air temperature may, in addition to the direct effects of rising temperatures, decrease the occurrence of turnover and thus modify levels of dissolved nutrients (Nõges et al. 2008). Milder winters may favor the onset of stratification earlier in spring, particularly in temperate lakes, with direct impacts on phytoplankton development (DeStasio et al. 1996; Jacquet et al. 2005; Peeters et al. 2007). Warming of surface waters may also intensify vertical stratification, increase the mixing resistance in autumn and lengthen the period of stratification, promoting the appearance of some microorganism and phytoplankton bloom formations (Walsby 1997). While not systematically reported in lakes, a deeper thermocline may take place, reducing the light availability due to a thicker mixed layer depth, thereby affecting phytoplanktonic production in the metalimnion (Huisman et al. 1999).

Among the indirect impacts on aquatic ecosystems relating to climate change, studies highlight the possible connection between the recent upsurge and expansion of the growth of cyanobacteria, as harmful algal blooms, and environmental change (Pearl and Huisman 2008). It is no longer possible to attribute such algal blooms solely to the nutrient overenrichment of waters by urban, agricultural and industrial development (Reynolds 1987; Pearl 1988): they are also related to higher water temperatures or more stable water columns. The poleward spreading of species originating from the subtropics, such as *Cylindrospermopsis*, support this hypothesis. (Ryan *et al.* 2003; Wiedner *et al.* 2007). Also, the dominance of cyanobacteria such as *Planktothrix Rubescens* during warm years, emphasises the competitive advantage of these buoyant species (that can exploit the water column by regulating their buoyancy) to strongly stratified waters (Jaquet *et al.* 2005; Fernald *et al.* 2007; Jöhnk *et al.* 2008). Potential sustained development of these algal blooms in the

future represents a real threat to the use of freshwater ecosystems and reservoirs for drinking water, irrigation, fishing and outdoor water activities (Codd 1995; Carmichael 2001; Chorus 2001; Paerl and Huisman 2009). For human health, ingestion or direct contact with these cyanotoxins may even cause pathologies ranging from skin allergies to severe liver and digestive diseases, leading in some cases to death (Carmichael 2001; Cox *et al.* 2003; Huisman *et al.* 2005). Ecological and economic consequences of cyanobacteria blooms are starting to be observed in lakes all around the world. In perialpine lakes, the problem is currently not as severe as in Lake Victoria (Verschuren *et al.* 2002), Lakes Erie and Michigan (Rinta-Kanto *et al.* 2005) or Lake Biwa (Maeda *et al.* 1992). However, since species such as the toxic cyanobacteria, *Planktotrix rubescens*, have already been recorded on occasion in Lake Geneva, Lake Bourget (Jacquet *et al.* 2005), Lake Zürich (Walsby and Schanz 2002), and Lake Pusiano, (Legnani *et al.* 2005), the evolution of these algae in large perialpine lakes and their development in high elevation water bodies in the Alps is a problem area which needs to be addressed. Such investigations should provide solutions designed to reduce economic and health-related risks.

This thesis is thus part of an interdisciplinary project that ultimately aims to assess the impacts of climate change on cyanobacteria blooms and their potential effects on water quality and health in different perialpine lakes. Addressing these complex questions requires extensive collaboration between scientists in order to develop an appropriate set of adaptation and mitigation options aiming at reducing the risk of infection. The goal of this project is to develop an integrated modelling system that associates climate and lake dynamics with biological processes within the aquatic milieu in order to determine whether health-threatening thresholds of cyanobacteria may be exceeded more frequently and over longer periods of time under certain climatic conditions.

The overall goals of the thesis are to investigate changes in the thermal structure of lakes in a future warmer climate resulting from enhanced atmospheric concentrations of greenhouse gases. Biological and health aspects are treated in a parallel study that does not form part of this manuscript. If many studies report on climatic impacts on thermal structure of American lakes, only a few perialpine lakes have been investigated with respect to global warming (Peeters et al. 2002; 2007). Due to the time required to calibrate and validate lake models, as well as difficulties to obtain full and long datasets in water bodies, we decided to focus on one lake only, but with the application of different techniques to assess changes in the lake's thermal structure in the future, under different global warming scenarios. These techniques are then certainly applicable to the other perialpine lakes. Lake Geneva, located at an altitude of 372 m a.s.l. between Switzerland and France, has thus been chosen to serve as an experimental laboratory to quantify thermal changes within the water column and to evaluate changes in qualitative aspects of the lake (such as the location of the thermocline. the occurrence of turnover and the timing of the onset of stratification). The choice of this particular lake is motivated by the long monitoring with deep lake soundings since the 1950s, and the fact that it has never been studied for such purposes until now. The depth of Lake Geneva makes it also particularly attractive as it allows quantifying the time response of a large lake to atmospheric perturbations.

To reach these objectives, the specific topics that this thesis covers include:

- an evaluation of the ability of numerical lake models, driven by atmospheric observations, to reproduce the thermal characteristics of the deep segment of Lake Geneva in a realistic manner. (Chapter 1)
- a numerical investigation of the response of Lake Geneva to atmospheric warming caused by enhanced concentrations of carbon dioxide. To reach this goal, a lake model driven by outputs from an atmospheric model simulates water temperature profiles through to the end of the 21th Century. While former experiments do not take into account the interaction between the lake and the atmosphere (Chapter 2), a

- method has been developed to allow the control of the feedbacks between the lake surface and the atmosphere (Chapters 3-4).
- an assessment of the sensitivity of the water temperature profiles to warmer climatic conditions by examining quantitative and qualitative changes in simulated mean daily water temperature profiles between a "current climate" and a "future climate" (Chapters 2 and 4). Outputs using both methods allow a comparison of energy budgets and validation of temperature trends.

As a background to the issues addressed in this study, a brief presentation of the lake features is provided in order to define the main terminology used in this work. Thereafter, a presentation of lake models developed to simulate profiles of lake water temperature and density is given, with an overall discussion on the thermodynamic processes included in these models. This chapter will enable an understanding of the criteria that have determined the choice of a particular lake model. Following this, an overview of atmospheric models developed to assess climate state forward in time is presented, together with a description of future emission scenarios. We will then explain the methods used to link expected changes in atmospheric variables with the thermal evolution of Lake Geneva waters. Finally, an overview of observed and expected changes in European and Swiss climate allows an estimation of the threat of these physical changes on perialpine water ecosystems.

0.1 Thermal structure of warm monomictic lakes

Heat energy exchanges at the lake-atmosphere interface as well as the surface wind stress are usually the main drivers of seasonal heat storage in lakes. In temperate areas, the thermal evolution of lakes over the different seasons thus generally follows a similar pattern. In winter, the structure of temperate perialpine lakes may however diverge, and lakes may thus be classified as being either dimictic (Lakes Zuerich, Pfaeffikon, Aegeri and Greifensee) or monomictic [Lakes Geneva, Lucern, Lugano and Constance, (Hendricks Franssen and Scherrer 2008; Dill 1993)]. Unlike monomictic lakes that are subjected to one spring turnover when temperatures homogeneised in the column are equal to or exceed 4°C, dimictic lakes mix twice during the cold season. Since this study focus on Lake Geneva, we will restrict our description of its thermal structure to warm monomictic lakes.

At the end of the winter season, water bodies are usually rather homogeneous, with waters at all depths close to 4°C or slightly warmer (Fig. 0.1a). Even though a moderately higher surface temperature may induce lower density overlying higher density layers, no significant amounts of energy are required for these layers to mix well together. Complete spring turnover may occur for some days or weeks. Wind-driven processes may prolong deep mixing in early spring and, jointly with the increase in air temperature, warm the entire column. However, when the amount of heat distributed downward is less than that stored at the surface, resistance to mixing increases. A warmer and less dense surface layer forms and bottom temperatures do not evolve much. Lakes are thus thermally structured in 3 strata (Fig. 0.1b).

- The surface layers, exposed to wind and rather turbulent, form the "epilimnion".
- The deep stratum of colder waters, over which the upper water floats, composes the hypolimnion.
- In between, the metalimnion is the stratum of thermal discontinuity, acting partially as a barrier to mixing.

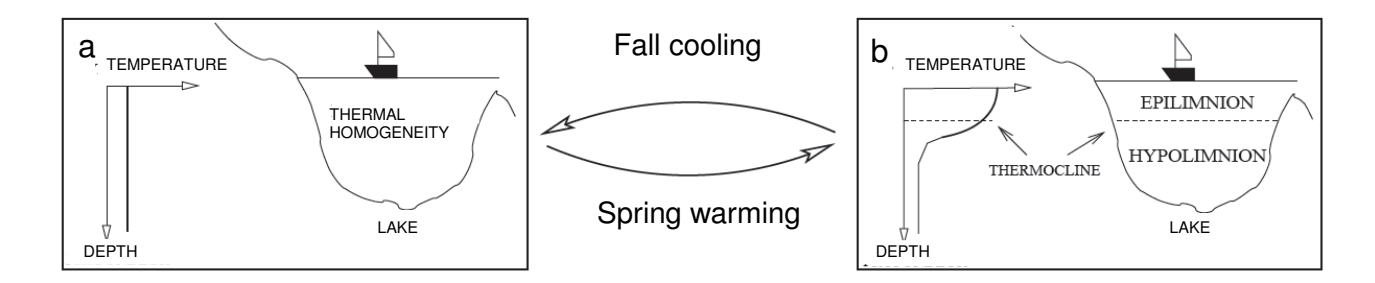


Figure 0.1. (a) Homogenised and (b) stratified thermal profiles in a freshwater body (Danis 2003).

The concept of stratification, widely discussed in the forthcoming chapters, refers to this segmentation of the lakes in three layers. The location and strength of the stratification (*i.e.*, strong when the thermal gradient is well-established) is largely dependent on meteorological conditions, since they drive the seasonal variations of the lake's thermal and dynamic properties.

Lake stratification lasts up to the end of summer when heat loss from the lake exceeds that gained from the atmosphere. At that time, colder surface waters, thus denser than in the underlying epilimnion, sink, mix to warmer waters, and erode the metalimnion. Depending on factors such as lake morphometry or meteorological conditions (Stewart and Haugen 1990), the lake basin may be either weakly stratified or well-mixed in winter. In deep lakes, such as the perialpine Lake Geneva, Lake Lucerne and Lake Maggiore, complete mixing only occurs occasionally (Lazzarotto *et al.* 2006; Buehrer and Ambuel 2001; Marchetto *et al.* 2001). This cyclic pattern is then repeated every year.

Since properties of the stratification determine surface water temperature and heat exchanges between surface and bottom waters, lake stratification will thus require particular attention in the assessment of the performance of the lake model discussed in Chapter 1.

0.2 Lake model

A lake can be viewed as a fluid that behaves according to the laws that govern fluid dynamics and thermodynamics applied to freshwater. The evolution of the salient characteristics of the water is governed by boundary conditions such as the bathymetry, surface and bottom stress, and energy balance. The specific variables that characterize the lake are the velocity field, the water density, its salinity and its temperature. The equation of state for fresh water, in the general case, relates the density of water to temperature and salinity around the point of maximum density (~4°C). The lake is forced by two major atmospheric inputs, namely the heat and momentum fluxes at its upper boundary. Heat energy exchanges at the lake-atmosphere interface are provided by the net solar S^* and infrared L^* radiation as well as by the sensible Q_H and latent Q_E heat fluxes, whereas the momentum exchange is described by the wind stress. All these physical processes, such as transport and mixing processes (advection, shear, molecular diffusion, turbulence and turbulent diffusion, entrainment, convection and dispersion) can be formulated mathematically and assembled in terms of a model, ultimately transcribed in the form of a computer program to enable numerical simulations. Lake models are similar to atmospheric models in that internal mechanisms are based on hydrodynamic and thermodynamic principles. Any code which attempts to model water bodies takes into account only a limited

number of environmental conditions. The numerical model focuses on certain key aspects of the lake system and thus is not a full representation of reality. A particular lake model is then used to represent its current state and predict its future behaviour, particularly under varying external factors. A lake may become stratified to the extent that apparent density discontinuities can be tracked. This has led to the design of models consisting of layers of water of different densities (Simon 1973) and with a sufficient resolution in the vertical to adequately represent temperature.

For the purpose of studying climate impacts on lake water quality and ecosystems, and for managing water resources, the stability of the water column and the seasonal dynamics of the vertical temperature profile are the most important parameters to model accurately. However, in order to improve the prediction of the evolution in a future climate due to the influence of a water surface, the lake surface temperature (LST) has to be carefully simulated. A more realistic estimation of the fluxes at the lake-atmosphere interface also allows to better control the heat content of the lake. In this case, the vertical thermal structure is also of importance as water stability controls the rate at which buoyancy forces damp turbulent mixing produced by external factors. Since the early to mid 1960's, a wide range of physically-based lake models have been developed to provide such information. Most of these models, called "one dimensional models" (1D models), assume that water bodies are represented by a vertical series of horizontal slabs that are well mixed laterally. Onedimensional lake and reservoir models have proven to be effective tools for analyzing internal lake and water quality problems because temperature and many water quality parameters tend to vary more along a vertical distance of tens of metres than along a horizontal distance of thousands of metres (Ford and Johnson 1986). These models have improved over the years, by including an increasing number of processes. In the former 1D models, radiative and convective heat exchanges taking place between the lake and the atmosphere were included, but only a few dynamic processes were represented. The model of Dake and Harleman (1969) for instance considered molecular diffusion of heat as the only means of downward transport outside the epilimnion. A complex frame of mixing related to wind action upon surface layers as well as in the meta-hypolimnion were progressively taken into account to simulate heat penetration though the water column. In some lakes, however, these models still present some limitations in the sense that horizontal variations in temperature and stratification may occur. Along the shore of a lake, for instance, the shallower depth than in the open-water region may favour differential heating over the lake. This topographical effect can result in the formation of a thermal bar (a thermal transition zone between homogenised open water and littoral stratified water favouring deep convective currents, Wetzel 2001), or produce significant horizontal advection. A river flowing into water layers of a different density also generates turbulence and induces horizontal variations. Basin-scale energy fluxes from the wind are also of particular interest because of their dominant role in setting the thermocline in motion and in initiating vertical and horizontal fluxes in a stratified lake beneath the surface layer (Hodges et al. 2000). Three-dimensional numerical lake models or 3D ocean models, customised for lakes, have thus been designed to resolve the effects of 3D transport and spatial heterogeneity (Hodges et al. 2000). However, we may also find some 1D models that have been developed to parameterized these 3D processes, i.e., that they retain the memory of what these processes do to the vertical structure (Copetti et al. 2005). For instance, the k-ε model of Goudsmit et al. (2002). SIMSTRAT, or the DYRESM model (Yeates and Imberger 2003) parameterize vertical exchanges between the epilimnion and the hypolimnion produced by basin scale oscillations. If wind-generated processes, such as shear and convective mixing are now common to 1D models, the numerical scheme makes them particularly unique. Generally, we may find eddydiffusion models (Orlob and Selna 1970; Henderson-Sellers et al. 1983), turbulence-based models (Kraus and Turner 1967; Imberger et al. 1978), in particular k- ε models (Burchard and Baumert 1995; Goudsmit et al. 2002; Stepanenko and Lykosov 2005), mixed-layer models (Stefan and Fang 1994; Goyette et al. 2000), or models based on similarity theory (Mironov 2008; Mironov et al. 2009).

The choice of a model is not so trivial. Due to lake morphometry or to lake-specific parameters, a model may not be applicable to all lakes (Orlob and Selna 1970; Markofsky and Harleman 1973; Swayne et al. 2005). In some cases, the vertical or horizontal resolution may be an issue. However, by means of some calibrations, a hierarchy of lake models turns out to be efficient in simulating thermal structure over multiple lakes. Swayne (2005) suggests selecting models with respect to the size of the lakes. In shallow lakes, a box model approach is accurate since the water column is usually well-mixed. In intermediate-size or deeper lakes (> 10 m), where horizontal thermal gradients are weak, a one-dimensional lake model approach can be used since aspects of stratification and seasonal thermal evolution are represented. For large lakes, 3D models that take into account horizontal distributions of heat and momentum should preferably be used. However, the choice of a lake model for simulating water temperature profiles depends primarily on the question to be addressed. Simulating water temperature profiles of a large water body for long term integrations may present a dilemma as to choosing between a 1D or a 3D model. If a 3D model is theoretically an appropriate option for Lake Geneva, three limitations appear. Firstly, unlike small lakes, large lake responses to a changing climate need more several decades to reach a steadystate. A 3 D approach may thus represent a high computational cost for climate-related applications (current 3 D simulations are usually run over periods shorter than a decade). Secondly, no climatologically-relevant data have been collected over the lake surface and thus no boundary conditions are available to drive the 3D lake models. Thirdly, the lack of observed profiles at different locations over the lake does not enable the validation of 3D models. Chapter 1 investigates the possibility of overcoming 3D constraints by using 1D lake models for the large and deep Lake Geneva. For deep lakes, the hypothesis of horizontal homogeneity for state variables (such as temperature and isotopic composition of water) is not inappropriate (Danis 2003) and has already been shown to be accurate to simulate thermal structure of such lakes (Hostetler et Bartlein 1990; Vassiljev et al. 1994; Benson and Paillet 2002; Peeters et al. 2002).

With the aim of evaluating the ability of 1D models to simulate Lake Geneva water temperature profiles, models have been selected on the basis of three main criteria. The models:

- 1. need to use different approaches in order to cover a wide range of possible hydrodynamic formulations, parameterizations, and numerical schemes
- 2. should be widely used and documented, with results published
- 3. have shown skill in simulating thermal profiles.

Since internal seiche oscillations are known to enhance mixing in Lake Geneva (Bohle-Carbonell 1986), models that implement this 3D process also had to be tested. The selected models thus include one eddy-diffusive lake model, the Hostetler model, a Lagrangian model, the one-dimensional Dynamic Reservoir Simulation Model "DYRESM", a k- ε turbulence model, "SIMSTRAT", and a model based on the concept of self-similarity of the temperature–depth curve, the Freshwater Lake model "FLake".

The performance of the models to reproduce water temperature profiles of Lake Geneva is evaluated on the ability of the models to capture the main characteristics of the vertical structure of the lakes, *i.e.*, surface and bottom water temperatures, thermocline depth and onset, and the duration of winter mixing (Chapter 1). The most accurate model is then chosen for evaluating the thermal response of Lake Geneva to a warmer climate (Chapters 2-4) and for coupling with the atmospheric single-column model (Chapter 3).

0.3 Modelling future climates

0.3.1 Climate models

In order to simulate the global or a just sub domain of the Earth's climate system, a hierarchy of models has been developed, ranging from the simplest energy-balance models (EBMs) to the more complex models that simulate fully interactive, three-dimensional (3D) climate processes (e.g., regional climate models, or RCMs, and global climate models, or GCMs). For particular applications, single column models (SCMs) that represent a single GCM or RCM atmospheric column have also been developed. The treatment of all physical processes occurring within SCMs may be identical in principle to those present in GCMs/RCMs. The main advantage of running a SCM over GCMs/RCMs is related to the much-reduced computational resources required in terms of speed and memory. In the SCM described below, techniques to prescribe the advective forcing and to nudge the atmospheric profiles have been developed in order to ensure the numerical stability for model simulations aimed at climatic timescales.

0.3.1.1 Approaching future climates with GCMs and RCMs

With the aim of assessing the state of perialpine ecosystems over coming decades, it is essential to predict how climate will evolve in the future. For this purpose, Global Climate Models (GCMs) are the most advanced tools to determine the climate's state with time and its response to future increases in greenhouse gases. These models represent dynamical processes related to atmospheric flows, and physical processes related to mass, heat, and momentum exchanges between the atmosphere and the surface (ocean, sea ice, subgridscale features such as lakes and land surfaces). They reproduce the large-scale atmospheric circulation and provide results related to the evolution of global climate using a three dimensional grid mesh. However, the relatively coarse horizontal resolution of the grid (100 km to 500 km. Randall et al. 2007) and the reduced number of vertical layers (10 to 20 layers) force GCM to use subgrid-scale parameterization to simulate important processes operating at scales smaller than the model grid. Cirrus and stratus cloud formation and dissipation, cumulus convection and turbulence and subgrid-scale mixing are some of the most important processes that are not explicitly resolved, but whose properties must however be represented on the grid. In addition, a better representation of the local climate, taking into account the effects of alpine topography on the study area and the surface features (e.g. vegetation and lake) of the Swiss Plateau would improve the assessment of expected changes in the perialpine aquatic environment. Among the methods used to refine GCM outputs, Regional Climate Models (RCMs) are one of the most widely implemented dynamical downscaling tools (Giorgi and Mearns 1999; Wang et al. 2004; Giorgi 2006; Laprise 2006). There are limited-area models designed for climate applications pioneered by Giorgi (1990) and his team (Dickinson et al. 1989) using the Pennsylvania State University mesoscale model (MM4) and then adopted and refined in many research institutions around the globe (Cullen 1993; Jones et al. 1995; Caya 1995; Christensen et al. 1996; Jacob and Podzen 1997). RCMs are nested in global or hemispheric coarse resolution atmospheric models which provide the lateral boundary conditions for the RCM, and use interactive land surface schemes. The limited area covered by these models allows a finer-scale horizontal spatial resolution (10-50 km). Despite their high computational demand, simulations can be undertaken for several decades, typically 20 to 30 years (Christensen et al. 2007), but also up to a century time scale for some applications (Mc Gregor 1999), thus allowing to better take into account sub-grid scale climate feedback mechanisms (Pesquero et al. 2010). Even with higher spatial resolution, parameterizations of sub-grid scale processes, such as surface-atmosphere exchanges or cloud microphysics (Bader et al. 2008) are still required. RCMs may thus make use of the parameterization package or physics of the parent GCM or include more sophisticated parameterizations [such as the Canadian Land Surface Scheme model, CLASS (Verseghy 1991; Verseghy et al. 1993), the Biosphere-Atmosphere Transfer

Scheme land model, BATS (Dickinson et al. 1986; 1993) or the Interaction Soil-Biosphere-Atmosphere land model, ISBA (Noilhan and Planton 1989; Noilhan and Mahfouf 1996)] or regional ocean models (Saucier et al. 2004). Lakes are not resolved in low resolution GCMs, but due to their importance on the momentum, heat and moisture exchanges with the atmosphere, first attempts have been made to include them in RCMs (Hostetler et al. 1993). If current surface water conditions can be deduced from observations, the large thermal response of water makes a realistic assessment of their future evolution difficult. Neglect of heat exchange between the earth surface and the atmosphere in a model may substantially bias the local climate response. To improve the accuracy of RCM outputs for climatic change studies, the incorporation of a lake component at the surface grid that takes into account these exchanges at the lake-atmosphere interface has been implemented (Goyette et al. 2000; Swayne et al. 2003). Due to the finer grid-mesh of RCMs, lakes may be fully resolved in a model grid cell or be part of a subgrid surface scheme. However, current experiments that use outputs from atmospheric models to drive lake models for long term climate applications are still confined to a stand-alone mode (Hostetler and Small 1999). First twoway coupling experiments between lake and atmospheric models have been successful, but over short periods of time and using 1D lake models only (Hostetler and Small 1999; Small et al. 1999; Leung and Ghan 1999; Song et al. 2004). Complex 3D lake models have been used to interact with the atmosphere in a stand-alone mode for coupling and regionalization issues (Swayne et al. 2005). The high computational costs and the large amount of data required to calibrate, validate and run these 3 D models are a further obstacle to their use for long term integrations (Leon et al. 2007). Since there is still a large degree of uncertainty on what lake models are optimal for certain environmental applications in order to well reproduce lake-atmosphere interactions, the Lake Model Intercomparison Project (LakeMIP) has been set up for testing purposes, for example in terms of lakes that are parameterised in numerical weather prediction (NWP) models and RCMs.

Since lake models implemented in RCMs are not currently used for long term integrations, a one-way technique of interfacing a lake model with the atmosphere is required in order to assess the evolution of lake thermal profiles. To link the outputs from GCMs or RCMs in a future climate to the impacts on physical features of lakes (Boyce *et al.* 1993; Peeters *et al.* 2002), the "delta method", widely adopted in many climate studies, is applied to lake surface temperature. It consists in adjusting the baseline observation by the difference between period-average results for the future and those for a current climate. In this study, the method has been improved to account for intra-monthly or daily variability of changes before being validated (chapter 2). Since stand-alone forcing uses a prescribed atmosphere, fluxes from the water surface cannot lead to changes in the atmosphere above. It is thus likely that this approach maximizes the sensitivity to climate change (Hostetler and Small 1999).

As mentionned in the 3rd Assessement Report of the IPCC (Giorgi et al. 2001), the better way to assess the full range of climate change for impacts studies and adaptation strategies would be to use jointly several GCMs and various downscaling methods. However, such a procedure can be computationally demanding, which has reduced the number of simulations for limnologic studies. Furthermore, by confronting RCM outputs to observations, it is not possible to state that a single model performs better than any other, while some may be more accurate at a specific grid point due the inclusion of a mesoscale process or a specific parameterization (Frei et al. 2006; Rinke et al. 2006). The EU PRUDENCE (Christensen et al. 2002) and ENSEMBLES (Hewitt and Griggs 2004) projects that attempts to assess general trends and uncertainties in climate simulations from an ensemble of simulations with RCMs over Europe, may help to gain confidence in the climate response using outputs from one RCM experiment only. The HIRHAM4 RCM of the Danish Meteorological Institute (Christensen et al. 1998) is one such model whose results correspond well with those of the other RCMs used in PRUDENCE. This latter was thus chosen to evaluate lake response to global warming in a first experiment detailed in chapter 2. Indeed, the fully-coupled oceanatmosphere general circulation model of the UK Hadley Centre, HADCM3 (Johns et al. 2003) has been used to drive the higher-resolution atmospheric HadAM3H model (Pope et al.

2000), that in turn provides the initial and boundary conditions for the RCM HIRHAM4. The model operates at a 50-km resolution and has completed two thirty-year simulations, *i.e.*, "current climate" or the "control simulation" for the period 1961-1990, and the future "greenhouse-gas climate" for the period 2071-2100. The future emissions of greenhouse-gases are based on the IPCC SRES A2 scenario (Nakicenovic *et al.* 2000). This point is discussed later on.

0.3.1.2 Simulating future climates with SCMs

To improve confidence in our understanding of lake response to global warming as a result of uncertainties related to surface scheme, we have conducted an experiment where effects from the lake on the atmosphere are included. The use of a single-column model (SCM) is an option for simulating the atmospheric conditions that may provide an economical framework compared to the computational burden of RCMs and GCMs (Ghan et al. 2000). The SCM may be seen as representing a GCM atmospheric column. It thus allows the isolation of the local, thermodynamic interactions and the evaluation of the feedbacks from the surface to the atmosphere. The use of SCM for testing feedbacks between the atmosphere and the surface appears in the works of Pitman (1994) that assessed the sensitivity of a land-surface scheme to the parameter values. Extension of this approach for feedbacks linked to air-water variations was proposed by Clayson and Chen (2002) using a coupled atmosphere-ocean SCM in the tropical Pacific. However, formerly, the SCM approach was designed to evaluate and improve physical parameterizations of atmospheric processes in climate models. One SCM for instance served to compute cloud formation and radiative transfer processes inside the column (Betts and Miller 1986; Grell et al. 1991; Bechtold et al. 2000), using convective and cloud parameterization (Jacobelis and Somerville 1991; Zhang and McFarlane 1995).

To drive SCMs, the data generally required includes an initial atmospheric profile, time series of surface boundary conditions (such as those for temperature, sensible and latent heat fluxes) and vertical profiles of large-scale vertical motion and of the tendencies of atmospheric variables linked to the horizontal advection are used as lateral boundary conditions (Randall *et al.* 1996; Ghan *et al.* 2000). Many SCMs are based on the same physics code and use the same subgrid-scale physical processes parameterization package as their parent GCM. If large scale dynamical tendencies are specified in SCMs, there are no interactions between parameterized processes and large-scale circulations. This is an advantage in that it allows simulations to be undertaken much more rapidly, and new parameterizations to be quickly tested; on the other hand, a major disadvantage is that biases may amplify with time in some studies.

In this study, the coupling of the one-dimensional lake model SIMSTRAT to a SCM, referred to as FIZC, has been achieved in order to study the effect of climate on lakes over long time spans at the closest grid point to Lake Geneva (chapter 3 and 4). The inclusion of a lake model, rather than prescribed surface conditions, as the surface boundary scheme is believed to better reproduce elements such as the evaporative or condensation rates, the likelihood of cloud formation and the stability of the air mass. It may in turn help better simulate the local climate characteristics through more realistic feedback mechanisms. FIZC takes advantage of the detailed archives of the second generation Canadian GCM (GCMii. McFarlane et al. 1992). Indeed, this model uses the tendencies due to the ensemble effects of the subgrid-scale physical processes as well as prognostic variables for prescribing the contributions to the dynamical tendencies. It also uses the physical parameterizations of GCMii. FIZC lateral boundary conditions could theoretically be provided by any RCMs or GCMs, limitations come from the lack of an adequate data archival frequency in many of these models. Since large-scale fields are saved only in the GCMii, FIZC is entirely dependent on this model data availability. GCMii operates at a 2.75° resolution and provides two thirty-year equilibrium climate, i.e., a "control climate" and a future "greenhouse-gas climate". Details on the future concentrations used for this study are discussed later on.

0.3.2 Emission scenarios

In order to investigate the evolution of the climate, models need to take into account key factors that may alter the energy balance of the climate system. In 1990, the IPCC analysed the evidence on the link between global warming (0.74 °C±0.18 °C from 1906 to 2005) and the increase in anthropogenic long-lived greenhouse gases since preindustrial time (IPCC 1990). While all anthropogenic GHG (CO₂, CH₄, N₂O and halocarbons) emissions have increased, carbon dioxide (CO₂) emissions is dominant (77% in 2004). CO₂ concentrations have increased from 288 in 1750 to 388 ppm in 2009 (Trans 2009). The representation of a possible future climate is thus based on assumptions about both natural and anthropogenic emissions of GHGs in the atmosphere as well as on the current understanding of the effects of increasing GHG and other pollutants on the atmosphere. The quantification of these emissions includes large uncertainties that depend on factors such as technologic development, economic activity, population growth, social criteria, policy choices, etc. Since the 90's, emission scenarios of GHGs in the 21st century have been designed. The most recent have been published in the IPCC Special Report on Emissions Scenario (SRES. Nakicenovic 2000). This has served as a reference to evaluate climatic and environmental impacts, assess mitigation and adaptation strategies for future GHG emissions, and negotiate possible agreements for the reduction of GHG emissions.

The SRES report proposes narrative storylines (or scenario families) for future development in social, economic, technological and policy dimensions, combined with associated quantitative values of GHG emissions. These scenarios do not assume explicit climate policy interventions. Based on specific quantification of driving forces (population, economy, technology, energy, land use), 40 emission scenarios were produced. Each belonged to one of the four scenario families (A1, A2, B1, B2). In order to reduce the number of scenarios, 6 marker scenarios (1 for each of the A2, B1 and B2, and 3 for A1) were selected and translated into CO₂ concentrations (Fig. 0.2). However, for the climate-water issue, as shown in this study simulating the evolution of the thermal structure of Lake Geneva, it is standard practise to focus on just one scenario (Hingray *et al.* 2007).

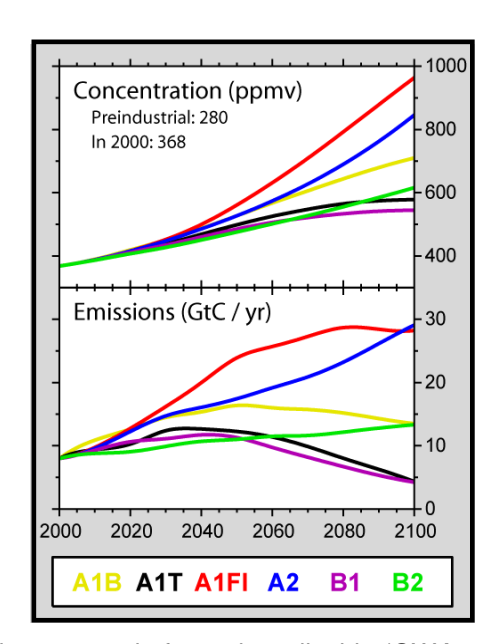


Figure 0.2. IPCC emissions scenario for carbon dioxide (GWA 2007).

Therefore, Chapter 2 uses IPCC A2 scenario changes in atmospheric properties for the period 2071-2100 compared to the reference period (1961-1990), which results from a gradual increase in atmospheric content of CO₂ and other greenhouse gases. The SRES A2 scenario projects an increase in CO₂ concentrations of about 800 ppm by 2100, *i.e.* 3 times

the preindustrial values as a result of an increasing global population and the development of regionally oriented economic growth, which is, however, slower than in other scenarios. Compared to most of the other scenarios, the A2 scenario provides an estimate of the upper boundary of climate futures discussed by the IPCC (2001) and thus drives one of the stronger responses of the climate system to greenhouse-gas increases.

The 2-way coupling experiment in Chapter 4 use results from a climate as it is likely to be at the time of a doubling of CO₂ compared to those achieved in a control "1 x CO₂" climate. This scenario is more of a medium range scenario since a doubling in CO₂ concentrations (660 ppm) corresponds to the value expected in the middle of 21th century in the A2 scenario and approximately to that of the SRES B2 scenario by 2100. In the B2 scenario, lower increase in CO₂ concentrations are expected due to a lower population growth, intermediate levels of economic development and less rapid and more diverse technological changes.

0.3.3 Evolution of European climate over the 20th and 21th Century

In order to more effectively measure the climatic impact of an increase in GHGs and to assess their threat to the aquatic environment, an overview of the climate's evolution in Europe and in Switzerland is presented. Over the last century, major trends in climatic changes were initially described in relation to observation. Later in the 21st century, as defined in emissions scenarios, these changes were characterized by the evolution of GHGs.

0.3.3.1 Climate change over the 20th century

The European climate has experienced more severe warming over the 20th century than the global mean, with an increase in surface air temperature reaching 0.90 ℃ (Jones and Moberg 2003). Annual precipitation trends also changed, but precipitation patterns show a more contrasting picture between the north and south of the continent. Land surface experienced increased precipitation (10 to 40%) from mid- to high latitude, but reduced precipitation in southern areas (up to 20%) (Voigt et al. 2005). Over the last century, Switzerland has also transitioned towards warmer conditions. An increase in mean air temperature of more than 1 °C was recorded, with significant variations between the northern (+1.3 °C and +1.6 °C in the western and eastern part respectively) and the southern Alps (+1 ℃, OcCC 2002). On a seasonal basis, the strongest changes have been in the increase in winter nocturnal minima of temperature at high altitude and the diurnal temperature in summer at low altitude (Jungo and Beniston 2001). Due to its central location in Europe, a clear trend in annual average precipitation has not been detected in Switzerland. If interannual variations are strong, the average amount of precipitation of the previous years is similar to that of the reference period (1961-1990, OcCC 2008). However, some changes in seasonal and regional precipitation have been observed. In eastern and western Switzerland, mean winter precipitation has increased by 10 to 20 % (Schmidli et al. 2002). Changes in precipitation regimes are also observed so that mean precipitation intensity has increased in northern and western Switzerland, as well as throughout much of the Alpine zone in autumn and winter (Schmidli and Frei 2005; Frei et al. 2006).

0.3.3.2 Climate change over the 21th century

Over the past few years, a large number and variety of simulations have been undertaken to provide information on global and regional climate change. By combining global and regional climate models, climate evolution over a specific area can be assessed. Based on a range of scenarios and models, changes are qualitatively consistent among models, while variations in the magnitude and geographical divergences may appear (Christensen *et al.* 2007). The climate model results available in the last assessment report on climate change agree that the mean trend observed in Europe over the 20th Century will continue in the following decades despite political and economic decisions (Alcamo *et al.* 2007). A surface mean air

temperature increase of 1 to 5.5°C is projected over the whole continent. The largest changes will occur in summer in the southern and central regions and in winter in the northern regions. Patterns of precipitation change are more spatially and seasonallydependant. It is projected that the quantity of annual precipitation will increase in the North, decrease in the South and both increase in winter and decrease in summer in central Europe. In some areas of southern and central Europe, summer precipitation may even decrease up to 70% according to scenario A2, (Räisänen et al. 2004) and cause summer droughts to be more frequent. The presence of the Alps plays a large role in Switzerland's climate and may contribute to major differences in terms of a changing climate (OcCC 2008). By the middle of the 21th century, temperature may rise by 2 °C in the winter and up to 2.5 °C in the summer (OcCC 2008). Projections in seasonal precipitation change confirm the observed trend over the 20th century, with an increase by as much as 8% in winter and a decrease of at least 15% in summer. Subsequently, changes by the year 2100 will to a large extent depend on the factors determining the evolution of GHGs. Compared with the period from 1960 to 1990, annual temperatures will continue to rise, with summer increases reaching between 3.5°C and 7°C (OcCC 2008). If mean summer temperature increase exceeds 4.5°C, it is likely that one summer out of two be warmer than the summer of 2003 (Schär et al. 2004). An increase in the mean winter precipitation is expected, with rain instead of snow at higher elevations. On the contrary, the mean summer precipitations are estimated to decrease by up to a maximum of 30%. While summer heat waves and droughts could be more frequent, the increasing mean temperature in winter may reduce the risk of extreme cold events (Christensen et al. 2007). While climate uncertainties suggest a wide range of possible changes, there is evidence that Switzerland will continue moving closer to a Mediterranean-type climate (Marinucci et al. 1995; Rotach et al. 1999).

Chapter 1

Simulation of multi-annual thermal profiles in deep Lake Geneva: a comparison of one-dimensional lake models

Marjorie Perroud^a, Stéphane Goyette^a, Andrey Martynov^b, Martin Beniston^a, and Orlane Anneville^c

a Climatic Change and Climate Impacts (C³I), University of Geneva, Carouge, Geneva, Switzerland b Canadian Regional Climate Modelling and Diagnostics (CRCMD) Network, University of Quebec in Montreal, Montreal, Quebec, Canada.

c French National Institute for Agricultural Research, INRA - Station d'Hydrobiologie Lacustre, Thonon-les-Bains Cedex, Haute-Savoie, France

Abstract

This study reports on the ability of four one-dimensional lake models to simulate the water temperature profiles of Lake Geneva, the largest water body in Western Europe, over a 10year period from 1996 to 2005, using lake models driven by a common atmospheric forcing. These lake models have already demonstrated their capability of reproducing the temperature distribution in smaller lakes and include one eddy-diffusive lake model, the Hostetler model; a Lagrangian model, the one-dimensional Dynamic Reservoir Simulation Model 'DYRESM'; a k- ε turbulence model, 'SIMSTRAT'; and, one based on the concept of self-similarity (assumed shape) of the temperature-depth curve, the Freshwater Lake model 'FLake'. Only DYRESM and SIMSTRAT reproduce the variability of the water temperature profiles and seasonal thermocline satisfactorily. In layers where thermocline variability is greatest, the temperature root mean square error is < 2°C and 3°C (at the time of highest stratification) for these models, respectively. It is possible to apply certain one-dimensional lake models that simulate the behavior of temperature to investigate the potential future warming of the water column in Lake Geneva. Importantly, the metalimnion boundary is successfully modeled, which represents an encouraging step towards demonstrating the feasibility of coupling biogeochemical modules, such as, for example, a phytoplanktonic model, to assess the possible biological responses within lakes to climate change.

Published in: Limnol. Oceanogr., 54(5), 2009, 1574-1594

1.1 Introduction

While peri-alpine lakes are generally renowned for their scenery, they also feature extensive biodiversity, support commercial fishing activities and are reservoirs of drinking water for thousands of inhabitants. In Switzerland, around 20% of domestic water supply comes from lakes (SVGW 2008). It is thus essential that the quality of these freshwater bodies be preserved. Many of the Swiss lakes were declared polluted following their eutrophication in the early 1950s (e.g., Lake Geneva shared by France and Switzerland, Lake Constance shared by Germany and Switzerland, the Swiss Lakes Neuchâtel, Biel and Zug), and political efforts were undertaken over the following decades in order to decrease their phosphorus or nitrate loads (SAEFL 1994).

Since nutrient concentrations have decreased to values associated with an improved trophic status, these lakes now face changes associated with present and future climate. Some of the reported thermal effects of global warming include earlier onset of stratification, less frequent complete winter overturning in large lakes, stronger thermal gradients in the thermocline, shallower depths of the thermocline and an overall warming of the entire water column (King et al. 1997; McCormick and Fahnenstiel 1999; Peeters et al. 2002). Climateinduced changes of lake water temperatures, dynamics and the intensity of stratification disturb the functioning of aquatic ecosystems (Gerten and Adrian 2000; Anneville et al. 2002; Straile et al. 2003). In some cases, they also promote the development of toxic cyanobacteria (Jöhnk et al. 2008; Shatwell et al. 2008) and delay the recovery of lakes following eutrophication (Anneville et al. 2002; 2004). Under such conditions, the presence of such toxic algae in the aquatic ecosystems of a number of peri-alpine lakes [e.g., Planktotrix rubescens in Lake Geneva, Lake Bourget (Jacquet et al. 2005), Lake Zürich (Walsby and Schanz 2002), and Lake Pusiano (Legnani et al. 2005)], indicates that this problem should be investigated further. Predictions of the thermal evolution of lakes will help to assess changes in frequencies of toxic blooms that are likely to occur in some particular lakes.

Numerical investigations of the thermal evolution of a few peri-alpine lakes in a warmer climate, such as the Lakes Constance and Zürich, have been reported in the literature, indicating significant changes in the long term (Peeters *et al.* 2002; 2007). However, Lake Geneva has never fully been studied in order to address this particular problem. Consequently, the main objective of this study is to simulate multi-annual cycles of temperature profiles at a deep lacustrine station in Lake Geneva using one-dimensional (also referred to as single-column) numerical models.

The assumption behind the use of one-dimensional lake models is that vertical gradients of temperature and salinity are significantly larger than the horizontal ones. This assumption is valid if density stratification is present, external forces resulting from wind stress are weak, in- and outflows are not very significant and other processes that may also generate horizontal gradients are negligible. The atmospheric variables driving the lake models are provided by the nearest onshore stations, and lake data used to validate the model simulations are limited by the poor temporal resolution of the water temperature soundings. Nevertheless, in this study, the underlying hypothesis regarding the application of one-dimensional models will be, to a large extent, verified if at least one model realistically reproduces seasonal temperature profiles when: 1) the original model formulation and parameterization do not need to be substantially modified for this particular lake; 2) the driving atmospheric variables do not include any significant ad hoc scaling factors other than the values found in the literature (e.g., the wind multiplication factor, Hornung 2002); and 3) there are no calibration parameters other than the ones found in the literature.

This study thus aims at evaluating the ability of one-dimensional numerical models, driven by common atmospheric observations, to reproduce thermal characteristics of the deep segment of Lake Geneva in a realistic manner. The choice of the models was undertaken

using three main criteria. The models have 1) to use different approaches in order to cover a wide range of possible hydrodynamic formulations, parameterizations, and numerical schemes, 2) to be widely used, and 3) have shown skill in simulating thermal profiles. The four models tested include one eddy-diffusive lake model, the Hostetler model (hereinafter referred to as 'HLM'); a Lagrangian model, the one-dimensional Dynamic Reservoir Simulation Model 'DYRESM'; a k- ε turbulence model, 'SIMSTRAT'; and one based on the concept of self-similarity (assumed shape) of the temperature-depth curve, the Freshwater Lake model 'FLake'. These models will be briefly described later. Three of them have already been tested on large lakes, yielding satisfactory results (Hostetler and Bartlein 1990; Boyce $et\ al.\ 1993$; Peeters $et\ al.\ 2002$).

In a first phase, calibrations pertaining to each model parameter and adjustments related to the location of the offshore station were carried out on data from three separate years (test samples) before being applied to the ten-year period under investigation. The comparison assesses monthly temperature profiles averaged over a number of levels in the mixed layer, in the metalimnion and in the hypolimnion, respectively. It then evaluates the metalimnion's thickness and the strength of the summer stratification.

This paper first gives a description of the experimental study site in terms of available lake and atmospheric data, and a short description of the model formulations and calibrations. It also defines the common atmospheric data driving the numerical models, as well the experimental design. Then, a validation of each model on the basis of available high-resolution vertical temperature soundings is presented, and finally results of the model comparison on the basis of their abilities to simulate the evolution of the monthly thermal characteristics of Lake Geneva are shown.

1.2 Methods

1.2.1 Study site

Bordered by the Alps to the South and the Jura mountains to the North, Lake Geneva is located at 46°26' latitude north, and 6°33' longitude east (mean geographic position). It is a fresh water body with a surface area of 580 km² shared by Switzerland and France, with a maximum length of 73 km and a maximum width of 14 km. It can be divided into 2 parts, the 'Grand Lac', on the eastern side and the 'Petit Lac' to the West, in its small and narrow section. The former, with a maximum depth of 309 m, represents more than 96% of the total water volume. As Lake Geneva remains stratified most of the year and surface waters do not freeze in the main body, it is considered a warm, monomictic lake, although complete winter mixing occurs very rarely in the Grand Lac. The last complete overturns took place consecutively in the winters of 2004-2005, and 2005-2006, 20 yr after the previous overturning (Lazzarotto *et al.* 2006; Lazzarotto and Rapin 2007). However, the shallower Petit Lac (max depth 76 m) mixes every winter.

The French National Institute for Agricultural Research (INRA) collects bi-monthly samples of thermal and bio-chemical properties of water such as temperature, conductivity, and oxygen at a deepest point of the lake (Database INRA of Thonon-Les-Bains, Data CIPEL) within the framework of a monitoring program coordinated by the International Commission for the Protection of Lake Geneva (CIPEL). This station, called SHL2, is located more or less in the middle of the Grand Lac (Fig. 1.1). Discrete measurements vary slightly within the time period of this study, but are presently recorded at 0, 2.5, 5, 7.5, 10, 15, 20, 25, 30, 35, 50,100, 150, 200, 250, 275, 290, 300, 305, and 309 m depths. Additionally, high-resolution vertical temperatures soundings ($\Delta z \approx 1$ m) are available for the purpose of this study. They are measured from the surface down to the bottom of the lake by a multiparameter probe ME

(Standart-ECO-Probe Version II) up to 2001 and then a conductivity temperature depth (CTD) 90 multiparameter probe (Sea-Sun Tech).

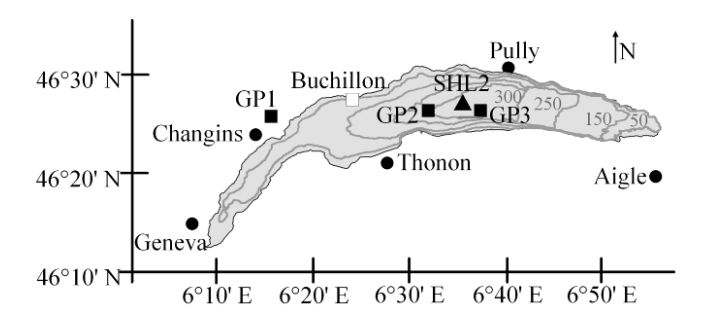


Figure 1.1. Map of Lake Geneva (longitude and latitude) with locations of the meteorological stations (black dots) and grid points of the COSMO model (black squares). The position of SHL2 (black triangle) and of a mast 100 m offshore (white squares) are indicated.

Penetration of solar radiation in the water column is closely correlated to water transparency. As no depth-dependent light extinction coefficient, $K_{\rm e}$, measurements exist, bi-monthly values are deduced on the basis of the secchi disk depth ($Z_{\rm SD}$) and interpolated through time in order to cover the period simulated by the lake models. $K_{\rm e}$ is then calculated through the Beer-Lambert model with light intensity at depth z corresponding to euphotic depth (1% of surface light intensity). Euphotic depth is estimated to 2.5 times the secchi disk depth (Capblancq 1995).

Density stratification of Lake Geneva depends mainly on the vertical water temperature gradients and to a very minor extent on salinity (here defined with the 'practical salinity scale', S), as well as on the suspended particles (Umlauf and Lemmin 2005). Even though the effects of these two last are negligible, they have been taken into account in the computation of the water density, $\rho_{\rm w}$. In each model, $\rho_{\rm w}$ depends on water temperature, $T_{\rm w}$, S, and depth induced pressure. Water conductivity, which is proportional to the concentration of dissolved ions, is currently used to derive S. In Lake Geneva, conductivity (normalized at 25 °C), κ_{25} , is measured. Composition of seawater and lake water is different and therefore the formula of practical salinity scale (UNESCO 1981; PSS78), which is based on salt water to retrieve salinity from conductivity, cannot be applied. A method has been used that reproduces local density conditions, without changing the density parameterization in each model. The density of Swiss lakes [defined by D. Imboden and R. Kifter (unpubl.) according to their ionic composition, as per the second term in Eq. 1] has thus been individually equalized with the density equation of each model

$$\rho_{w}(T_{w},S) = \rho_{w}(T_{w})(1+\beta_{k} \kappa_{20}). \tag{1}$$

 κ_{20} is then converted into 'density equivalent' salinity by a linear regression of $T_{\rm w}$ [0 - 20 °C]

on S [0 - 0.5] as per the approach described by Wüest et~al. (1996). This approximate fresh water density equation based on the dominance of ions in Swiss lakes and rivers, namely calcium and bicarbonate, is given through κ_{20} and β_{κ} , the specific expansion coefficient for κ_{20} through Ca(HCO₃)₂. κ_{25} has been changed into κ_{20} by the empiric formula described in Bührer and Ambühl (1975):

$$\kappa_{20} = \kappa_{\rm T} \left(1.72118 - 0.0541369 \, T + 1.14842 \times 10^{-3} \, T^2 - 1.222651 \times 10^{-5} \, T^3 \right)$$
(2)

with κ_T the conductivity at temperature T.

1.2.2 Model descriptions

Among the range of one-dimensional lake models developed to simulate the evolution of the water temperature profiles, two kinds of models may be distinguished, *i.e.*, eddy-diffusion and turbulence-based models. They have all been shown to realistically reproduce multiple aspects of the lake thermal profiles. Therefore, the choice of a specific model depends more on the exact questions to be addressed in the particular study. Eddy-diffusion models simulate the vertical transport of heat in the water using a mixing parameterization based on an eddy-diffusion approach (Orlob and Selna 1970; Henderson-Sellers *et al.* 1983). Turbulence-based models compute the production and available amount of turbulent kinetic energy, parameterize the vertical transport by eddies (Kraus and Turner 1967; Imberger *et al.* 1978; Burchard and Baumert 1995), and consider the dissipation of energy.

The models selected for the purpose of this project include an eddy-diffusion model based on a diffusion coefficient, HLM (Hostetler 1987; Hostetler and Bartlein 1990); an updated version of the DYRESM Lagrangian model developed by Imberger *et al.* (1978); an extended version of the k- ε turbulence model, SIMSTRAT (Goudsmit 2002); and, a two-layer self-similarity based bulk model, FLake (Mironov 2008). Technical details, calibration, parameter optimization, and other simulation characteristics referring to these models are summarised in Table 1.1. In addition, governing equations of these models are summaries in Appendix 1.1 – 1.4.

Numerical schemes have grown in complexity, since earlier one-dimensional lake models considered molecular diffusion of heat as the only means of downward transport outside the epilimnion (Dake and Harleman 1969). Parameterizations of vertical mixing have also progressively improved so that the effects of winds upon surface layers as well as in the meta-hypolimnion through seiching are an option for two of these models.

The HLM uses the parameterization of Henderson-Sellers (1985) as an approximation to the eddy-diffusion coefficient. This equation is highly dependent on the surface friction velocity, u_{\cdot} , obtained from the surface wind speed, v_{\cdot} , and the aerodynamic drag coefficient, $c_{\rm D}$, and the ratio between the strength of the stratification and the shear stress, provided by the depth-dependent Richardson number (Appendix 1.1). In this model, the heat diffusion is responsible for the evolution of the thermal profiles. Density instabilities are solved by mixing of the unstable layers.

The Dynamic Reservoir Simulation Model (DYRESM) is a one-dimensional turbulence-model using a Lagrangian approach developed by the Centre for Water Research (CWR), University of Western Australia. It is designed to simulate the distribution of heat and salinity in the water column of lakes and reservoirs. The first version has been described in detail by Imberger *et al.* (1978), Imberger and Patterson (1981), and has been improved more recently by Yeates and Imberger (2003). The public-domain version DYRESM V4.0.0-b2 is used in this study. DYRESM is structured in layers of uniform properties but of variable thickness that need to be defined by the user. Layer mixing occurs when the turbulent kinetic energy (TKE), which is stored in the topmost layers and produced by convective overturn, wind stirring and shear, exceeds a potential energy threshold (Appendix 1.2). Moreover, DYRESM accounts for diffusion created by basin-scale internal waves. It uses the lake number, L_N , to evaluate the amplitude of the internal wave and to parameterize the turbulence created by the damping of the motion of seiches on the bottom boundary and the shear mixing in the interior of the lake.

Table 1.1. Model name, type, calibration, characteristics, and reference.

Model	Туре	Calibration and parameter optimization	Simulation characteristics	Other characteristics	Reference
HLM [§]	energy balance with eddy diffusivity and convective mixing	no calibration $V_{\text{lake}} = \text{fct } (v^*)$ $C_{\text{D}} = C_{\text{DM}} = C_{\text{D}} (v_{\text{lake}})^+$	timestep = 1 h archival frequency = 1 d ⁻¹ layer depth = 1 m	Inflow and outflow : set to 0 Variable $K_{\rm e}$	Hostetler and Bartlein 1990
DYRESM	process-based, vertical mixing as an extension of the Kraus–Turner deepening law (Kraus and Turner 1967).	$V_{\text{lake}} = \text{fct } (v)$ $C_{\text{D}} = 0.0018$ VMC = 700	timestep = 1 h archival frequency = 1 d ⁻¹ layer depth = variable (0.5 - 3 m)	Lagrangian layer scheme include seiches parametrization inflow and outflow : set to 0 Constant K_e	Yeates and Imberger 2003 Kraus and Turner 1967
SIMSTRAT	turbulent kinetic energy production and dissipation diffusive mixing	$v_{\text{lake}} = \text{fct } (v)$ $C_{\text{D}} = C_{\text{D}} (v_{\text{lake}})$ $\alpha_{\text{seiche}} = 0.012$ $q = 0.9$	timestep = 10 min archival frequency = 1 d^{-1} layer depth ≈ 0.75 m	include seiches parametrization inflow and outflow : set to 0 Variable $K_{\rm e}$	Goudsmit et al. 2002
FLake	bulk heat and kinetic energy budgets	no calibration virtual bottom at 60 m if deeper than 60 m $C_{\rm D} = C_{\rm DM}^{\dagger}$	timestep = 1 h archival frequency = 1 d ⁻¹ layer depth = variable (2 layers: mixing layer and thermocline)	no hypolimnion	

[§] Hostetler Lake model
* v represents the hourly wind speed recorded at a land station, vlake the corresponding over the lake surface at SHL2.
+ formulation used for momentum drag only

The third model, SIMSTRAT, the buoyancy-extended k- ε model (Rodi 1984; Burchard *et al.* 1998), has been updated to include the effects of internal seiches on the production of *TKE*. Turbulent mixing is solved by the two dependent equations of production and dissipation of *TKE* (Appendix 1.3). The source of *TKE* is generated by shear stress from the wind and buoyancy production in case of unstable stratification. Seiching developed under the action of the wind increases *TKE* in the interior of the lake due to loss of seiche energy by friction at the bottom.

The fourth model, 'Freshwater Lake model' or FLake is based on the concept of the selfsimilarity of the thermocline structure, drawn from numerous observations of oceanic mixing layer dynamics (Kitaigorodskii and Miropolsky 1970). A two-layer structure is assumed, consisting of a mixing layer with constant temperature and of a thermocline, extending between the mixing layer and the lake bottom. The water temperature shape in the thermocline is parameterized by a fourth-order polynomial function of the depth that depends on a shape coefficient C_T (Appendix 1.4). The mixed-layer temperature, the bottom-water temperature, the mixed-layer depth, and the shape coefficient C_T determine the water temperature profile. The same concept of parametric shape functions is applied to other elements of lake systems: sediment layer, ice and snow layers, with linear shape functions for ice and snow. The model calculates the temporal evolution of an ensemble of lake structure parameters that balance thermal fluxes on internal and external boundaries. The mixed-layer depth dynamics include convective entrainment, wind-driven mixing and volumetric solar radiation absorption. The two-layer water thermal structure used in FLake precludes its application to deep lakes, since the hypolimnion is usually present between the thermocline and the lake bottom. To avoid this limiting factor, a virtual bottom is usually placed at 60 m, whenever the lake depth exceeds 60 m.

1.2.3 Meteorological data

Lake models need to take into account components of the energy budget as well as other atmospheric variables and their evolution in time. The energy transfer that drives these models is based on the surface energy budget computed as $QS^* + QL^* - (Q_E + Q_H)$ as well as on the wind stress forcing. The energy budget involves net solar radiation $QS^* = QS \downarrow - QS \uparrow$, taking into account incoming solar radiation, $QS \downarrow$, and reflected solar radiation, $QS \uparrow$; the net atmospheric infrared radiation $QL^* = QL \downarrow - QL \uparrow$, considers $QL \downarrow$, the infrared radiation emitted by the atmosphere down to the surface and, $QL \uparrow$, the infrared flux emitted by the surface and, finally, the latent (Q_E) and sensible heat (Q_H) fluxes, respectively. Positive values of the latter indicate heat extraction from the lake to the atmosphere. These components are computed as common inputs to the lake models, but incident solar radiation, $QS \downarrow$, is prescribed from observations.

The required meteorological variables are provided as hourly values of air temperature, *T*, horizontal wind magnitude, *v*, relative humidity, *hr*, and cloud cover, *C*. Meteorological records in the vicinity of the lake are supplied by the Automatic Network (ANETZ) of the Federal Office of Meteorology and Climatology, Meteoswiss (Bantle 1989), and by a MeteoFrance inland weather station nearby. Locations of the four land stations are indicated in Fig. 1.1. Meteorological inputs used to drive the models are taken from the land station Changins due to its central location and because its wind data are not perturbed by surrounding land surface characteristics (Table 1.2). Surface air temperatures were adjusted according to the station altitude differences compared to the water surface of the lake. In order to remove the bias of inland wind speed recordings and to generate values over open water at station SHL2, a correction factor has been implemented. It takes into account wind outputs from a numerical weather forecast model, COSMO (Consortium for Small-scale Modeling; Bettems 2002) provided by MeteoSwiss at three model grid points (GP1, GP2, and GP3, respectively, as shown in Fig. 1.1).

Table 1.2. Hourly meteorological value recorded at Changins over the 10-year period 1996-2005.

	T (°C)	v (m s ⁻¹)	hr (%)	<i>QS</i> ↓ (W m ⁻²)	p (hPa)
Mean	10.6	2.3	73.2	142	966
Min	-10.7	0	13.4	0	928
Max	36.3	17.8	100	1040	988

hr, relative humidity, $QS\downarrow$, incident solar radiation, p, surface pressure

A common parameterization based on the bulk transfer method has been employed for the surface sensible and latent heat fluxes. The scheme uses the atmospheric vapor pressure e_a (hPa), computed on the basis of hr (%) and on the saturation vapor pressure e_o (hPa) function of the surface air temperature. Hostetler and Bartlein (1990) propose to use the Richards' equation (1971) to compute e_o , as follows:

$$e_0 = 1013.25 \,\mathrm{e}^{\left(13.3185t_{\rm K} - 1.976t_{\rm K}^2 - 0.6445t_{\rm K}^3 - 0.1299t_{\rm K}^4\right)}$$
 (3)

where

$$t_{\rm K} = 1 - \left[\frac{373.15}{T_{\rm w} + 273} \right] \tag{4}$$

Infrared radiation flux density emitted by the water surface is approximated by the Stefan Boltzmann law with water emissivity set to 0.97 in all models (Henderson-Sellers 1986). Downward atmospheric infrared radiation to the water surface is given by standard formulation based on ε_a , effective atmospheric emissivity. A wide range of formulations to calculate ε_a have been compared and presented in detail in Henderson-Sellers (1986). The formulation for ε_a that depends on the cloud cover fraction, C, is proposed by Hostetler and Bartlein (1990), as follows:

$$\varepsilon_{\rm a} = 0.84 - \left(0.1 - 9.973 \times 10^{-6} \, e_{\rm a}\right) \left(1 - C\right) + 3.491 \times 10^{-5} \, e_{\rm a} \qquad ; 1 - C \ge 0.4$$
 (5a)

$$\varepsilon_{\rm a} = 0.87 - (0.175 - 29.93 \times 10^{-6} e_{\rm a})(1 - C) + 2.693 \times 10^{-5} e_{\rm a}$$
; $1 - C < 0.4$ (5b)

The cloud cover fraction is taken as the mean value between two station observations, Geneva and Aigle, that is located east of the lake.

The albedo, α , that is used to compute the solar flux reflected at the surface accounts for the solar zenith angle and the solar declination angle (Bonan 1996):

$$\alpha = 0.05 (\mu + 0.15)^{-1} \tag{6}$$

with μ , the cosine of the local solar zenith angle.

1.3 Experimental setup

The four models are run in a 'stand-alone' mode over the lake station SHL2 where a common set of atmospheric driving variables are prescribed for a ten-year period on an hourly basis. In order to compare simulated lake profiles, observed or derived values of T, $QS\downarrow$, $QL\downarrow$, v, and e_a for the period 1996-2005 are used as input variables for the models, also on an hourly basis. A common module then explicitly computes $QS\uparrow$, $QL\uparrow$, Q_E , and Q_H at each time step. The transfer of energy from wind to water has been standardized using the friction velocity u-, defined in Appendix 1.1 – 1.4. The only difference regarding input variables concerns the light extinction coefficient. The user's interface of DYRESM does not allow modifying the value which is then set to the annual average. The morphometry is common to all models and consists of height-area values characteristic of the water body as illustrated in Fig. 1.1.

Due to the low frequency of complete turnover in Lake Geneva, an initial homogenized temperature and salinity profile cannot be used as it would create shifts that cannot easily be recovered during the following seasons. The previously described vertical profiles of water temperature and salinity conducted at SHL2 were used to initialize the conditions prevailing in the lake at the beginning of simulations. Each yearly simulation runs from the last sounding of the previous year to 31 December of the following year. Each model has its own time-marching scheme and time-step interval. Water temperature profiles were archived daily at the exact same time to facilitate comparison.

1.3.1 Model calibrations and wind-speed adjustment

The calibration phase initially focuses on specific model parameters that cannot be inferred from measurements (Table 1.1). Since buoys do not record meteorological variables at the center of the lake, it remains difficult to assess the specific influence that each driving variable produces. Therefore, no calibration procedure is undertaken on those components as the error is detrimental to all models. However, since surface roughness may be considerably different over land than it is over water, a correction to the hourly wind-speed values is allowed. Additionally, a drag coefficient is adjusted since there are large uncertainties in the roughness height over the water surface.

The calibration considers a sample of three disconnected years, namely 1996, 2000, and 2004. For calibration, simulated data ($Tsim_w$) are compared to bimonthly observed temperature profile ($Tobs_w$) over a number m of layers (I). Validation and model comparison are made on the basis of observed and simulated water temperatures where the root mean square of the errors (T_{rmse}), the mean error (T_{rmse}), the standard variation of the error (T_{stdev}) and the improvement of the T_{rmse} by calibration, Imp_{rmse} (%) are computed as follows:

$$\operatorname{error}(t_i, l_i) = T \operatorname{sim}_{w}(t_i, l_i) - T \operatorname{obs}_{w}(t_i, l_i)$$

$$(7)$$

$$T_{\text{me}} = \frac{1}{\sum_{i=1}^{n} m_{i}} \sum_{i=1}^{n} \sum_{j=1}^{m_{i}} \left(\text{error} \left(t_{i}, l_{j} \right) \right)$$
 (8)

$$T_{\text{stdev}} = \sqrt{\left\{ \frac{1}{\sum_{i=1}^{n} m_i - 1} \sum_{i=1}^{n} \sum_{j=1}^{m_i} \left[\text{error} \left(t_i, l_j \right) - T_{\text{me}} \right]^2 \right\}}$$
 (9)

$$T_{\text{rmse}} = \sqrt{\left[\frac{1}{\sum_{i=1}^{n} m_{i}} \sum_{i=1}^{n} \sum_{j=1}^{m_{i}} \operatorname{error}(t_{i}, l_{j})^{2}\right]}$$

$$(10)$$

$$Imp_{\text{rmse}} = 100 - \left[\left(\frac{T_{\text{rmse_cal}}}{T_{\text{rmse_ref}}} \right) 100 \right]$$
 (11)

where j = 1,2,...,m; i = 1,2,...,n; n is the number of days in which a sounding has been taken, and $T_{\text{rmse ref}}$ and $T_{\text{rmse cal}}$ are the T_{rmse} before and after calibration.

In order to characterize the thermal layers with some degree of accuracy, the water column was partitioned into three groups of depths: GD1 (0 to 10 m), GD2 (15 to 35 m), and GD3 (50 to 300 m). Model calibrations were performed through the optimization of values. The optimal value of all specific parameters is determined through minimizing the three annual $T_{\rm rmse}$ compared to a reference value, *i.e.*, before calibration.

The large surface area of Lake Geneva and the topography of its surroundings cause wind speed and direction to be spatially heterogeneous with regard to the scale of the processes that initiate them (Lemmin and D'Adamo 1996). A correction factor to observed values is determined in order to remove the bias in the wind speed generated by the inland station as a surrogate to SHL2 winds. Hourly data simulated by the COSMO model for 2004 serves to establish this factor. Two linear regressions using wind speed at the closest land grid to Changins (GP1) and on those at grid points near SHL2, GP2, and GP3 are determined. The resulting average regression gives a linear relation for wind forcing v of the form for SHL2:

$$v = 0.47 + 1.04 v_{\text{land}}$$
 (12)

where v_{land} is the wind speed recorded inland at Changins.

The varying wave height that is a function of the aerodynamic drag coefficient, c_D , is optimized (Table 1.1). Momentum exchange from wind to water is parameterized by default using a constant drag coefficient. As reported in Wüest and Lorke (2003), typical values of c_D as a function of wind speed vary from 0.0011 for 5 m s⁻¹ to 0.0021 for 25 m s⁻¹, the latter for well-developed waves. Nevertheless, the state of wave saturation is generally never reached in lakes where there is limited wind stress on the surface and short fetch. Studies have demonstrated that surface roughness increases when young waves are growing (Geernaert et al. 1987; Smith et al. 1992). Thus, c_D can largely exceed values for open waters with a long fetch. In Lake Geneva, Graf et al. (1984) have analyzed the drag with respect to wave heights at a mast located 100 m offshore of station Buchillon (Fig. 1.1), a data set for wind speed ranging from 7 to 17.5 m s⁻¹. Consequently, c_D is greater over Lake Geneva than the reference value. Thus, at 17.5 m s⁻¹, c_D is 0.0027. For wind speed below 3 m s⁻¹, Bradley et al. (1991), Lin et al. (2002) have shown that c_D increases unexpectedly with decreasing wind

speeds. In order to consider the key role of c_D in momentum transfer to the water and its implications for the process of mixing, a non-constant value for c_D has been used to consider the increased values at extremes of both high and low wind speed. Simulations included an empirical drag parameterization for low wind speeds (from 3 m s⁻¹, c_D increases as wind speed decreases, Wüest and Lorke 2003) as well as an extra one obtained during the Lake Geneva campaign for higher wind speeds (Graf *et al.* 1984) and that correlates c_D with the increase of wind speed.

In HLM, changes in the value of the momentum drag coefficient $c_{\rm D}$ can be undertaken only through the parameterization of surface friction velocity. However this procedure does not modify the $T_{\rm rmse}$ to any significant extent. Temperature profiles are slightly improved by scaling the wind speed according to Eq. 12 in GD1 and GD2 (for both, improvement of 4%, Fig. 1.2a).

DYRESM is considered as a calibration-free model, containing generic parameters that are obtained by field measurement or lab experiments (Hornung 2002; Gal et al. 2003; Hamilton and Schladow 1997). However, it is possible to calibrate the vertical mixing coefficient (VMC) used in the formulation of vertical heat diffusion, in addition to layer thickness defined by the user (Hornung 2002; Yeates and Imberger 2003; Tanentzap et al. 2007). While generic values normally do not need any modification, parameters related to formulations of TKE in the surface mixed layer (Appendix 1.2, e.g., shear production efficiency), have also been varied with the values found in the literature (Gal et al. 2003; Yeates and Imberger 2003; Tanentzap et al. 2007). The VMC is set to 200 by default, a value found empirically by Yeates and Imberger (2003). Simulations were performed with VMC varying from 200 to 1500. In addition, the maximum layer thickness was set from 1 to 5 m. With a minimum layer thickness set to 0.5 m (Hornung 2002), the smallest $T_{\rm rmse}$ were found for maximum thickness of 3 m and of 3.5 m (not shown). Then, a range of values for VMC and c_D (since winddependent c_D cannot be implemented in this version of the model) are tested with and without the wind correction factor. Increasing c_D and VMC decreases slightly the T_{rmse} in GD1 (improvement of 2%), and reduces it further in GD2 (improvement of 28%, Fig. 1.2b). When the wind correction factor is added, the $T_{\rm rmse}$ decrease significantly (25% in GD1 and 48% in GD2). These results emphasize the lack of heat penetration before calibration and the need to increase the intensity of the mixing process. In GD3, small values of $T_{\rm rmse}$ are also affected by varying these three parameter values (improvement of 12% without wind correction and 33% with wind correction). Improvements of T_{rmse} in GD1 and GD2 are found with a doubling of the shear production efficiency (0.8) and of the wind stirring (0.12). However, they remain very low, below 5% and 10%, respectively, and do not concern each of the calibrated years. Consequently, modifications in the parameter files are not justified. The sensitivity of the model to variations of the constant light extinction coefficient was tested in order to assess whether the constant imposed by DYRESM may affect the quality of the results. DYRESM was run with various values of K_e distributed around the annual average value (\pm 50%). Whereas a strong decrease of K_e tends to reduce the error in GD1 and GD2, simulations with higher K_e do not improve the thermal profile. The maximum improvement (7% in GD1 and 21% in GD2) represents a 50% decrease of K_e , but is not representative of real conditions as this is what is observed during the period of minimum turbidity and would imply no biological effects on light penetration. For a more realistic decrease of K_e (25%), in GD1 and GD2, there is a gain of about 1%, but predicted temperatures are clearly less accurate in GD3.

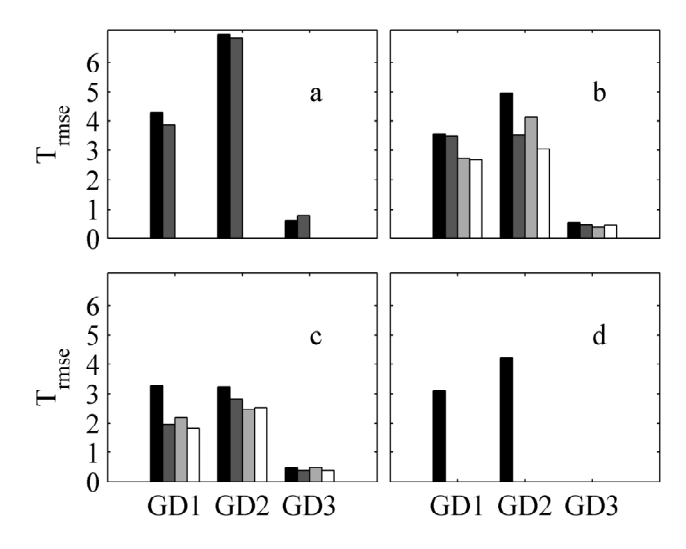


Figure 1.2. Mean of $T_{\rm rmse}$ (1996), $T_{\rm rmse}$ (2000), and $T_{\rm rmse}$ (2004) for GD1 (first group of bars), GD2 (second group of bars), and GD3 (third group of bars) according to (a) HLM, in black: no calibration, v_{land} , in dark gray: v; (b) DYRESM, in black: no calibration, VMC=200, c_D =0.0013, v_{land} , in dark gray: VMC=500, c_D =0.0022, v_{land} , in light gray: VMC=200, $c_{\rm D}$ =0.0013, $v_{\rm t}$ in white: VMC=700, c_D =0.0018, v; (c) SIMSTRAT, in black: no calibration, α_{seiche} =0.006, c_{D} =0.0013, q=0.75, v_{land} , in dark gray: α_{seiche} =0.013, c_D taken from Graf et al. (1984) and Wüest and Lorke (2003), q = 0.9, v_{land} , in light gray: $\alpha_{\text{seiche}} = 0.006$, $c_{\text{D}} = 0.0013$, q = 0.75, v, in white: α_{seiche} =0.012, c_{D} taken from Wüest and Lorke (2003), q = 0.9, v; and (d) FLake, in dark: no calibration, v_{land} .

SIMSTRAT uses two parameters related to the seiche activity, $\alpha_{\rm seiche}$ and q. The former determines the fraction of energy transferred by the wind to the seiche motion and the latter determines the vertical distribution of energy loss from the seiching motion (Goudsmit *et al.* 2002). The two $c_{\rm D}$ parameterizations, described above, for both high and low wind speeds, are implemented in the model code and tested both separately and jointly. Whether or not a correction to wind speeds is applied, $T_{\rm rmse}$ are reduced at all depths with stronger $\alpha_{\rm seiche}$ (Fig. 1.2c). Using wind observations at the Changins station, the error is further reduced when both $c_{\rm D}$ parameterizations are included (improvement of 52% in GD1, 35% in GD2, and 8% in GD3). However, when Eq. 12 is used, even smaller $T_{\rm rmse}$ are found when only the low wind-speed parametrization is employed for $c_{\rm D}$ (improvement of 56% in GD1, 41% in GD2, and 9% in GD3). In fact, when the $c_{\rm D}$ parameterization for high wind speed minimizes the $T_{\rm rmse}$ in GD2, the latter increases in GD1. Since slight shifts of the thermocline produce high $T_{\rm rmse}$, it was decided to favour the $c_{\rm D}$ parameterization for low wind speed. Higher wind speeds compensate for the decrease of energy induced by lower values of $c_{\rm D}$ (Fig. 1.2c).

The FLake model does not require any particular calibration. The water surface roughness length is calculated with respect to wind velocity, using the Charnock formula (Charnock 1955), where the Charnock parameter is obtained from the wind fetch, using an empirical equation. The wind fetch used as the model input parameter is no longer required since a common formulation for the momentum flux has been introduced into the models, and $c_{\rm D}$ becomes a parameter that can be adjusted if required. The high $T_{\rm rmse}$ in GD1 and particularly in GD2 (Fig. 1.2d) means that too much heat penetrates deeper layers and implies that further mixing is not necessary.

1.3.2 Validation

The model comparison was carried out on a bimonthly basis of high resolution vertical soundings over a 10-yr period from 1996 to 2005. Temperature profiles were reset at the beginning of each annual run with the last lake sounding of the previous year. Hence, a bias in the thermal profile produced one year does not affect the following year's simulation. The optimal parameter values were prescribed after minimizing $T_{\rm rmse}$ in the calibration procedure. Simulated temperatures profiles were analyzed in terms of time and depth averages (Figs. 1.3 – 1.6). The five depth classes are 1 - 5 m (D_{0-5}), 5 - 10 m (D_{5-10}), 10 - 15 m (D_{10-15}), 15 - 50 m (D_{15-50}), and 50 - 100 m (D_{50-100}). Depths below 100 m were not taken into account in the validation as water temperatures did not vary significantly over an annual cycle. Surface temperature is also an important variable that requires validation. The strength and the onset of stratification are thermodynamic aspects of the lake that were considered in the model

validation with respect to their essential role in biological processes, particularly for studying species composition, abundance and distribution. In addition, these characteristics are associated with the thickness of the metalimnion and serve to explain the temperature errors that arise in the simulated profiles. The stability of the water column with respect to small vertical displacements was deduced from the Brunt-Väisälä frequency $N(s^{-1})$ as follows:

$$N^2 = \frac{g}{\rho_{\rm w}} \left(\frac{\mathrm{d}\rho_{\rm w}}{\mathrm{d}z} \right) \tag{13}$$

in which g is the acceleration due to gravity, z the depth and $\rho_{\rm w}$ was calculated using the UNESCO equation of state (UNESCO 1981), function of $T_{\rm w}$, S and hydrostatic pressure. Here S is fixed to 0.

A diagnostic index for the onset of thermal stratification (Jacquet *et al.* 2005) has been reformulated for Lake Geneva. The maximum depth where a 1 $^{\circ}$ C difference appears between the 100 m and 2 m layer is used to diagnose the lowest bound of the metalimnion, M_{LB} , as well as the first occurrence of M_{LB} to date the beginning of stratification for each simulated years.

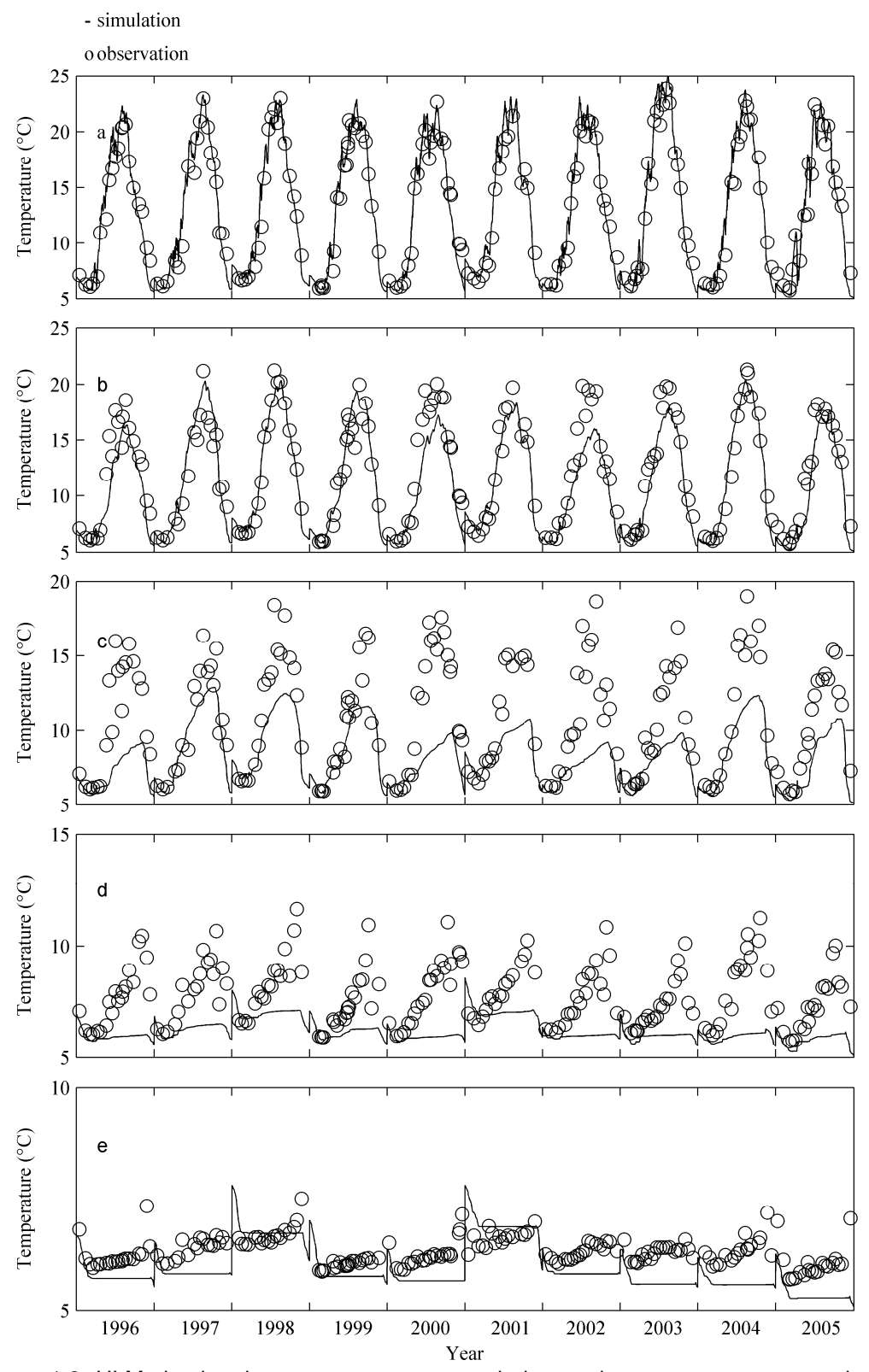


Figure 1.3. HLM simulated water temperatures and observed temperatures averaged over the intervals (a) 0 - 5 m, (b) 5 – 10 m, (c) 10 – 15 m, (d) 15 – 50 m, and (e) 50 – 100 m from 01 January 1996 to 31 December 2005.

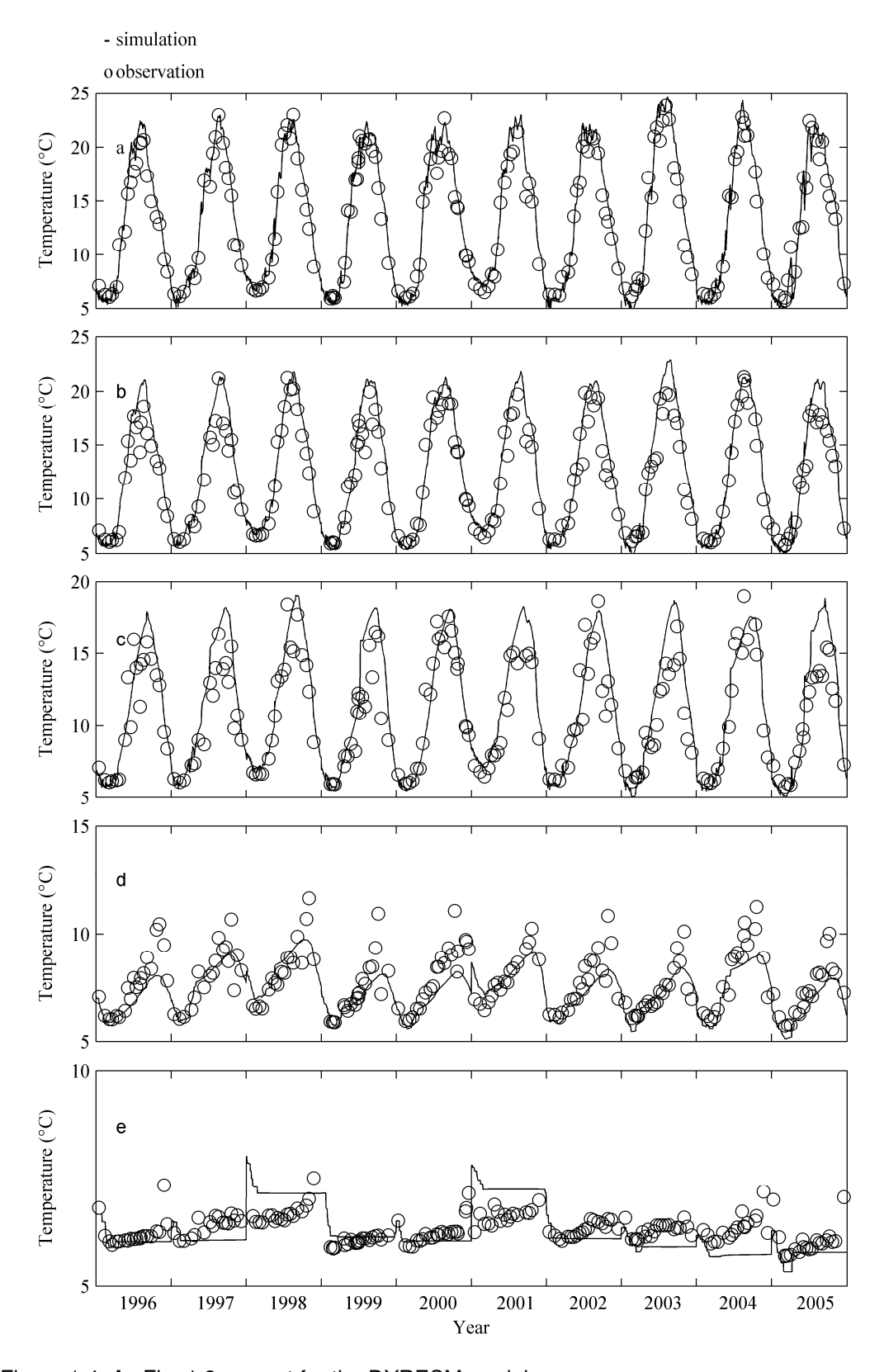


Figure 1.4. As Fig. 1.3, except for the DYRESM model.

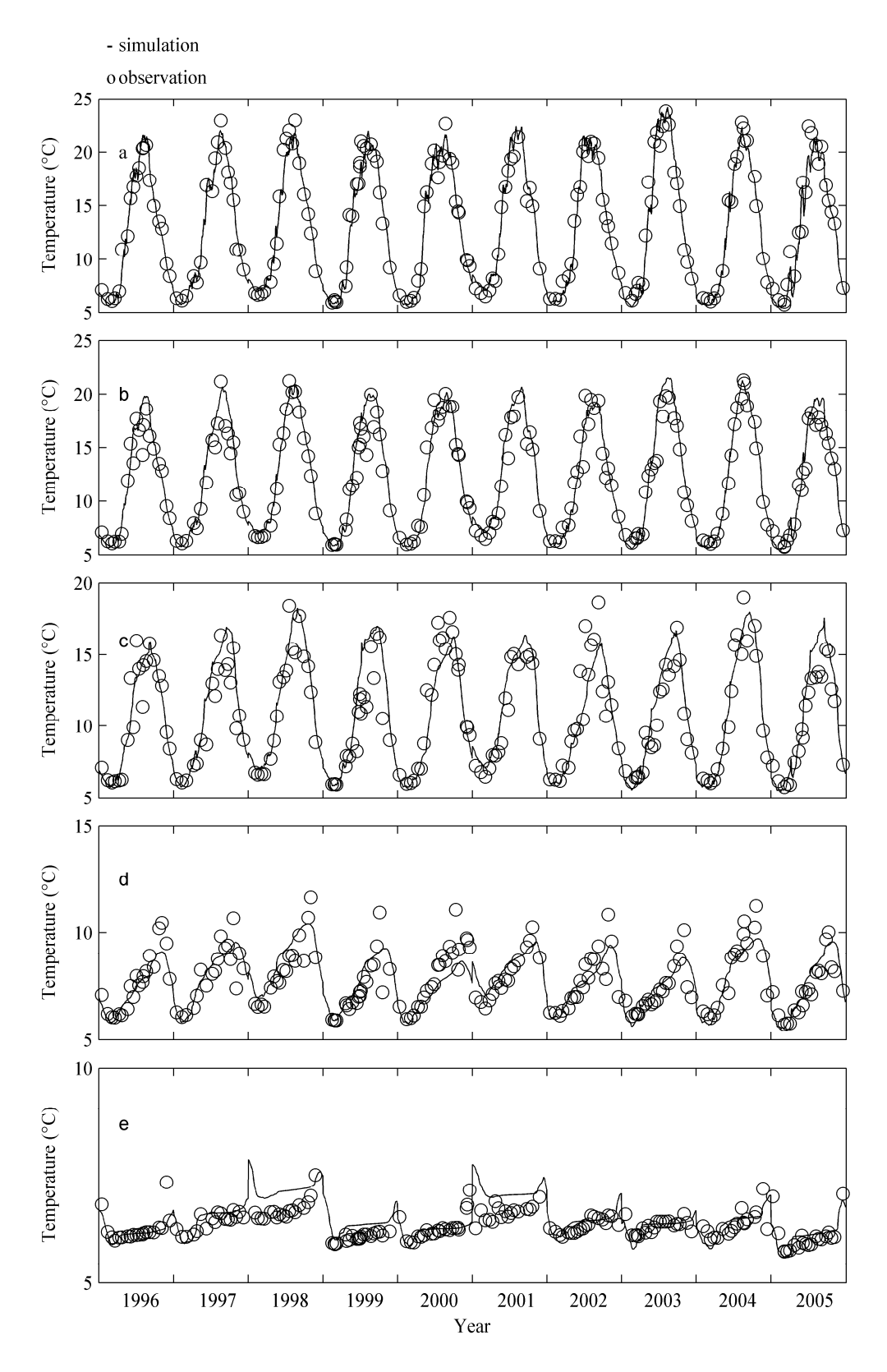


Figure 1.5. As Fig. 1.3, except for the SIMSTRAT model.

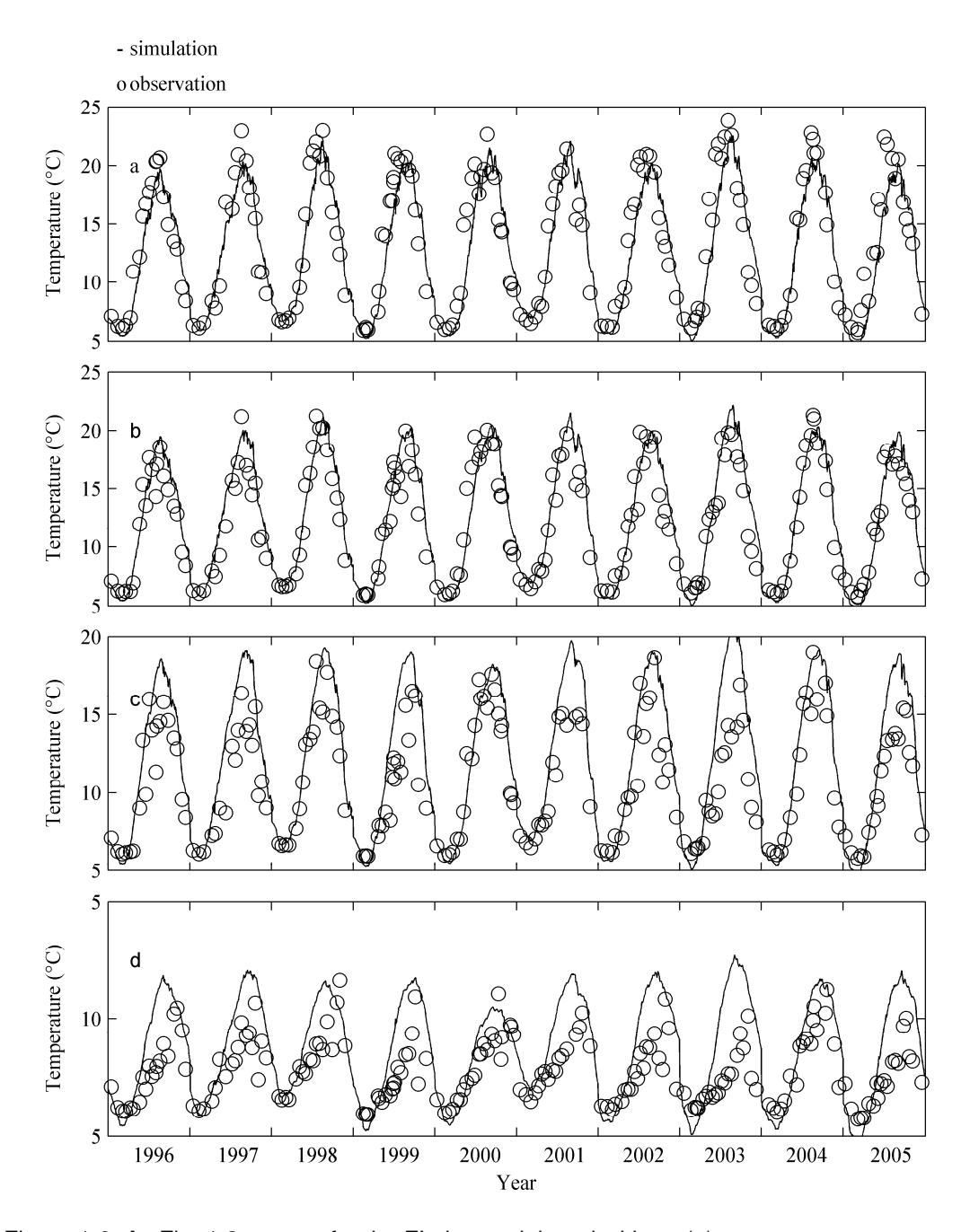


Figure 1.6. As Fig. 1.3, except for the FLake model, and without (e).

1.4 Results

As stated previously, the different adjustable parameters and model configurations make a simple comparison difficult. Due to the different parameter values and parameterization schemes used for VMC, $\alpha_{\rm seiche}$, q, and $c_{\rm D}$, we will focus on the ability of the models to reproduce the monthly-mean temperature profiles, the strength of the stratification and $M_{\rm LB}$ over a ten-year period. The $T_{\rm rmse}$ and $T_{\rm me}$ were used to evaluate the water temperature differences between observed and simulated data (Fig. 1.7).

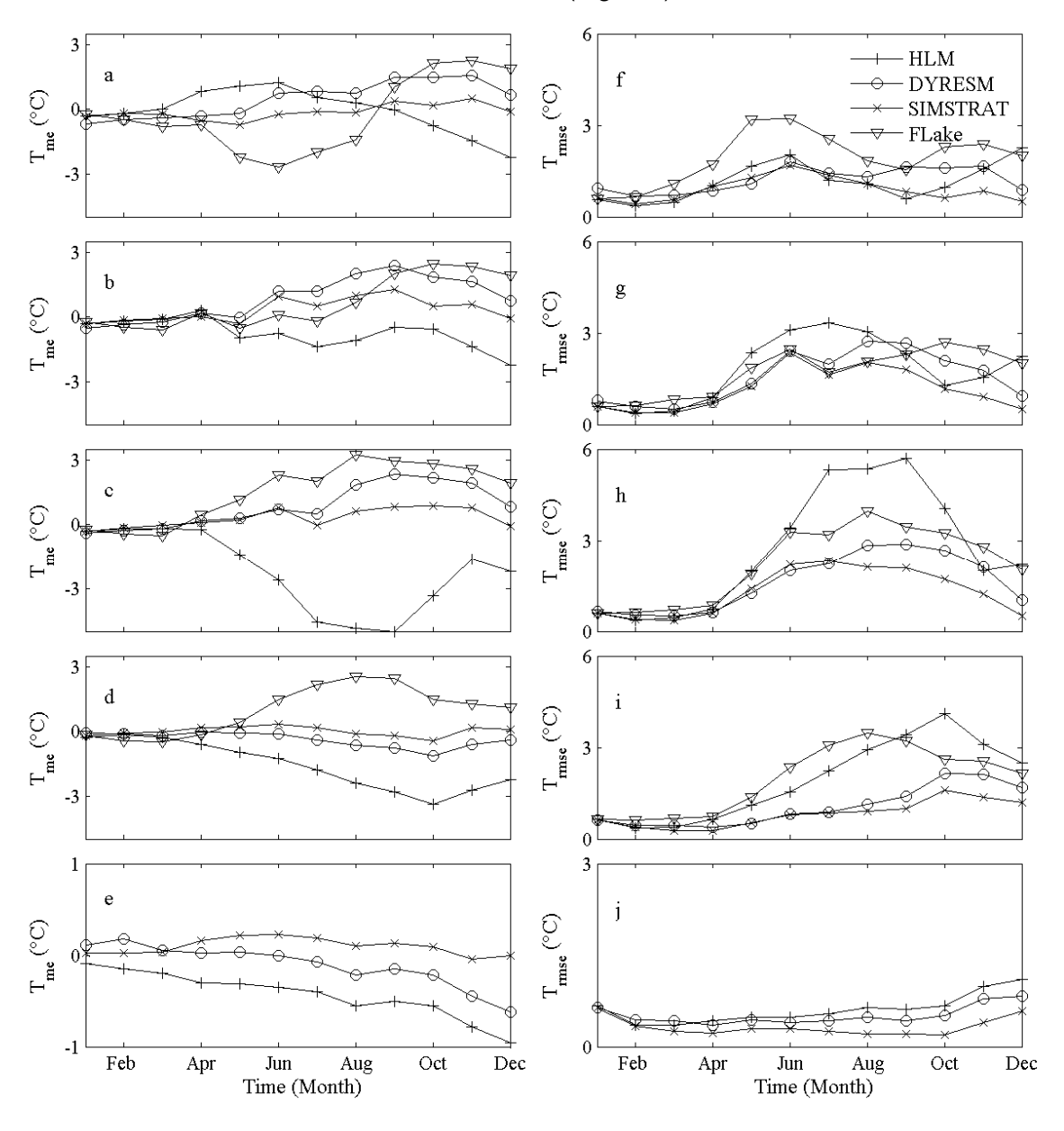


Figure 1.7. Monthly mean HLM, DYRESM, SIMSTRAT and FLake T_{me} (left column) and T_{rmse} (right column) for depth intervals (a and f) 0 - 5 m, (b and g) 5 - 10 m, (c and h) 10 - 15 m, (d and i) 15 - 50 m, and (e and j) 50 - 100 m from 01 January 1996 to 31 December 2005.

In Fig. 1.3 and those that follow, the observed water temperature soundings show strong seasonal variations at station SHL2 and are characterized by a seasonal lag and reduced amplitude with increasing depth. From D_{0-5} to D_{50-100} , the lowest mean temperatures were recorded in February-March lying between 6.0 and 6.5 °C. The warmest mean temperature,

21.3 and 18.9°C for the depth classes $D_{0.5}$ and D_{5-10} , respectively, were recorded in August. In deep layers, the observed delay in the seasonal occurrence of maximum temperatures is caused by the finite heat diffusion and thus generates the warmest temperatures in September in D_{10-15} at 15.6°C and in October in D_{15-50} at 9.7°C. Below 50 m, seasonal variation is less pronounced with a mean change of only +0.6°C in November. In summer, when the thermocline is well established, $\Delta T_{\rm w}$ between D_{0-5} and D_{50-100} is roughly 15°C, and the strength of stratification, N^2 , reaches 2.7x10⁻³ s⁻². Onset of stratification, using the first occurrence of $M_{\rm LB}$, usually takes place between 20 March and 20 April, on average; this interval is based on the observed bimonthly high-resolution temperature profiles.

1.4.1 HLM

The HLM performs well in $D_{0.5}$ (Fig. 1.3a) with monthly $T_{\rm rmse}$ generally below 1 °C except during the months of May and June, November and December where higher values (1.5 °C to 2 °C) coincide with the stratification and destratification periods. This model's annual mean bias \pm standard deviation is 0.08 ± 1.25 °C. In D_{5-10} , $T_{\rm rmse}$ exceeds 2 °C from May to September with a maximum of 3.4 °C in July, and in D_{10-15} from May to December, with a maximum of 5.7 °C in September. These $T_{\rm rmse}$ correspond to monthly $T_{\rm me}$, respectively, of -0.5 ± 2.3 °C to -1.38 ± 3.05 °C and of -1.40 ± 1.42 °C to -5.00 ± 2.77 °C, thus indicating systematic underestimation of the simulated temperatures over this ten-year period (Fig. 1.3b,c). This underestimation is the result of an HLM-simulated metalimnion that is thinner than observed. In Fig. 1.8a, it is noticed that $M_{\rm LB}$ values stands close to 20 m during the whole period of stratification, whereas observations show that those limits should deepen down to 50 m. Therefore, this model overestimates the maxima of N^2 (Fig. 1.9a), reducing the heat diffusion in deeper layers (Fig. 1.3d). Any deep-water variations are then generated only by winter turnover (Fig. 1.3e).

1.4.2 DYRESM

DYRESM effectively simulates surface layers water temperatures (Fig. 1.4a) and produces small monthly $T_{\rm rmse}$, from 0.5 to 1.7 °C, in D_{0-5} , where monthly $T_{\rm me}$ is positive. Annual $T_{\rm me}$ during these ten years is $0.5 \pm 1.2 \,^{\circ}$ C. During the warm season, the values of T_{rmse} increase at all depths and reach close to 3 °C in D_{5-10} and D_{10-15} ; this bias is due to overestimations of temperature (Fig. 1.4b,c), with maxima of T_{me} in August of 2.00 \pm 1.88 $^{\circ}$ C and 1.84 \pm 2.15 $^{\circ}$ C, respectively. On the contrary, in D_{15-50} , the maximum T_{rmse} in October over 2°C, jointly with a T_{me} of -1.12 ± 1.84 °C indicate that the model underestimates the temperatures; in this case, the difference may be due to insufficient heat diffusion from above (Fig. 1.4 b-d), as explained by the positive surface temperature bias. Even though increased mixing during model calibration tends to reduce $T_{\rm rmse}$ in the lower metalimnion (GD2), there is not sufficient heat diffusion in the deeper layers after the onset of stratification. There is a correlation between simulated and observed MLB in spring (Fig. 1.8b). Later in the season, the MLB shows that the deepening rate of the thermocline is too low, even though the values of N^2 are simulated realistically (Fig. 1.9b). Below 50 m, where observations indicate a slight increase of water temperature, simulated values do not exhibit any significant variation, with the exception of a temperature adjustment that produces a rapid cooling following the yearly initialization (Fig. 1.4e).

1.4.3 SIMSTRAT

In D_{0-5} , $T_{\rm rmse}$ between 0.5 and 1.3 °C indicate that temperatures are realistically simulated (Fig. 1.5a). Small monthly $T_{\rm me}$ indicate that no systematic bias exists, corresponding to an annual $T_{\rm me}$ of -0.12 \pm 1.02 °C. As is the case with DYRESM, the same behaviour with depth is simulated (Fig. 1.5 b-d), producing highest $T_{\rm rmse}$ during the warm season, but of smaller

magnitude (Fig. 1.7g,h). Thus, $T_{\rm rmse}$ lie closer to 2°C in D_{5-10} and in D_{10-15} . The maximum of $T_{\rm rmse}$ is also reached in October at 1.5°C in D_{15-50} . In terms of $T_{\rm rms}$, maxima are, respectively, 0.97 ± 2.15°C in D_{5-10} , 0.80 ± 2.07°C in D_{10-15} in June, and -0.44 ± 1.53°C in D_{15-50} in October. The monthly $T_{\rm rms}$ in D_{15-50} is positive throughout most of the year, even in November and December, which means that heat diffuses to sufficient depths (Fig. 1.5d). The negative bias in autumn may be the result of insufficient deepening of the thermocline at the beginning of destratification. Also, as indicated by the values of N^2 shown in Fig. 1.9c, the strength of the stratification is well simulated over this ten-year period, and the deepening of $M_{\rm LB}$ agrees with observations (Fig. 1.8c), even during strong stratification periods. Seasonal variations of water temperature in D_{50-100} are also well captured (Fig. 1.5e).

1.4.4 Flake

This model simulates water temperature profiles that produce high $T_{\rm rmse}$ (between 2 and 4°C) very rapidly. During the water warming period, a maximum monthly $T_{\rm me}$ negative in $D_{0.5}$ (-2.67°C ± 1.82°C in June) is predicted, whereas during the destratification period, maximum monthly $T_{\rm me}$ in $D_{0.5}$ (2.27 ± 0.75°C in November) and $D_{5.10}$ (2.46 ± 1.14°C in October) are positive. This emphasizes a significant lag in the temporal evolution of the simulated temperature (Fig. 1.6a,b). During the same periods (as shown in Fig. 1.6d), temperatures in the deeper layers were overestimated (monthly $T_{\rm me}$ between 0.42 ± 1.29°C and 2.56 ± 2.38°C in $D_{15.50}$). This trend is the result of the formation of a thermocline too thick in spring and which, instead of being steepest in the topmost layers, declines monotonically to the bottom and prevents accurate development of the thermocline later in the year. Therefore $M_{\rm LB}$ develops at greater depth than observed (Fig. 1.8d), and the slope of the thermocline is less abrupt, explaining the high $T_{\rm rmse}$ through the profile and smaller values of N^2 (Fig. 1.9d). Due to the virtual bottom of the lake set at 60 m, heat loss was enhanced during non-stratified periods.

1.4.5 Additional assessments

The date of first occurrence of M_{LB} (O_T) was diagnosed each year for both the simulations and observations. Due to the fact that temperature soundings have not been made with the same frequency as those of the model water temperature archives, O_T is diagnosed when the thermocline is well established in the observed profiles. It is difficult to have accurate estimates of O_T because of the sparsity of the soundings (every 2 wk), since the thermocline can develop any time between one sounding and the next. Nevertheless, it seems that O_T simulated by DYRESM, SIMSTRAT and FLake is quite similar and appears either in one sounding or in the time that elapsed between two soundings. In HLM, stratification always appeared earlier than the other models, but however between the same two soundings, with three exceptions.

Finally, for a set of 182 observed and simulated surface water temperatures (0.4 m), the correlation coefficients are r > 0.98 for HLM, DYRESM, and SIMSTRAT and 0.91 for FLake. Annual $T_{\rm me}$ are -0.1 \pm 1.1 °C, 0.27 \pm 1.14 °C and -0.44 \pm 0.99 °C for HLM, DYRESM, and SIMSTRAT, respectively. Overall, FLake produces lower surface temperatures, with a $T_{\rm me}$ of -0.84 \pm 2.4 °C.

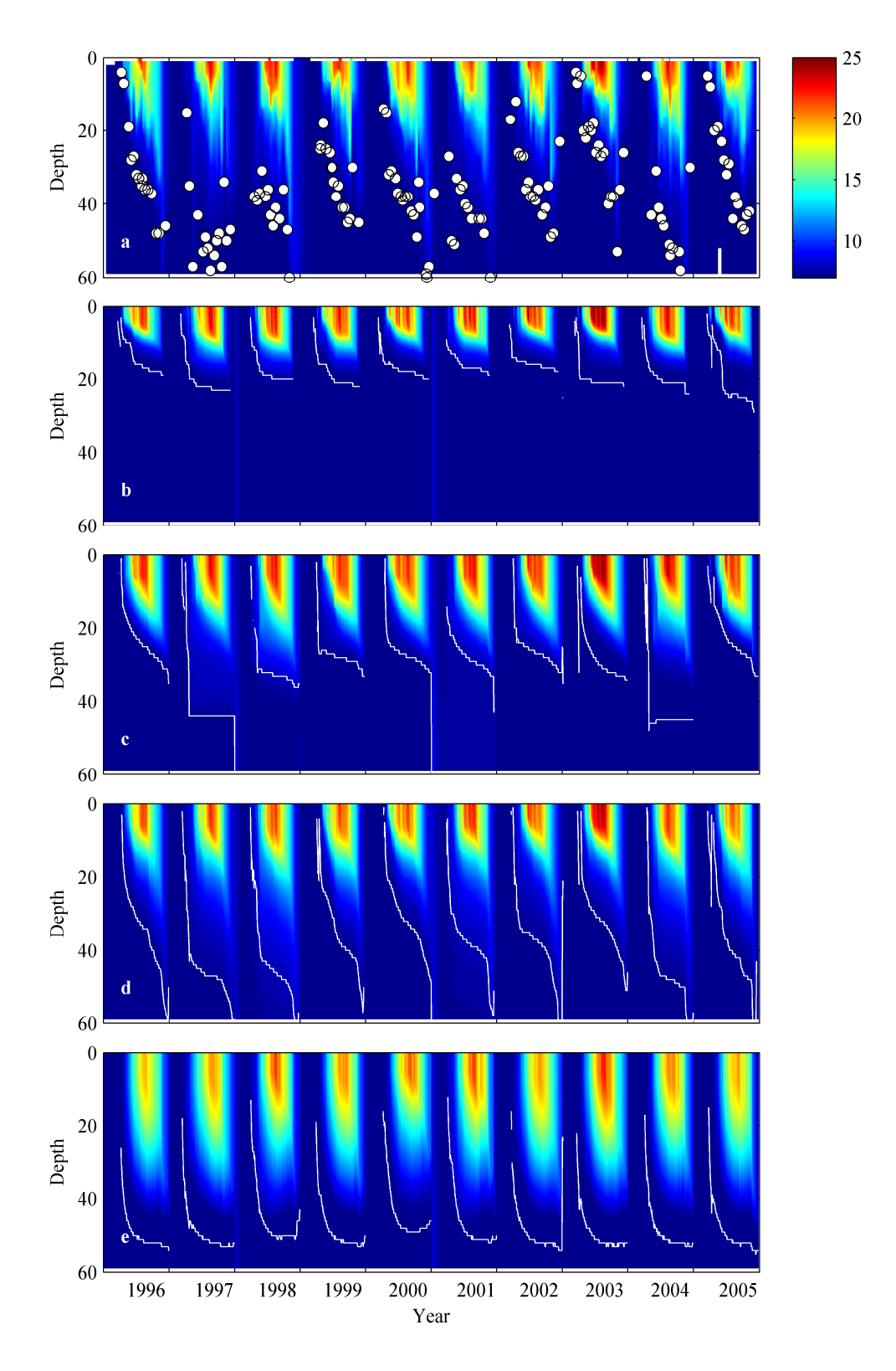


Figure 1.8. Temperature contour plots of (a) the interpolated observed data, and of simulated data with (b) HLM, (c) DYRESM, (d) SIMSTRAT, and (e) FLake, from 01 January 1996 to 31 December 2005. The observed M_{LB} and the M_{LB} of each model are indicated in white from 01 May to 31 October of years 1996-2005

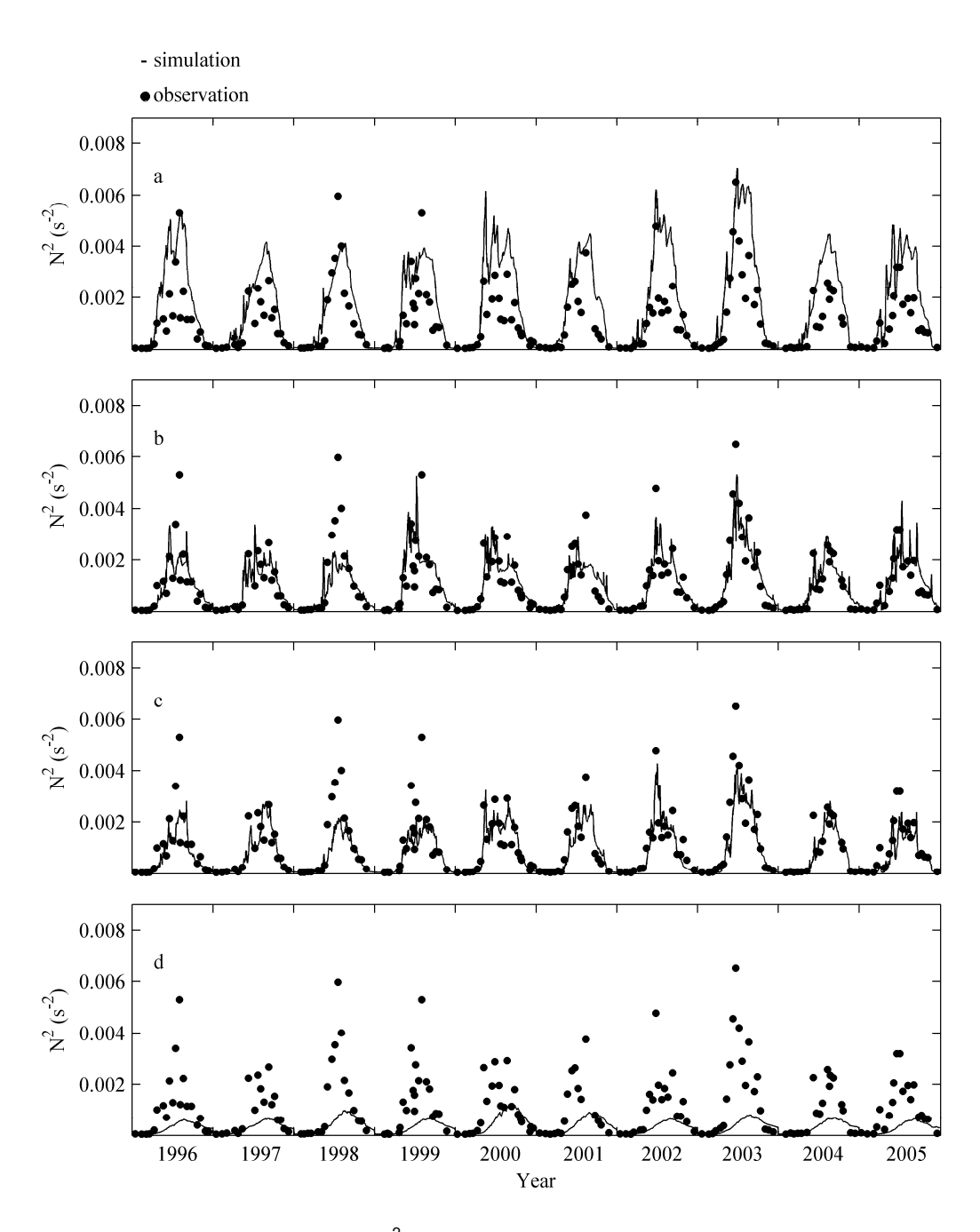


Figure 1.9. Index of stratification N^2 from 01 January 1996 to 31 December 2005 for the observed data and for data simulated with (a) HLM, (b) DYRESM, (c) SIMSTRAT, and (d) FLake.

1.5 Discussion

The main goal of this study was to evaluate the suitability of one-dimensional lake models to reproduce the evolution of water temperature profiles in the deep peri-alpine Lake Geneva. Despite controversy regarding the application of one-dimensional models to large and deep lakes, particularly because atmospheric conditions are heterogeneous over extensive water surface areas, and because horizontal advection is neglected in the lake and seiching motion is parameterized in a rather rudimentary way, we have nevertheless shown that some models, after slight calibration and with no significant changes to model formulations, are able to predict seasonal evolution of water temperature profiles with reasonable accuracy.

It has already been shown that for shallower lakes [e.g., Pyramid Lake (100 m), Yellowstone Lake (98 m), and Sparkling Lake (20 m) in the United States], HLM and FLake accurately predicted temperature profiles (Hostetler and Bartlein 1990; Hostetler and Giorgi 1995; A. Martynov unpubl.). However, at Lake Geneva's deep station (SHL2), it appears that HLM and FLake limitations have been reached in terms of simulating thickness and seasonal deepening of the thermocline. Consequently their temperature profiles are not well reproduced. On the one hand, the FLake model tends to generate too strong a mixing and the HLM simulates too weak a mixing that consequently affects the timing and position of the thermocline. As both momentum and heat are similarly exchanged at the air-lake interface, the discrepancies in the intensity of the mixing are probably due to internal structure and processes involved in each model. The onset of stratification, earlier in HLM than in the other models, is related to a thermocline that hardly deepens and with a largely underestimated MIB. Once the threshold of maximum increase of eddy-diffusion coefficient is reached, the values then level off with increasing wind speed. After inaccurate reproduction of the mixedlayer depth with a similar eddy diffusion model, McCormick and Meadows (1988) had already identify such a problem. It appears that the seiche parameterization is a missing fundamental process that should increase the actual value of eddy-diffusion coefficients in highly stratified layers and improve the prediction of heat penetration in deeper layers. In order to explain the disagreements between observations and FLake simulations, one should remember that physical processes, such as heat diffusion, are not explicitly evoked in this model; instead they are based on self-similarity concepts of the temperature-depth curve. However, the virtual bottom of the FLake model may be the primary source of error and a limiting factor for application to lakes where the annual variability is still important at 60 m depth. The model simulates excessive cooling in winter as heat lost is concentrated in a reduced volume that enables complete overturn. A good representation of the profiles during the cold period is essential as those produced before stratification determine the future evolution of the thermocline. Furthermore, the observed thermocline in spring often develops close to the surface with a steeper slope in shallow water. Such a curve cannot be reproduced in FLake since the thermocline is located between the lower limit of the mixed layer and the bottom of the lake. This definition of the thermocline may, on such occasions, be detrimental to development of future temperature profiles. On the other hand, the surface temperature predictions of HLM, with an annual $T_{\rm me}$ of the order of -0.1 ± 1.1 °C and in $D_{0.5}$ of 0.08 ± 1.25 °C, are remarkable.

This model intercomparison shows that DYRESM and SIMSTRAT are capable of reproducing multiple aspects of the evolution of water temperature profiles at station SHL2. The best agreement between predicted and observed data is at the surface and in $D_{0.5}$. Accurate results are also found in layers between 5 and 50 m, with slightly better agreement for SIMSTRAT. The main challenge for the models lies in the D_{5-10} and the D_{10-15} layers in order to correctly simulate the location and the slope of the seasonal thermocline. Even minor disagreements in the deepening of the thermocline in summer may generate large $T_{\rm rmse}$. Compared to HLM and FLake, both DYRESM and SIMSTRAT have the advantage of parameterizing certain three-dimensional processes such as seiching effects on mixing, and may explain the accurate prediction of the simulated profiles. Nevertheless, due to intrinsic inability of one-dimensional models to reproduce physically all processes in lakes,

displacements of the thermocline during such seiching events are not accurately resolved. Soundings taken during or soon after those events may increase the temperature variability, thereby affecting $T_{\rm rmse}$. Due to the poor temporal resolution of the water temperature soundings, pronounced thermocline displacements are, however, rarely observed, and systematic offsets cannot be identified. However, while $T_{\rm rmse}$ of both the DYRESM and SIMSTRAT models reproduced similar temperature profiles from quasi vertical isothermal conditions until the beginning of summer, SIMSTRAT performed better (Fig. 1.7 g-i) during the period of strongest stratification (< 2°C for SIMSTRAT, < 3°C for DYRESM in D_{5-10} and D_{10-15}).

Overestimation of temperature in D_{5-15} and its underestimation below as well as the lack of seasonal variability of the MLB simulated by DYRESM indicate insufficient heat below the thermocline. Similar hypolimnion temperature predictions were simulated in a number of lakes with a combination of hypotheses to explain those differences, primarily ensuing from field data or model structure (Romero and Melack 1996; Rutherford et al. 1996; Copetti et al. 2006). As also shown in Tanentzap et al. (2007), the calibration does not enable one to identify a particular mixing parameter that would systematically reduce the error. The enhanced surface mixed-layer algorithm and the new deep-mixing algorithms implemented in DYRESM improved predictions of the thermal structure of various lakes (Yeates and Imberger 2003). Additionally, the new version has reduced disagreement between observed and simulated data in the hypolimnia of some of those lakes (Gal et al. 2003; Yeates and Imberger 2003). However, the underestimated variability of temperatures exhibited in the lower metalimnion and hypolimnion show that the parameterization of internal mixing might not yet be appropriate for Lake Geneva. Despite a similar 240 m depth, simulation with DYRESM over Lake Ontario produced lower surface temperature and a deeper thermocline (Boyce et al. 1993). It is difficult to assume in this study that the constant K_e may be responsible for the temperature errors throughout the year and water depth (Gal et al. 2003; Tanentzap et al. 2007). While the sensitivity analysis did not affect the performance of the model, temporal agreement between profiles differed depending on the value of $K_{\rm e}$. This result emphasizes the need to account for seasonal effects of light penetration induced by changing phytoplankton populations.

Due to the higher heat diffusion in the D_{15-50} and D_{50-100} layers, SIMSTRAT is the only model that significantly accounts for seasonal deep hypolimnion temperature variations. Despite the accurate correlation in the upper layers, the smoothed hypolimnetic seasonal temperature cycles predicted by DYRESM may cause an issue over multi-year simulations. Insufficient heat storage with depth may increase discrepancies in the water column over the years and eventually change the extent of the dynamic processes as the lake does not overturn regularly, and so temperature through the column may not be homogenized each winter.

It has been shown above that a one-dimensional lake model can be used to simulate thermal profiles at SHL2 providing that some adjustments are made that influence heat diffusion. The sensitivity of the models to variable or wind-speed dependent $c_{\rm D}$ has been tested, and lower $T_{\rm rmse}$ between observed and simulated profiles were found when $c_{\rm D}$ is higher than the constant default value or accounts for wind speed. Similarly, a seiching parameterization reduces the $T_{\rm rmse}$ as heat diffusion does not cease in highly stratified layers. The scaling of the wind speed at the land station has proven beneficial for simulation of the thermal profile, since it better represents conditions over the lake at station SHL2.

This is the first time that several one-dimensional models, with common external driving variables and common heat flux parameterizations, have been compared in order to assess their capacity in reproducing temperature profiles in the deep domain of Lake Geneva (station SHL2). Owing to inclusion of detailed physics, SIMSTRAT and DYRESM perform better at this particular location. Based on these rather encouraging results, the use of lake models to investigate other aspects of Lake Geneva in a changing climate clearly becomes possible. Issues that need to be addressed concern the temperature increases related to enhanced atmospheric CO₂ concentrations over a much longer period than that investigated

here, where the thermal response of the lake will be investigated numerically in terms of the amount of heat stored over a century time scale. Initial experiments conducted on deep Swiss lakes have shown the significant effect of a temperature increase on the entire column and the need to use a continuous modelling approach for lakes that do not freeze each year. Typically, heat is stored in the hypolimnion and accumulates year after year (Peeters *et al.* 2002) within lakes, which are rarely dimictic, especially those that are deep.

If, as shown in this paper, models are capable of adequately simulating the timing of the onset of stratification, the thickness of the metalimnion, and the maximum stability of the thermocline, then there is room for further studies involving, for example, coupled physical and biological models. Such coupled model experiments can help understand changes in biogeochemical processes under shifting conditions of lake temperature and stratification. Such changes could have an effect on the proliferation of toxic algae and other aquatic pathogens, that could ultimately result in a reduction of water quality and possibly to problems of public health. However, even though DYRESM and SIMSTRAT have shown genuine skill in simulating temperature profiles down to deep layers, the lake model required for biological applications needs to perform accurately through the whole water column as it may affect the performance of coupled biochemical models. DYRESM discrepancies in the bottom layer may not only potentially neglect inter-annual temperature variations, but also alter the biological and chemical properties in the upper layers. Furthermore, one should keep in mind that the models presented here do not consider all mixing processes observed in the lakes and limits may therefore be reached. The Rhone River underflows (Loizeau and Dominik 2000) or cascades of cold water due to rapid cooling from the shallow Petit Lac or shallow lake areas in winter (Fer et al. 2002) are, for instance, not considered. By omitting deep winter convection related to these intrusions, oxygen supply to the deep water could be underestimated and phosphorus release overestimated, with effects on biogeochemical processes. The results presented in this paper suggest that models can today be used for applications beyond solely physical-process investigations; they are now in a position to attempt effects-oriented modeling for issues such as water quality in a changing climate.

1.6 Acknowledgments

We are grateful to S. W. Hostetler from the US Geological Survey, the Centre for Water Research (CWR), the Swiss Federal Institute of Aquatic Science and Technology (EAWAG), in particular M. Schmidt and D. Mironov from the German Weather Service (DWD) for providing us the lake models and technical support. We are thankful to the French 'Station d'Hydrobiologie Lacustre' of Lake Geneva (managed by the French National Institute for Agricultural Research, INRA) for collecting water temperature profiles at station SHL2 over the period 1996-2005 and to make these available for the purpose of this study. We would like to thank particularly S. Jacquet for his scientific remarks and advice, and his efforts to make the collaboration possible between our two institutes. We also thank the reviewers for their helpful suggestions made on this manuscript. Their comments were particularly valuable and enhanced the quality of the text.

1.7 Appendix

Appendix 1.1. Governing equations of Hostetler model (Hostetler and Bartlein 1990)

$$\frac{\partial T}{\partial t} = \frac{1}{A(z)} \frac{\partial}{\partial z} \left\{ A(z) \left[\kappa_m + K(z,t) \right] \frac{\partial T}{\partial z} \right\} + \frac{1}{A(z)} \frac{1}{C_w} \frac{\partial \left[\Phi A(z) \right]}{\partial z}$$

$$K(z,t) = \frac{v_k u \cdot z}{P_o} e^{(-k^* z)} (1 + 37 Ri^2)^{-1}$$

$$u^{\star} = \sqrt{\frac{\rho_a}{\rho_o} c_D v^2}$$

Definitions:

A(z) lake area at depth z (m²)

 c_D drag coefficient

 C_w volumetric heat capacity of water (J m⁻³ °C⁻¹)

K(z, t) eddy diffusivity, (m² s⁻¹)

 k^* Latitudinally dependent parameter of the Ekman profile

 P_o neutral value of the turbulent Prandtl number (1.0)

t time (s)

Ri Richardson number

T water temperature (°C)

v wind speed 2 m above the water surface

 U_* surface friction velocity (m s⁻¹)

 v_k von Karman constant (0.4)

z depth from the surface (m)

 κ_m molecular diffusion of water, (m² s⁻¹)

 ρ_o density of lake surface (kg m⁻³)

 ρ_a air density (kg m⁻³)

 Φ heat source term (W m⁻²)

Appendix 1.2. Governing processes and equations of the DYRESM model (Yeates and Imberger 2003)

Surface mixed layer

$$KE_{conv} = \eta_{p} \rho_{j} A_{j-1} \omega^{3} \Delta t$$

$$KE_{stir} = \eta_{s} \rho_{j} A_{j} u^{3} \Delta t$$

$$KE_{shear} = \frac{\eta_{k}}{2} \frac{M_{j} M_{j-1}}{M_{j} + M_{j-1}} (U_{j} - U_{j-1})^{2}$$

$$U^{*} = \sqrt{\frac{\rho_{a}}{\rho_{o}}} c_{D} v^{2}$$

$$PE_{mix} = g \{ (M_{j} + M_{j-1}) \zeta_{j-1}^{*} - (M_{j} \zeta_{j} + M_{j-1} \zeta_{j-1}) \}$$

Deep mixing

$$F_{i}^{T} = \frac{200 N_{i}^{2} A_{i} K_{m} \Delta t}{L_{N} N_{\text{max}}^{2} \left(\frac{\delta_{i} + \delta_{i+1}}{2}\right)}$$

$$F_{i}^{I} = \begin{cases} \frac{F_{i}^{T} \tanh(B_{N})(L_{N} - 1)}{L_{N}} L_{N} > 1 \\ 0 & \text{otherwise} \end{cases} \text{ and } F_{i}^{B} = F_{i}^{T} - F_{i}^{I}$$

Definitions

 A_i surface area of layer j (m²)

 A_i surface area of layer *i* below the surface mixed layer (m²)

 B_N Burger number

 C_D surface drag coefficient

 δ_i thickness of layer *i* below the surface mixed layer (m)

 F_i^B benthic boundary layer volume exchange (m³)

*F*¹ internal volume exchange (m³)

 F_i^T total volume exchange between two layers (m³)

g acceleration due to gravity (m s⁻²)

 κ_m molecular diffusion coefficient for heat (m² s⁻¹)

KE_{conv} turbulent kinetic energy due to convective mixing (kg m² s⁻²)

 KE_{stir} turbulent kinetic energy due to wind stirring (kg m² s⁻²)

KE_{shear} turbulent kinetic energy due to shear mixing (kg m² s⁻²)

 L_N lake number

 M_j mass of layer j (kg)

j surface layer index

 N^2 square of buoyancy frequency (s⁻²)

```
maximum buoyancy frequency squared in a 'portable Flux Profiler' profile (s<sup>-2</sup>)
N_{\text{max}}^2
           potential energy to mix layers D and D-1 (kg m<sup>2</sup> s<sup>-2</sup>)
PE_{mix}
           speed of layer j (m s<sup>-1</sup>)
U_i
           surface friction velocity (m s<sup>-1</sup>)
И×
           wind speed at height H above the lake surface (m s<sup>-1</sup>)
V_H
           model time step (s)
\Delta t
           efficiency coefficient associated to the TKE due to shear mixing
\eta_k
           efficiency coefficient associated to the TKE due to convective mixing
\eta_p
           efficiency coefficient associated to the TKE due to wind stirring
\eta_s
           air density (kg m<sup>-3</sup>)
\rho_a
           water density at layer i (kg m<sup>-3</sup>)
\rho_i
           density of lake surface (kg m<sup>-3</sup>)
\rho_o
           turbulent velocity scale due to convective overturn (m s<sup>-1</sup>)
ω×
           center of mass of layer j before mixing (m)
\zeta_i
           center of mass of layer j after mixing (m)
5*,
```

This model is based on a Lagrangian layer scheme in which the lake is modelled by a series of horizontal layers of uniform property but variable thickness. Mixing is represented by the amalgamation of layers. Properties of the amalgamated layer are volumetrically averaged. When combining two layers, say j and j+1, the conservation laws for a given property noted C in layer i such as water temperature, T, salt, S, and momentum, U, can be generalised as:

$$C_j^* = \frac{C_j \Delta M_j + C_{j+1} \Delta M_{j+1}}{\Delta M_j + \Delta M_{j+1}}$$

where ΔM is the change of water mass in layer j and j+1. While this framework remained essentially unchanged, this later version of DYRESM includes a pseudo two-dimensional benthic boundary layer structure as described above.

Appendix 1.3. Governing equations of the k- ε model and extensions included in SIMSTRAT (Goudsmit *et al.* 2002)

$$\frac{\partial T}{\partial t} = \frac{1}{A} \frac{\partial}{\partial z} \left(A(v_t + \kappa_m) \frac{\partial T}{\partial z} \right) + \frac{1}{\rho_t c_\rho} \frac{\partial H_{sol}}{\partial z} + \frac{\partial}{\partial z} \frac{A}{A \rho_t c_\rho}$$

$$\frac{\partial U_u}{\partial t} = \frac{1}{A} \frac{\partial}{\partial z} \left(A(v_t + v) \frac{\partial U_u}{\partial z} \right) + f U_v$$

$$\frac{\partial U_v}{\partial t} = \frac{1}{A} \frac{\partial}{\partial z} \left(A(v_t + v) \frac{\partial U_v}{\partial z} \right) - f U_u$$

$$\frac{\partial k}{\partial t} = \frac{1}{A} \frac{\partial}{\partial z} \left(Av_k \frac{\partial k}{\partial z} \right) + P + P_{seiche} + B - \varepsilon$$

$$\frac{\partial \varepsilon}{\partial t} = \frac{1}{A} \frac{\partial}{\partial z} \left(Av_k \frac{\partial \varepsilon}{\partial z} \right) + \frac{\varepsilon}{k} \left[c_{\varepsilon 1} (P + P_{seiche}) + c_{\varepsilon 3} B - c_{\varepsilon 2} \varepsilon \right]$$

$$P = v_t \left[\left(\frac{\partial U_v}{\partial z} \right)^2 + \left(\frac{\partial U_v}{\partial z} \right)^2 \right] \qquad B = -v_t N^2$$

$$v_t = c_\mu \frac{k^2}{\varepsilon}$$

$$v_t = c_\mu \frac{k^2}{\varepsilon}$$

$$v_t = \frac{c_\mu k^2}{\sigma_k \varepsilon}$$

$$v_\varepsilon = \frac{c_\mu k^2}{\sigma_\varepsilon \varepsilon}$$

$$v_\varepsilon = \frac{c_\mu k^2}{\sigma_\varepsilon \varepsilon}$$

Constant of the k- ε model:

 $c_{\mathcal{E}l}$ 1.44

 $c_{\mathcal{E}2}$ 1.92

 $c_{\mathcal{E}3}$ -0.4 if B < 0, else 1

 c_{μ} 0.09

 c'_{μ} 0.072

 σ_k 1.00

 $\sigma_{\mathcal{E}}$ 1.3

Definitions:

A cross sectional area at z (m²)

B buoyancy flux (W kg¹) c_p specific heat of lake water (J kg¹ K⁻¹) c_D surface drag coefficient f Coriolis parameter (s¹¹) t time (s) k turbulent kinetic energy per unit of mass (J kg¹¹) H_{sol} solar radiation at depth z (W m²²)

H_{geo}	geothermal heat flux (W m ⁻²)
N	brunt-Väisälä frequency (s ⁻¹)
Т	water temperature (°C)
V_{U}	horizontal air velocity west-east (m s ⁻¹)
U_u	horizontal velocity west-east (m s ⁻¹)
V_{V}	horizontal air velocity south-north (m s ⁻¹)
U_{v}	horizontal velocity south-north (m s ⁻¹)
P	production of <i>k</i> due to shear stress (W kg ⁻¹)
P _{seiche}	production of <i>k</i> due to internal seiching (W kg ⁻¹)
Z	depth (positive upward) (m)
ε	dissipation rate of k (W kg ⁻¹)
$ ho_a$	air density (kg m ⁻³)
$ ho_r$	reference density of lake water (kg m ⁻³)
$ ho_o$	density of lake surface (kg m ⁻³)
τ	surface wind stress (m ² s ⁻²)
v	molecular viscosity, 1.5 x 10 ⁻⁶ m ² s ⁻¹
K_m	molecular diffusivity, 1.5 x 10 ⁻⁷ m ² s ⁻¹
v_t	turbulent viscosity (m ² s ⁻¹)
\mathbf{v}_t'	turbulent diffusivity (m ² s ⁻¹)
$V_{arepsilon}$	turbulent diffusivity of ε (m ² s ⁻¹)
V_k	turbulent diffusivity of $k \text{ (m}^2 \text{ s}^{-1})$

Appendix 1.4. Governing equations of Flake model (Mironov 2008)

The shape of the water temperature profile is prescribed: the self-consistent profiles, described by the universal non-dimensional functions Φ are used.

$$T(z) = \begin{cases} T_{surf} & 0 \le z \le h \\ T_{surf} - (T_{surf} - T_{bot}) \Phi_{T}(\zeta) & h \le z \le D \end{cases}$$

$$\Phi_{\tau}(\zeta) = \left(\frac{40}{3}C_{\tau} - \frac{20}{3}\right)\zeta + \left(18 - 30C_{\tau}\right)\zeta^{2} + \left(20C_{\tau} - 12\right)\zeta^{3} + \left(\frac{5}{3} - \frac{10}{3}C_{\tau}\right)\zeta^{4}$$

$$z - h$$

$$\zeta = \frac{z - h}{D - h}$$

$$u = \sqrt{\frac{\rho_a}{\rho_o} c_D v^2}$$

Definitions

 c_D drag coefficient

 C_T shape parameter

h mixed-layer depth (m)

T water temperature (°C)

 T_{surf} surface water temperature (°C)

 T_{bot} bottom water temperature (°C)

v wind speed 2 m above the water surface

z depth (m)

 u_* surface friction velocity (m s⁻¹)

 ρ_a air density (kg m⁻³)

 ρ_o density of lake surface (kg m⁻³)

Other characteristics

D = virtual bottom at 60 m

1.8 References

- Anneville, O., S. Souissi, F. Ibanez, V. Ginot, J. C. Druart, and N. Angeli. 2002. Temporal mapping of phytoplankton assemblages in Lake Geneva: Annual and interannual changes in their patterns of succession. Limnol. Oceanogr. 47: 1355-1366.
- Anneville, O., S. Souissi, S. Gammeter, and D. Straile. 2004. Seasonal and inter-annual scales of variability in phytoplankton assemblages: comparaison of phytoplankton dynamics in three peri-alpine lakes over a period of 28 years. Freshw. Biol. 49: 98-115.
- Bantle, H. 1989. Programm Documentation for Climatic-Database at RZ-ETH Zürich. MeteoSwiss Publication. (written in German)
- Bettems, J. M. 2002. EUCOS Impact study using the limited-area non-hydrostatic NWP model in operational use at MeteoSwiss. COSMO, Tech. Rep. 5.
- Bonan, G. D. 1996. A land surface model (LSM version 1.0) for ecological, hydrological, and atmospheric studies. Technical description and user's guide. NCAR Technical Note NCAR/TN-417+STR, National Center for Atmospheric Research, Boulder.
- Boyce, F. M., P. F. Hamblin, L. D. Harvey, W. M. Schertzer, and R. C. McCrimmon. 1993. Response of the thermal structure of Lake Ontario to deep cooling water withdrawals and to global warming. Journal of Great Lakes Research 19: 603-616.
- Bradley, E., P. Coppin, and J. Godfrey. 1991. Measurements of sensible and latent heat flux in the western equatorial Pacific ocean. J. Geophys. Res. 96: 3375-89.
- Burchard, H., and H. Baumert. 1995. On the performance of a mixed layer model based on the k-ε turbulence closure. J. Geophys. Res. 100: 8523-8540.
- Burchard, H., O. Petersen, and T. P. Rippeth. 1998. Comparing the performance of the Mellor-Yamada and the κ - ϵ two-equation turbulence models. J. Geophys. Res. 103: 10543-10554.
- Bührer, H., and H. Ambühl. 1975. The discharge of treated waste water into lakes. Schweiz. Z. Hydrol. 37: 347-369. (written in German)
- Capblancq, J. 1995. Autotroph primary production, p. 228-252. *In* R. Pourriot and M. Meybeck [eds.], General limnology. Masson. (written in French)
- Charnock, H. 1955. Wind stress on a water surface, Q. J. R. Meteorol. Soc. 81: 639–640.
- Copetti, D., G. Tartari, G. Morabito, A. Oggioni, E. Legnani, and J. Imberger. 2006. A biogeochemical model of lake Pusiano (North Italy) and its use in the predictability of phytoplankton blooms: first preliminary results. J. Limnol. 65: 59-64.
- Dake, J. M. K., and D. R. F. Harleman. 1969. Thermal stratification in lakes analytical and laboratory studies. Water Resour. Res. 5: 484-495.
- Fer, I., U. Lemmin, and S. A. Thorpe. 2002. Winter cascading of cold water in Lake Geneva. J. Geophys. Res. 107: 2236–2569.
- Gal, G., J. Imberger, T. Zohary, J. Antenucci, A. Anis, and T. Rosenberg. 2003. Simulating the thermal dynamics of Lake Kinneret. Ecol. Modell. 162: 69-86.

- Geernaert, G. L., S. E. Larsen, and F. Hansen. 1987. Measurements of the wind stress, heat flux, and turbulence intensity during storm conditions over the North Sea. J. Geophys. Res. 92: 13127-13139.
- Gerten, D., and R. Adrian. 2000. Climate-driven changes in spring phytoplankton dynamics and the sensitivity of shallow polymictic lakes to the North Atlantic Oscillation. Limnol. Oceanogr. 45: 1058-1066.
- Graf, W. H., N. Merzi, and C. Perrinjaquet. 1984. Aerodynamic drag: Measured at a nearshore platform on Lake Geneva. Arch. Meteor. Geophys. and Bioclim. 33: 151-173.
- Goudsmit, G.-H., H. Burchard, F. Peeters, and A. Wüest. 2002. Application of k-ε turbulence models to enclosed basins: The role of internal seiches, J. Geophys. Res. 107: 3230-3243, doi:10.1029/2001JC000954.
- Hamilton, D. P., and S. G. Schladow. 1997. Prediction of water quality in lakes and reservoirs: Part I Model description. Ecol. Modell. 96: 91–110, doi:10.1016/S0304-3800(96)00062-2.
- Henderson-Sellers, B., M. J. McCormick, and D. Scavia. 1983. A comparison of the formulation for eddy diffusion in two one-dimensional stratification models. Appl. Math. Model. 7: 212-215.
- Henderson-Sellers, B. 1985. New formulation of eddy diffusion thermocline models. Appl. Math. Model. 9: 441-446.
- Henderson-Sellers, B. 1986. Calculating the surface energy balance for lake and reservoir modeling: A review. Rev. Geophys. 24: 625-649.
- Hornung, R. 2002. Numerical modelling of stratification in Lake Constance with the 1-D hydrodynamic model DYRESM. M.S. thesis. Univ. of Stuttgart.
- Hostetler, S.W. 1987. Simulation of lake evaporation with an energy balance-eddy diffusion model of lake temperature: model development and validation, and application to lake-level variations at Harney-Malheur Lake. Ph.D. thesis. Univ. of Oregon.
- Hostetler, S. W., and P. J. Bartlein. 1990. Simulation of lake evaporation with application to modelling lake-level variations at Harney-Malheur Lake, Oregon, Water Resour. Res. 26: 2603–2612.
- Hostetler, S. W., and F. Giorgi. 1995. Effects of a 2 x CO2 climate on two large lake systems: Pyramid Lake, Nevada, and Yellowstone Lake, Wyoming. Glob. And Plan. Change 10:43-54.
- Imberger, J., J. C. Patterson, B. Hebbert, and I. Loh. 1978. Dynamics of reservoir of medium size. J. Fluid Mech. 78: 489-512.
- Imberger, J., and J. C. Patterson. 1981. A dynamic reservoir simulation model: DYRESM5, p. 310-361. *In* H. B. Fischer [ed.], Transport models for inland and coastal waters, Academic Press.
- Jacquet, S., J. F. Briand, C. Leboulanger, L. Oberhaus, G. Paolini, J. C. Druart, O. Anneville, and J. F. Humbert. 2005. The proliferation of the toxic cyanobacterium *Planktothrix rubescens* following restoration of the largest natural French lake (Lake Bourget). Harmful Algae 4: 651-672.

- Jöhnk, K., J. Huisman, J. Sharples, B. Sommeijer, P. Visser, and J. Stroom. 2008. Summer heatwaves promote blooms of harmful cyanobacteria. Glob. Change Biol. 14: 495-512.
- Kitaigorodskii, S. A., and Y. Z. Miropolsky, 1970. On the theory of the open ocean active layer. Izv. Akad. Nauk SSSR. Fizika Atmosfery i Okeana 6: 178-188.
- King, J. R., B. J. Shuter, and A. P. Zimmerman. 1997. The response of the thermal stratification of South Bay (Lake Huron) to climatic variability. Can. J. Fish. Aquat. Sci. 54: 1873–1882.
- Kraus, E. B., and J. S. Turner. 1967. A one dimensional model of the seasonal thermocline: II. The general theory of its consequences. Tellus. 19: 98-106.
- Lazzarotto, J., P. Nirel, and F. Rapin. 2006. Physical-chemical changes in the waters of Lake Geneva, p. 31-63. *In* CIPEL [eds.], Report of the international commission for the protection of the waters of lake Geneva against pollution, Campaign 2005. (written in French)
- Lazzarotto, J., and F. Rapin. 2007. Physical-chemical changes in the waters of Lake Geneva, p. 33-57. *In* CIPEL [eds.], Report of the international commission for the protection of the waters of lake Geneva against pollution, Campaign 2006. (written in French)
- Lin, W., L. P. Sanford, S. E. Suttles, and R. A. Valigura, 2002: Drag coefficients with fetch limited wind waves. J. Phys. Oceanogr. 32: 3058–3074.
- Legnani, E., D. Copetti., A. Oggioni, G. Tartari., M. T. Palumbo, and G. Morabito. 2005. Planktothrix rubescens'seasonal dynamics and vertical distribution in Lake Pusiano (North Italy). J. Limnol. 64: 61-73.
- Lemmin, U., and N. D'Adamo. 1996. Summertime winds and direct cyclonic circulation: Observations from Lake Geneva. Ann. Geophys. 14: 1207–1220.
- Loizeau, J.-L., and J. Dominik. 2000. Evolution of the Rhone river discharge during the last 80 years and some implications for Lake Geneva. Aquat. Sci. 62: 54-67.
- McCormick, M. J., and G. A. Meadows. 1988. An intercomparison of four mixed layer models in a shallow inland sea. J. Geophy. Res. 93: 6774-6788.
- McCormick, M. J., and G. L. Fahnenstiel. 1999. Recent climatic trends in nearshore water temperatures in the St. Lawrence Great Lakes. Limnol. Oceanogr. 44: 530-540.
- Mironov, D. V. 2008. Parameterization of lakes in numerical weather prediction. Description of a lake model. COSMO Technical Report 11. Deutscher Wetterdienst.
- Orlob, G. T., and L. G. Selna. 1970. Temperature variations in deep reservoirs. J. Hydraul. Div. Proc. 96: 393-410.
- Peeters, F., D. M. Livingstone, G. Goudsmit, R. Kipfer, and R. Forster. 2002. Modeling 50 years of historical temperature profiles in a large central European lake. Limnol. Oceanogr. 47: 186-197.
- Peeters, F., D. Straile, A. Lorke, and D. M. Livingstone. 2007. Earlier onset of the spring phytoplankton bloom in lakes of the temperate zone in a warmer climate. Glob. Change Biol. 13: 1898-1909.

- Richards, J. M. 1971. Simple expressions for the saturation vapor pressure of water in the range −50 to 140 °C. Brit. J. Appl. Phys. 4: L15–L18.
- Rodi, W. 1984. Turbulence models and their application in hydrodynamics a state of the art review, 2nd Int. Assoc. Hydraul. Res.
- Romero, J. R., J. P. Antenucci, and J. Imberger. 2004. One- and three- dimensional biogeochemical simulations of two differing reservoirs. Ecol. Modell. 174: 143–160.
- Rutherford, J. C., S. M. Dumnov, and A. H. Ross. 1996. Predictions of phosphorus in Lake Rotorua following load reductions. N. Z. J. Mar. Freshwat. Res. 30: 383-396.
- SAEFL, Swiss Agency for the Environment, Forests and Landscape. 1994. The state of lakes in Switzerland, Cahier de l'environnement 237. (written in French)
- Shatwell, T., J. Köhler, and A. Nicklisch. 2008. Warming promotes cold-adapted phytoplankton in temperate lakes and opens a loophole for Oscillatoriales in spring. Glob. Change Biol. 14: 1-7.
- Smith, S. D., R. J. Anderson, W. A. Oost, C. Kraan, N. Maat, J. DeCosmo, K. B. Katsaros, K. L. Davidson, K. Bumke, L. Hasse, and H. M. Chadwick. 1992. Sea surface wind stress and drag coefficients: the HEXOS results. Bound.-Layer Meteorol. 60: 109-142.
- Straile, D., D. M. Livingstone, G. A. Weyhenmeyer, and D. G. George. 2003. The response of freshwater ecosystems to climate variability associated with the North Atlantic Oscillation, p. 263–279. *In J. W. Hurrell, Y. Kushnir, G. Ottersen and M. Visbeck, [eds.], The North Atlantic Oscillation: Climatic significance and environmental impact. AGU Geophysical Monograph Series 134.*
- SVGW. 2008. Swiss company of water and gas industry. Information on drinking water. TWI 12. (written in German)
- Tanentzap, A. J., D. P. Hamilton, and N. D. Yan. 2007. Calibrating the dynamic reservoir simulation model (DYRESM) and filling required data gaps for 1-dimensional thermal profile predictions in a boreal lake. Limnol. Oceanogr. Meth. 5: 484-494.
- Umlauf, L., and U. Lemmin. 2005. Interbasin exchange and mixing in the hypolimnion of a large lake: The role of long internal waves. Limnol. Oceanogr. 50: 1601-1611.
- Unesco. 1981. The practical salinity scale 1978 and the international equation of state of seawater 1980. Tenth Report of the Joint Panel on Oceanographid Tables and Standards. Unesco Techn. Pap. in Mar. Sci. Unesco. Division of Marine Sciences.
- Walsby, A. E., and F. Schanz. 2002. Light-dependent growth rate determines changes in the population of Planktothrix rubescens over the annual cycle in Lake Zürich, Switzerland. New Phytol. 154: 671-687.
- Wüest, A., and A. Lorke. 2003. Small-scale hydrodynamics in lakes. Annu. Rev. Fluid Mech. 35: 373-412.
- Wüest, A., G. Piepke, and J. D. Halfman. 1996. Combined effects of dissolved solids and temperature on the density stratification of Lake Malawi, p. 183-202. *In* T. C. Johnson and E. O. Oada [eds.], The limnology, climatology and paleoclimatology of the East African Lakes. Gordon and Breach.

Yeates, P. S., and J. Imberger. 2003. Pseudo two-dimensional simulations of internal and boundary fluxes in stratified lakes and reservoirs. Intl. J. River Basin Management 1: 279-319.

Chapter 2

Impacts of a warmer climate on Lake Geneva water temperature profiles

Marjorie Perroud and Stéphane Goyette

Climatic Change and Climate Impacts (C³I), University of Geneva, Carouge, Geneva, Switzerland

Abstract

The impact of climate warming caused by the increase of greenhouse gases in the atmosphere on the thermal profiles of Lake Geneva, Switzerland, is investigated using a k- ε turbulence lake model. To assess the thermal response of this lake, two sets of 130-year time series of hourly meteorological variables are used to drive the lake model. In the control simulation, the lake model is driven by a series representative of the period 1981 - 1990, and in the perturbed experiment, deltas derived from outputs of the HIRHAM Regional Climate Model run under the IPCC A2 scenario in the framework of the 5th EU programme PRUDENCE, have been used. Changes in the lake water temperature profiles indicate an increase in monthly epilimnic and hypolimnic temperatures of 2.32 °C to 3.8 °C and 2.2 °C to 2.33 °C respectively. The warming of epilimnic temperatures correspond to 55 - 98% of the monthly increase in air temperature. The stratification period lasts longer and the lake stability increases. Thus the lake is likely to retain its mixing regime, but this will be of shorter duration.

Published in: Boreal Env. Res., 15, 2010

2.1 Introduction

The mean global surface warming of the earth caused by the increase of greenhouse gas (GHG) concentrations over the 20th century (0.74°C from 1906 to 2005, IPCC 2007) has induced a wide-range of impacts in many parts of the world (Alcamo *et al.* 2007). In lakes, thermal response to recent atmospheric warming reveals that the first signs of change are already observed in many regions. Most studies agree on an increase in the temperature of surface waters, and sometimes also at the bottom of lakes. In all cases, the temperature increase is observed to be higher in the epilimnion than in the hypolimnion; there is currently an earlier onset and strengthening of the summer stratification, and a shorter duration of ice cover during the freezing season (Robertson and Ragotzkie 1990; Schindler *et al.* 1996; King *et al.* 1997; McCormick and Fahnenstiel 1999; Peeters *et al.* 2002; Livingston 2003).

GHG emissions are likely to increase at an accelerating rate in coming decades with stronger impacts that up till now (IPCC 2007). Estimates of warming vary largely due to the GHG emissions scenario (cf. SRES - the Special Report on Emission Scenarios; Nakicenovic *et al.* 2000) as well as to the climate model used. In Europe for instance, models project an increase of 1 - 4°C for the SRES B2 scenario and 2.5 - 5.5°C for the A2 scenario in the 2070 - 2099 timeframe compared to the baseline, or "current", (1961 - 1990) climate (Alcamo *et al.* 2007). An increase in mean global temperature of 1.5 to 2.5°C may also induce changes in ecosystem structure and function, ecological interactions between species and their geographical ranges, often with negative consequence for biodiversity and ecosystems (Fischlin *et al.* 2007). Impacts of a warmer climate on the thermal evolution of lakes and therefore on organisms dependent on water temperature thus need to be investigated.

In this study, particular attention has been devoted to Lake Geneva, a warm and deep monomictic lake in which effects of warmer meteorological conditions have recently been observed (Lazzarotto *et al.* 2004; Dokulil *et al.* 2006). Since the early 1970s, an increase of more than 1°C in the annual mean surface temperature has been monitored, as shown at a depth of 5 m (Lazzarotto *et al.* 2004). In addition, bottom temperatures increased progressively from the 4.5°C measured in 1960s to the maximum 5.98°C measured in 2002. The occurrence of occasional cold winters has served to cool bottom temperatures, but these have never reverted to the values observed in the 1960s. Other studies also highlight indirect effects of changes due to warming trend notably on phytoplanktonic community composition (Anneville *et al.* 2005) and on fish communities (Gerdeaux 2004; Gillet and Quétin 2006).

With the purpose of examining the thermal evolution of Lake Geneva on the long term, a k- ε one-dimensional numerical lake model, called SIMSTRAT (Goudsmit et~al.~2002), has been chosen to simulate water temperature profiles of this large lake. To explore how Lake Geneva might be affected by changes in current and future climate conditions, meteorological data used to drive the model have been perturbed using the outputs of the HIRHAM regional climate model (RCM), described in Christensen et~al.~(1998). A method, referred to as the decile method, based on the difference in the distribution of meteorological variables between current and future periods will be presented. This latter is broadly similar to previous methods in that meteorological data are modified according to differences between future and current climates simulated by global circulation models (GCM) or by RCMs. However, the method differs in the manner by which perturbations are segmented (according to the deciles from a distribution, i.e. at each 10% increment of the probability distribution function) instead rather than using just the average temperature difference.

The response of a deep warm monomictic lake to expected changes in weather conditions needs to be analysed on the long term, especially when deep mixing does not cool deeper layers on regular time intervals. Indeed, the heat transported downward and stored over several years is a determinant for bottom temperatures (Coats 2006). For such water bodies, a long historical meteorological dataset is useful to study the trend in deep waters when daily variability is taken into account (Peeters *et al.* 2002). Unfortunately, long time series tend to

be rare and thus strategies for running long-term simulations need to be developed. For Lake Geneva, hourly meteorological data required to run the lake model have been collected for the past 30 years, but only ten years (1981 - 1990) cover the period prior to the intense warming trend of the past 20 years. A meteorological data generator in which variable distributions match the observations has thus been developed that allows running numerical simulations over several decades. This generator is designed to reproduce the mean and variability of the current meteorological conditions. The simulated water temperature profiles, when the SIMSTRAT lake model is driven by meteorological observations, are validated against observed profiles. Next, the weather generator is used to produce a series of pseudo-random data that will serve to drive a long simulation representing the current climate conditions. In addition, this long series of pseudo-random data representative of the current conditions will be perturbed by the decile method and then be used to drive simulations, as a proxy for future climate conditions. Thermal properties of Lake Geneva as simulated for the last decade of the 21st century is assessed by analysing monthly changes in epilimnic and hypolimnic water temperatures. Variations in the onset of the stratification, depth of the thermocline and strength of the stratification will serve to explain differences in the warming of surface and bottom layers. Particular attention will also be paid to the way radiative, sensible and latent heat fluxes evolve with respect to changes in air temperature and surface water temperature. A final discussion will then relate the evolution of thermal properties and stratification in Lake Geneva to results from other studies concerned with global warming in other lakes.

2.2 Material and methods

2.2.1 Study site and lake data

Lake Geneva, the deepest in Western Europe (309 m), is a large water body located in the western peri-alpine area of Switzerland, bordered by France on the southern shore. It is composed of two basins, a main basin, referred to as the "Grand Lac", that represents more than 96% of the total water volume and an adjacent shallower and narrow downstream basin that forms the "Petit Lac" (Fig. 2.1). It is considered as a warm monomictic lake even though overturns rarely reach the bottom of the "Grand Lac" (Lazzarotto *et al.* 2006; Lazzarotto and Rapin 2007).

Within the framework of a monitoring program coordinated by the International Commission for the Protection of Lake Geneva (CIPEL), discrete measurements of water temperature profiles and bio-chemical properties are collected twice a month at station SHL2, located at its deepest point by the French National Institute for Agricultural Research (INRA). As sampling depths vary slightly with time, only depths of 0, 2.5, 5, 7.5, 10, 15, 20, 30, 35, 50,100, 150, 200, 250, 300 meters (Database INRA of Thonon-Les-Bains, Data CIPEL) are employed in the following analysis.

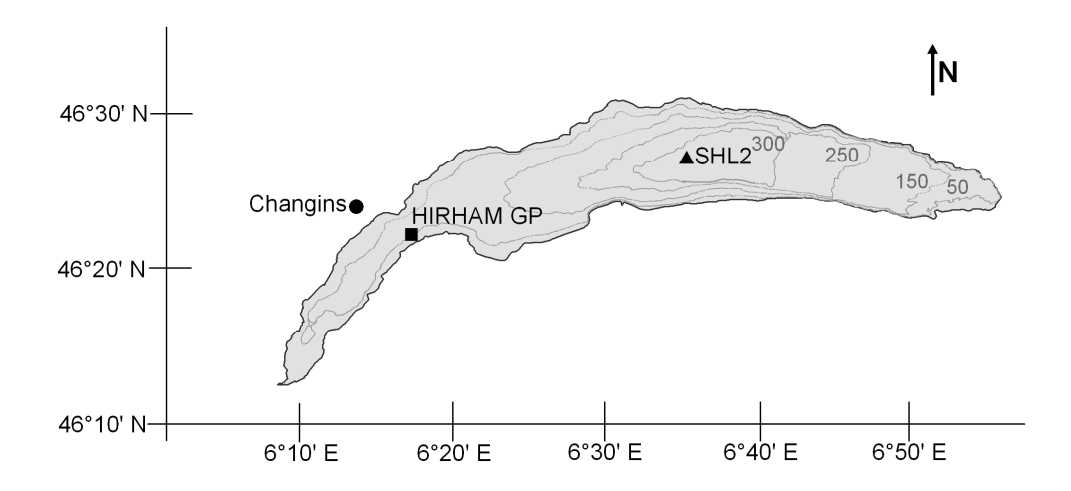


Figure 2.1. Map of Lake Geneva (longitude/latitude) with locations of the meteorological station Changins, of the HIRHAM RCM grid point over Lake Geneva and of the lake sounding station SHL2.

2.2.2 Lake model

For climatological applications, one-dimensional (1D) lake models are usually used because of their computational efficiency and the realistic temperature profiles that they produce. A wide range of 1D lake models have proven efficient in reproducing multiple aspects of thermal profiles in larges lakes in stand-alone mode (Hostetler and Bartlein 1990; Boyce et al. 1993; Peeters et al. 2002; Perroud et al. 2009). Depending on the numerical schemes used, we may find eddy-diffusion models (Orlob and Selna 1970; Henderson-Sellers et al. 1983), turbulence-based models (Kraus and Turner 1967; Imberger et al. 1978), in particular $k-\varepsilon$ models (Burchard and Baumert 1995; Goudsmit et al. 2002; Stepanenko and Lykosov 2005), mixed-layer models (Stefan and Fang 1994; Goyette et al. 2000), or models based on similarity theory (Mironov 2008; Mironov et al. 2010). If turbulent processes such as those generated by shear stress or density instabilities are generally numerically resolved in 1D models, it is true that many processes explicitly implemented in 3D lake models are missing (Bennett 1978; Kelley et al. 1998; Hodges et al. 2000). 1D lake models may miss for instance horizontal advection or mixing induced by progressive or long standing waves, and particularly on large lakes when the effects of earth rotation are neglected (e.g. Kelvin seiches). However, 3D lake models present two main disadvantages; first they are too timeconsuming for century scale applications and secondly the small number of meteorological stations recording data around the lake cannot provide the adequate boundary conditions required for simulations with 3D models. Despite the obvious limitations associated with the use of 1D lake models, the simulation of thermal profiles in Lake Geneva at SHL2 has been previously assessed using four different 1D lake models (Perroud et al. 2009). Two of them were clearly capable of simulating water temperature profiles over ten independent annual cycles. Indeed, these latter had the advantage of parameterizing 3D processes, i.e., the vertical mixing due to the effects of seiching on the metahypolimnion.

SIMSTRAT (Goudsmit *et al.* 2002; Peeters *et al.* 2002), has been used in this study to examine the evolution of temperature profiles in a changing climate. In this model, turbulent diffusivity is estimated from the production k and dissipation ε of turbulent kinetic energy, TKE. Apart from buoyancy and shear, SIMSTRAT extends the production of TKE to mixing processes from seiching motion, *i.e.*, from the release of TKE by friction on the bottom boundary. The version employed in this study has different boundary conditions from those of Goudsmit (2002). First, a new formulation for albedo has been introduced to account for the time-dependent solar zenith angle. Secondly, the varying wave height has been

parameterized by using two empirical equations for the drag coefficient c_D , one to relate increasing wind speed to higher c_D and the other for variation of c_D with wind speed below 3 m s⁻¹. Details on these modifications are given in Perroud *et al.* (2009).

Table 2.1: Energy fluxes at the water-atmosphere interface and calibration parameters.

Model parameter	Value	Unit	Remarks
L↓	$(1-r_a)\varepsilon_a\sigma T_a^4$	W m ⁻²	downward atmospheric longwave
r _a	0.03	-	reflection of infrared radiation from water
\mathcal{E}_a	$1.24 (1 + 0.17 C^2) \left(\frac{e_a}{T_a}\right)^{1/2}$	-	atmospheric emissivity
С		-	cloud coverage
σ	5.67 x 10 ⁻⁸	$\mathrm{W}\;\mathrm{m}^{2}\;\mathrm{K}^{4}$	Stefan-Boltzmann constant
T_a		K	absolute atmospheric temperature
e_a		hPa	atmospheric water-vapour pressure
L↑	$-\varepsilon_{\scriptscriptstyle W}\sigma{\cal T}_{\scriptscriptstyle W}^4$	W m ⁻²	emitted longwave
\mathcal{E}_{W}	0.97	-	longwave emissivity of water
T_w		K	absolute temperature of water
Q_{h}	$Bf_{u}(T_{w}-T_{a})$	W m ⁻²	sensible heat flux
f_u	$4.4 + 1.82 \sqrt{U_{10}^2 + V_{10}^2} + 0.26 (T_w - T_a)$	$\mathrm{W}~\mathrm{m}^{\text{-2}}~\mathrm{K}^{\text{-1}}$	transfer function
В	0.61	-	Bowen ration
Q_e	$f_u(e_w-e_a)$	W m ⁻²	latent heat flux
e_w	$f_w \times 10 \frac{0.7859 + 0.03477 T_w}{1 + 0.00412 T_w}$	hPa	water vapour saturation at T_w
f_w	$0.61\left[1+10^{-6}p_a\left(4.5+6\times10^{-5}T_w^2\right)\right]$	W m ⁻² hPa ⁻¹	transfer function
p _a		hPa	air pressure

^{*} T_a has been adjusted in this study with respect to conditions at the lake surface, $T_a = T_L$).

In order to calculate the evolution of water temperature profiles, the energy budget and wind stress forcing need to be estimated at each time step. The energy components are thus either given as input to the model if they are measured to the meteorological station close to the lake, or deduced from a given parameterization (Table 2.1). The model time step is set at 10 minutes for a vertical grid spacing of 0.75 m.

Meteorological data collected at the land station Changins (Fig. 2.1) are supplied by the Automatic Network (ANETZ) of the Federal Office of Meteorology and Climatology, Meteoswiss (Bantle 1989), from 1980 to 2006. This latter provides as input to the model hourly values of air temperature, T, horizontal wind magnitude, v, wind direction, dir, relative humidity, RH, surface pressure, p, downward solar radiation, $S \downarrow$, and cloud cover, C. T is adjusted to account for the difference of elevation $\Delta z = z_{\text{station}} - z_{\text{L}}$ between the land station, z_{station} , and the lake reference, z_{L} , as follows:

$$T_{\rm L} = T_{\rm station} + \Delta z \gamma$$
 (1)

where T_L is the temperature over the lake, $T_{\rm station}$ is the temperature at Changins, and γ the vertical lapse rate fixed at 6.5 K km⁻¹. A scaling factor is also applied to v in order to be more representative of the conditions over the lake open water (Perroud *et al.* 2009).

The penetration of S^{\downarrow} through the water column is modulated by the light extinction coefficient, $K_{\rm e}$, from the Beer-Lambert law. The euphotic depth (1% of surface light intensity) is calculated from bi-monthly measurements of the secchi disk depth. Values are then linearly interpolated to cover the missing daily data.

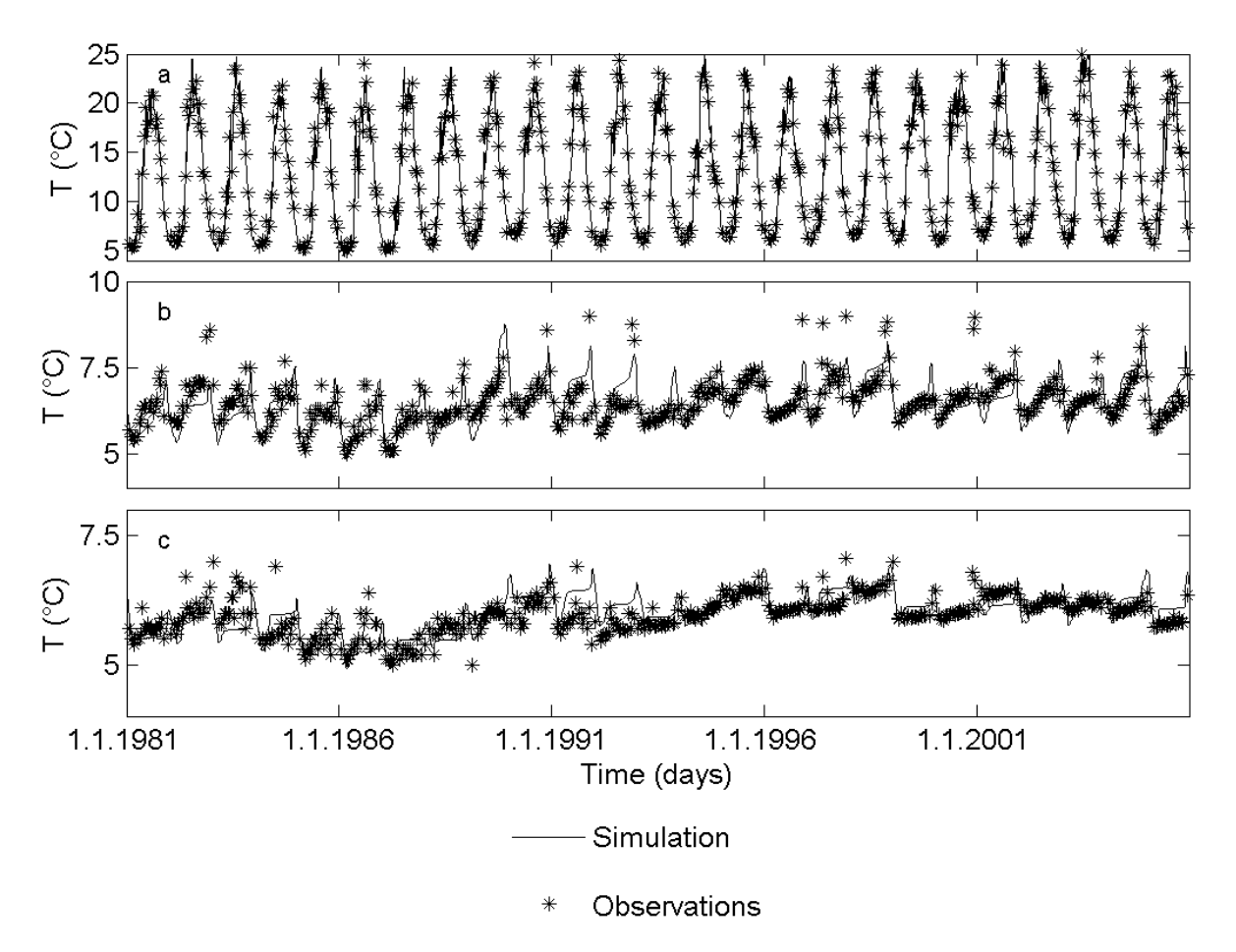


Figure 2.2. Map of SIMSTRAT simulated water temperatures and observed temperatures at (a) the surface, (b) 10 m deep and (c) 100 m from January 1, 1981 to December 31, 2005.

To ensure that the model does not drift when run over a long period, a simulation with a 26-year meteorological record is first carried out. The simulation is initialized with the last temperature profiles taken at SHL2 in December 1980 and is then run through to December $31^{\rm st}$ 2005. Since the model has been calibrated for Lake Geneva for individual years (Perroud *et al.* 2009), a new calibration procedure covering continuous years is completed by adjustment of the two empirical parameters, α and q, both used in the algorithm of boundary mixing and related to seiche activity. Calibration is undertaken for two 5-year periods (1981 - 1986 and 2000 - 2005) by minimizing the root mean square error (RMSE) between observed and simulated water temperatures. The values are first adjusted to fit the first period before being tested against the second dataset for validation. The temperature profiles simulated over 26 years show that the model remains remarkably stable and reproduces fairly accurately the temperature variations at all depths (Fig. 2.2).

A statistical analysis applied on more than 500 soundings collected at SHL2 indicates that the RMSEs are below 1.5 °C, except between 10 m and 15 m where errors are likely due to difficulties to locate the exact depth of the thermocline. The mean error ME and standard deviation σ are -0.91 °C ± 1.16 °C at the surface, -0.05 °C ± 1.63 °C at 10 m, -0.24 °C ± 0.54 °C at 50 m and lower than -0.2 °C ± 0.3 °C below (Table 2.2).

Table 2.2: Mean error, standard deviations of the error and root mean square error between observed and simulated water temperature profiles from December 1980 to December 2005.

Depth	Mean error (℃)	Standard deviation ($^{\circ}$ C)	Root mean square error
Surface	-0.91	1.16	1.47
2.5 m	-0.74	1.09	1.31
5 m	-0.33	1.35	1.38
7.5 m	-0.15	1.43	1.44
10 m	-0.05	1.63	1.63
15 m	-0.22	1.54	1.56
20 m	-0.26	1.22	1.25
30 m	-0.25	0.93	0.96
35 m	-0.38	0.78	0.87
50 m	-0.24	0.54	0.59
100 m	-0.20	0.29	0.35
150 m	-0.16	0.23	0.28
200 m	-0.07	0.23	0.24
250 m	-0.01	0.27	0.27
300 m	0.03	0.29	0.29

2.2.3 Model Inputs for long term simulations

2.2.3.1 Current data set

In order to capture the evolution of the thermal signal in the deep hypolimnion of this monomictic lake, it is necessary to drive the model with atmospheric inputs over a longer time period. The meteorological dataset that is created to run the model on the long term needs to have similar statistics to those of the reference period of 1981 to 1990. In addition, the long term average water temperature profiles simulated by SIMSTRAT, also need to be fairly similar to those obtained from the ten years of observation. A novel concept thus needs to be developed to fulfil two requirements: 1) these long series of data will help identify meteorological variables whose variability is essential in reproducing water temperature profiles; 2) generate longer series of realistic variables to drive SIMSTRAT to ensure that the model water temperatures do not drift with time.

First, a one-year sequence of hourly mean meteorological variable \overline{X}_i (for i=[T, v, RH, dir, C, $S\downarrow$]) is produced by averaging hourly data covering the ten year period. \overline{X}_i is then concatenated 10 times to produce a series of same length as the period of observations. Then, simulated water temperature profiles driven with current observations and with hourly average observations are compared. These results show that water temperatures are generally underestimated (Fig. 2.3a). In fact, hourly averages tend to reduce the supply of heat penetrating into the water column.

To analyse the importance of a variable on the fluxes that generate the necessary heat transfer with depth, hourly averages are replaced in turn with the original time series. Results indicate that the variability of the winds only, the other variables keeping their hourly mean values, decreases the RMSE by 88% and the mean error is reduced at all depths of the profile (Fig. 2.3a). In order to generate a long sequence of winds, a weather generator is used to create a pseudo-random time series to avoid reproducing periodic events.

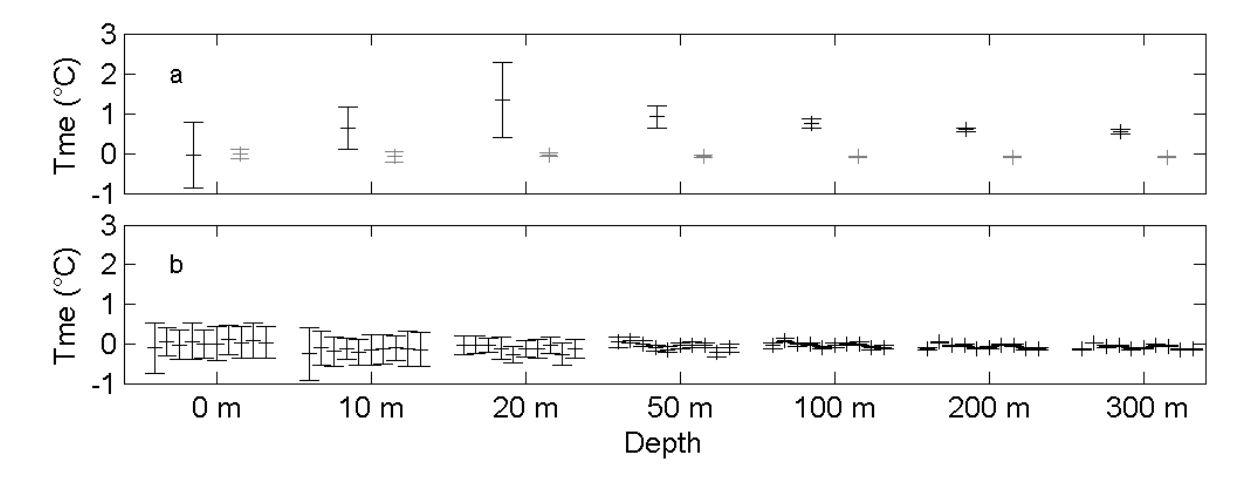


Figure 2.3. (a) Mean error and standard deviation for decadal mean simulated water temperatures when driven with current observations (1981 - 1990) and hourly average observations (bar 1), except for wind (bar 2) at different depths. (b) Mean error and standard deviation of mean simulated water temperatures when driven with current observations (1981 - 1990) and ten individual decadal datasets of mean daily values of $S\downarrow$ and C, and pseudo-random series of v, dir, T and RH.

Second, since potential changes in *T* and *RH* will be investigated in the next section, their variability will also be reproduced with the generator.

The pseudo-random meteorological data generation consists in the creation of meteorological variables m_i (for i=[v, dir, T, RH]) whose distribution properties are similar to

those of the current observations. This means that the monthly mean distribution μ D, the intra-day standard deviation, σ IAD, and the inter-day standard deviation, σ IED, of a variable must be similar to the ten-year observations. The generation of pseudo-random data (Appendix) follows basically the same procedure for v, RH and T and data finally produced by the generator fits observations in terms of μ D, σ IAD and σ IED (Fig. 2.4).

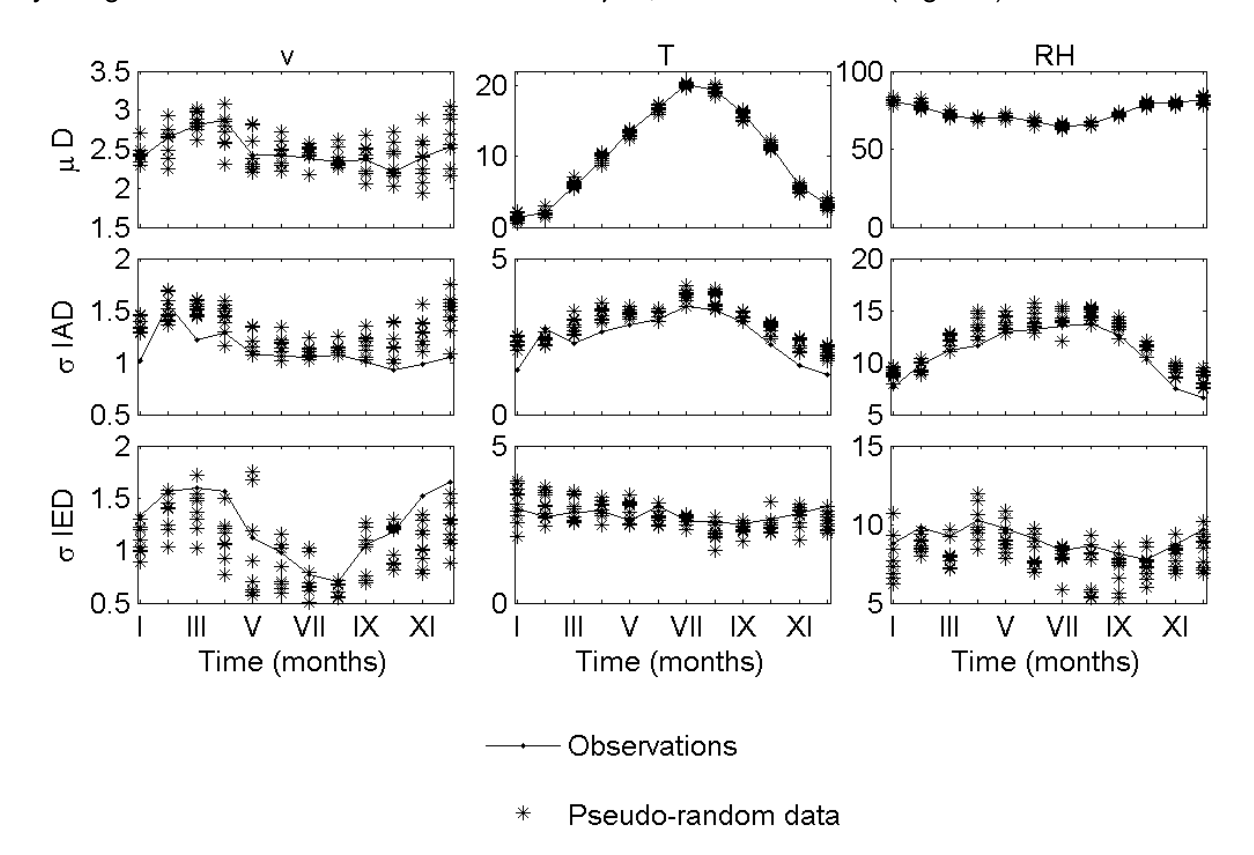


Figure 2.4. Monthly means, μ *D*, (upper row), monthly mean intra-day standard deviation, σ *IAD*, (middle row), and monthly mean inter-day standard deviation, σ *IED*, (lower row), of ten years of pseudo-random ν , T and RH are compared individually to the averaged monthly means recorded at Changins over the period 1981 - 1990.

A 100-year sequence of m_i has been created in order to validate this method for the model's ability to reproduce the water temperature profile (mean and variance), when driven by such time series. Profiles thus simulated are averaged to produce ten decadal daily profiles. Each of them reproduces accurately decadal mean daily profiles and lies inside their daily extrema found within the ten-year period (Fig. 2.5). Maximum mean errors (< 0.25 °C) are found in the metalimnic layers, e.g. at 10 m below the surface (Fig. 2.3b). It is noticed that no systematic drift appears (Fig. 2.6). Mean daily values of $S\downarrow$ and C, combined with pseudo-random v, dir, T and RH thus form a dataset suitable to drive SIMSTRAT in order to simulate water temperature profiles representative of the current period over long time period of time.

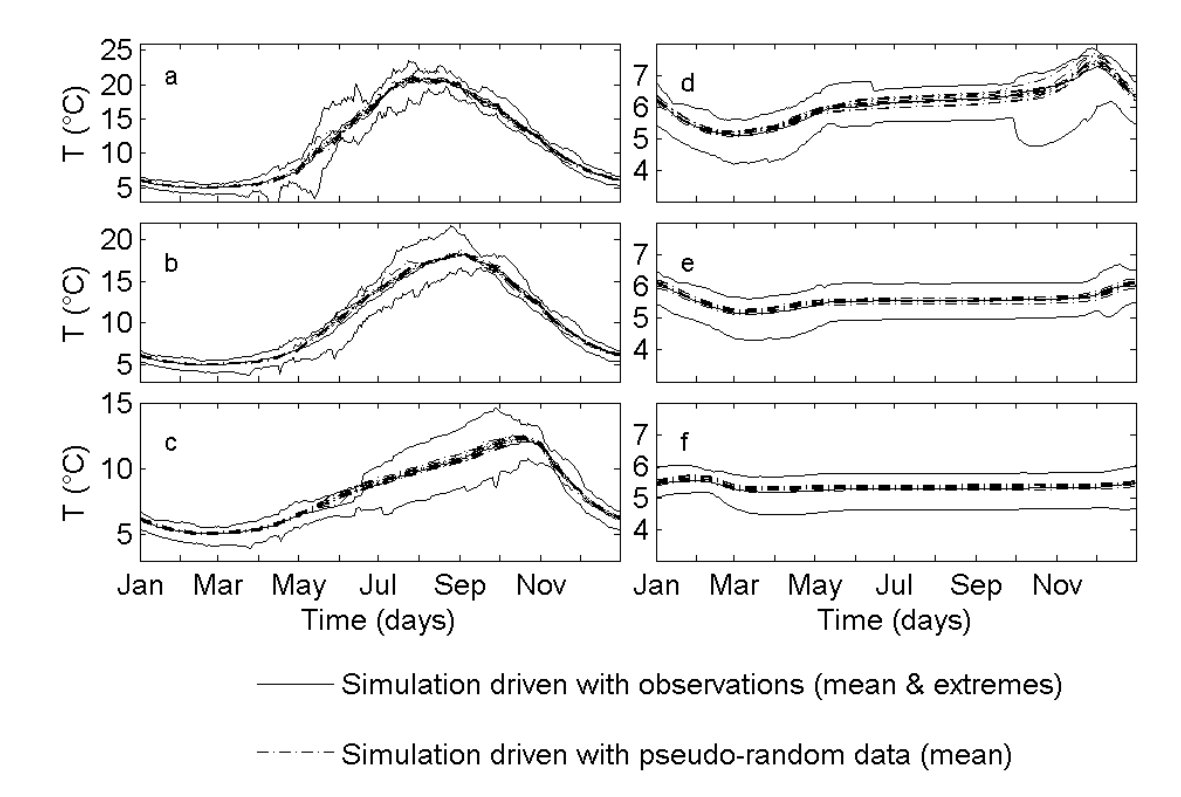


Figure 2.5. Mean daily water temperature profiles per decade are obtained from a 100-year simulation driven with pseudo-random v, dir, T and RH and observation (1981 - 1990) at (a) the surface, (b) 10 m, (c) 20 m, (d) 50 m, (e) 100 m and (f) 200m.

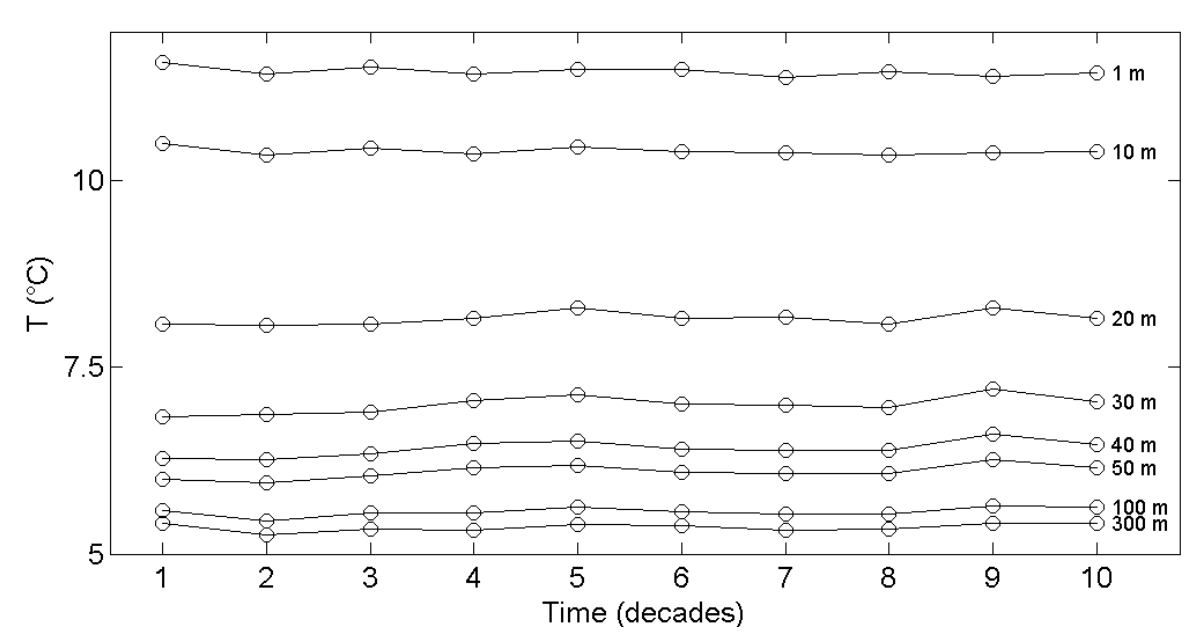


Figure 2.6. Mean decadal temperature profiles obtained from a 100-year simulation driven with pseudo-random series of v, dir, T and RH.

2.2.3.2 Data set perturbed using the decile method

To assess changes in the water temperature of Lake Geneva in response to a changing climate, daily mean outputs obtained from the HIRHAM Danish Regional Climate model used in the framework of the 5th EU programme PRUDENCE (Christensen *et al.* 1998) are taken into account. The hourly observed meteorological input variables driving the lake model are thus perturbed according to changes diagnosed with the HIRHAM outputs. This model provides two sets of daily meteorological variables, covering respectively the period 1961 - 1990 and 2071 - 2100, at 21 grid points over Switzerland. The atmospheric CO₂ concentrations projected in the model follow the IPCC A2 emissions scenario (IPCC 2001).

In many climate studies, physical characteristics prescribed at grid points compared to observation site (e.g., land cover) as well as low archival frequency of GCM data prevent using RCM outputs as input data to run subsequent models. Therefore, the approach that is usually proposed to investigated climate forcing on environmental systems consists in adding a delta increment, Δ , to observations, or a ratio r obtained by linking past and future outputs from a RCM (Boyce $et\ al.\ 1993$; Mortsch and Quinn 1996; Stefan $et\ al.\ 1998$, Fang and Stefan 1999). As shown in Fang and Stefan (1996; 1999), Δ or r are not uniform throughout the year and may vary from one month to another. To better represent the time change of the data over the year, Δ or r should vary on a seasonal or monthly basis since trends are not the same. Based on this approach, the method for the present study can thus be described as follows:

$$\varphi_{i} = \chi_{i} + \lambda \Delta \tag{2}$$

where φ_i are the hourly meteorological variables expected in the future, $\lambda = [0,...,1]$ is an empirical scaling parameter and Δ is the monthly difference between HIRHAM future and current data. Jungo and Beniston (2001) show that minima, maxima and mean temperatures will not change in the same way. A single Δ may omit the large variability of this parameter moving away from the mean. Uhlmann et al. (2009) proposed to calculate several forms of Δ during a same period, that is Δ 's that characterize the mimimum, maximum and mean temperatures. In this study, estimates of Δ follow a more detailed approach than that of Uhlmann et al. (2009). Monthly data distribution of the current and future periods are divided into deciles, d_i (i=1,...,10); values delimited by the same two deciles are grouped to form a class and then averaged to produce one mean value per class. Ten values per month and per variable are thus obtained for the current period and an equivalent number of values for the future period. Differences between respective classes of deciles for the first and second period produce ten different values of Δ per month. The Δ produced for the smallest values of a distribution ($< d_1$) may be rather different to the Δ produced for the highest values ($> d_9$). Observed data are scaled by the Δ corresponding to the class (defined by d_i from HIRHAM data distribution for the period 1961 - 1990) in which they belong.

With regards to the monthly Δ determined for the 5 input variables (Table 2.3) driving the lake model, the air temperature T and dew point temperature Td at screen level for the grid point over Lake Geneva are the most sensitive to future modifications. As RH is not provided by HIRHAM outputs, Td is used. Perturbations to observed hourly data will thus be applied only to T and Td. The adjustment of variables for the difference in elevation $\Delta z = z_H - z_L$ is made as follows:

$$T_{L} = T_{H} + \Delta z \gamma \tag{3}$$

$$RH_{H} = f(T_{H}, Td_{H}) \tag{4}$$

$$Td_{L} = f(T_{L}, RH_{H})$$
 (5)

with the subscript $_{\rm H}$ and $_{\rm L}$, for the HIRHAM and the lake variables. Monthly bias of T and Td between the HIRHAM variables and observations, $\Delta_{\rm H-L}$, are calculated. While monthly $\Delta_{\rm H-L}$ is low for T (\pm 1 $^{\circ}$ C), HIRHAM generally overestimates the moisture level of the atmosphere ($\Delta_{\rm H-L}$ for Td = [1.5 $^{\circ}$ C; 4.5 $^{\circ}$ C] from January to August). $\Delta_{\rm H-L}$ is considered thereafter.

Unlike T, Δ for Td cannot be deduced from distribution of Td only. A same value of Td may indicate that the atmosphere is saturated (if T equals Td) or unsaturated (if T is higher than Td). The bigger the difference between T and Td is, the drier the conditions are. Thus, changes in RH are obtained by calculating monthly Δ on the basis of the distribution of T-Td. Even though current data distribution is different for HIRHAM and the Changins meteorological observing site, it is hypothesised that Δ for Td, henceforth ΔTd , are devoid of model bias. Therefore, new d are calculated from the monthly T-Td distribution at Changins and Δ are added on those new classes.

Table 2.3: Monthly differences between HIRHAM RCM future and current data.

Month	S↓ (W m ⁻²)	С	T (℃)	Td (℃)	<i>v (</i> m s ⁻¹ at 10 m)
January	-9.68	0.06	4.12	3.00	0.127
February	-17.05	0.1	2.97	2.70	0.066
March	-20.37	0.07	1.71	2.24	0.057
April	0.48	-0.03	3.03	2.78	-0.041
May	19.80	-0.06	3.50	2.83	0.008
June	26.10	-0.09	4.18	2.96	-0.003
July	13.04	-0.07	4.52	2.18	0.037
August	26.38	-0.12	6.87	1.26	0.030
September	16.03	-0.08	6.03	1.57	-0.050
October	-0.39	-0.02	4.50	2.88	-0.030
November	6.75	-0.05	4.02	0.86	-0.087
December	-3.00	0.01	4.12	2.18	0.043

In order to verify the validity of the method, monthly Δ are added to the current data generated by the HIRHAM model (*i.e.*, 1961 - 1990) and the new distribution compared to the one predicted for the future (*i.e.*, 2071 - 2100). It is shown that $T + \Delta T$ (ΔT being Δ for T) and $Td + \Delta Td$ (ΔTd being Δ for Td) are quite similar with the expected values at any time of the year (Fig. 2.7a,b). ΔT indicate that greatest warming is observed for maxima of T (> d_9) from April to October and for minima from December to March (< d_1). Overall, the ΔT are more pronounced in summer than in winter. ΔT in the median class (between d_5 and d_6) is

 $6.79\,^{\circ}$ C in August whereas it reaches only $4.13\,^{\circ}$ C in January. Even though predictions for both T and Td point out a shift in the distribution towards higher values, these variables will not evolve in the same manner. Therefore, it is likely that difference between T and Td increases further due to a lower augmentation of Td, thus impacting on RH; this is true for the whole year except in March. Changes concern mainly the months of July, August and September (e.g. high difference at Julian day 180, Fig. 2.7a,b) where the decrease of RH reaches 15% on average during this period, in line with the findings of Christensen and Christensen (2003). ΔTd above d_5 are also expected to be the largest. This means that reduction in RH will be observed principally for dry atmospheric conditions but that the number of days close to saturation will not necessarily decrease.

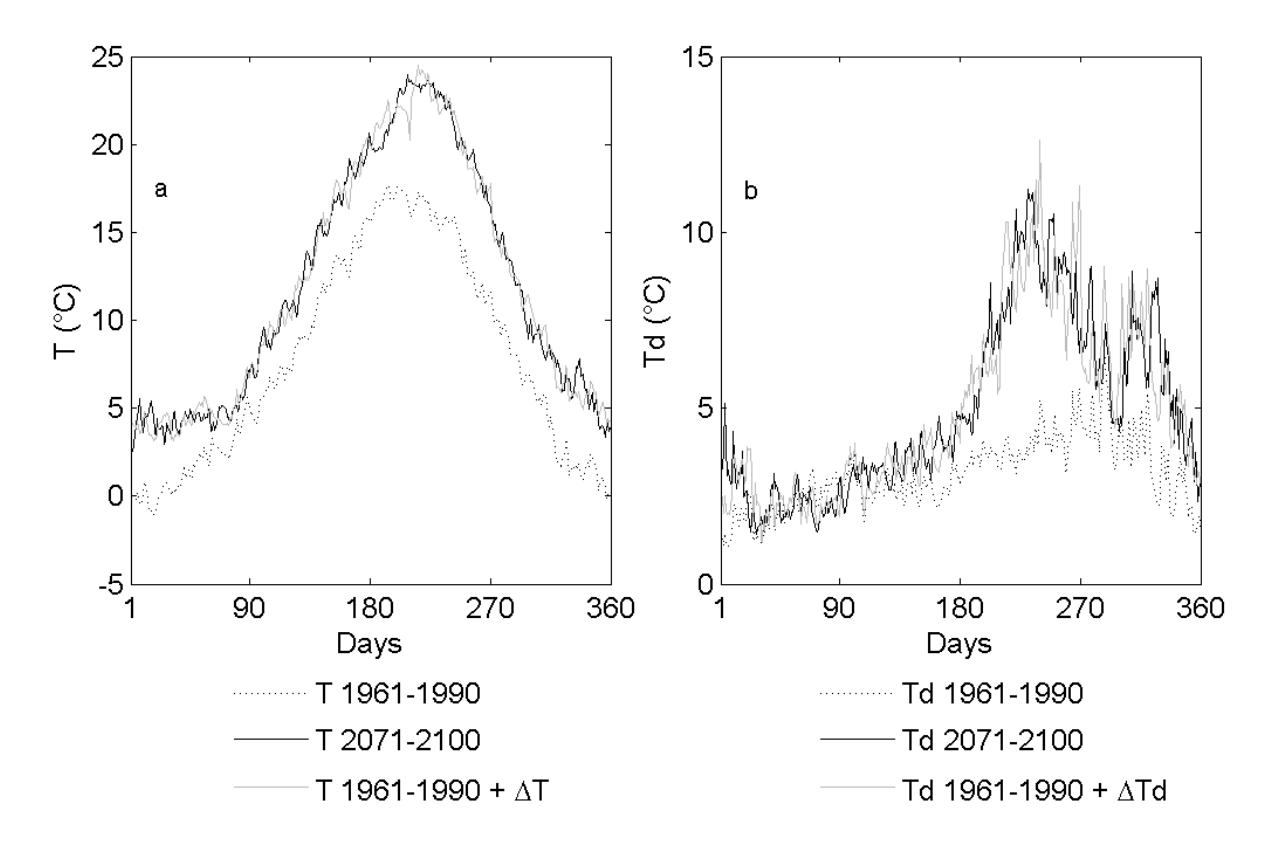


Figure 2.7. Mean daily distribution of (a) temperature and (b) dew point temperature according to the HIRHAM outputs for the current and future period, as well as when monthly Δ are added to HIRHAM current data.

2.2.4 Experimental setup

To simulate the evolution of Lake Geneva temperature profiles well beyond the observation period, a pseudo-random meteorological data generator is used to reproduce a 130-year sequence of meteorological data representative of the conditions recorded between 1961 and 1990. According to the amplitude of climate change simulated by the HIRHAM RCM, another dataset is produced by perturbing this long time series according to Eq. 2. The first ten years serve to spin up the water temperatures ($\lambda = 0$, *i.e.*, no perturbation is applied) and the following 110 years to reproduce the evolution of the climate from the current to the future period. In the following, λ is equal to 0 in 1976 (median year for the first period) and increases linearly up to 1 in 2086 (median year for the second period), followed by an extra ten years using a fixed $\lambda = 1$ in order for a new equilibrium to be reached (Fig. 2.8). A number of simulations are then run with current (reference simulation) and future conditions over this

long time period. Daily water temperature profiles produced during the last decade are averaged daily to produce 365 profiles and serve to estimate the changes.

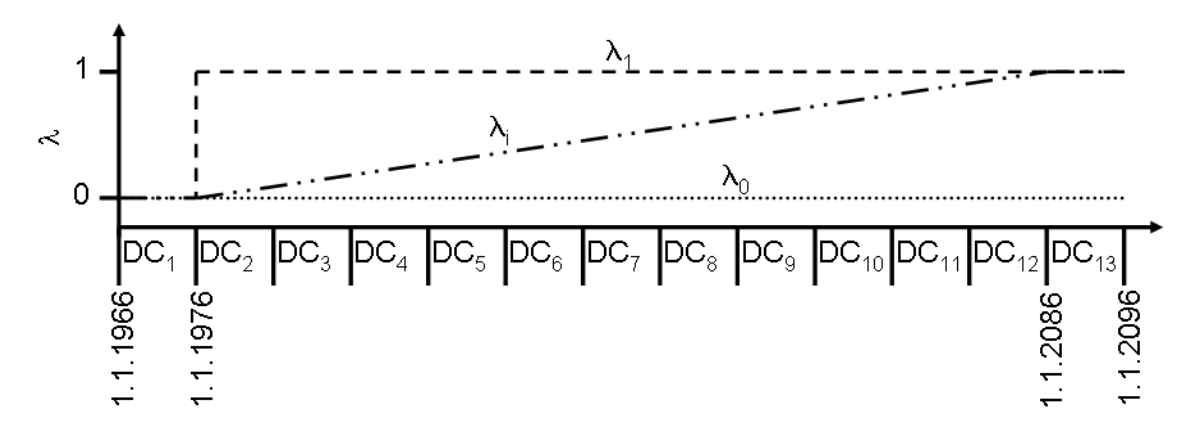


Figure 2.8. Possible yearly values taken by the empirical scaling parameter λ to perturb the reference dataset over the 13 decades of simulation.

The thermal response of the lake to a constant λ (λ =1 from year 11 to year 130) is also investigated for comparison since many studies concerned with climatic effects on lakes usually perturb historical weather recorded data with a unique and constant value (Fig. 2.8). This will provide a quantification of the time spent to reach the second equilibrium. Hereinafter, λ is referred to as λ_0 when λ is equal to zero (reference simulation), as λ_i when λ is increasing over the period, and as λ_1 when λ is held constant and equal to 1 (Fig. 2.8).

Since no coupled-biochemical model is used, existing measurements of K_e serve to produce daily values. However, in order to dampen the effects of high eutrophic status measured prior to 1990 on the absorption of solar radiation by the lake water, daily K_e have been averaged for similar Julian days over a period that covers the years 1981 to 2006. Water temperature variability resulting from fixed average values in K_e is then discussed below.

Changes in water temperature profiles are investigated in term of volume-weighted temperatures in the epilimnion $T_{\rm epi}$ and in the hypolimnion $T_{\rm hyp}$. The epi-hypolimnion boundary $z_{\rm lim}$ is then set at the depth z corresponding to the highest water temperature gradient (for a layer spacing of 1 m). As $z_{\rm lim}$ evolves dynamically, the depth of the thermocline is defined as the average value of $z_{\rm lim}$ over the summer-fall stratification period (Hambright et al. 1994). The onset of the stratification, OS, as well as the stability of the water column (given by the stability parameter, N) at $z_{\rm lim}$, are considered with regard to their potential influence on biological processes. OS is diagnosed when a 1 °C difference appears between the 100 m and 2 m layer (adapted from Jacquet et al. 2005 and detailed in Perroud et al. 2009).

Surface energy exchanges and the resulting budgets are also computed (Table 2.1) since they determine the cooling/heating of the water body due to climatic forcings.

2.3 Results

Water temperatures profiles have been produced with SIMSTRAT driven by a 130-year pseudo-random hourly series. These results will allow quantifying changes due to global warming compared to the reference simulation. As shown previously with the 100-year simulation (Fig. 2.6), mean decadal temperature profiles are reproduced in a realistic manner over the decades and simulate profile statistics similar to these obtained by using observations (1981 - 1990) (Fig. 2.5). At the bottom, mean water temperature is of 5.33 °C by the 13th decade. From the bottom up to 100 m depth, mean decadal temperatures increase but do not exceed 0.2 °C. It is mainly above 100 m that changes are the most significant, particularly above 50 m. Temperatures are thus 6.10 °C at 50 m, 7 °C at 30 m, 10.3 °C at 10m and 11 °C at the surface. $T_{\rm epi}$ is the strongest in August where it reaches 17.45 °C and the lowest in February (5.09 °C). $T_{\rm hyp}$ lie between 5.25 °C (March) and 5.88 °C (November), thus showing the shift in the cooling (heating) of the hypolimnion.

2.3.1 Projected Lake water temperature changes using the decile method

Two simulations driven by perturbed data based on a linear increase of the atmospheric perturbation were run. In the first, monthly perturbations were applied only to temperature (Sim_T) and in the second to temperature and relative humidity (Sim_{T,RH}). In both cases, an increase in water temperature was simulated in the entire water column. The annual temperature increase from 35 m depth down to the bottom varies between 2.35 °C and 2.57 °C (Sim_T) and between 2.10 °C and 2.28 °C (Sim_{T,RH}). Temperatures then rise strongly from 35 m up to the surface, so the increase for Sim_T and Sim_{T,RH} is respectively 2.54 °C and 2.27 °C at 20 m, 3.31 °C and 2.83 °C at 10 m and 3.9 °C and 3.16 °C at the surface. Intrannual variability indicates that during the winter months, the warming through the column lies between 2.37 °C and 2.93 °C for Sim_T and 2.11 °C and 2.72 °C for Sim_{T,RH}. Then, after the onset of the stratification, the lake can be partitioned into three segments with distinct warming trends: the surface layers are expected to warm the most, the metalimnic layers below the thermocline the least, and the temperature in the hypolimnion to rise to values similar to those observed prior to stratification (Fig. 2.9).

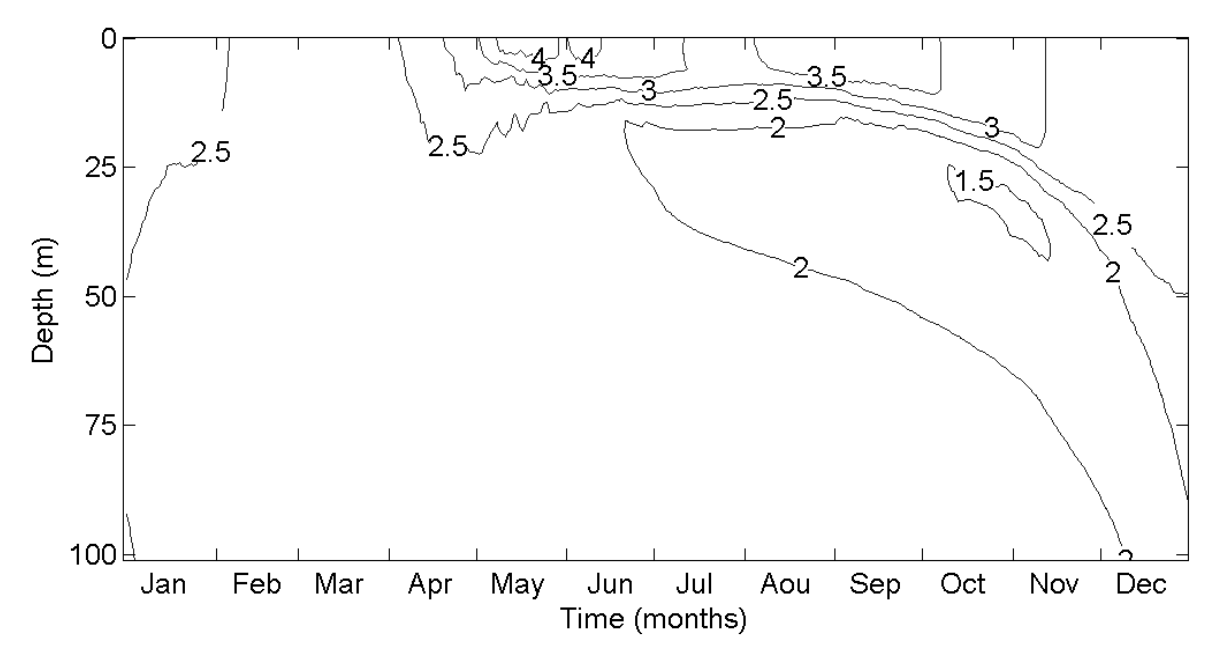


Figure 2.9. Coutour plots of mean daily temperature differences in the first 100 m below the surface between simulated profiles beyond the 13th decade under future and current conditions.

As heat entering the lake is not homogeneously mixed above z_{lim}, variability in water temperature may be important (Fig. 2.9). In the epilimnion, the warming varies between 2.80 °C and 6.07 °C for Sim_T and 2.40 °C and 4.17 °C for Sim_{T,RH}, the highest temperature increase being simulated at shallower depths, and mostly from early August to late September for Sim_T (> 5 °C), and from mid-May to mid-June for Sim_{T,RH} (> 4 °C). Compared to the values simulated at the depth of the lower metalimnion before stratification, water temperatures warm. However, Sim_T and Sim_{T,RH} show that the warming below the thermal gradient will be lower than further down in the column, and particularly from early July (Fig. 2.9). These layers evolve dynamically downwards with a deepening of the thermocline. A minimum of 1.59 °C for Sim_T and 1.62 °C for Sim_{T,RH} are thus found at 18 m and 23 m, respectively, in early September. From the bottom up to this limit, daily variability in the thermal increase lie within 2.42 °C and 2.63 °C for Sim_T and 2.15 °C and 2.33 °C for Sim_{T,RH}. This indicates that predictions for Sim_T impacted more strongly on water temperature than $Sim_{T,RH}$ (Fig. 2.10). Similarly, the monthly increases of T_{epi} were between 2.58 °C (March) and 5.35 (August) for Sim_T, whereas they ranged from 2.32 °C and 3.83 ° for Sim_{T,RH}. Likewise, monthly T_{hyp} rose by 2.50 °C to 2.63 °C for Sim_T and by 2.20 °C and 2.33 °C for Sim_{T,RH}. A T_{epi} slightly lower or similar to T_{hyp} ($\leq 0.3 \,^{\circ}\text{C}$) simulated under current conditions from January to March was also observed under both future projections, but only in February and March (≤ 0.2) .

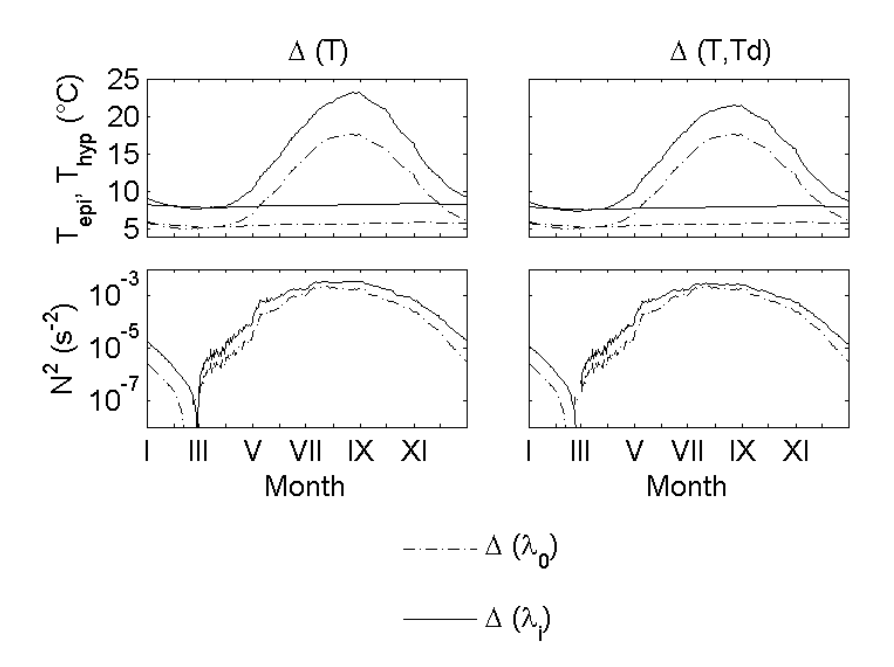


Figure 2.10. Mean daily volume-weighted temperatures in the epilimnion $T_{\rm epi}$ and in the hypolimnion $T_{\rm hyp}$, for SIMSTRAT simulations under present and future conditions, when T and both T and Td are perturbed (upper row). Similar results are shown for daily values of water column stability, N^2 (lower row).

The main changes in the metalimnic properties concerned the overall greater stability of the lake. In spring, N^2 is 3 times higher in the future (Fig. 2.10) and 1.5 times larger in summer. During summers, z_{lim} generally agrees under current and future conditions, but the thermocline depth in fall moves closer to the surface in the future (2 to 4 m upwards on average), thus indicating a longer period of stratification (up to 11 days more). Moreover, the lake will stratify earlier, slightly more than one week on average, so that the length of the stratification period is of more than 3 weeks longer than under current climate.

Total daily energy amount for each flux component was averaged per decade in order to analyse the differences observed in the water column between both perturbed simulations and to diagnose the amount of heat gain or loss by the lake (Fig. 2.11). Air temperature

dependent fluxes, $L\downarrow$, Q_h , Q_e , are analysed since they strongly impact upon the lake surface energy budget, and thus on the amount of heat available to warm the lake water column. However, omitting the decrease in RH, the atmospheric emissivity, ε_a , is overestimated, producing higher values of $L\downarrow$ (Table 2.4). The reduction in water vapour e_a (Table 2.1) following drying of the atmosphere, jointly with surface water temperature changes, is seen to cool the water by evaporation more intensively than in Sim_T alone (Table 2.4).

Table 2.4: Mean energy components calculated over the 13th decade of simulation under current (reference simulation) and future conditions (Sim_T , $Sim_{T.RH}$).

FLUXES (MJ day ⁻¹ m ⁻²)	Reference simulation (LDP)	Sim _T	Sim _{T,RH}
S↓	11.97	11.97	11.97
S^{\uparrow}	0.88	0.88	0.88
<i>S</i> *	11.95	11.09	11.09
$L \!\!\downarrow$	24.93	27.54	27.01
L↑	-31.30	-32.97	-32.54
<i>L</i> *	-6.24	-5.43	-5.61
Q_{h}	-0.73	-0.56	-0.17
Q_e	-4.11	-5.12	-5.34
Energy budget	-0.02	-0.03	-0.04

At the same time that perturbations were linearly increased in Sim_T and $Sim_{T,RH}$, it appears that $L\downarrow$ increased under the new climatic conditions at a mean rate of 0.21 and 0.17 MJ day⁻¹ m⁻², respectively, per decade. The other fluxes, whose values also depend on the lake surface temperature, remained negative on an annual average basis. Due to higher surface water temperature, there were additional 0.14 and 0.11 MJ day⁻¹ m⁻² that were extracted by the loss of infrared energy. In addition, more negative values of Q_e further cooled the lake at a mean rate of 0.07 and 0.09 MJ day⁻¹ m⁻² respectively. Even though Q_h is still negative, the amount of energy lost from this latter component were decreasing at a mean rate of 0.015 and 0.049 MJ day⁻¹ m⁻² respectively. Compared to the reference simulation, the energy budget indicated that the mean multi-decadal energetic gain is 0.036 and 0.0273 MJ day⁻¹ m⁻² for Sim_T and $Sim_{T,RH}$, respectively.

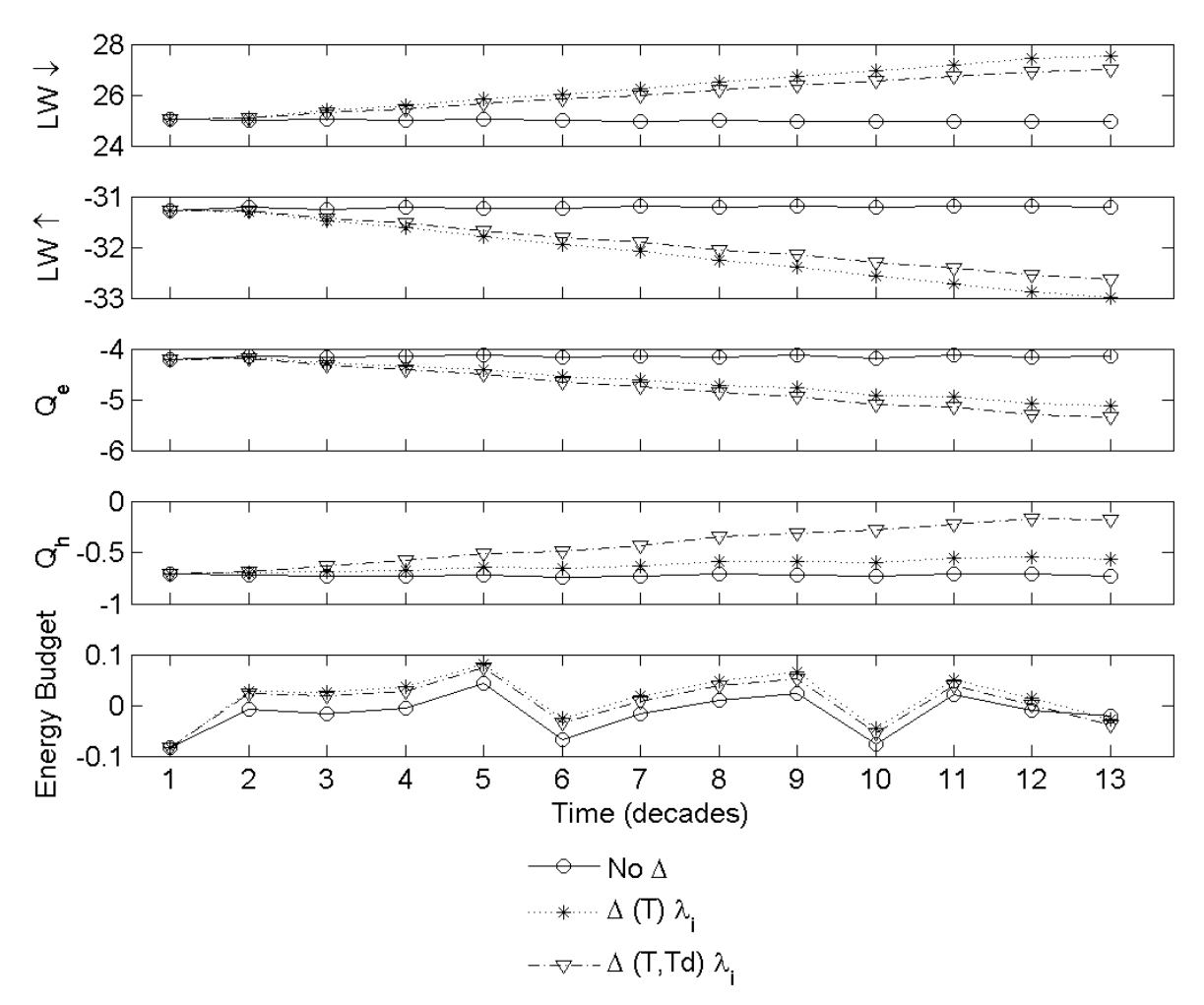


Figure 2.11. Total daily energy amount for $L\downarrow$ and $L\uparrow$, infrared gain or loss at the lake surface, $Q_{\rm e}$, latent heat flux, $Q_{\rm h}$, sensible heat flux and total energy budget, averaged per decade for the reference simulation and for both perturbed simulations ${\rm Sim_{T,RH.}}$ Units are in MJ day⁻¹ m⁻².

2.3.2 Sensitivity of the lake water temperature to changes in air temperature.

Two additional simulations have been undertaken with a bulk increase in air temperature of $1\,^{\circ}\text{C}$ (Sim_{T_1}) and $4\,^{\circ}\text{C}$ (Sim_{T_4}). The lake response to various increases in air temperature will allow to conclude whether nonlinearities appear in the system. In any case, an increase of $1\,^{\circ}\text{C}$ or more produces a warming of the entire water column over the year. Seasonal variability of changes in the water temperature profile is $0.6\,^{\circ}\text{C}$ to $0.68\,^{\circ}\text{C}$ below 75 m (Sim_{T_1}) and $2.73\,^{\circ}\text{C}$ to $2.95\,^{\circ}\text{C}$ (Sim_{T_4}) below 85 m. From that limit up to the surface, changes for Sim_{T_1} and Sim_{T_4} are higher and reach respectively a maximum of $0.75\,^{\circ}\text{C}$ and 3.16 in winter, $0.98\,^{\circ}\text{C}$ and $4\,^{\circ}\text{C}$ in spring, $1.06\,^{\circ}\text{C}$ and $4.05\,^{\circ}\text{C}$ in summer and $0.90\,^{\circ}\text{C}$ and $3.60\,^{\circ}\text{C}$ in autumn. As for Sim_{T,RH}, weaker changes appear in the area situated below the thermocline in summer and fall, with minima of $0.52\,^{\circ}\text{C}$ (Sim_{T_1}) and $2.35\,^{\circ}\text{C}$ (Sim_{T_4}). The warming of the water temperature due to an increase of $1\,^{\circ}\text{C}$ or $4\,^{\circ}\text{C}$ in air temperature produces seasonal ratios through the column that ranges from 3.8 to 4.6. Smallest ratios are found above the thermocline. Furthermore, it is during summer and fall that the values lower than 4 were calculated, *i.e.*, in the first 10 m (Sim_{T_1}) and 8 m (Sim_{T_4}) below the surface. During these stratified periods, the highest ratio (> 4.4) are found in the metalimnion.

The monthly increase in $T_{\rm epi}$ varies between 0.70 °C (February) and 1.26 °C (March) for Sim_{T1} and between 3.01 °C (February) and 4.23 °C (July) for Sim_{T4} . Similarly, changes in $T_{\rm hyp}$, with

respect to the increase in air temperature, are of $0.64\,^{\circ}$ C to $0.69\,^{\circ}$ C and $2.81\,^{\circ}$ C to $2.97\,^{\circ}$ C for Sim_{T_1} and Sim_{T_4} , respectively.

2.3.3 Variability of light extinction coefficient on lake water temperature

The sensitivity of the light extinction coefficient on the thermal profiles has been tested on $Sim_{T,RH}$ by varying K_e in the range of \pm 25%. Deeper penetration of $S\downarrow$ in the lake, followed by a reduction of $K_{\rm e}$, increased water temperature with depth and reduced it at the surface. However, changes in water temperature through the profile for a low K_e (- 25%) are only significant above 30 m and for all seasons except during winters. Below 30 m and as in winter, mean temperatures change (compared to the reference simulation) by less than 0.1 °C. In spring, summer and fall, the highest temperature increase with depth is simulated at 12 m (0.09°C), at 11 m (0.81°C) and 16 m (0.64°C). The decrease in near-surface temperature is mainly observed in spring and summer and affects the first 5 - 6 m below the surface (respectively - 0.14 °C and - 0.26 °C at the most). A maximum decrease of 0.49 °C is simulated at the surface in August. In fall, temperatures are even warmer in the surface layers, probably due to mixing processes appearing between the hypolimnic (warmer with respect to the reference simulation) and epilimnic layers. On the contrary, near-surface water temperatures increase at the expense of deeper layers under an increase in K_e . Again, variations of water temperature are observed only in the first 25 m of the profile and in summer and fall. Outside those periods, seasonal changes are less than 0.05 ℃. The strongest decrease in temperature (- 0.86 °C) is simulated at 9 m in summer and at 14 m in fall (- 0.34 °C). The temperature increase observed in the near-surface water reaches 0.22 °C at maximum (surface layer). On a daily average, temperatures increase exceeds occasionally 0.7 °C in August.

Variability in $T_{\rm epi}$ is balanced by the fact that $z_{\rm lim}$ lie much deeper than the increase (- 25% $K_{\rm e}$) / decrease (- 25% $K_{\rm e}$) in near-surface temperature. Depending on $K_{\rm e}$ variability, the maximum monthly differences between simulations with maximum range of variation (± 25%) are of 0.33 °C in $T_{\rm epi}$ and 0.05 °C in $T_{\rm hyp}$.

2.3.4 Variability of wind speed on lake water temperature

Changes in wind speed, as simulated by HIRHAM, are expected to be small in the future according to the IPCC A2 scenario. The mean annual difference is 0.01 m s⁻¹ and no significant bias appears through the months (Table 2.3). Since Δv is rather not significant, the decile method could not be applied on this variable. However, sensitivity of water temperature profiles to variations of \pm 20% of ν has been tested on Sim_{T,RH}.

Under stronger wind conditions, the onset of the stratification is delayed (1 weak on average) and, once established, strength of the statification is weaker (1.5 x in summer) and the thermocline is lowered by 3 m on average. Compared to $Sim_{T,RH}$, the profiles are warmer, except in the upper layers in spring, summer and autumn. The additional increase in the seasonal temperature profiles varies between $0.6\,^{\circ}\text{C}$ and $0.86\,^{\circ}\text{C}$ in winter, and rises to $0.67\,^{\circ}\text{C}$ (45 m) in spring, $1.9\,^{\circ}\text{C}$ (20 m) in summer and $2\,^{\circ}\text{C}$ (30 m) in fall. In the upper layers, the cooling is particularly important in summer (- $0.98\,^{\circ}\text{C}$) and fall (- $0.21\,^{\circ}\text{C}$). The downward shift of the thermocline from the onset to the destratification is larger than in $Sim_{T,RH}$. It stands 1 m deeper than in $Sim_{T,RH}$ in summer and 7 m in fall.

Weaker winds produce an opposite effect. The thermocline is thus established earlier (1 week) and the stratification becomes stronger (1.5 x in summer). Less wind leads to a thermocline 3 m on average closer to the surface than in $Sim_{T,RH}$ and to a reduction of heat penetration. Compared to $Sim_{T,RH}$, this latter leads to an overall cooling of the water temperature profile. Negative changes lie within 0.71 °C and 1 °C in winter or vary between no difference (where the thermoclines meet) and 0.26 °C in spring (36 m), 2.3 °C m in summer

(16 m) and 2.5 °C in fall (24 m). The downward movement of the thermocline is very smooth and temperature gradient lasts longer. The thermocline is located 1 m shallower than in Sim_{T,RH} in summer and 5 m in fall. Heat that accumulates in the upper layers during the stratified period warms the water up to 0.26 °C, 0.89 °C and 0.25 °C in spring, summer and fall.

A 20% increase of the wind speed in $Sim_{T,RH}$ cools T_{epi} only during the stratified months and inversely following a reduction of the wind speed. Thus T_{epi} may decrease by $0.02\,^{\circ}\text{C}$ (April) to $1.12\,^{\circ}\text{C}$ (July) or increase by $0.24\,^{\circ}\text{C}$ (October) to $1.06\,^{\circ}\text{C}$ (July). During the coldest months, due to missing or low stratification, T_{epi} evolves with respect to T_{hyp} Variability of T_{hyp} ranges between $0.6\,^{\circ}\text{C}$ and $0.75\,^{\circ}\text{C}$ for higher wind speed and $0.7\,^{\circ}\text{C}$ and $0.84\,^{\circ}\text{C}$ for lower wind speed.

2.3.5 Variability of cloud cover on lake water temperature

Cloud cover changes expected in the future are small ($\Delta C < 0.02$). The trend shows a slight increase in C during the winter month and a clearer sky the rest of the year. Similarly, as for v, variations were not sufficiently large to allow the decile method to be applied. Sensitivity to variations of C was assessed by running $\mathrm{Sim}_{\mathsf{T},\mathsf{RH}}$ with the C variable increased and then decreased by 10%. The lake temperatures did not vary significantly in changes up to 10%. An increase or a decrease of the C warmed or cooled the seasonal water temperature by 0.14 $^{\circ}$ C to 0.17 $^{\circ}$ C and 0.13 $^{\circ}$ C to 0.16 $^{\circ}$ C from 18 m down to the bottom with respect to $\mathrm{Sim}_{\mathsf{T},\mathsf{RH}}$. Variability increased in the upper layer: the largest changes were observed at the surface in spring (+ 0.22 $^{\circ}$ C / - 0.20 $^{\circ}$ C) and the smallest in fall (+ 0.14 $^{\circ}$ C / - 0.12 $^{\circ}$ C).

Changes evolve symetrically in $T_{\rm epi}$ and in $T_{\rm hyp}$ with respect to the increase and decrease of C. Thus, the monthly amplitude went from 0.24 °C (September) to 0.42 °C (May) in $T_{\rm epi}$ and were equal to 0.30 °C in $T_{\rm hyp}$.

2.3.6 The decile method with a linear increase vs a constant Δ .

The effects of a constant increase of atmospheric perturbations on the simulated water temperatures were estimated when both the temperature and relative humidity (Sim_{T,RH,1}) were allowed to change. Simulated profiles with λ_1 (Fig. 2.8) were averaged per decade at each depth to produce 13 decadal profiles. Each decadal profiles DP_i (i=[1,..., 13]) obtained using λ_1 were compared to the last decadal mean profile simulated with λ_i (LDP). Water temperature from Sim_{T,RH,1} rapidly increased during the simulation, so that the maximum water temperature difference between DP₂ and LDP (Fig. 2.12) was of only 0.8 °C. Then, the difference between both DP_3 and DP_4 and LDP became even smaller. However, compared to the LDP, water temperatures were slightly overestimated above 13 m and 80 m respectively and still underestimated below. From DP5, values at each depth fluctuated around those averaged in the *LDP* and the mean error to the *LDP* was - 0.039 °C ± 0.06 °C at the depth where the maximum difference occurs, i.e., 12 m. The lake may thus be considered as evolving towards a mean steady state after the fourth decade following the perturbation. As a consequence of the constant temperature change during the second decade, the lake energy budget became highly positive, 0.41 MJ day 1 m-2, and then fluctuated around zero on average. Compared to the reference simulation, there is even a mean energetic loss of 0.0279 MJ day⁻¹ m⁻² from DP_3 to DP_{12} . Simulations with λ_1 are almost identical to LDP during the last decade where the same values are driving the model. A maximum difference of 0.019 °C is recorded at the bottom whereas the minimum (0.02 °C) is observed at the surface.

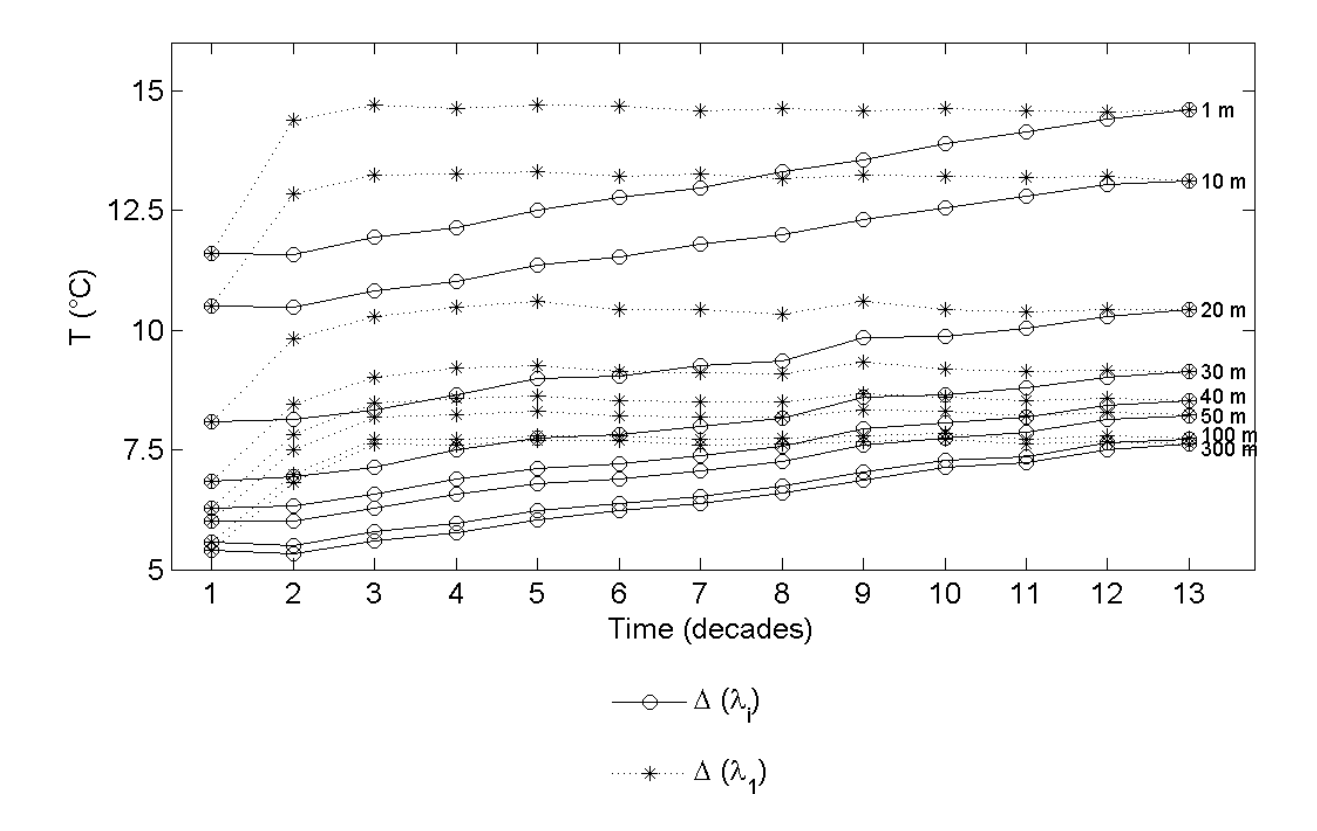


Figure 2.12. Mean decadal temperature profiles obtained from the 130-year perturbed simulations $Sim_{T,RH}$ and $Sim_{T,RH,1}$.

2.4 Discussion

The pseudo-random weather generator is a useful tool to drive the lake model in order to investigate the evolution of water temperature over periods that are longer than historical meteorological records. Moreover, the similarity between water temperature profiles produced by the reference simulation over decades shows that the generator is able to reproduce long and realistic datasets.

The decile method that has been applied to perturb the pseudo-random series used to drive the SIMSTRAT lake model indicates that warming of the thermal profiles is likely to occur, whether T or both T and RH are used. Compared to the reference simulation, a run using modified conditions warms the whole water column. This is caused by an increase in the surface longwave budget L^* and a decrease in heat lost by sensible heat Q_h . The cooling by stronger evaporation cannot compensate the positive flux towards the lake, thus producing a mean energy gain of 0.036 MJ day⁻¹ m⁻² (Δ applied to T) and 0.0273 MJ day⁻¹ m⁻² (Δ applied to T and RH) over the 110 years period. However, changes in surface water temperature induced by the reduction of RH, as predicted by the HIRHAM model under future condition at the grid point over Lake Geneva, were significantly different from Sim_T outputs, leading to a decrease in water temperatures. Comparison of water temperature profiles from Sim_T and $Sim_{T,RH}$ revealed differences at all depths, particularly important in T_{epi} where it may reach 1.5 °C in August. The cooling that follows this decrease in RH is caused by a reduction of L* as well as by an increase in the loss of heat by evaporation. Interestingly enough, an increase in surface temperature according to Sim_T leads to less evaporation than a simulation producing lower water surface temperature. This is due to a smaller water vapour

deficit at the air-lake interface in Sim_T , indicating that changes induced by a decrease in RH have a larger impact on the rate of evaporation than the increase in surface temperature only. The way the energy exchanges at the lake-atmosphere interface are affected by changes in saturation properties of air reveals the need to include this component in the simulations. A shift appears between the months during which data were most severely modified with respect to drier conditions and the maximum differences simulated in $T_{\rm epi}$, *i.e.*, one month on average. Therefore, the perturbation specified on a monthly basis seems to be a crucial component and should not be omitted when seasonal and monthly variability is concerned.

It has been shown that the sensitivity in daily profiles to the values of $K_{\rm e}$ (± 25%) in the future is only significant at certain depths. The seasonal increase (+ 25% $K_{\rm e}$) vs decrease (- 25% $K_{\rm e}$) in near-surface layers water temperature produce changes generally below 0.25°C. Also, seasonal variations in water temperature below 30 m are in any case below 0.1°C. At some depths above 30 m, the largest changes are simulated in the range of ±0.9°C for summer and between - 0.34°C (+ 25% $K_{\rm e}$) and 0.64°C (- 25% $K_{\rm e}$) for fall. In reality, these high differences result from changes in the depth of the thermocline (deeper when $K_{\rm e}$ is reduced) and not from strong variations in the water temperature profiles. Monthly changes lie within 0.2°C for $T_{\rm epi}$ and 0.05°C for $T_{\rm hyp}$. Therefore $T_{\rm epi}$ and $T_{\rm hyp}$ would remain essentially unchanged even though $K_{\rm e}$ vary within those limits in the future.

HIRHAM outputs indicate that T and Td are expected to change in the future according to the IPCC A2 warming scenario. However, the sensitivity performed with the other driving variables, v and C, show that the response of the lake would be significatively different. Actually, changes would concern only v. In effect, sensitivity of Lake Geneva to variations in C (± 10%) implies monthly changes lower to 0.22 °C in $T_{\rm epi}$ and 0.16 °C in $T_{\rm hyp}$. The largest seasonal change, observed at the surface, is of $0.22 \,^{\circ}$ C only. On the contrary, variations of vmay induce seasonal changes of at least 0.6°C through the column under unstratified conditions and changes reaching up to 2°C below the thermocline during the stratified period. At the surface, where temperature changes are inversed compared to those below the thermocline, differences may be higher than 0.89 °C. The evolution of the lake waters is strongly related to the behaviour of the thermocline. In fact, a 20% increase in v is sufficient to delay the formation of the thermocline and weaken the stratification in Lake Geneva. As a consequence, surface waters heated in spring mix easily with deeper waters, thereby warming deeper layers of the column at the expense of surface waters, and fostering the development of a deep thermocline, 3 m deeper than current. This latter also serves to explain the large shift in temperatures observed in summer and fall. During the stratified period, less stability also eases heat exchanges between the epilimnion and the hypolimnion, providing heat to deeper layers. A reduction of 20% in v would imply reverse processes, and thermal effects of the same order. Large monthly amplitudes in $T_{\rm epi}$ (2.18°C) and $T_{\rm hyp}$ (1.60 °C) resulting from ± 20% change of v emphasis the need to be careful when assessing the impact of climate change on such a large water body.

Sim_{T,RH} produces a strong increase in $T_{\rm epi}$ that lies generally below that of the air temperatures, generally given by the smallest monthly ΔT . However, one exception is observed in March when the increase in $T_{\rm epi}$ exceeds the increase in air temperature of the ninth highest value of monthly ΔT . This suggests that even though ΔT are the smallest during this month for all classes and shift in $T_{\rm epi}$ the lowest, the mixing of epilimnic water with part of hypolimnic water volume as well as the short duration of colder conditions prevent intensive cooling of surface waters, keeping the entire water column close to mean hypolimnic temperatures. The shift in surface water temperatures during the coldest periods is then related more to minimum monthly $T_{\rm hyp}$ than to the increase in air temperature. The monthly increases in $T_{\rm epi}$ simulated in this study are slightly less than the average annual increase in air temperature (3.9 °C) and, with the exception of March, represent 55 - 98% of the increase in monthly mean air temperature. From mid-May to mid-June, water surface temperatures may even exceed the average annual air temperature increase. This conclusion is in close

agreement with the results from many studies that concluded also to a higher warming in air temperature than in epilimnic temperature (Hondzo and Stefan 1993; Stefan *et al.* 1993; DeStasio *et al.* 1996; Peeters *et al.* 2002; 2007). Similar predictions have drawn similar conclusions for Lake Constance, located between Switzerland and Germany (Peeters *et al.* 2007). In the latter, epilimnic temperatures are only slightly lower than the fixed increase of 4° C that perturbed a long time series of observed data whereas the increase observed in April may even exceed this threshold. However, monthly maximum increases in the epilimnic temperatures are not predicted at the same time in Lake Constance (April) and Lake Geneva (August). Since the highest perturbations are applied in August to Lake Geneva, it is likely that those differences arise from the monthly Δ T used.

Unlike earlier studies (Robertson and Ragotzkie 1990; Hondzo and Stefan 1991; DeStasio *et al.* 1996; Stefan *et al.* 1998) that predicted a slight increase in the bottom water temperatures and in some cases, even a decrease, simulations of Lake Geneva temperature profiles indicate that the warming may be strong and even exceed 2.3 °C in *T*_{hyp.} This finding is similar to results predicted for other peri-alpine deep lakes, such as Lake Constance (Peeters *et al.* 2007) and Lake Zurich (Peeters *et al.* 2002). In those lakes, a fixed 4 °C increment to air temperature records raised the hypolimnion temperatures at all seasons inducing a mean difference exceeding 2 °C and of 1.4 °C respectively. In order to explain this trend that is observed in monomictic lakes, Peeters *et al.* (2002) assumes that complete mixing that may potentially occur in the future will not cool the bottom temperature of monomictic lakes to values lower than the minimum epilimnic temperatures. Since the minimum epilimnic temperatures are expected to increase, hypolimnic temperatures will also increase in accordance with the trend observed during the coldest part of the year.

Lake stability has been studied by many authors with respect to perturbations in air temperature and wind speed for example (Hondzo and Stefan 1991; 1993, DeStasio 1996; Stefan et al. 1998). These studies generally agree on a more intense stratification. Consistency with those assumptions is found in Lake Geneva, since the warming of the whole water column is stronger for $T_{\rm epi}$ than for $T_{\rm hyp}$. Temperature difference may reach + 0.88 °C. This hypothesis is reinforced by the higher $N^{\rm e}$ values that have been calculated for the future conditions. As a consequence of this higher stability, the penetration of heat decreases. As a matter of fact, heat is stored in the upper layers and rises the temperatures of surface waters, thus leading to a differential warming of the water column (Fig. 2.9). Succession patterns of daily profiles highlights a lower metalimnion where the expected increase in water temperature was less important than the smallest changes observed in the hypolimnion. In fact, strenghtening of the stratification in the future may impact strongly on metaliminic properties. A higher stability may reduce epi-hypolimnic heat exchanges compared to today's regime. This point may be relevant for species that would be more temperature dependent than stability or light penetration dependent. However, the persistence of $T_{\rm epi}$ in late winter below $T_{\rm hyp}$ under a warmer climate as well as a similar increase in epilimnic and hypolimnion temperatures in March suggests that overturns might still occur occasionally (Fig. 2.10), or at least as frequently as today. The period of time for which T_{epi} is less or equal to T_{hyp} is expected to be reduced, thus impacting on the events of partial or complete turnover. Likewise, frequency of complete mixing in some deep lakes (projected to become monomictic, if not already the case) is expected to decrease and the period of mixing to be of shorter duration (Croley 1994; Peeters et al. 2002).

Changes in the duration of summer stratification (> 3 weeks) match the predictions of many other authors (Robertson and Ragotzkie 1990; Boyce *et al.* 1993; Stefan *et al.* 1996; Stefan *et al.* 1999). In Lake Geneva, the increase in the period of stratification is almost equally due to changes at the start and end of stratification.

Sensitivity of Lake Geneva to a constant increase of air temperature, as deduced from Sim_{T4}, may serve as a tool to evaluate what the more complex decile method has brought to the prediction of water thermal profiles. This assessement is allowed since the mean annual temperature difference between HIRHAM current and future data is of 4°C. The comparison

between water temperature profiles simulated by Sim_{T4} and Sim_T shows that the differences can largely be attributed to variabilities of ΔT . An increase of $4^{\circ}C$ is higher than any ΔT calculated by the decile method from February to April, and lower to at least the third smallest increment from July to October. As a result, Sim_{T4} overestimates T_{eoi} before the onset of stratification whereas the warming is much too low at time of stratification (< 1.5 ℃ in August and September). Even though less heat accumulates in $T_{\rm epi}$ in summer, the lack of variability of ΔT in early spring contributes to the more intense warming of T_{hyp} (+ 0.3 °C) and to the reduction of the mixing period duration. Furthermore, sensitivity of Lake Geneva to various increases in air temperatures has shown that linearities in the thermal response of the lake exist. The ratio deduced from respective changes in water temperature due to an increase of 4°C and 1°C in air temperatures, is of 4.1 ± 0.3, at any time and any depths, with the exception of the metalimnion. Here, the slight nonlinearities can be explained by the shallower position of the thermocline during the stratified month simulated for a 1 °C increase in air temperature. Even though the stratification is also weaker, the shallower thermal gradient reduces the depth of heat penetration. This analysis confirms the strong link that exists between the increase in air and water temperature and the need to include at least the monthly variations.

Whether climate change is applied abruptly or progressively to atmospheric data driving the lake model, the resulting water temperature profiles as well as energy budgets are very similar. However, data perturbed according to λ_1 provided during the first perturbed decade slightly more energy to the lake than the total amount added over the 11 decades when data are perturbed progressively. The overestimated temperatures in the upper waters and underestimated temperature in the lower waters for former decades indicate that the lake needs more than a decade to equal values of the LDP. The continuous multi-decadal energy loss thus reduces the high amount of energy obtained during the first perturbed decade (for the λ_1 simulation) over the following decades up to a steady state. Lake Geneva reacts guite rapidly to a change in weather conditions. For a lake as deep as Lake Geneva, at least four decades are required to reach a steady state. Impacts on the water temperature profiles of modified meteorological data produce realistic results from the fourth perturbed decade onwards. This is true even though it is only from the eight perturbed decade that the mean energetic balance equals the one of LDP. While the goal is to estimate the increase in water temperature by the end of the century, the insignificant bias between profiles obtained using λ_1 or λ_i (< 0.014°C) reveals that both methods can be used as long as the simulation with λ_1 is run over a sufficiently long period.

2.5 Conclusion

This study has investigated the evolution of Lake Geneva water temperature profiles under conditions of global warming using the one-dimensional lake model SIMSTRAT. Long simulations are required to take heat storage into account in the deep hypolimnion and to accurately assess future water temperatures profiles. A 130-year simulation has thus been undertaken with variables representative of the current period and others perturbed according to expected changes in monthly distribution.

The statistical method used to produce meteorological datasets has been shown to represent a reasonable alternative when long term historical records are missing. Moreover, this technique randomly produces extreme events or particular periods over the period and removes those that would appear spuriously if only observed data were used. During its development process, it has been shown that variability of the wind on the accuracy of simuled temperature profiles is essential.

The runs done over a large number of years allow to track the heat accumulation in the deep hypolimnion and to have a measure of confidence regarding the projected changes at the bottom. However, this study has shown that 40 years are required to stabilize the heat exchange at the lake-atmosphere interface and to obtain accurate temperature changes throughout the water column when a constant perturbation is applied to current data.

The decile method developed in this paper to reproduce future climate from RCM outputs superimposed on the observed data has proven genuine skill to drive the lake model. This method accounts not only for changes in the mean but also in the different parts of the probability density function, such as maxima and minima. It should be noted that changes presented here result from projections provided by the HIRHAM RCM only; the mean annual difference in temperature simulated by this RCM (3.9 °C at grid point over Lake Geneva) lies within the range of values defined by other RCMs for Europe under the A2 scenario (Déqué et al. 2005; Alcamo et al. 2007; Beniston et al. 2007). Therefore, the thermal response of the lake can be considered as a good approximation of the mean increase projected by a set of RCMs.

The sensitivity of the water temperature profiles to the meteorological variables as drivers of climate change demonstrated the need to include more than just the temperature. The water temperature increases which result from the perturbation of T and RH is significant, exceeding $4\,^{\circ}\text{C}$ at the surface, and reaching $3.83\,^{\circ}\text{C}$ in the epilimnion and $2.33\,^{\circ}\text{C}$ in the hypolimnion.

It is likely that these increases will impact on the ecosystem of Lake Geneva. Based on these findings, rigorous investigations of climate change impacts on various aspects of lake ecological systems need to be addressed. Among them, special attention should be given to the frequency of occurrence of harmful algal blooms, such as the cyanobacteria *Planktothrix* Rubescens that has been observed in Lake Geneva (Jacquet et al. 2005). As a result of higher temperatures, increased stability of the water column and reduction of the vertical turbulent mixing, lakes and particularly eutrophic lakes are likely to be more regularly affected in the future by these toxic algae (Jöhnk et al. 2008; Roelke and Buyukates 2002; Kanoshina et al. 2003; Shatwell et al. 2008). Changes in vertical mixing within the water column relating to thermal stratification are extremely important as they are usually accompanied by changes in the availability of nutrients and light (Anneville et al. 2005; Winder and Hunter 2008). Therefore, findings from this study could also suggest ways to assess the timing of the phytoplankton spring bloom, growth capacity of phytoplankton and changes in phytoplanktonic communities. To study the possible responses of aquatic ecosystems to a warmer climate, the complexity of processes and exchanges taking place through the water column also implies that a coupled ecological model needs to be used.

2.6 Acknowledgments

We would like to thank Martin Beniston for the helpful discussions, valuable suggestions in preparing this paper and also for proof-reading the manuscript.

We also wish to thank the EU-PRUDENCE project for online data availability (http://prudence.dmi.dk/). We also thank the reviewers for their comments on this manuscript.

2.7 Appendix

Steps in the development of pseudo-random meteorological data generation extending the series from 10 years to 130 years

Step 1: All values taken by a variable from 1981 to 1990 at 0000 UTC, x_{i0} (i=[T, v, RH, dir] and 0 = 0000 UTC)), for each day at a particular month are selected and sorted out to determine the shape of the distribution (Fig. a1).

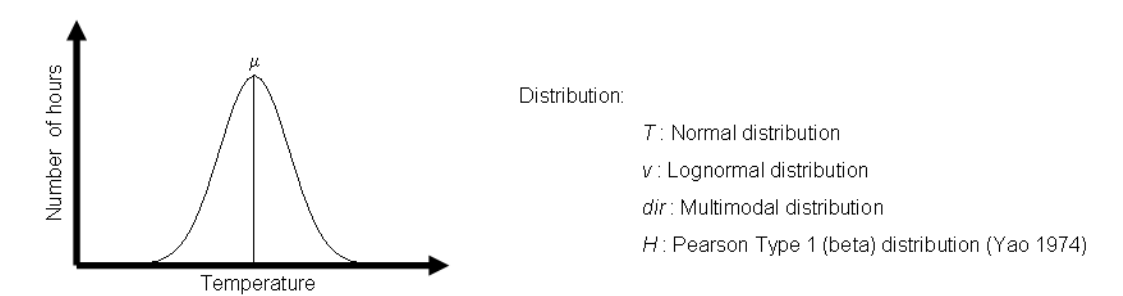


Figure a1: Temperature normal distribution function over the period 1981 - 1990 at 0000 UTC for a particular month.

Step 2: A value of m_i is then randomly selected according to the distribution curve defined in step 1 and is given the value m_{i0} (Fig. a2). For instance, a normal distribution would increase the probability to have a m_{i0} close to the mean μ .

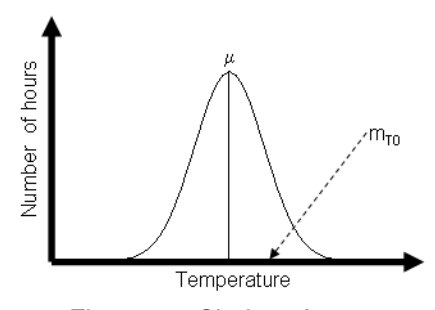


Figure a2: Choice of a temperature value for m_{T0} according to the distribution function defined in Figure a1.

Step 3: Values at 0100 UTC are strongly dependent of the data at 0000 UTC, those at 0200 UTC of data at 0100 UTC and so on. Unfortunately, the recurrence of this approach (step 1 and step 2) from one hour to the next is not adequate as it would artificially increase intra-day variability. Therefore, the classification method suitable for the distribution at 0000 UTC partitions the values in different classes. All data at 0000 UTC that stands in the same class as m_{i0} (Fig. a3) are found and serve to select their respective value at 0100 UTC.

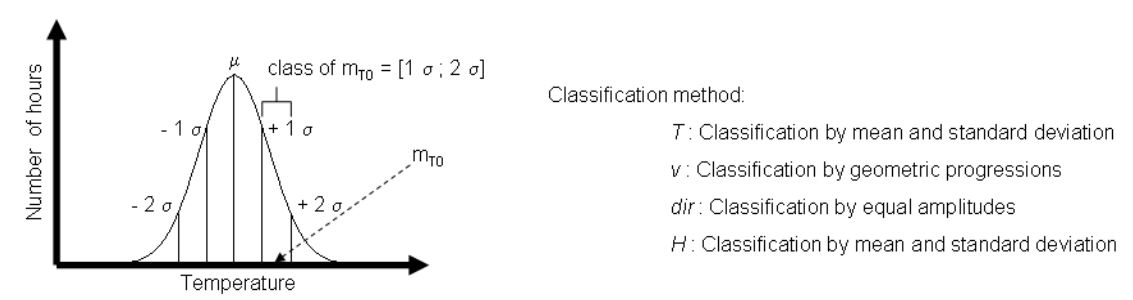


Figure a3: Selection of values that stand in the same class as m_{T0}.

Step 4: The selected values at 0100 UTC compose a new dataset, DS_1 (1 for 0100 UTC) (Fig. a4). The random selection of a value for 0100 UTC, m_{T1} , must consider the new distribution curve of DS_1 . In DS_1 , T still follow a normal distribution (normality test of Kolmogorov-Smirnov, Massey 1956) but distributions for v, dir and RH are more chaotic and not related to the original distribution. While a pseudo-random value drawn from normal distribution in DS_1 is given to m_{T1} , statistical properties of the other variables serve at bordering the range of possible random values. The procedure for T (step 3 and 4) is repeated for the following hours, which means that each m_i is evaluated according to the condition that precedes it.

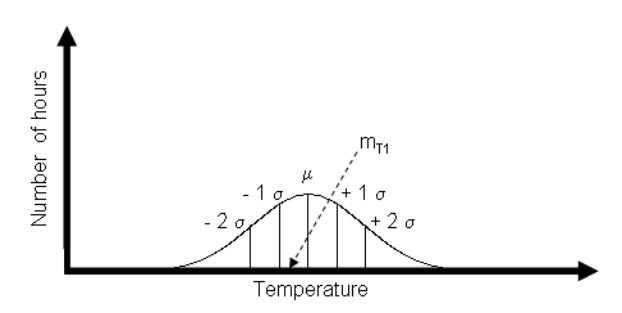


Figure a4: Choice of a temperature value for m_{T1} according to the temperature distribution curve of DS_1 .

A set of techniques are tested in order to find values for $m_{\text{V1-23}}$ and $m_{\text{RH1-23}}$ that reasonably reproduce the μ D, the σ IAD and the σ IED. These include the random selection of a number over a uniform distribution limited by the minimum and maximum or by the $\mu \pm 1,1.1,...,2$ σ of DS₁, or over a normal distribution defined by parameters of DS₁. The same procedure is applied to the following hours on the basis of the value selected at the preceding hour. The best results are obtained when $m_{\text{V1-23}}$ is drawn randomly from a uniform distribution in the range $\mu \pm 1.6\sigma$ (Fig. 2.4) and $m_{\text{RH1-23}}$ from a normal distribution (Fig. 2.4). The selection method for RH has been adopted since more than 90% of the DS₁₋₂₃ follow a normal distribution.

The approach is different for $m_{\rm dir1-23}$ as wind direction does not follow any regular daily pattern. $m_{\rm dir0}$ is randomly chosen between 0° and 360° and $m_{\rm dir1}$ is selected according to the probability of occurrence after a given $m_{\rm dir0}$. Directions are then partitioned in 16 classes and those to whom $m_{\rm dir0}$ and $m_{\rm dir1}$ belong are defined. Then, the succession of these two classes of directions is searched during the month and $m_{\rm dir2}$ is pseudo-randomly selected based on the occurrence probabilities of each class after such a configuration. The same pattern is then extended to $m_{\rm dir3-23}$.

2.8 References

- Alcamo, J., J.M. Moreno, B. Nováky, M. Bindi, R. Corobov, R.J.N. Devoy, C. Giannakopoulos, E. Martin, J.E. Olesen, and A. Shvidenko. 2007. Europe. In: M.L. Parry, O.F. Canziani, J.P. Palutikof, P.J. van der Linden and C.E. Hanson (eds), Climate Change 2007: Impacts, Adaptation and Vulnerability. Contribution of Working Group II to the Fourth Assessment Report of the Intergovernmental Panel on Climate Change, Cambridge University Press, Cambridge, pp. 541-580.
- Anneville, O., S. Gammeter, and D. Straile. 2005. Phosphorus decrease and climate variability: mediators of synchrony in phytoplankton changes among European perialpine lakes. Freshw. Biol. 50: 1731-1746.
- Bantle, H. 1989. Programmdokumentation Klima-Datenbank am RZ-ETH Zürich. MeteoSwiss Publication, Zürich.
- Beniston, M., D. B. Stephenson, O. B. Christensen, C. A. T. Ferro, C. Frei, S. Goyette, K. Halsnaes, T. Holt, K. Jylhä, B. Koffi, J. Palutikoff, R. Schöll, T. Semmler, and K. Woth. 2007. Future extreme events in European climate; an exploration of Regional Climate Model projections. Clim. Change 81: 71-95.
- Bennett, J. R. 1978. A three-dimensional model of Lake Ontario's summer circulation: II. A diagnostic study. J. Phys. Oceanogr. 8: 1095-1103.
- Burchard, H., and H. Baumert. 1995. On the performance of a mixed layer model based on the k-e turbulence closure. J. Geophys. Res. 100: 8523-8540.
- Boyce, F.M., P.F. Hamblin, L.D. Harvey, W.M. Schertzer, and R.C. McCrimmon. 1993. Response of the thermal structure of Lake Ontario to deep cooling water withdrawals and to global warming. J. Great Lakes Res. 19: 603-616.
- Christensen, J.H., and O.B. Christensen. 2003. Severe summertime flooding in Europe. Nature 421: 805-806.
- Christensen, O. B., J. H. Christensen, B. Machenhauer, and M. Botzet. 1998. Very high-resolution regional climate simulations over Scandinavia Present climate. J. Climate 11: 3204-3229.
- Coats, R., J. Perez-Losada, G. Schladow, R. Richards and C. Goldman. 2006. The warming of Lake Tahoe. Clim. Change 76: 121-148. doi: 10.1007/s10584-005-9006-1.
- Croley, T. E. 1994. Hydrological impacts of climate change on the Laurentian Great Lakes. Trends in Hydrology 1: 1-25.
- De Stasio, B. T., D. K. Hill, J. M. Kleinhans, N. P. Nibbelink, and J. J. Magnuson. 1996. Potential effects of global climate change on small north-temperate lakes: Physics, fish and plankton. Limnol. Oceanogr. 41: 11361149.
- Déqué, M., R. G. Jones, M. Wild, F. Giorgi, J. H. Christensen, D. C. Hassell, P. L. Vidale, B. Rockel, D. Jacob, E. Kjellström, M. de Castro, F. Kucharski, and B. van den Hurk. 2005. Global high resolution versus Limited Area Model climate change projections over Europe: quantifying confidence level from PRUDENCE results. Clim. Dynam. 25: 653-670.

- Dokulil, M. T., A. Jagsch, G. D. George, O. Anneville, T. Jankowski, B. Wahl, B. Lenhart, T. Blenckner, and K. Teubner. 2006. Twenty years of spatially coherent deepwater warming in lakes across Europe related to the North Atlantic Oscillation, Limnol. Oceanogr. 51: 2787-2793.
- Fang, X., and H. G. Stefan. 1996. Projections of potential climate change effects on water temperature, dissolved oxygen and associated fish habitat in small lakes of the contiguous U.S., Vol. I Effects of past climate conditions. Project Report 393. St. Anthony Falls Laboratory, University of Minnesota, Minneapolis.
- Fang, X., and H. G. Stefan. 1999. Projection of climate change effects on water temperature characteristics of small lakes in the contiguous U.S. Clim. Change 42: 377-412.
- Fischlin, A., G. F. Midgley, J. T. Price, R. Leemans, B. Gopal, C. Turley, M. D. A. Rounsevell, O. P. Dube, J. Tarazona, A. A. Velichko. 2007. Ecosystems, their properties, goods, and services. In: M.L. Parry, O.F. Canziani, J.P. Palutikof, P.J. van der Linden and C.E. Hanson (eds), Climate Change 2007: Impacts, Adaptation and Vulnerability. Contribution of Working Group II to the Fourth Assessment Report of the Intergovernmental Panel on Climate Change, Cambridge University Press, Cambridge, pp. 211-272.
- Gerdeaux, D. 2004. The recent restoration of the whitefish fisheries in Lake Geneva: the roles of stocking, reoligotrophication, and climate change. Ann. Zool. Fennici 41: 181-189.
- Gillet, C., and P. Quetin. 2006. Effect of temperature changes on the reproductive cycle of roach in Lake Geneva from 1983 to 2001. J. Fish. Biol. 69: 518-534.
- Goudsmit, G.-H., H. Burchard, F. Peeters, and A. Wüest. 2002. Application of k-ε turbulence models to enclosed basins: The role of internal seiches. J. Geophys. Res. 107: 3230-3243. doi: 10.1029/2001JC000954.
- Goyette, S., N. A. McFarlane, and G. Flato. 2000. Application of the Canadian Regional Climate Model to the Laurentian Great Lakes Regions. Implementation of a Lake Model. Atmos. Ocean. 38: 481-503.
- Hambright, K.D., M. Gophen, and S. Serruya. 1994. Influence of long term climatic changes on the stratification of a tropical, warm monomictic lake. Limnol. Oceanogr. 39: 1233-1242.
- Henderson-Sellers, B. M., J. McCormick, and D. Scavia. 1983. A comparison of the formulation for eddy diffusion in two one-dimensional stratification models. Appl. Math. Model. 7: 212-215.
- Hodges, B., J. Imberger, A. Saggio, and K. B. Winters. 2000. Modeling basin-scale internal waves in a stratified lake. J. Limnol .Oceanogr. 45: 1603-1620.
- Hondzo, M., and H. G. Stefan. 1991. Three case studies of lake temperature and stratification response to warmer climate. Water Resour. Res. 27: 1837-1846.
- Hondzo, M., and H. G. Stefan. 1993. Regional water temperature characteristics of lakes subjected to climate change. Clim. Change 24: 187-211.
- Hostetler, S. W., and P. J. Bartlein. 1990. Simulation of lake evaporation with application to modelling lake-level variations at Harney–Malheur Lake, Oregon. Water Resour. Res. 26: 2603-2612.

- Imberger, J., J. C. Patterson, B. Hebbert, and I. Loh. 1978. Dynamics of reservoir of medium size. J. Fluid Mech. 78: 489-512.
- IPCC. 2001. Climate Change 2001: The Scientific Basis, vol. 1. The Third Assessment Report of the Intergovernmental Panel on Climate Change (IPCC). University Press, Cambridge.
- IPCC. 2007. Climate Change 2007: The Physical Science Basis. Contribution of Working Group I to the Fourth Assessment Report of the Intergovernmental Panel on Climate Change. S. Solomon, Qin, D., Manning, M., Chen, Z., Marquis, M., Avery, K.B., Tignor, M. and Miller, H.L. (eds.), Cambridge University Press, Cambridge.
- Jacquet, S., J. F. Briand, C. Leboulanger, L. Oberhaus, G. Paolini, J. C. Druart, O. Anneville, and J. F. Humbert. 2005. The proliferation of the toxic cyanobacterium Planktothrix rubescens following restoration of the largest natural French lake (Lake Bourget). Harmful Algae 4: 651-672.
- Jöhnk, K.D., J. Huisman, J. Sharples, B. Sommeijer, P. M. Visser, and J. M. Stroom. 2008. Summer heatwaves promote blooms of harmful cyanobacteria. Glob. Change Biol. 14: 495-512.
- Jungo, P., and M. Beniston. 2001. Change in the anomalies of extreme temperature anomalies in the 20th century at Swiss climatological stations located at different latitudes and altitudes. Theor. Appl. Clim: 69: 1-12.
- Kanoshina, I., U. Lips, and J.-H. Leppänen. 2003. The influence of weather conditions (temperature and wind) on cyanobacterial bloom development in the Gulf of Finland (Baltic Sea). Harmful Algae 2: 29-41.
- Kelley, J.G.W., J. S. Hobgood, K. W. Bedford, and D. J. Schwab. 1998. Generation of Three-dimensional lake model forecasts for Lake Erie. Weather and Forecasting. 13: 659-687.
- King, J. R., B. J. Shuter, and A. P. Zimmerman. 1997. The response of the thermal stratification of South Bay (Lake Huron) to climatic variability. Can. J. Fish. Aquat. Sci. 54: 1873-1882.
- King, J.R., B. J. Shuter, and A. P. Zimmerman. 1999. Empirical links between thermal habitat, fish growth and climate change. Trans. Am. Fish. Soc. 128: 656-665.
- Kraus, E.B., and J. S. Turner. 1967. A one dimensional model of the seasonal thermocline: II. The general theory of its consequences. Tellus 19: 98-106.
- Lazzarotto, J., and F. Rapin. 2007. Evolution physico-chimique des eaux du Léman. In: CIPEL (eds.), Rapp. Comm. int. prot. Eaux Léman contre pollut., Campagne 2006, pp. 33-57.
- Lazzarotto, J., F. Rapin, and C. Corvi. 2004. Physical—chemical changes and tests for metals and various micropollutants in the waters of Lake Geneva. In: CIPEL (eds.), Rapp. Comm. Int. prot. Eaux Léman contre pollut., Campagne 2003, pp. 31-58.
- Lazzarotto, J., P. Nirel, and F. Rapin. 2006. Evolution physico-chimique des eaux du Léman. In: CIPEL (eds.), Rapp. Comm. int. Prot. eaux Léman contre pollut., Campagne 2005., pp. 31-63.

- Livingstone, D. M. 2003. Impact of secular climate change on the thermal structure of a large temperate central European lake. Clim. Change 57: 205-225.
- Massey, F. J. 1956. The Kolmogorov-Smirnov Test for Goodness of Fit. J. Am. Stat. Ass. 46: 68-78.
- McCormick, M. J., and G.L. Fahnenstiel. 1999. Recent climatic trends in nearshore water temperatures in the St. Lawrence Great Lakes. Limnol. Oceanogr. 44: 530-540.
- Mironov, D. V. 2008. Parameterization of lakes in numerical weather prediction. Description of a lake model. COSMO Technical Report, No. 11, Deutscher Wetterdienst, Offenbach am Main, Germany, 41 pp.
- Mironov, D., E. Heise, E. Kourzeneva, B. Ritter, N. Schneider, and A. Terzhevik. 2009. Implementation of the lake parameterisation scheme FLake into numerical weather prediction model COSMO. Boreal Env. Res. 15: 218-230.
- Mortsh, L., and F. Quinn. 1996. Climate change scenarios for Great Lakes Basin ecosystems studies. Limnol. Oceanogr. 41: 903-911.
- Nakicenovic, N., J. Alcamo, G. Davis, B. de Vries, J. Fenhann, S. Gaffin, K. Gregory, A. Grübler, T. Y. Jung, T. Kram, E. L. La Rovere, L. Michaelis, S. Mori, T. Morita, W. Pepper, H. Pitcher, L. Price, K. Riahi, A. Roehrl, H.-H. Rogner, A. Sankovski, M. Schlesinger, P. Shukla, S. Smith, R. Swart, S. van Rooijen, N. Victor, and Z. Dadi. 2000. Special Report on Emissions Scenarios, Working Group III, Intergovernmental Panel on Climate Change (IPCC). Cambridge University Press, Cambridge.
- Orlob, G.T., and L. G. Selna. 1970. Temperature variations in deep reservoirs. J. Hydraul. Div. Proc. 96: 393-410.
- Peeters, F., D. Straile, A. Lorke, and D. M. Livingstone. 2007. Earlier onset of the spring phytoplankton bloom in lakes of the temperate zone in a warmer climate. Glob. Change Biol. 13: 1898-1909.
- Peeters, F., D. M. Livingstone, G.-H. Goudsmit, R. Kipfer, and R. Forster. 2002. Modeling 50 years of historical temperature profiles in a large central European lake. Limnol. Oceanogr. 47: 186-197.
- Perroud, M., S. Goyette, A. Martynov, M. Beniston, and O. Anneville. 2009. Simulation of multiannual thermal profiles in deep Lake Geneva: A comparison of one-dimensional lake models. Limnol. Oceanogr. 54: 1574-1594.
- Robertson, D.M., and R. A. Ragotzkie. 1990. Changes in the thermal structure of moderate to large sized lakes in response to changes in air temperature. Aquatic Sciences 52: 360-380.
- Roelke, D., and Y. Buyukates. 2002. The diversity of harmful algal bloom-triggering mechanisms and the complexity of bloom initiation. Hum. Ecol. Risk Assess. 7: 1347-1362.
- Schindler, D. W., S. E. Bayley, and B. R. Parker. 1996. The effect of climatic warming on the properties of boreal lakes and streams at the experimental lakes area, Northwestern Ontario. Limnol. Oceanogr. 41: 1004-1017.

- Shatwell, T., J. Köhler, and A. Nicklisch. 2008. Warming promotes cold-adapted phytoplankton in temperate lakes and opens a loophole for Oscillatoriales in spring. Glob. Change Biol. 14: 2194-2200.
- Stefan, H. G., and X. Fang. 1994. Dissolved oxygen model for regional lake analysis. Ecol. Model. 71: 37-68.
- Stefan, H. G., M. Hondzo, and X. Fang. 1993. Lake water quality modeling for projected future climate scenarios. J. Environ. Qual. 22: 417-431.
- Stefan, H. G., M. Hondzo, and X. Fang. 1996. Simulated long-term temperature and dissolved oxygen characteristics of lakes in the north-central United States and associated fish habitat limits. Limnol. Oceanogr. 41: 1124-1135.
- Stefan, H. G., X. Fang, and M. Hondzo. 1998. Simulated Climate Changes Effects on Year-round Water Temperatures in Temperate Zone Lakes. Clim. Change 40: 547-576.
- Stepanenko, V. M., and V. N. Lykosov. 2005. Numerical simulation of heat and moisture transport in the "lake-soil" system. Russian Journal of Meteorology and Hydrology 3: 95 104.
- Uhlmann, B., S. Goyette, and M. Beniston. 2009. Sensitivity analysis of snow patterns in Swiss ski resorts to shifts in temperature, precipitation and humidity under condition of climate change. Int. J. Climatol. 29: 1048-1055. doi: 10.1002/joc.1786.
- Winder, M., and D. A. Hunter. 2008. Temporal organization of phytoplankton communities linked to physical forcing. Oecologia 156: 179-192.
- Yao, A.Y.M. 1974. A statistical model for the surface relative humidity. J. Appl. Meteor. 13: 17-21. doi: 10.1175/1520-0450(1974)013.

Chapter 3

Interfacing a one-dimensional lake model with a single-column atmospheric model: Application to the deep Lake Geneva, Switzerland

Stéphane Goyette and Marjorie Perroud

Climatic Change and Climate Impacts (C³I), University of Geneva, Carouge, Geneva, Switzerland

Abstract

A novel Single Column Model (SCM) is described in this paper. As a test case, a onedimensional lake model employed in the framework of this SCM is applied to the deep Lake Geneva in Switzerland. This coupled model requires a minimal set of adjustable parameters to reproduce the local temperature, moisture and wind observations. It is interfaced with a one-dimensional k- ε lake model where few calibration parameters are needed to reproduce the evolution of the thermal profiles. The coupling interface between the lower atmosphere and the lake surface is also described. It involves the solar and infrared fluxes and the vertical components of turbulent fluxes of momentum, sensible and latent heat, as a function of the surface albedo and a drag coefficient. In addition, strong wind events, parameterized as a function of a prescribed wind profile based can be activated. Regarding the lake water temperature, one of the most important parameters is related to the simulation of the windspeed average and variability that impacts on the momentum transfer between the atmosphere and the surface water. This process influences the intensity of the lake upperlayer mixing and thus on the surface water temperature modulating the boundary-layer stability conditions. Consequently, the feedbacks between the lake and the lower atmosphere indicate that the simulated surface water and air temperature, and the windspeed respond in a non linear fashion to most of the model adjustable parameter values. A number of simulations have been performed to produce a sorted set of optimal model parameters that reproduces the mean and the variability of the seasonal evolution of the thermal profiles in the lake as well as those of the mean and the variability of the surface air temperature, moisture and windspeed. The lake water temperature is reproduced in a realistic manner using the optimal calibration parameter values with a seasonal- and depthaveraged error of 0.41°C in Summer, -0.15°C in Autumn, 0.01°C in Winter, and 0.27°C in Spring when compared to the lake observational database. Also, the errors of the seasonally-averaged simulated anemometer-level windspeed, screen-level air temperature and specific humidity to the station-derived values are 0.04 m s⁻¹, 1.04°C, and 0.74 g kg⁻¹, respectively.

Submitted to: Ecological Modelling

3.1 Introduction

As the horizontal resolution of numerical models of weather and climate increases, more demands are being made for access to accurate lower boundary conditions of inland fresh water body temperatures. Lake parameterizations for use in Numerical Weather Prediction (NWP) and Regional Climate Models (RCM) become an important issue when the surface computational grid includes a large number of individual "inland water" grid points. Different approaches and modes have been used to resolve the lake thermal regimes. In the so-called "stand-alone mode", i.e., when the forcing is provided by observations, one can afford a more detailed lake model to resolve the evolution of the water temperature profiles. However, efficiency becomes the major constraint for their use in the case of NWP and RCM models that exploit in practice the surface temperature only. Due to their finer horizontal grid spacing, thus allowing resolving a larger number of lakes, NWP models may use highly parameterized lake models using self-similarity of the temperature-depth profiles (Mironov 2008). On the other hand, RCMs employing a relatively coarse grid spacing, e.g. roughly 50-km in the case of the EU/FP5 project PRUDENCE (Christensen et al. 2002) and 25-km in the case of the EU/FP6 project ENSEMBLES (Hewitt and Griggs 2004), may use either Lagrangian-based models (Swayne et al. 2005), eddy-diffusion models (Hostetler et al. 1993) or a mixed-layer model (Goyette et al. 2000). More complex lake models, such as those based on turbulence kinetic energy production and dissipation (e.g., k-ε), are not yet implemented routinely in NWP models, nor in RCMs, due to the high computational costs involved. However, one of them has been tested in a stand-alone mode (Peeters et al. 2002) over a number of annual cycles with a realistic reproduction of thermal profiles; it was also noticed that simulations conducted with increased air temperatures produced an increase in lake water temperatures at all depths. The turbulence-based model SIMSTRAT (Goudsmit et al. 2002) has been tested with prescribed atmospheric forcing over lake Geneva, Switzerland for a 10-year period, and results show a very good agreement with observed thermal profiles (Perroud et al. 2009). Stand-alone forcing uses a prescribed atmosphere; therefore fluxes from the water surface cannot lead to changes in the atmosphere above. This technique proved useful in lake-model developments, but nonlinear effects between the atmosphere and the water body cannot be resolved, and may thus produce misleading results, as is the case for land-surface schemes forced by observations (e.g., Koster and Eagleson 1990).

In order to circumvent this problem, in addition to avoiding the computational load of an RCM, the use of a single-column model (SCM) provides a practical and economical framework for assessing the sensitivity of water temperature profiles to current and perturbed climatic conditions. SCMs that encompass a variety of approaches and hypotheses have proven useful in the development of physical parameterization of atmospheric processes, predominantly for clouds and radiation; for example convection in weather and climate models (Betts and Miller 1986), as well as the atmospheric solar and infrared radiation transfers (Stephens 1984). Using an SCM, Stokes and Schwartz (1994) studied the processes that influence atmospheric radiation; Randall et al. (1996) analysed the parameterization of convection and of cloud amount; lacobellis et al. (2003) and Lee et al. (1997) used such an approach to study and validate interactions of clouds with radiation parameterizations, and also to study nocturnal stratocumulus-topped marine boundary layers (Zhu et al. 2005); different cloud schemes have been compared within the framework of an SCM (Lohmann et al. 1999); Girard and Blanchet (2001) evaluated the impact of aerosol acidification on the lower ice crystal layer and humidity using an SCM. Other applications of SCMs include the sensitivity of a land surface scheme to the distribution of precipitation (Pitman et al. 1993), the development of a parameterization of rainfall interception (Dolman and Gregory 1992); Randal and Cripe (1999) proposed alternative methods for prescribing advective tendencies combined with a relaxation forcing that nudge the model's temperature and humidity towards observed profiles within the framework of an SCM; Ball and Plant (2008) compared different stochastic parameterizations in a SCM. Then, owing to the possible interactions between the atmosphere and the surface which cannot be reproduced with stand-alone experiments, Pitman (1994) assessed the sensitivity of a land-surface scheme to the parameter values using an SCM. A coupled atmosphere—ocean SCM has also been developed for testing tropical atmosphere-ocean interactions in tropical areas of the Pacific (Clayson and Chen 2002).

No SCM known to the authors has yet been coupled to lake models to simulate the long-term fresh water temperature profiles. An evaluation of the performance of such a coupled model is needed to assess the reliability of the coupling variables and fluxes at the model air-water interface of a number of lakes, such as the temperature and the windspeed, as well as of the various components of the energy budget.

Although the experimental configurations and applications of these SCMs have gained in complexity, most of them neglect or oversimplify the dynamical feedbacks of the atmospheric circulation. Such simplifications in SCMs reported in the literature, although making them computationally efficient, have introduced errors that may have confused and compromised their atmospheric prognostics, especially in the long term. Nevertheless, these SCMs are locatable over any part of the globe, principally if the parameterization of the unresolved dynamical processes is not too restrictive.

In this paper, a novel type of SCM, named FIZC, has been developed to include the contributions to the evolution of large-scale circulation dynamics in combination with diabatic contributions as parameterized in General Circulation Models (GCMs), thus allowing for a realistic time evolution of the prognostic atmospheric temperature, moisture and winds. In SCMs, the importance of large-scale dynamics has been demonstrated by Hack and Pedretti (2000). When prescribed, these contributions of the dynamical tendencies drive the evolution of the prognostic variables towards a given solution. FIZC is based on the second-generation Canadian GCM physical parameterization package (GCMii described in McFarlane *et al.* 1992). It also takes advantage of the detailed archives of GCMii that include the tendencies due to the ensemble effects of the subgrid-scale physical processes. A specific procedure of prescribing the contributions to the dynamical tendencies makes FIZC locatable over any surface of the globe, thus avoiding the development of a specific parameterization of the dynamical tendencies that is dependent on the location.

For this study, FIZC is coupled with the turbulence-based k- ε lake model SIMSTRAT (Goudsmit 2002) to assess the potential for long term integrations of the current and future warming climate conditions of Lake Geneva in Switzerland (Goyette and Perroud 2008).

In the following discussion, the coupled FIZC-SIMSTRAT model sensitivity experiments on the temperature profiles of the deep Lake Geneva in Switzerland is investigated with respect to a number of adjustable parameters that control the evolution of the Dynamics; these relaxing the vertical profiles of temperature, moisture and windspeed components to the GCMii archives, as well as those lake parameters controlling the evolution of the thermal profiles.

3.2 Methodology

3.2.1 The concepts at the base of the atmospheric model

The numerical modelling approach - termed FIZ, where "FIZ" stands for "Physics" - is based on the conceptual aspects of the physically-based regional climate interpolator for off-line downscaling of GCM's "FIZR", developed by Goyette and Laprise (1996). It may be considered as a column version of the Canadian GCMii (McFarlane *et al.* 1992) where, in the latter, atmospheric prognostic variables are evolving with time schematically as follows:

$$\frac{\partial u, v}{\partial t} = D_{u,v} + P_{u,v} \tag{1}$$

$$\frac{\partial T}{\partial t} = D_T + P_T \tag{2}$$

$$\frac{\partial q}{\partial t} = D_q + P_q \tag{3}$$

including the momentum equation (1), the thermodynamic equation (2) and the vapour continuity equation (3) where [u, v] are the components of the horizontal wind vector, T the air temperature, and q the specific humidity function of space. The adiabatic dynamical terms, operating essentially in the horizontal, are represented symbolically by "D" in each equation. The other members in the right hand side of these equations represent the source and sink terms of momentum $(P_{u,v})$, of heat energy (P_T) and of water vapour (P_0) . These subgrid sources and sink terms represent the contributions of processes which have important impacts on the larger resolved scales; they cannot be neglected and must therefore be parameterized. These processes are operating essentially in the vertical. The term $P_{u,v}$ represents, in principle, the acceleration due to vertical and horizontal momentum flux divergence, essentially turbulent in nature. The heat energy term, P_T , may be generated by solar and infrared radiation processes, turbulent diffusion of heat or by release of latent heat due to water vapour condensation. Turbulent diffusion of heat may result, in principle, in local heating due to vertical or horizontal flux divergence. Moisture in the form of water vapour can be redistributed by means of differential water vapour flux in the vertical or in the horizontal, and can be depleted by condensation. The vertical flux of moisture includes the effects of convection and other turbulent vertical fluxes.

A simplified field equation for $\Psi = (u, v, T, q)$ can therefore be written symbolically as follows:

$$\frac{\partial \Psi}{\partial t} = D_{\Psi} + P_{\Psi} \tag{4}$$

This partial differential equation allows for a forward integration in time when appropriate initial and boundary conditions are provided. During the GCMii simulations, the atmospheric prognostics, Ψ , were archived at regular time intervals and the contribution to the Physics tendencies were cumulated and archived at 24-hourly intervals, whose values are symbolized by \overline{P}_{Ψ} . Consequently, the mean contributions to the Dynamics can be retrieved as follows:

$$\overline{D}_{\Psi} = \frac{\partial \Psi}{\partial t} - \overline{P}_{\Psi} \tag{5}$$

That Dynamics, also a function of space and time represented by 24-h average values, will then be prescribed to FIZ and will serve to compute the atmospheric profiles as described next.

3.2.2 The FIZC approach

The column version of FIZ, called FIZC, is a one-dimensional atmospheric model applicable anywhere over the earth's surface. The prognostic variables $\Psi = \{u(\varphi_0, \lambda_0, \eta, t), v(\varphi_0, \lambda_0, \eta, t), T(\varphi_0, \lambda_0, \eta, t), \text{ and } q(\varphi_0, \lambda_0, \eta, t)\}$, are a function of the altitudinal coordinate, η , where φ_0 and λ_0 denote a fixed point of latitude and longitude, and are evolving with time as follows:

$$\frac{\partial \Psi}{\partial t} = D_{\Psi}^{\star} + P_{\Psi}^{\star} \tag{6}$$

where,

$$D_{\Psi}^{\star} = R_{\Psi,\eta} \, \overline{D}_{\Psi} \tag{7}$$

Equation (7) represents the prescribed contributions to the tendencies due to the Dynamics computed on the basis of GCMii archives in the column, $\overline{D}_{\Psi} = (\varphi_0, \lambda_0, \eta, t)$, which is superimposed on white noise, $R_{\Psi,\eta} = S_{\Psi,\eta} R^*$. $S_{\Psi,\eta}$ are scaling parameters allowed to vary in the vertical for each prognostic variable and R^* is a random number ranging from -1 to +1. The small archival frequency of GCMii outputs that are used to compute \overline{D}_{Ψ} (Eq. 7) led to use this stochastic component in the parameterization, as following the general ideas described in Wilks (2008). At each time step white noise is combined to the resolved scales of the GCMii dynamical tendencies, the latter being determined by the spatial resolution, and by the archival frequencies of its outputs in the present context. Consequently, the introduction of noise in the above parametrisation is intended to re-inject the unresolved variability in the dynamical processes that is present in the real atmosphere (e.g., sub-daily advection processes), but is lost in this SCM. This version allows a different scaling, i.e., a different intensity, to each of the contributions to the Dynamic tendencies, but the mean subdaily frequency variability is similar to all of these. Although a more sophisticated parameterisation could be derived for D_{Ψ}^* , the method used here is considered satisfactory because the flow fields computed by this single-column model do not interact with adjacent atmospheric columns; therefore no feedback on the GCMii dynamical tendencies are considered. Work is currently underway to implement sub-daily variability for subgrid-scale dynamical processes based on other types of noise (e.g., red noise spectra) in order the simulated flow fields Ψ match the observed local atmospheric variability in the atmospheric column. In Eq (6) the term p_{Ψ}^* , represents the contributions to the tendencies due to the Physics computed at each time step throughout the atmospheric column on the basis of the GCMii physics package. As is the case for GCMii, the Dynamics are contributions to the tendencies of processes operating essentially in the horizontal, whereas the Physics are contributions to the tendencies of processes operating in the vertical. Therefore, the evolution of Ψ in an atmospheric column over a fixed point (φ_0, λ_0) is computed in FIZC schematically as follows:

$$\Psi_{n,\ell} = \Psi_{n-1,\ell} + \Delta t \left(\mathcal{D}_{\Psi_{n-1,\ell}}^* + \mathcal{P}_{\Psi_{n-1,\ell}}^* \right)$$
 (8)

where time is evolving in a discrete manner as $t = t_0 + n \Delta t$, with t_0 as the initial time and Δt the model timestep and the vertical levels are labelled by ℓ . FIZC thus considers the following contributions to the tendencies: a prescribed Dynamics, D_{Ψ}^* , which is interpolated at each time step, as well as a recomputed Physics in the atmospheric column, P_{Ψ}^* , using the standard GCMii physics package (McFarlane *et al.* 1992). In addition to the simple forward-in-time marching scheme shown in (8), a model option may also allow for using a second-order centered method for time differencing combined with a weak time filter developed by Asselin (1972). The timestep, Δt , used in FIZC is kept the same as that used in GCMii although there is no upper bound for it due to the restriction regarding dynamical instabilities. No attempts are made in the present paper to increase Δt further.

FIZC is then interfaced with the lake model via a coupling interface described below.

3.2.3 Nudging interface

An FIZC option allows nudging the vertical profiles of Ψ towards the GCMii archived profiles. "Nudging" means that the prognostic variables computed in FIZC from (8), such as temperature, moisture and winds, are "relaxed" toward the GCMii values found in the archives in the column. The difficulty is to find a nudging coefficient suitable for preventing FIZC from drifting too far from the GCMii prognostics, but at the same time allowing it to develop its own structures and variabilities. The variability may turn out to be necessary to drive a lake model in a realistic manner since GCMii prognostic variables have been resolved using a spatial resolution and surface conditions different to that of FIZC. Part of the variability is brought about by the prescribed contributions to the Dynamics tendencies (Eq. 7), and the other by the contribution to the Physics tendencies through processes such as the diurnal and seasonal cycles of the solar radiation, the atmospheric instabilities, which enable vertical diffusion of momentum, heat and moisture, etc. The nudging procedure is as follows:

$$\Psi_{m,\ell} = N_{\Psi,\ell} \Psi_{GCMii,m,\ell} + (1 - N_{\Psi,\ell}) \Psi_{F/ZC,m,\ell}$$
(9)

where the values of $\Psi_{m,\,\ell}$ at step m and at level ℓ is a combination of computed FIZC and GCMii archived values controlled by $N_{\Psi,\ell}$, the nudging parameter, whose value is 1 for a complete nudging to GCMii archives, and 0 for no nudging; m denotes the discrete time archival frequency, $t_A = m \Delta t_A$, being 1 per 12 hours. Variables are thus allowed to be nudged independently of each other at all levels at 12 hour intervals.

3.2.4 Vertical levels

The vertical levels in FIZC are originally the same used by GCMii (McFarlane *et al.* 1992). The hybrid coordinate system, η , has been developed by Laprise and Girard (1990) and is a function of the local pressure, p, as follows:

$$p = p_o \eta + (p_s - p_o) \left(\frac{\eta - \eta_T}{1 - \eta_T}\right)^2$$
(10)

where p_s is the surface pressure, p_o is a specified reference pressure and η_T is the value of the upper boundary coordinate, chosen at a finite pressure of 5 hPa. The coordinate surfaces are terrain-following in the lower troposphere, but become nearly coincident with isobaric surfaces as p decreases. In this scheme, Ψ are is defined on full levels (η_t) and the

diagnostically determined vertical motion variable η is defined on the staggered levels ($\eta_{\ell_1/2}$) as shown in Table 3.1. The reference pressure p_o is 1013 hPa. In addition, the surface pressure may be hydrostatically adjusted according to the difference between the altitude of a station and that resolved by GCMii at the point (φ_0 , λ_0).

Table 3.1. Position of the unstaggered layers in GCMii, and in the 10-layer version of FIZC.

Layer (l)	ηℓ	η{+½
		0.005 (Top)
1	0.012	0.020
2	0.038	0.056
3	0.088	0.120
4	0.160	0.200
5	0.265	0.330
6	0.430	0.530
7	0.633	0.736
8	0.803	0.870
9	0.915	0.960
10	0.980	1.000

3.2.5 Wind gust parameterization

Another FIZC option allows generation of random strong wind events between November 1st and March 1st of each simulated year as follows:

$$[u,v]_{FIZC} = [u,v]_s \tag{11}$$

where the horizontal wind components are fixed to a prescribed wind profile $[u, v]_s$. Consequently, the simulated wind speed may be set to a profile determined on the basis of station observations during windstorms. This procedure is done independently to the nudging

procedure (Section 2.3) in order to apply these profiles to consecutive timesteps which is not possible to reproduce with a 12-hourly wind prescribed on the basis of the GCMii archives.

3.2.6 The k- ε SIMSTRAT lake model

The one-dimensional SIMSTRAT lake model, a buoyancy-extended k- ε model described in Burchard et~al.~(1998), has been updated to include the effects of internal seiches on the production of turbulent kinetic energy (TKE). Turbulent mixing is solved by the two dependent equations of production and dissipation of TKE. The source of TKE is generated by shear stress from the wind and buoyancy production in case of unstable stratification. The seiching motion developed under the action of the wind increases the TKE in the interior of the lake due to loss of seiche energy by friction at the bottom. Governing equations of the k- ε model and extensions included in SIMSTRAT are fully described in Goudsmit et~al.~(2002). This model takes into account the bathymetry, thus providing better parameterization of the seiche energy production. The influence of river inflows and outflows is, however, not taken into account, so that the lake water-balance remains fixed. In addition, two adjustable parameters relevant for the simulation of the thermal evolution of lake waters are prescribed in the seiches parameterization, $\alpha_{\rm seiche}$ and $q_{\rm seiche}$. For the current application, no lake-ice module is used in conjunction with this lake model.

3.2.7 Coupling FIZC with SIMSTRAT lake model

The lake model is interacting with the lower atmosphere of FIZC through a coupling interface. The coupling is realised at each FIZC time step using the GCMii physics package to compute the incoming solar, $R_{S,sfc}^{\downarrow}$, downward atmospheric infrared, $R_{L,sfc}^{\downarrow}$, the reflected solar, $\alpha_w R_{S,sfc}^{\downarrow}$ and emitted infrared, $\varepsilon_w \sigma T_{sfc}^4$. The radiation fluxes at the surface depend on the water albedo, α_w , the surface water temperature, $T_{sfc} = T_w \left(z = 0\right)$ and the water emissivity ε_w (fixed at 0.97), where z is the lake-depth vertical coordinate and σ is the Stefan-Boltzmann constant. In addition, the GCMii physics package computes the subgrid-scale vertical component of the turbulent fluxes of sensible and latent heat, taking into account the surface drag coefficient as well as the differences of the air temperature and moisture in the vertical at the water-atmosphere interface. The formulation of these fluxes is described in McFarlane et al. (1992). The albedo, α_w , that is used to compute the reflected solar flux at the surface accounts for the solar zenith angle (Bonan 1996):

$$\alpha_w = 0.05 (\mu + 0.15)^{-1}$$
 (12)

with μ being the cosine of the local solar zenith angle. In the lake model, the exchanges occurring at the air-water interface are realised mainly through conduction and by the absorption of solar radiation in the water column; the solar flux reaching any depth z is given by $R_S^{\downarrow} = R_{S,sfc}^{\downarrow} e^{-az}$, where the decay is controlled by the extinction coefficient a (m⁻¹) prescribed as a function of lake depth.

The vertical component of the turbulent flux of momentum prescribed at the lake surface is parameterized using the anemometer level windspeed $[u, v]_{anem}$, computed in the GCMii physics package as follows (Goudsmit *et al.* 2002):

$$\tau_{sfc} = \frac{c_D \rho_a}{\rho_o} [s_u u, s_V v]_{anem}^2$$
 (13)

where ρ_a represents the air density and ρ_o the surface water density. The parameters s_u and s_v are applied to the anemometer-level wind speeds to scale the simulated values in order to match those of the station observations. This can be done without altering the prognostic variables since the anemometer-level windspeed is a diagnostic quantity. The evolution of the lake thermal profiles is also dependent on the value of the surface drag coefficient, c_D .

3.3 Data and experimental setup

The deep Lake Geneva is used for the numerical investigations during a 10-year period. This period is deemed sufficient for the lake-parameter validation procedure (Perroud *et al.* 2009). This lake is a fresh water body of 580 km^2 surface area, shared by Switzerland to the north and France to the south at 372 m a.s.l. It is divided into 2 basins, the deep or "Grand Lac" ($z_{\text{max}} = 309 \text{ m}$) to the east, and the shallower "Petit Lac" to the west. It remains stratified most of the year and surface waters do not freeze. It is considered as a warm monomictic lake for which complete winter mixing occurs rarely in the deep lake.

The French National Institute for Agricultural Research (INRA) collects bi-monthly samples of thermal profiles at the deepest point of the lake (Database INRA of Thonon-Les-Bains, Data management by the Commission Internationale pour la Protection des Eaux du lac Léman, CIPEL) at the SHL2 station. It is located between Lausanne, Switzerland ($46.52^{\circ}N$; $6.63^{\circ}E$), and Evian, France ($46.38^{\circ}N$; $6.58^{\circ}E$). Discrete temperature measurements have been made available since 1957 where samples are currently recorded at z = 0, 2.5, 5, 7.5, 10, 15, 20, 25, 30, 35, 50,100, 150, 200, 250, 275, 290, 300, 305 and 309 meters depths. The penetration of solar radiation into the water column is a function of the water transparency. As no depth-dependent light extinction coefficient measurements exist, bi-monthly values are deduced on the basis of the Secchi disk depth and interpolated through time in order to cover the period simulated by the lake models.

Meteorological records of hourly mean temperature and wind speed of the inland meteorological station to SHL2 (*i.e.*, Changins, 46.38°N; 6.22°E) for comparison with simulated values are supplied by the Automatic Network (ANETZ) of the Federal Office of Meteorology and Climatology, Meteoswiss (Bantle 1989) for a 10-year period centred on 1981. To simulate the effects of windstorms, the windspeed is set to a prescribed wind profile determined on the basis of observations made at the Swiss Climatological Station Payerne (46.8°N, 6.9°E, 490 m a.s.l.). Surface air temperatures are hydrostatistically adjusted owing to the station altitude differences compared to the water surface of the lake. In order to remove the bias of inland windspeed recordings, and to generate values over the lake open water at station SHL2, a correction factor applied to the observed winds has been developed (Perroud *et al.* 2009). Unfortunately, no measurements are made and available for comparison with SHL2.

For these investigations, the simulated GCMii current climate (1 x CO₂ case in Boer *et al.* 1992) flow fields, as well as the contributions to the Physics tendencies, are employed to provide the necessary information to drive the FIZC model; these fields serve to compute the contributions to the Dynamic tendencies (Eq. 5) and to specify the flow fields required in the nudging procedure (Eq. 9). FIZC is positioned over the location of station SHL2 of Lake Geneva. The computational timestep of 20 min is the same for both models, and the altitude

difference between the observed lake altitude and the surface level diagnosed in GCMii is 16 m, so that surface pressure is hydrostatically adjusted in FIZC. Since ice cover rarely appears in the deep Lake Geneva, the lack of an ice module is not an issue in the present context.

FIZC and the k- ε lake models contain numerical parameters, and it is important to establish the sensitivity of the coupled model results to reasonable variations of these parameters. Sensitivity tests on the lake thermal water profiles, as well as on the atmospheric temperature and windspeed statistics, involve the intensity and the number of vertical levels of the nudging of the air temperature, the moisture and the horizontal component of the wind, $N_{\Psi,\ell}$ (Eq. 9), towards GCMii archived values. Another parameter, allowed to vary in the vertical to scale the contribution to the Dynamics tendencies, $S_{\Psi,\ell}$, is tested. A parameter introduced to scale the simulated anemometer windspeed to fit the observed statistics is also tested. The windgust parameterization can be activated or not, thus impacting on the intensity of mixing during strong wind events. Additional runs investigate some of the lake calibration parameters, such as the surface drag coefficient c_D , as well as those relevant for the seiches parameterization, $\alpha_{\rm seiche}$ and $q_{\rm seiche}$. The vertical grid spacing of SIMSTRAT is fixed at 0.75 m, so that 412 levels are needed for the simulation at the hydrological station SHL2.

This coupled atmosphere-lake model is run over a 10-year period, starting January 1st. The initial lake temperature profile is based on the mean December 1980 and January 1981 observations. The greenhouse gas concentrations are fixed at current levels (*i.e.*, 1 x CO₂ case). The archival frequencies are fixed at 12-hourly (0000 and 1200 UTC) for the simulated lake profile, and hourly for the mean screen-level temperature and humidity, as well as for the anemometer-level windspeed.

3.4 Results

The goal of these modelling experiments is to reproduce optimally the observed atmospheric surface conditions and the lake thermal profiles by adjusting parameter values within reasonable limits, and to analyse the sensitivity of the lake-water temperature profiles to the variation of these parameters. The sensitivity analysis is carried out by way of the comparison of seasonal means of a number of variables simulated using the optimal combination of parameter values with a number of sets of experiments with modified parameter values. The comparison is performed using simulated and observed hourly-mean atmospheric screen-level temperature and anemometer winds as well as those of twice-daily water temperature profiles, seasonally averaged.

3.4.1 Preliminary test: the "lake" vs "no-lake" experiments

Prior to investigating the sensitivity of the adjustable parameter values on the lake thermal profiles, this preliminary test is designed to assess the role of the underlying surface on the surface temperature and on the vertical structure of the atmosphere, including both "lake" and "no lake" experiments. For these experiments, a set of ad hoc parameters has been devised. These are $N_{\Psi,\ell} = 0.1$, $S_{\Psi,\ell} = 6$, $\Psi = (T, q, u, v)$, $\ell = 10$, $s_u = s_v = 0.6$, and the wind gusts parameterization is not activated. The lake parameters are fixed at $\alpha_{\text{seiche}} = 0.01$, and $q_{\text{seiche}} = 0.9$ (Perroud *et al.* 2009). The ground surface characteristics and the land-use of the "no lake" case are the same as those used in the GCMii (McFarlane *et al.* 1992). Figure 3.1 shows the evolution of the surface temperatures when the lake model and the GCMii force-restore approach are interfaced separately with FIZC over a one-year cycle for the same

geographical location (φ_0 = 46.5°N, λ_0 = 6.5°E) in Switzerland, starting August 1st. The experiments used the same initial surface temperature of 20.8°C. The moments in time when the lake surface temperature reaches the annual minima and maxima are delayed in the lake case due to the larger thermal inertia of the water compared to that of the solid ground surface. The minimum surface water temperature is reached in early March at 5.2°C, whereas that of the soil is reached in early January at -23°C; the lake surface maximum temperature is reached in late August at 22.1°C, whereas the ground surface maximum is reached at 39°C in late June, both after using a 6-day running average for comparison as shown in Fig. 3.1. Consequently, the daily and annual temperature amplitudes of the water are significantly reduced compared to the solid soil surface. The seasonality, in terms of the time it takes to reach these extremes, is also modified; there is a two-month lag in the deep Lake Geneva compared to the soil case, even though the atmospheric dynamical forcing is similar in magnitude, thus emphasizing the role of the thermal characteristics of such a large body of water.

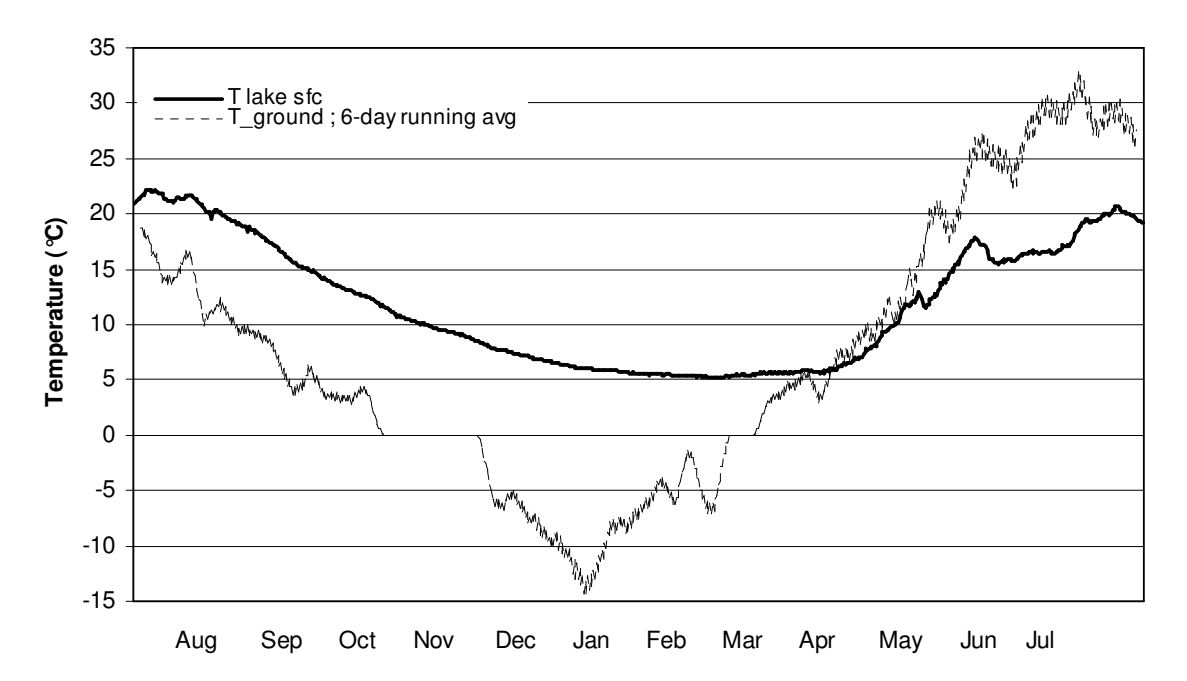


Figure 3.1. The simulated lake surface temperature using the k- ε lake model and ground surface temperature using the land-surface energy budget approach of GCMii (McFarlane *et al.* 1992) under a similar annual surface forcing. Both modules are interfaced with FIZC over a one-year cycle for the same geographical location (φ_0 , λ_0) in Switzerland. Temperatures are archived at 12-hourly intervals and the ground surface temperature is displayed after filtering the time series with a 6-day running average in order to smooth out the diurnal cycles.

A number of variables and fluxes, seasonally averaged, are shown in Table 3.2 for the "lake" and the "no lake" cases. The different surface radiation and thermal characteristics (the lake has a lower albedo and a larger heat capacity than the soil) have thus a strong impact on the surface radiation and heat flux components that changed completely the surface net heat budget. The lake absorbs a large quantity of heat during the spring and summer seasons and releases a larger quantity during the autumn and winter seasons. The sign and intensity of surface latent and sensible heat fluxes changed markedly in the lake case. These fluxes are a function of the vertical gradient of specific humidity and temperature, and of the surface-layer bulk Richardson number, which relates vertical static stability and the vertical shear serving to compute drag coefficients as in McFarlane *et al.* (1992). A Richardson

number less than a critical value ($R_{iB,c} = 0$ in this parameterisation) implies a dynamically unstable surface layer that is likely to become or remain turbulent. The atmospheric conditions are unstable on average over the lake surface, whereas over the solid surface stability prevails on the average during the nights. This is due to the rapid warming/cooling of the soil surface, consequence of the smaller thermal inertia compared to that of the lake. During this annual cycle, the mean energy budget of the soil surface is close to zero but that of the lake is in excess of 48 W m⁻², meaning that the lake stored energy to warm up the water of about 1 ℃, on average in the column. The values of individual surface heat fluxes are also modified: the upward latent heat flux is less intense over the lake than over the soil in the spring (46 vs 85 W m⁻²) and summer (78.9 vs 136.6 W m⁻²) seasons, but more intense during the autumn (71.4 vs 49.8 W m⁻²) and winter (44.4 vs 22.8 W m⁻²) seasons; the sensible heat flux is less intense over the lake than over the soil in the spring (7.9 vs 17.2 W m⁻²) and summer (16.4 vs 23.5 W m⁻²) seasons, and even changes direction (i.e. upward instead of downward in the "no-lake" case) during the autumn (13.2 vs -3.2 W m⁻²) and winter (-16.5 vs 2.2 W m⁻²) seasons. The precipitations are similar for both cases during the autumn (2.55 vs 2.57 mm d⁻¹) and winter (3.13 mm d⁻¹ in both cases) seasons, but smaller over the lake surface during the spring (3.12 vs 3.46 mm d⁻¹) and summer (1.99 vs 2.58 mm d⁻¹) seasons. Also, cloudiness is not much modified during the autumn (0.46 in both cases), little during the winter (0.55 vs 0.57 for the "no-lake" and "lake" cases respectively) and the spring (0.58 vs 0.56 for the "no-lake" and "lake" cases respectively), and more during the summer (0.46 vs 0.43 for the "no-lake" and "lake" cases respectively). These changes are also consistent with the absorbed short- and longwaves in the atmosphere where temperature, but also clouds, are playing a role in the atmospheric column as described below. The strong coupling between the lake surface and the atmosphere thus has an impact on the dynamical and thermodynamical vertical structure of the atmosphere.

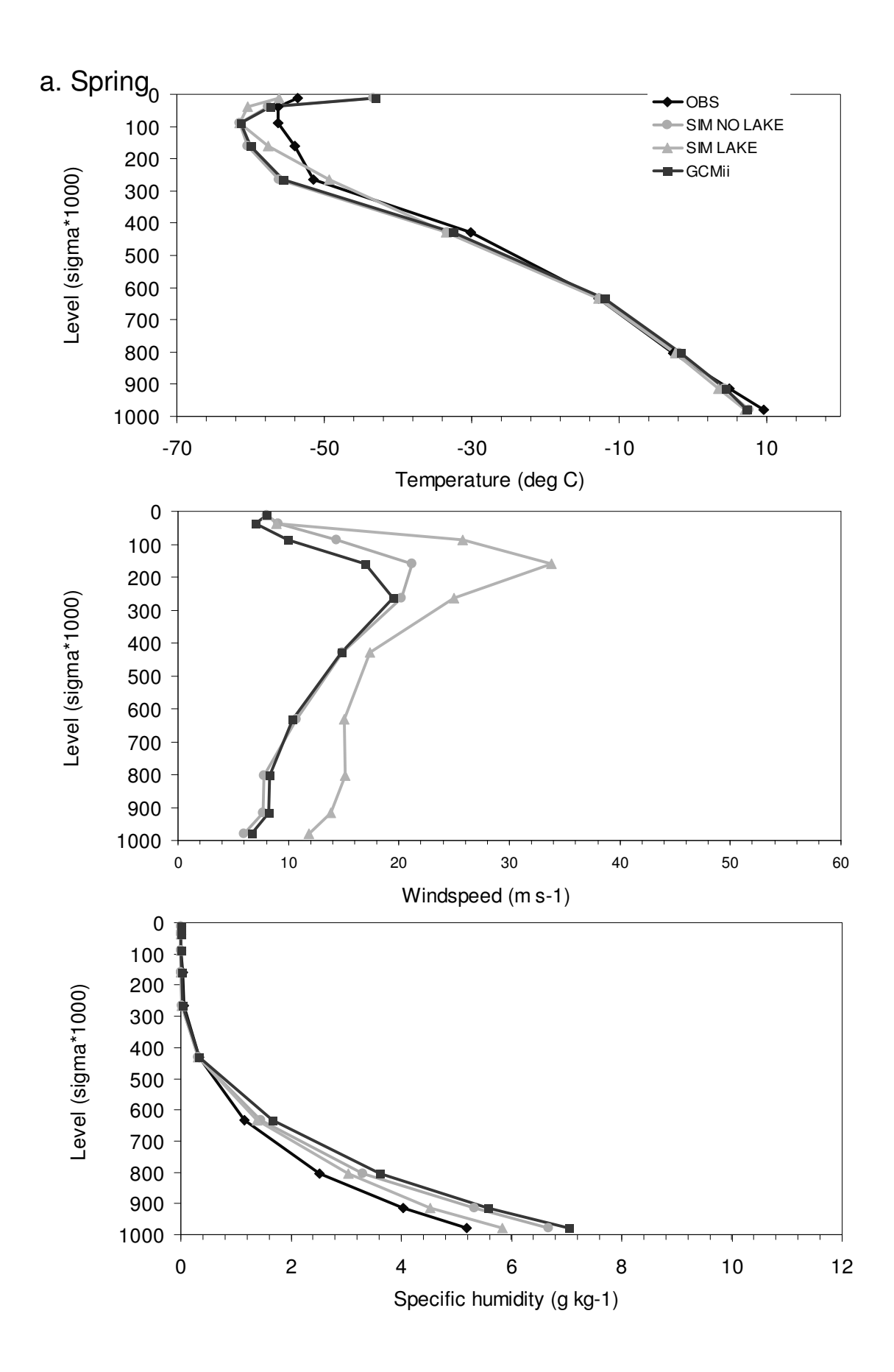
Figure 3.2 shows the seasonally-averaged temperature, horizontal windspeed, and specific humidity profiles simulated by FIZC for the "lake" and the "no-lake" experiments. These can be compared to these of GCMii found in the original archive for the same column, as well as to the vertical soundings measured at the Payerne Climatological Station in Switzerland (up to 30-35 km high) and downloaded from the University of Wyoming, Department of Atmospheric Science web site. One year in the 1980s has thus been arbitrarily chosen for this comparison. Seasonal averages are based on the 0000 and 1200 UTC profiles, and observed profiles are aggregated into the FIZC/GCMii vertical levels to ease the comparison. Unfortunately, the observed horizontal windspeed profiles are not displayed due to the lack of in-depth and continuous measurements that prevent us from producing meaningful seasonal averages throughout the atmospheric column. In these experiments, as the nudging parameter values are expected to be less than 1 (i.e. $N_{\Psi,\ell} = 0.1$), the FIZC vertical profiles are generally not the same as these of GCMii. Moreover, a set of optimal parameters have been devised for the "no-lake" case to reproduce very closely the atmospheric structure, the surface variables and the various fluxes found in the GCMii archives (not shown); however, these values are not necessarily suited for the "lake" case and are therefore not considered further. The seasonally-averaged wind profiles in the "no-lake" case are close to these computed using the GCMii archives. In the "lake" case, however, the horizontal winds are stronger than in the "no-lake" case in the column due to the smaller surface roughness height of the water surface compared to that of the solid surface. The seasonal temperature profiles in both the "no lake" and the "lake" experiments match well those observed, despite a cold bias generally found above a level corresponding to a height of roughly 8 km above the surface. In the "lake" case during the summer season, the air above the surface up to an altitude of roughly 1500 m is generally colder compared with the "no-lake" case, in line with the reduced sensible heat and downward longwave fluxes at the surface; during the winter season this is quite the opposite where the air is generally warmer and the sensible heat and downward longwave fluxes at the surface are stronger than the "no-lake" case. The shape of seasonal specific humidity profiles match well those observed, despite a systematic moist bias found below roughly 5 km. In the "lake" case, during the

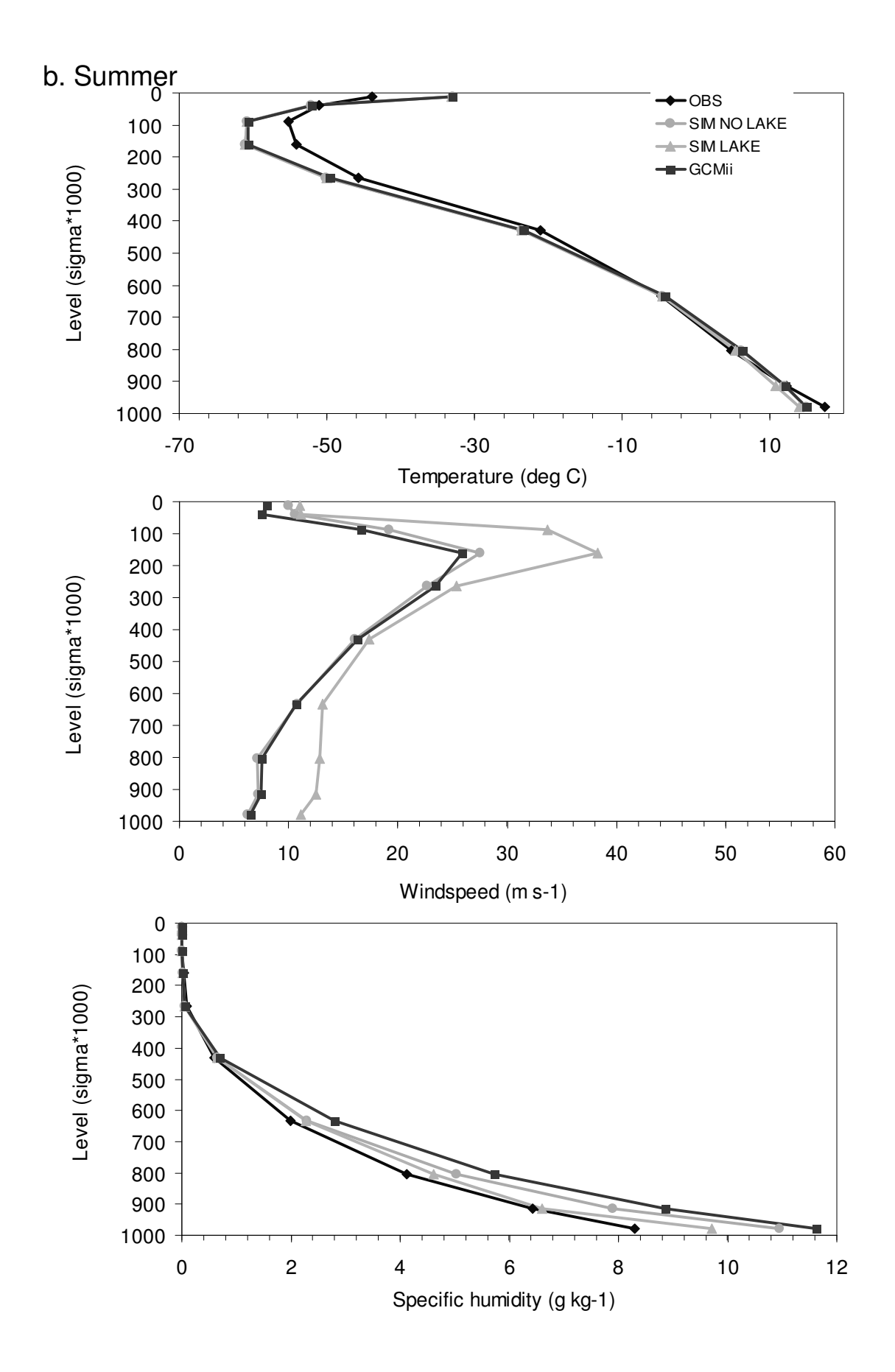
spring and summer seasons, the specific humidity in the lower atmosphere is generally less than that in the "no-lake" case, in line with the reduced evaporation-evapotranspiration (or latent heat flux), with the increased downward solar radiation at the surface, as well as with the reduced cloudiness as shown in Table 3.2. The reverse occurs in the autumn and winter seasons for the "lake" case where the specific humidity is higher in the lowest atmospheric levels, in line with the increased evaporation, a decrease in the downward solar radiation at the surface, as well as with the increase (modest in autumn) in the cloudiness when compared to the "no-lake" case.

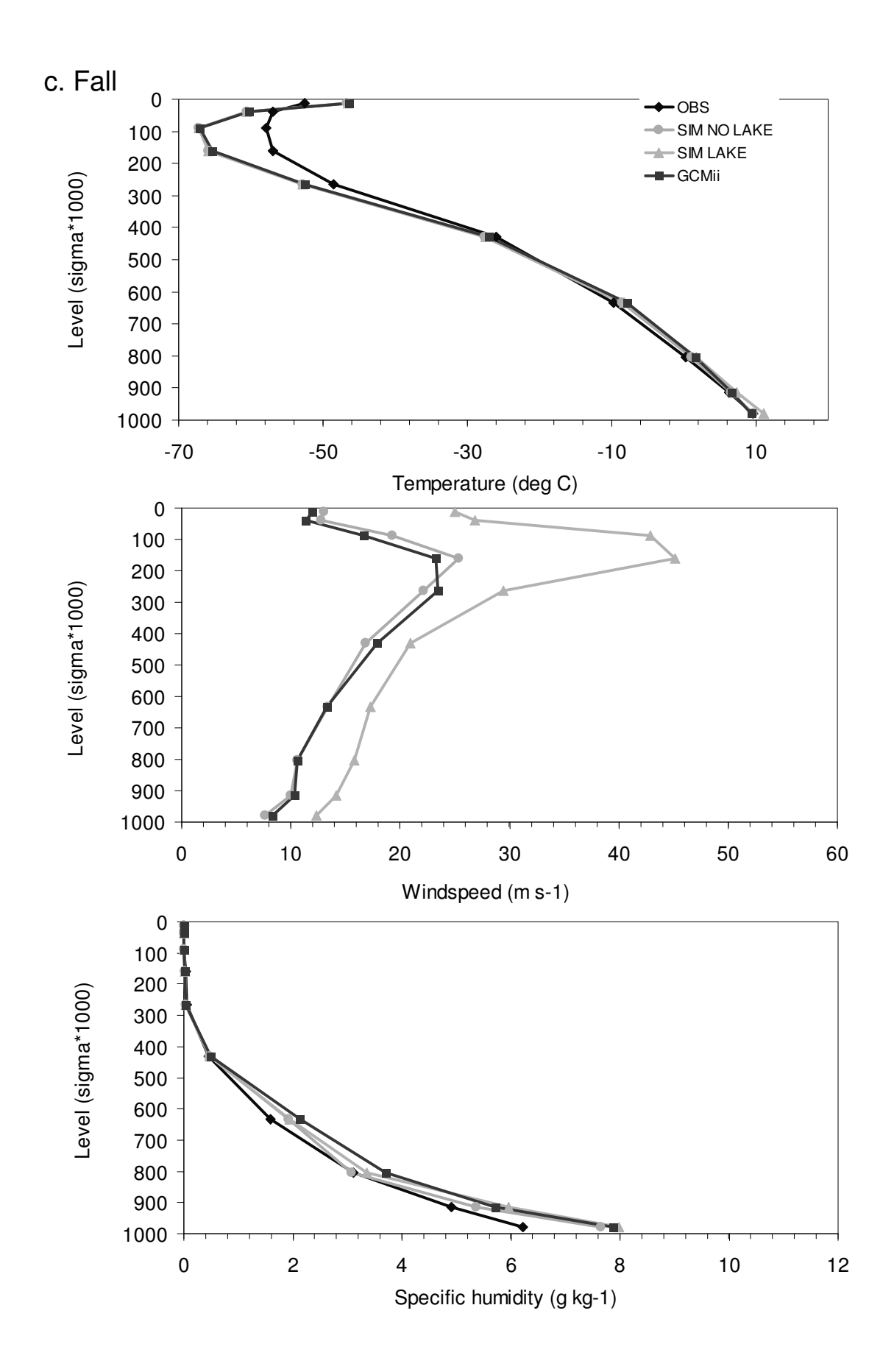
Consequently, these results showed that a change from a land to a lake surface in this SCM led to consistent modifications in the atmospheric profiles, as well as in the surface variables and fluxes, despite similar atmospheric dynamical forcing. The minimum and maximum values of the lake surface temperatures are delayed and the daily temperature amplitude is significantly reduced compared to the land surface. Thus, these modifications emphasize the role played by the surface conditions taken accounted for in the lake model and these of the vertical exchanges in the atmospheric column accounted for in the contributions to the Physics tendencies. This conclusion is based on 12-hourly outputs and for the relatively small value of the nudging parameters.

Table 3.2: Comparison of seasonal averages of selected variables and fluxes between the "lake" and "no-lake" experiments over one annual cycle; averages are computed over the March, April, May (MAM), June, July, August (JJA), September, October, November (SON), and December, January, February (DJF) months. Precipitation (pcp) is displayed in the units of mm d⁻¹, total cloudiness ranges from 0 to 1, downward longwave radiation flux at the surface, $R_{L,sfc}^{\downarrow}$, absorbed longwave by the atmosphere, $R_{S,atm}^{*}$, absorbed shortwave at the surface, $R_{S,sfc}^{*}$, latent and sensible heat flux, respectively Q_{E} and Q_{H} , and the net energy at the surface, $Q_{N,sfc}$ (W m⁻²), are in the units of W m⁻². The sign convention is positive downward for $R_{L,sfc}^{\downarrow}$, positive for net absorbed radiation for $R_{L,sfc}^{*}$, $R_{S,atm}^{*}$, $R_{S,sfc}^{*}$, and $Q_{N,sfc}$. R_{IB}^{*} is the bulk Richardson number (dimensionless), values for the day (D) and night (N). Surface temperature is computed by the GCMii land-surface module in the "no lake" experiment, and the lake surface temperature (*i.e.* z = 0 m) in the "lake" experiment by the k- ε lake model.

	MAM		J	JA	A S		D	JF
	no lake	Lake	no lake	lake	no lake	lake	no lake	lake
$R_{L,sfc}^{\downarrow}$ (W m ⁻²)	324.3	314.3	351.6	337.4	311.2	329.8	291.0	312.5
$R_{L,sfc}^{\star}$ (W m ⁻²)	-154.2	-144.6	-175.8	-160.4	-154.9	-155.0	-132.4	-133.5
$R_{S,atm}^*$ (W m ⁻²)	58.7	55.2	80.9	75.8	37.2	37.6	19.2	19.6
$R_{S,sfc}^*$ (W m ⁻²)	137.4	154.3	204.4	234.3	95.6	96.0	48.0	46.1
\mathcal{T}_{sfc} (°C)	8.9	8.7	16.2	16.5	10.1	13.6	4.0	8.3
$Q_{\rm H}$ (W m ⁻²)	17.2	7.9	23.5	16.4	-3.2	13.2	-16.5	2.2
$Q_{\rm E}$ (W m ⁻²)	85.0	46.0	136.6	78.9	49.8	71.4	22.8	44.4
pcp (mmd ⁻¹)	3.5	3.1	2.6	1.9	2.6	2.6	3.1	3.1
Clouds	0.58	0.56	0.46	0.43	0.46	0.46	0.55	0.57
$Q_{\rm N,sfc}$ (W m ⁻²)	2.2	57.3	-0.1	77.2	-1.5	-42.1	0.0	-43.9
$R_{ m iB}$	N D 3895	N D 0305	N D .58	N D 0909	N D .54	N D 115	N D .48 .15	N D 107







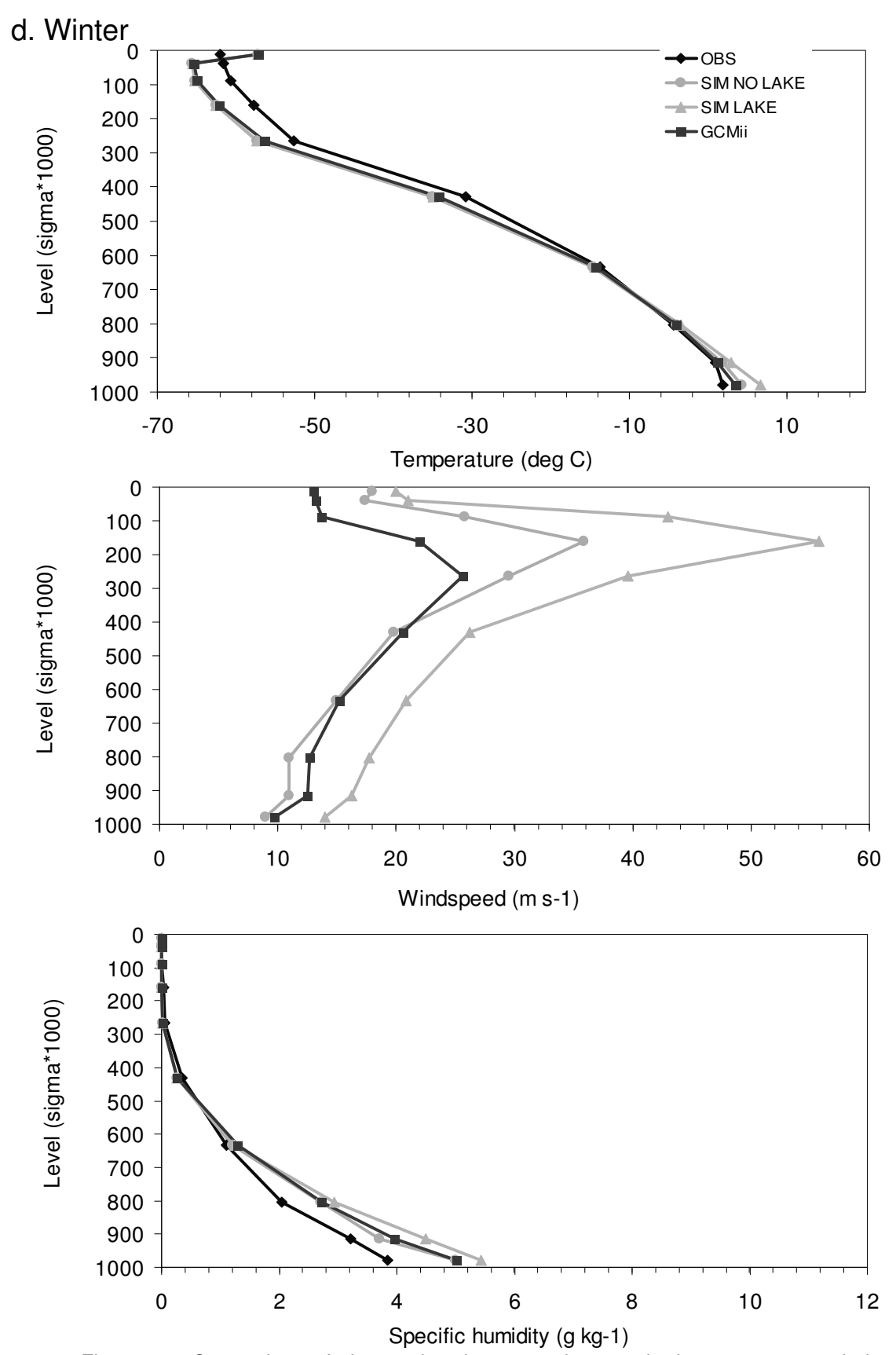


Figure 3.2. Comparison of observed and computed atmospheric temperature, windspeed and specific humidity profiles. The simulated profiles are produced by FIZC interfaced with the lake model and land-surface energy budget approach as described in Fig. 3.1. The station observation is located in Payerne, Switzerland. The observed profiles are collected from radiosoundings at 0000 and 1200 UTC aggregated onto FIZC vertical levels. Profiles are seasonally averaged; a) Spring, b) Summer, c) Autumn, and d) Winter.

3.4.2 Coupled-model optimal parameter values

Prior to assessing the sensitivity of the lake water temperature to the coupled-model parameter values, an arbitrary combination of values has been devised. This combination aims at reproducing the observed water temperature profiles by using the smallest nudging parameter, $N_{\Psi,\ell}$, is a unique value for the scaling of the contributions to the Dynamics tendency applied at all vertical levels, $S_{\Psi,\ell}$, Ψ represents atmospheric prognostics of T, q, u and v, $\ell=10$, and a scaling of the anemometer level wind speed that reproduces the observed windspeed, s_u and s_v when the windgust parameterization is not activated. Simulated hourly-mean atmospheric temperature and screen level specific humidity are also compared with the station observations (Table 3.3).

A set of 50 simulations has been performed using the following combinations, $S_{\Psi,\ell} = [1, 3, 5, 6, 7, 8, 9]$, s_u and $s_v = [0.5, 0.6, 0.7, 0.8, 1.0]$ and $N_{\Psi,\ell} = [0.1, 0.5]$. The comparison between simulated and observed mean seasonal water temperature, evaluated through the RMSEs for four groups of depths (GD1: 0-10 m, GD2: 15-50 m, GD3: 100-200 m, GD4: 275-309 m), serve to devise the calibration that produce the smallest bias.

When $N_{\Psi,\ell} = 0.5$, three combinations reproduced realistic water temperature profiles with RMSEs ranging from $1.04\,^{\circ}\text{C}$ to $1.24\,^{\circ}\text{C}$ in GD1, from $0.32\,^{\circ}\text{C}$ to $0.42\,^{\circ}\text{C}$ in GD2, from $0.21\,^{\circ}\text{C}$ to $0.24\,^{\circ}\text{C}$ in GD3, and from $0.5\,^{\circ}\text{C}$ to $0.53\,^{\circ}\text{C}$ in GD4. For these, s_u and $s_v = 0.5$, and $s_{\Psi,\ell} = [7, 8, 9]$; $s_{\Psi,\ell} = 9$ performed the best in GD1 and GD2, but the worst was in GD3 and GD4. Since the variability of the RMSEs is larger in the first 100 m below the surface, the latter is more appropriate. For all these simulations, the bias between simulated and observed mean screen (*i.e.* 2 m) air-temperature and specific humidity is positive. However, it turns out that $s_{\Psi,\ell} = 9$ produces the smallest bias (Fig. 3.3). Furthermore, for s_u and $s_v = 0.5$, the bias diminishes with increasing $s_{\Psi,\ell}$ (Table 3.3). The bias varies between $0.03\,^{\circ}\text{C}$ (Winter) and $1.58\,^{\circ}\text{C}$ (Spring) at the surface, $-0.08\,^{\circ}\text{C}$ (Winter) and $0.84\,^{\circ}\text{C}$ (Summer) at 15 m, $-0.41\,^{\circ}\text{C}$ (Autumn) and $0.23\,^{\circ}\text{C}$ (Winter) at 50 m, and $0.03\,^{\circ}\text{C}$ (Autumn) and $0.23\,^{\circ}\text{C}$ (Spring) at 100 m.

The same analysis has been performed using a smaller nudging parameter value, $N_{\Psi,\ell}=0.1$. The lowest RMSEs are reached for s_u and $s_v=0.6$ and $s_{\Psi,\ell}=7$. The RMSEs are of the order of $0.75\,^{\circ}$ C in GD1, $0.38\,^{\circ}$ C in GD2, $0.24\,^{\circ}$ C in GD3 and $0.15\,^{\circ}$ C in GD4. The nudging can thus be reduced to values as low as 0.1 without any negative effects on the simulation of the lake water temperature profiles. The bias between observed and simulated atmospheric variables is even reduced (Table 3.3). The seasonal water temperature profiles produced with this latter combination will serve as a reference for the sensitivity analysis, thus producing realistic seasonal water temperature profiles as shown in Figure 3.3. The seasonal water temperature profiles show generally a small negative bias. At the surface, the error is maximal in autumn (-0.92 $^{\circ}$ C), at 15m in spring (+0.48 $^{\circ}$ C), and at 50m and 100m (-0.65 $^{\circ}$ C and 0.37 $^{\circ}$ C) in autumn.

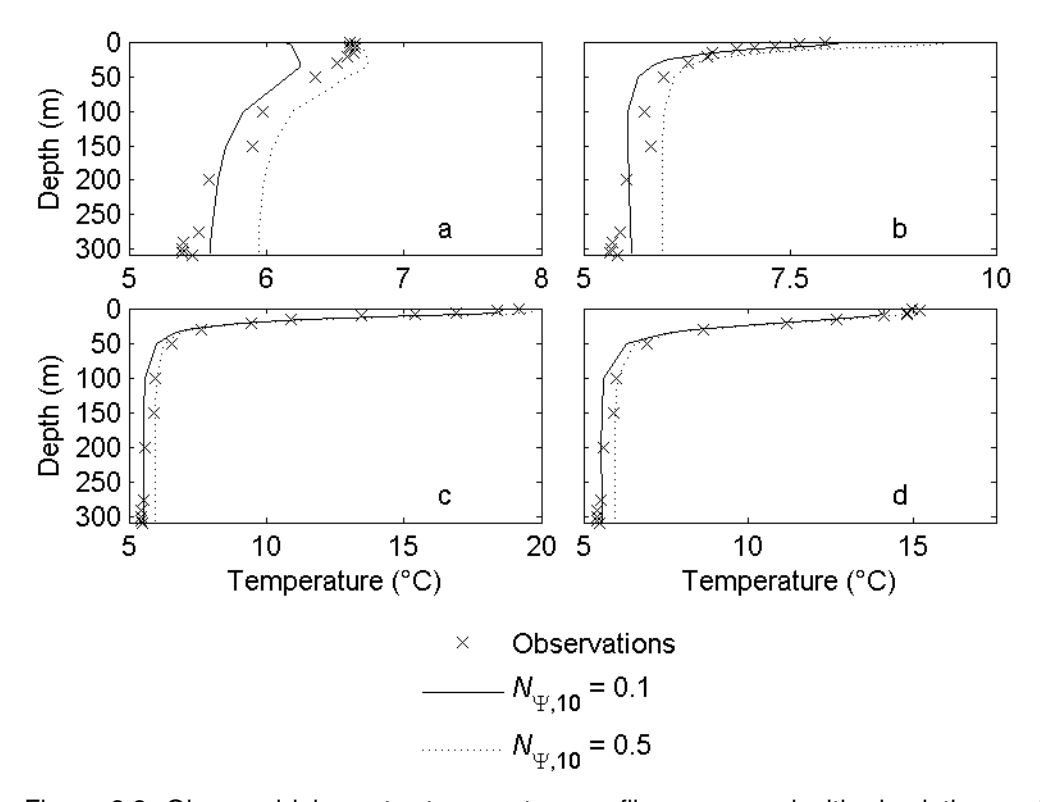


Figure 3.3. Observed lake-water temperature profiles compared with simulations using two different values for the nudging towards the GCMii archived values; Ψ stands for T, q, u and v, and $\ell = 10$. Profiles are seasonally averaged; a) Winter (DJF), b) Spring (MAM), c) Summer (JJA), and d) Autumn (SON).

Table 3.3. Comparison of the station observation statistics (annual mean \pm standard deviation) with simulated quantities of anemometer-level windspeed, screen-level air temperature and specific humidity as a function of the FIZC parameter values for the nudging technique, $N_{\Psi,\ell}$, for the scaling of the contribution to the tendencies due to the Dynamics, $S_{\Psi,\ell}$ and for the scaling of the anemometer-level windspeed, s_u and s_v . Here, Ψ stand for all prognostic variables, T, q, u, and v, and ℓ for the number of vertical levels above the surface on which the nudging and the scaling of the contributions to the Dynamics are applied. This comparison is partitioned into the optimisation phase, as well as into different sensitivity experiments involving the nudging and scaling intensities to the screen-level temperature and anemometer level windspeed.

	Wind speed (m s ²)	Temperature (°C)	Specific humidity (g kg ¹)
Observations at Cha	angins (1981-1990)		
$N_{\Psi} = 0.5$ $S_{\Psi} = 7$ $S_{u,v} = 0.5$	2.47 ± 1.65	12.67 ± 5.86	7.99 ± 3.17
$N_{\Psi} = 0.5$ $S_{\Psi} = 8$ $s_{u,v} = 0.5$	2.54 ± 1.75	12.50 ± 5.75	7.81 ± 3.09
$N_{\Psi} = 0.5$ $S_{\Psi} = 9$ $s_{u,v} = 0.5$	2.60 ± 1.84	12.33 ± 5.63	7.64 ± 3.02
$N_{\Psi} = 0.1$ $S_{\Psi} = 7$ $S_{u,v} = 0.6$	2.89 ± 1.82	11.31 ± 5.48	6.86 ± 2.69
Nudging			
$\begin{aligned} N_{\Psi} &= 0.3 \\ S_{\Psi} &= 7 \\ su, v &= 0.6 \end{aligned}$	2.87 ± 1.91	12.56 ± 5.65	7.75 ± 3.03
$N_{\Psi} = 0.5$ $S_{\Psi} = 7$ $s_{u,v} = 0.6$	2.98 ± 1.92	12.66 ± 5.61	7.91 ± 3.08
$N_{q,T} = 0.5$ $N_{u,v} = 0.1$ $S_{\Psi} = 7$ $s_{u,v} = 0.6$	2.76 ± 1.89	12.76 ± 5.65	7.96 ± 3.11
$N_{\Psi,\ell} = 1 = 0.1$ $S_{\Psi} = 7$ $s_{u,v} = 0.6$	3.08 ± 2.14	12.56 ± 5.31	7.64 ± 2.97
$N_{\Psi,\ell} = 3 = 0.1$ $S_{\Psi} = 7$ $s_{u,v} = 0.6$	2.82 ± 1.84	11.79 ± 5.44	7.13 ± 2.79
Scaling of the contri	butions to the Dynamics tend	dencies	
$N_{\Psi,\ell} = 10 = 0.1$ $S_{u,v} = 1$ $S_T = [1,3,7]$ $S_q = [1,3,7]$ $S_{u,v} = 0.6$	1.83 ± 0.94	12.75 ± 6.7	7.82 ± 3.4
$N_{\Psi,\ell} = 10 = 0.1$ $S_{u,v} = 7$ $S_T = [1,3,7]$ $S_q = [1,3,7]$ $S_{u,v} = 0.6$	2.94 ± 1.8	11.35 ± 5.5	7.02 ± 2.7
Scaling of the anem	ometer-level windspeed		
$N_{\Psi} = 0.1$ $S_{\Psi} = 7$ $s_{u,v} = 0.5$	2.40 ± 1.52	11.34 ± 5.82	6.92 ± 2.82
$N_{\Psi} = 0.1$ $S_{\Psi} = 7$ $S_{u,v} = 0.8$	3.85 ± 2.45	11.26 ± 4.78	6.74 ± 2.41

3.4.3 Sensitivity to the nudging.

Sensitivity to the nudging is analysed first by relaxing prognostic variables towards the GCMii archives with a set of values, *i.e.*, $N_{\Psi,\ell} = [0.1, 0.3, 0.5]$, and then by fixing one value to a given variable and relaxing independently the three others with values of $N_{\Psi,\ell} = 0.1$ and 0.5; in these experiments, the nudging is applied to all vertical levels ($\ell = 10$).

As shown in Figure 3.4 the water temperature profiles warm throughout the column as the intensity of the nudging towards the GCMii archived values increases. The seasonal differences with the reference simulation vary between $0.58\,^{\circ}$ C and $0.6\,^{\circ}$ C for the minima, and $0.84\,^{\circ}$ C and $1.5\,^{\circ}$ C for the maxima when $N_{\Psi,\ell}=0.3$. For a nudging of 0.5, the warming continues and the differences range respectively from $0.7\,^{\circ}$ C to $0.77\,^{\circ}$ C and $0.98\,^{\circ}$ C to $1.63\,^{\circ}$ C. The largest differences are observed from the surface down to 20 m. Even though the mean wind speed does not differ significantly from the reference simulation, a stronger nudging has an impact on warming the mean screen-level air temperature and increasing the screen-level specific humidity (Table 3.3), and thus serve to explain the warm shift of the water temperature profile.

It is noticed that the simulated water temperature profiles resulting from nudging the temperature and specific humidity to 0.5, and the wind speed to 0.1, are similar to that produced when a nudging of 0.5 is applied to all of the variables. The largest water temperature difference is 0.26 °C at 30 m depth. On the contrary, when the wind speed is nudged to 0.5 and the other variables are nudged to the value of 0.1, the water temperature profile is similar to the reference profile. This indicates that the screen-level atmospheric temperature and specific humidity are more sensitive to the large nudging values. The increase of the screen-level temperature and specific humidity is thus similar to mean values defined for a nudging of 0.5.

The nudging has also been tested on a reduced number of vertical levels. A nudging on & levels implies that $N_{\Psi,\ell}$ of less that one is applied on the ℓ layers above the surface (Eq. 9), whereas a value of one is applied otherwise. Nudging the prognostic variables from 4 to 10 levels above the surface does not significantly impact on the surface conditions. The screenand anemometer-level variables remain essentially unchanged and the water temperature profiles vary within 0.1 °C. The effects are significant when nudging 3 levels and less. Screenlevel temperature and specific humidity increase, whereas mean wind speed remains essentially unchanged, except when only 1 level is considered. From a nudging on 10 to 1 levels, the average values of the screen-level temperature, specific humidity and anemometer-level windspeed increase (Table 3.3); this warms the water column and temperature RMSEs increase in all groups of depths. However, it turns out that the increase in the mean of these atmospheric variables by a nudging of 0.1 on 3 levels reduces the RMSE in GD1 (-0.69 °C), GD2 (-0.24 °C) and GD3 (-0.23 °C), but increases in GD4 (+0.53 °C). Despite this, the bias between observed and simulated screen-level variables does not decrease further (Table 3.3). At the surface, the water temperature error lies between 0.01 °C (Winter) and -0.43 °C (Autumn), at 15 m between 0.07 °C (Winter) and 0.65 °C (Summer), at 50 m between 0.22 °C (Winter) and -0.35 °C (Autumn), and at 100 m between 0.01 (Autumn) and 0.21 °C (Winter).

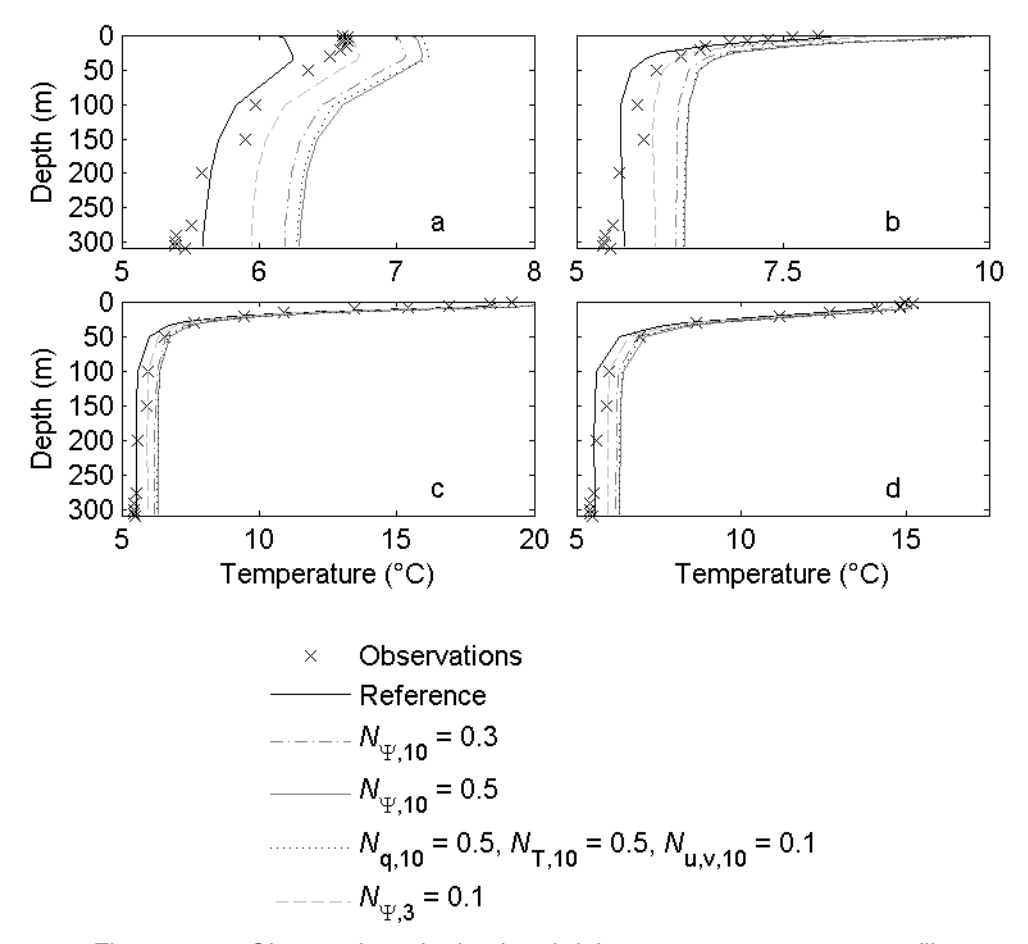


Figure 3.4. Observed and simulated lake-water temperature profiles, seasonally averaged for a) DJF, b) MAM, c) JJA, and d) SON. Simulations use a fixed scaling of the contributions to the Dynamics tendencies ($S_{\Psi}=7$) and of the anemometer wind speed ($s_{\rm u}$, $s_{\rm v}=0.6$), but varying values for the nudging $N_{\Psi,\ell}$ and the number of level in the vertical on which these are applied.

3.4.4 Sensitivity to the scaling of the contributions to the Dynamics tendencies

The analysis has been done by allowing the scaling parameters $\mathcal{S}_{\Psi,\ell}$ to vary independently to the contributions to the Dynamics tendencies (Eq. 7). The optimal ad hoc scaling was found to be 7, so this value is fixed for at least one variable, whereas for the other variables it takes the values of 1 and 3, thus producing 19 simulations.

The seasonal water temperature profiles simulated using the various scaling values all behave differently, while the location of the thermocline and water temperature produce 3 groups of profiles as shown in Figure 3.5. The analysis of the water temperature profiles shows that the scaling of the contributions to the wind Dynamics is the most important. The smaller the scaling, the colder the bottom water temperatures are, and the steeper is the temperature gradient in the thermocline. The $S_{\rm u}$ and $S_{\rm v}$ components explain 99% of wind variance, 95% of temperature variance and 81% of specific humidity variability. Their increase raises the mean wind speed and its standard deviation, whereas they reduce those for the atmospheric temperature and specific humidity at the screen level (Table 3.3). The mean anemometer-level windspeed with $S_{\rm u}$ and $S_{\rm v}=7$ agrees with that of the observation, whereas the bias in the atmospheric temperature and specific humidity averages is positive, whatever the values given to $S_{\rm T}$ and $S_{\rm q}$.

Small variations in the screen-level variable averages are observed according to the combinations of values taken by S_T and S_q . For given S_u , S_v and S_T values, it appears that

mean atmospheric temperature and specific humidity decrease with increasing S_q . However, their effects on the water temperature profiles are small. For instance, the mean of the seasonal RMSEs in layers 0-10 m varies between 1.48 °C and 1.80 °C (S_u and $S_v = 1$), 1.15 °C and 1.30 °C (S_u and $S_v = 3$), 0.7 °C and 0.76 °C (S_u and $S_v = 7$), for any given values of S_T and S_q .

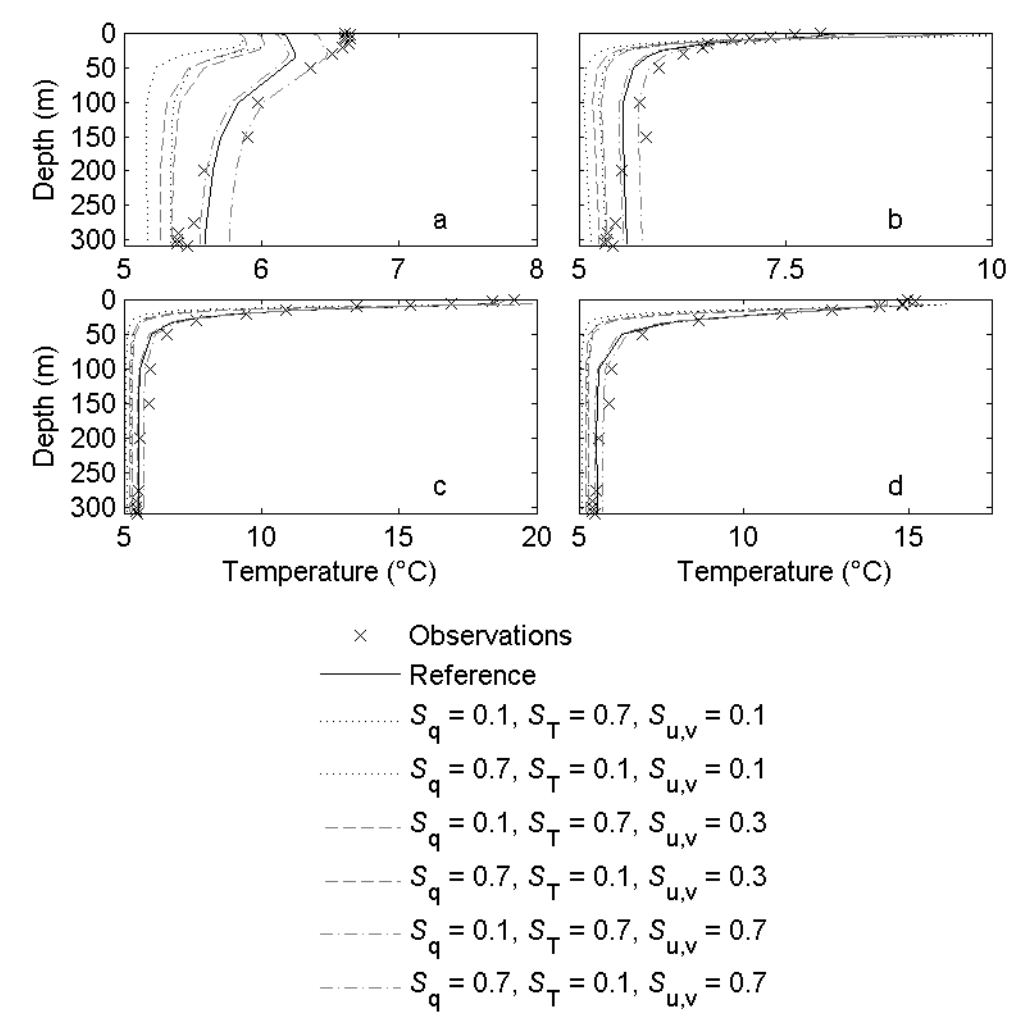


Figure 3.5. Observed and simulated lake-water temperature profiles, seasonally averaged for a) DJF, b) MAM, c) JJA, and d) SON. Simulations use a fixed scaling for the anemometer wind speed (s_u , $s_v = 0.6$) and for the nudging towards the GCMii archived values ($N_{\Psi,\ell} = 0.1$), but varying values are applied to the scaling of the contributions to the Dynamics tendencies $S_{\Psi,\ell}$.

The scaling parameters that produce the lowest RMSE with regard to the whole water column are as follow: $S_q = 1$, $S_T = 7$, S_u and $S_v = 7$. The simulated water temperatures fit with lake observations at all depths and for all seasons as shown in Figure 3.6; the bias varies between -0.67 °C (autumn) and 0.49 °C (Spring) at the surface, -0.19 °C (Winter) and 0.63 °C (Summer) at 15 m, -0.49 °C (autumn) and 0.01 °C (Winter) at 50 m, and -0.18 °C (Autumn) and 0.03 °C (Spring) at 100 m.

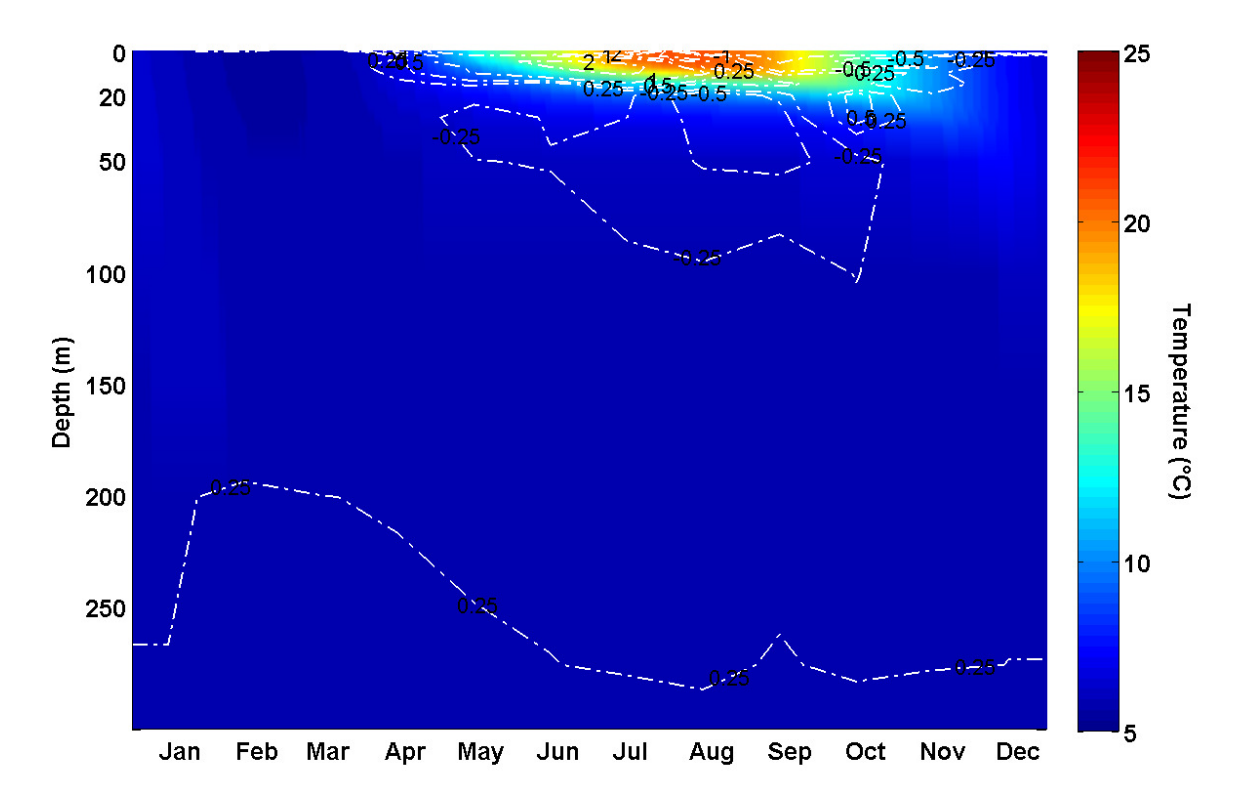


Figure 3.6. Time-depth vertical cross section of simulated lake water temperature using the optimal parameter values: $N_{\Psi,\ell} = 0.1$, $S_{\Psi,\ell} = 7$, where $\Psi = \{T, u, v\}$, $S_{\Psi,\ell} = 1$ for $\Psi = q$, $\ell = 10$; s_u , $s_v = 0.6$, wind gust parameterization is not activated, $\alpha_{\text{seiche}} = 0.01$, $q_{\text{seiche}} = 0.9$; lake depth is in meters and the colour scale is in °C. Differences (°C) between observed and simulated temperatures are in dotted lines.

3.4.5 Sensitivity to the scaling of the anemometer-level windspeed

The effect of the intensity of the simulated anemometer-level windspeed on the thermal profile has been evaluated by varying its scaling around the value of the reference calibration. Therefore, the scaling s_u and s_v is varied from 0.5 to 0.8.

As shown in Figure 3.7, the reduction of s_u and s_v produces a warming of the topmost 2.5 m of water in Spring (difference of + 0.11 °C) and the first 7.5 m in Summer (difference of +0.58 °C), when compared to the reference profile. Below, the average cooling reaches -0.63 °C at 50 m and -0.47 °C at 100 m. Reverse effects are noticed when s_u and s_v both increase. The higher these values are the colder the surface temperature, the warmer the bottom temperature and the smoother the temperature gradient are in the thermocline. For instance, a scaling of 0.8 produces a cooling of 1.19 °C at the surface and a warming of 1.84 °C at 15 m, 1.49 °C at 50 m and 1.03 °C at 100 m during Summer. Table 3.3 shows that the scaling of the anemometer-level wind speed produces large variations of the mean windspeed, but does not affect significantly the atmospheric temperature and specific humidity. As the mean wind speed attains higher values, the warming of deeper layers is explained by the increase of the mixing processes and by the loss of heat in the surface layer due to heat penetration to deeper layers.

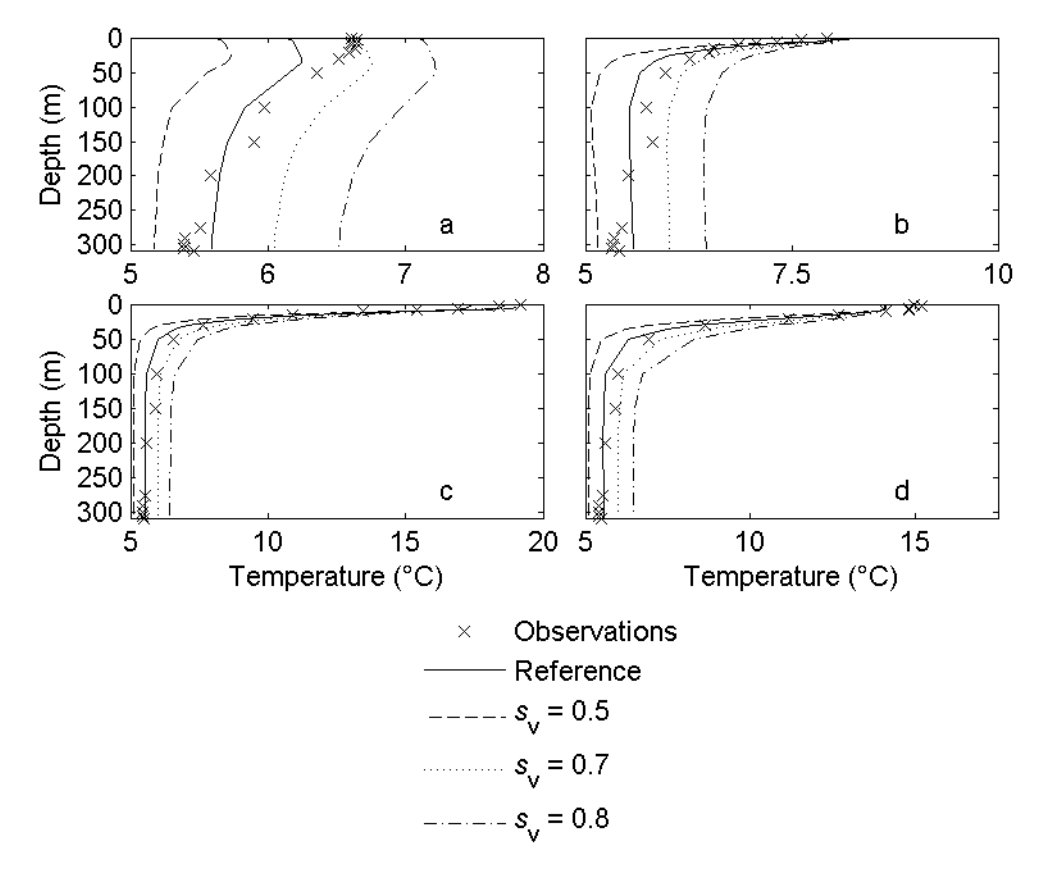


Figure 3.7. Observed and simulated lake-water temperature profiles seasonally-averaged for a) DJF, b) MAM, c) JJA, and d) SON. Simulations use a fixed scaling of the contributions to the Dynamics tendencies ($S_{\Psi,\ell} = 7$) and of the nudging towards GCMii archived values ($N_{\Psi,\ell} = 0.1$), but varying values are applied to the scaling of the anemometer wind speed, $s_{\rm u}$ and $s_{\rm v}$.

3.4.6 Sensitivity to the wind gust parameterization

Wind gust parameterization has been activated in order to produce high wind events. The number of consecutive timesteps upon which the parameterization is applied influences the sensitivity test on the water temperature profiles. The module is thus activated during 72 time steps (1 day), 144 timesteps (2 days) and 216 timesteps (3 days). The mean seasonal water temperature profiles are rather insensitive to such short periodic events of a given magnitude (Eq. 11). The increase of the mean anemometer-level wind speed caused by the activation of the parameterization over 3 days is of the order of 0.03 m s⁻², causing maximum differences with the reference profile of $0.04\,^{\circ}$ C.

3.4.7 Sensitivity to the surface drag and the seiches parameterization

The two lake-model specific parameters used to calibrate the production/dissipation of TKE due to seiches have been tested; $\alpha_{\rm seiche} = 0.006$ instead of 0.01, and $q_{\rm seiche} = 0.6$ instead of 0.9. Variations of $q_{\rm seiche}$ do not modify significantly the lake water temperature, apart from a 2-m shift in the thermocline position. On the contrary, the lake profile is sensitive to the variations of $\alpha_{\rm seiche}$, as this value serves to calibrate the amount of mixing in the interior of the lake due to the energy transfer from the wind to seiche motions. Therefore, its reduction causes less heat to penetrate deeper into the lake. As a result, from 10 m down to the bottom, the cooling of the water temperature is systematic. Below 100 m the decrease is on average 0.3 °C, whereas it ranges between 0.26 °C (Spring) and 0.69 °C (Summer) at 15 m and between 0.31 °C (Winter) and 0.56 °C (Autumn) at 50 m, due to the stronger temperature

gradient simulated in the thermocline. At the surface, seasonal temperature differences are weak compared to the annual variability (< 0.3 °C). Screen- and anemometer-level variables are not significantly affected by the lake calibration.

Finally, a new parameterization of the surface drag coefficient that accounts for the wind speed is tested. Since this parameterization increases the wind energy acting upon the surface, a more intense mixing smears out the temperature gradient in the thermocline and warms the column at all times of the year, with one exception in Summer from the surface down to 7.5 m. As a result, the water temperature error is lower than 0.13 °C from 50 m down to 150 m during the stratification periods, and the warming of the simulated water profiles decreased the RMSEs in GD1, GD2, and GD3. The temperature increase varies between 0.3 °C (Winter) and 0.82 °C (Summer) at 15 m and between 0.35 °C (Spring) and 0.7 °C (Autumn) at 50 m. From 100 m and below, the increase ranges between 0.27 °C and 0.38 °C. Screen- and anemometer-level variables do not vary significantly either. Unlike the seiche parameterization, the varying surface drag coefficient produces a similar RMSE between simulated and the observed water temperature profile, except in the 100 m layer above the bottom.

3.5 Discussion and concluding remarks

The above results indicate that the model's adjustable parameters have an impact on the simulated water temperature profiles, on the screen-level temperature and humidity, as well as on the anemometer-level windspeed. However, devising an optimal combination is challenging because of the non-linear effects generated by the coupling technique. These parameters modulate the surface turbulent and radiation fluxes that couple the lower atmosphere to the lake, drive the surface water temperature and then feed back on the atmospheric boundary layer that modulates the values of surface atmospheric variables. The differences between observed and simulated downward solar and infrared fluxes at the surface are generally from 3 to 74 W m⁻² for the solar flux, and from -4 to 28 W m⁻² for the infrared flux respectively, where the clouds are the major factors explaining these differences. Yet, a combination of these parameter values has been found to produce seasonal water temperature profiles and surface atmospheric variables in a realistic manner.

While nudging the atmospheric variable towards the GCM profiles tends to increase the mean screen-level atmospheric temperature and specific humidity, a higher scaling of the contributions to the Dynamics tendencies tends to reduce their values. However, their individual effects on the water temperature profiles are similar. In both cases, a warming is observed throughout the whole water column. While the mean anemometer-level wind speed is not significantly affected by a stronger nudging, a higher scaling increases its mean and variability. This increase in the momentum flux towards the water surface, and thus more energy is available to transfer heat with depth and the effects of colder air temperature, does not impact on the water column. To cool the water temperature, it is thus necessary to modify the parameter that scales the anemometer-level wind speed without significantly modifying the other variables. This is achieved by scaling down the anemometer-level wind speed, together with increasing the scaling of the contributions to the Dynamics tendencies. This shows that the effects of a reduction of the nudging towards the GCMii profiles can be compensated by varying the scaling of the contribution to the Dynamics tendencies and the anemometer-level windspeed.

Parameters optimisation using a weak nudging towards the GCMii archived values ($N_{\Psi,\ell}$ = 0.1) can realistically reproduce the observed water temperature profiles as well as the atmospheric screen variables. A constant value for the scaling of the contributions to the Dynamics tendencies ($S_{\Psi,\ell}$ = 7) and an adequate value for the scaling of the anemometer-

level windspeed (s_u , s_v = 0.6) generate RMSEs of 0.75 °C in GD1, 0.38 °C in GD2, 0.24 °C in GD3 and 0.15 °C in GD4. Despite a small negative bias in the seasonal water temperature profiles, the mean error of the screen-level air temperature, specific humidity and anemometer-level windspeed are respectively 0.09 m s⁻², -0.87 °C and -0.4 g kg⁻¹. However, the sensitivity analysis revealed that the water temperature profiles can more closely approximate to seasonal observations. Even though the scaling of the contributions to the Dynamics tendencies was proven to impact mainly on the anemometer-level wind speed, a different scaling of the temperature and specific humidity may slightly shift the temperature profiles. Therefore, the most accurate results were found when S_q was lowered to 0.1. The RMSEs was reduced to 0.73 °C in GD1, to 0.25 °C in GD2, to 0.15 °C in GD3 but increased to 0.34 °C in GD4. The mean value of the anemometer-level wind speed is reduced (0.04 m s⁻²), but the mean values of temperature and specific humidity are increased, 1.04 °C and 0.74 g kg⁻¹ respectively.

Variations in the number of levels on which the nudging is applied also influenced the RMSEs in GD1, GD2 and GD3. When the strongest nudging towards the GCMii profiles is applied on more than 6 levels (*i.e.*, $N_{\Psi,\ell>6}=1$), screen- and anemometer-level variables react to an increase in the value of the nudging, but more weakly. A nudging on 1 level (that is 9 levels with $N_{\Psi}=1$) produces less variations than a nudging of 0.3 on 10 levels. Therefore a nudging on 3 levels was shown to improve the water temperature profile without negatively affecting the simulation of the atmospheric variables. However, this improvement is due to the negative bias of the simulated water temperature profile. Since the effects of the nudging of the atmospheric variables imply a warming of the water column, the simulated profile necessarily crosses the observation and may reduce the bias. By applying a nudging on 3 levels to the previous calibration obtained using the following scaling values, $S_q=1$, $S_T=7$, S_u and $S_v=7$), the influence of the GCMii on the water profile is very strong and produces a positive bias. Since the wind gust function has a negligible effect on the atmospheric variables, the optimal calibration does not make use of it.

The anemometer-level windspeed showed no significant changes following the application of the extreme winds parameterization, perhaps because we prescribed only the wind profiles regardless of the temperature and of the specific humidity profiles. Also, the nudging procedure should be modified during these extreme events.

Even though the lake surface temperatures are sensitive to variations of lake-model parameters $\alpha_{\rm seiche}$, $q_{\rm seiche}$, and to $c_{\rm D}$, mean screen-level atmospheric variables do not vary significantly. The temperature gradient in the thermocline is less accurately resolved by decreasing the value of $\alpha_{\rm seiche}$. On the contrary, a varying surface drag coefficient improves the simulation of the thermocline. The variations of $c_{\rm D}$ due to increasing wind speeds allow heat to penetrate deeper, reducing the RMSEs down to 150 m. However, compared to the calibration with varying S_{Ψ} , the RMSEs are higher.

The optimal parameter values combination found in this study is applicable only for Lake Geneva. Other parameter values would presumably be required for other lakes. The coupled FIZC/ k- ε is currently being tested on other lakes in order to cover a range from shallow to deep, non freezing to freezing, low altitude to high altitude and crystal clear to turbid waters, but also other lake types, *i.e.*, monomictic, dimictic, etc., such as that depicted in the LakeMIP project (www.unige.ch/climate/lakemip/index.html). Consequently, this coupled model is further tested against a variety of configurations in order to adequately reproduce the atmosphere-water interactions and the lake thermal profiles. These include an increased number of vertical levels of FIZC to refine the vertical profiles, as well as to better represent the momentum and the energy fluxes in the boundary layer, but also other numerical time-marching schemes, etc. Other tests aim at reducing the number of vertical levels of the k- ε lake model to reduce the computational load that may be a limiting factor in regional climate simulation over a lake-rich region. Finally, if one plans to run a GCM or a RCM with the intention of outputting the contributions to the Physics tendencies \overline{P}_{Ψ} , or

ultimately those of the Dynamics \overline{D}_{Ψ} , an archival frequency higher than 24-h would better represent the diurnal cycle of the large-scale circulation through their effects on the lateral advection of temperature, moisture and momentum.

3.6 Acknowledgements

Dr. Douglas Cripe (GEOS) made helpful comments on a draft of this manuscript. We would also like to thank Dr. Warren Lee of the Canadian Centre for Climate modelling and analysis (CCCma) for providing the second version General Circulation Model (GCMii) simulated archives needed to run the FIZC atmospheric model.

3.7 References

- Asselin, R. A. 1972. Frequency filter for time integrations. Mon. Wea. Rev. 100: 487-490.
- Ball, M. A., and R. S. Plant. 2008. Comparison of stochastic parametrization approaches in a single-column model. Phil. Trans. R. Soc. A. 366: 2603-2621. doi:10.1098/rsta.2008.0050.
- Betts, A. K, and M. J. Miller. 1986. A new convective adjustment scheme. Part II: Single column tests using GATE wave, BOMEX, ATEX and arctic air-mass data sets. Quart. J. Roy. Meteor. Soc. 112: 693-709.
- Boer, G.J., N.A. McFarlane, and M. Lazare. 1992. Greenhouse Gas-induced Climate Change Simulated with the CCC Second-Generation General Circulation Model. J. Clim. 5: 1045-1077.
- Bonan, G. D. 1996. A land surface model (LSM version 1.0) for ecological, hydrological, and atmospheric studies. Technical description and user's guide. NCAR Technical Note NCAR/TN-417+STR, National Center for Atmospheric Research, Boulder.
- Christensen, J. H., T. Carter, F. Giorgi. 2002. PRUDENCE Employs New Methods to Assess European Climate Change. EOS. 83: 147.
- Clayson, C. A., and A. Chen. 2002. Sensitivity of a coupled Single-Column model in the Tropics to treatment of the interfacial parameterizations. J. Clim.15, 1805-1831.
- Dolman, A. J. and D. Gregory. 1992. A parameterization of rainFall interception in GCMs. Q. J. R. Meteorol. Soc. 118: 455-467.
- Girard, E, J.-P. Blanchet. 2001: Simulation of arctic diamond dust and ice fog and thin stratus using an explicit aerosol-cloud-radiation model. J. Atmos. Sci., 58, 1199-1221.
- Goudsmit, G.-H., H. Burchard, F. Peeters, and A. Wüest. 2002. Application of k-ε turbulence models to enclosed basins: The role of internal seiches. J. Geophys. Res. 107: 3230-3243. doi:10.1029/2001JC000954.
- Goyette, S. and M. Perroud. 2008. Interfacing Single Column Lake and Atmospheric Models: Application over Lake Geneva for Observed and Climate Warming Scenario. Fall meeting, San Francisco (USA), December 2008.
- Goyette, S., N. A. McFarlane, and G. M. Flato. 2000. Application of the Canadian Regional Climate Model to the Laurentian Great Lakes region: Implementation of a lake model. Atmos.-Ocean. 38: 481-503.
- Goyette, S., and R. Laprise. 1996. Numerical investigation with a physically based regional interpolator for off-line downscaling of GCMs: FIZR. J. Climate. 9: 3464-3495.
- Hack, J. J., and J. A. Pedretti. 2000. Assessment of solution uncertainties in single-column modeling frameworks. J. Climate. 13: 352-365.
- Hewitt, C. D and D. J. Griggs. 2004. Ensembles-based predictions of climate changes and their impacts. EOS. 85: 566.

- Hostetler, S. W., Bates, G. T. and Giorgi, F. 1993. Interactive coupling of a lake thermal model with a regional climate model. J. Geophys. Res. 98: 5045-057.
- lacobellis, S. F., G. M. McFarquhar, D. L. Mitchell, and R. C. J. Somerville. 2003. The sensitivity of radiative fluxes to parameterized cloud microphysics. J. Clim. 16: 2979-2996.
- Koster, R. D., P. S. Eagleson. 1990: A one-dimensional interactive soil-atmosphere model for testing formulations of surface hydrology. J. Clim. 3: 593-606.
- Laprise, R. and C. Girard. 1990. A spectral general circulation model using a piecewise-constant finite element representation on a hybrid vertical coordinate system. J. Clim. 3: 32-52.
- Lee, W. H., S. F. Iacobellis, and R. C. J. Somerville. 1997. Cloud radiation forcings and feedbacks: General circulation model tests and observational validation. J. Clim. 10: 2479-2496.
- Lohmann, U., N. McFarlane, L. Levkov, K. Abdella, and F. Albers. 1999. Comparing different cloud schemes of a single column model by using mesoscale forcing and nudging technique. J. Clim. 12: 438-461.
- McFarlane, N. A., G. J. Boer, J.-P. Blanchet, and M. Lazare. 1992. The Canadian climate centre second generation general circulation model and its equilibrium climate. J. Climate. 5: 1013-1044.
- Mironov, D. V. 2008. Parameterization of lakes in numerical weather prediction. Description of a lake model. COSMO Technical Report, No. 11, Deutscher Wetterdienst, Offenbach am Main, Germany, 41 pp.
- Peeters, F., D. M. Livingstone, G. Goudsmit, R. Kipfer, and R. Forster. 2002. Modeling 50 years of historical temperature profiles in a large central European lake. Limnol. Oceanogr. 47: 186-197.
- Perroud M., S. Goyette, A. Martynov, M. Beniston and O. Anneville. 2009. Simulation of multiannual thermal profiles in deep Lake Geneva: A comparison of one-dimensional lake models. Limnol. Oceanogr. 54: 1574-1594.
- Pitman, A. J. 1994. Assessing the sensitivity of a land-surface scheme to the parameter values using a single column model. J. Climate. 7: 1856-1869.
- Pitman, A.J., Yang, Z-L. and A. Henderson-Sellers. 1993. Sub-grid Scale Precipitation in AGCMS: Re-assessing the Land Surface Sensitivity using a Single Column Model. Clim. Dyn. 9: 33-41.
- Randall, D. A., D. G. Cripe. 1999. Alternative methods for specification of observed forcing in single-column models and cloud system models. J. Geophys. Res. 104: 24,527-24545.
- Randall, D. A., K.-M. Xu, R. J. C. Somerville, and S. Iacobellis. 1996. Single column models and cloud ensemble models as links between observations and climate models. J. Climate. 9: 1683-1697.
- Swayne, D., D. Lam, M. MacKay, W. Rouse, W. Schertzer. 2005. Assessment of the interaction between the Canadian Regional Climate Model and lake thermal-hydrodynamic models. Env. Mod. Soft. 20: 1505-1513.

- Stephens, G. I. 1984: The parameterization of radiation for numerical weather prediction and climate models. Mon. Wea. Rev. 112: 826-867.
- Stokes, G. M., and S. E. Schwartz. 1994. The atmospheric radiation measurement (ARM) program: Programmatic background and design of the cloud and radiation test bed. Bull. Amer. Meteor. Soc. 75: 1202–1221.
- University of Wyoming, Department of Atmospheric Science web site: http://weather.uwyo.edu/upperair/sounding.html.
- Wilks, D: S., 2008: Effects of stochastic parametrization on conceptual climate models. Phil. Trans. R. Soc. A. 366: 2475-2488. doi:10.1098/rsta.2008.0005.
- Zhu, P., C. S. Bretherton, M. Köhler, A. Cheng, A. Chlond, Q. Geng, P. Austin, J.- C. Golaz, G. Lenderink, A. Lock, and B. Stevens. 2005. Intercomparison and interpretation of Single-Column Model simulations of a nocturnal stratocumulus-topped marine boundary layer. Mon. Wea. Rev. 133: 2741-2758.

Chapter 4

Thermal response of the deep Swiss Lake Geneva under a 2 x CO₂ global climate change

Marjorie Perroud and Stéphane Goyette

Climatic Change and Climate Impacts (C3I), University of Geneva, Carouge, Geneva, Switzerland

Abstract

The response of the deep Swiss lake, Lake Geneva, to global warming caused by an increase in atmospheric carbon dioxide concentration (i.e., 2 x CO₂) was investigated using a coupled lake-atmosphere model. The one-dimensional k- ε lake model SIMSTRAT has thus been interfaced with the single column atmospheric model FIZC. Compared to former uncoupled experiments where atmospheric variables were used to drive the lake model without being modified, coupling the models allowed for strong feedbacks between the lake surface and the atmosphere and produced changes in atmospheric moisture and cloud cover that further modified the downward radiation fluxes. The time evolution of atmospheric variables as well as those of the lake's thermal profile could be reproduced realistically by devising a set of adjustable parameters. In a "control" 1 x CO₂ climate experiment, the coupled FIZC-SIMSTRAT model demonstrated genuine skills in reproducing epilimnic and hypolimnic temperatures, with annual mean errors and standard deviations of 0.26 °C ± 0.27 °C and 0.31 °C ± 0.14 °C respectively. Following this, several decades were needed to spin up the water temperature in order to reach equilibrium in the 2 X CO₂ climate. Doubling CO₂ concentration induced an atmospheric warming that impacted the lake's thermal structure, increasing the stability of the water column and extending the stratified period by 3 weeks. Epilimnic temperatures were seen to increase by 2.6 ℃ to 4.2 ℃ while hypolimnion temperatures increased by 2.2°C. Climate change modified components of the surface energy budget through changes mainly in air temperature, moisture and cloud cover. During summer, reduced cloud cover resulted in an increase in the annual net solar radiation budget. A larger water vapor deficit at the air-water interface induced a cooling effect in the lake.

Submitted to: Water Resour. Res.

4.1 Introduction

European climate experienced a surface air temperature warming of 0.9 ℃ during the 20th century (Jones and Moberg 2003), resulting in a wide-range of impacts that followed the first signs of change (Alcamo et al. 2007). According to projections made for future climate, southern and central Europe would experience the largest changes in mean air temperature during summer while the northern regions would be more strongly affected during winter. The warming would also have a number of impacts on the distribution of precipitation throughout Europe (Christensen et al. 2007). Annual precipitation is predicted to increase in the North. decrease in the South and increase during winter but decrease during summer in Central Europe, resulting in more frequent summer droughts. In Switzerland, the recent trends of these variables are consistent with projections for central Europe (Schmidli et al. 2002; OcCC 2008). In the Alps, changes in winter precipitation have reduced the length of the snow season and the amount of snow (Beniston 1997) and with higher summer temperatures, have caused glacial mass wasting (Paul et al. 2004). In the lowlands, the more severe heat waves and heavier precipitation of the last decades (Luterbacher et al. 2004; Della-Marta et al. 2007), have caused crop losses, water shortages, like in the regions of the Swiss Jura and Swiss Plateau during the summer heat wave of 2003, and large flood events (De Bono et al. 2004; Voigt et al. 2005).

In many western-European lakes changing climate has resulted in increased water column stability, longer stratified periods, and warmer temperatures in the epilimnion (Peeters *et al.* 2002; Livingston 2003). These findings are in agreement with the observations for other midand high-latitude lakes (Robertson and Ragotzkie 1990; Schindler *et al.* 1996; King *et al.* 1997; McCormick and Fahnenstiel 1999). While the impacts of changes in climate in the Alps have been reported by many authors (Theurillat and Guisan 2001; Abegg *et al.* 2007; Uhlmann *et al.* 2009; Beniston *et al.* 2010), very few studies have attempted to relate future climate projections to their potential impacts on perialpine lakes (Peeters *et al.* 2002; 2007; Perroud and Goyette 2010). This enhances the need to lead investigations on a variety of lakes, grabbing the opportunity to develop new methods

This study examines the thermal evolution of the waters of Lake Geneva, which is located at an altitude of 372 m a.s.l. between Switzerland and France. Long term monitoring (since the 1950s) of Lake Geneva at its deepest point (309 m), has shown that the lake has changed in response to recent warmer conditions (Lazzarotto *et al.* 2004; Dokulil *et al.* 2006). Despite large interannual variability, trend analyses have shown that bottom temperatures have risen over the last 50 years from 4.5 °C to ~ 6 °C in 2002. The annual mean surface temperatures have increased by more than 1 °C since the early 1970s (Lazzarotto *et al.* 2004).

The objective of this study is to investigate the lake response with a coupled lake-atmosphere model. This approach, as described in Goyette and Perroud (2010), might also ultimately contribute to understanding the impacts of Lake Geneva on global warming. In such numerical experiments, results, as it is likely to be at the time of a doubling of CO₂, are compared to those achieved in a control "1 x CO₂" climate. This method, used in former studies, assume initial concentrations of GHG in the atmosphere close to the one recorded in the second half of the 20th Century (*i.e.*, 1 x CO₂) and then the final concentrations (*i.e.*, 2 x CO₂) similar to these projected by the IPCC-SRES A2 scenario in the middle of 21th Century, (Nakicenovic *et al.* 2000).

Using coupled models to numerically investigate long-term lake-atmosphere interactions is innovative. Currently lake sensitivity analyses use meteorological forcing computed by atmospheric models rather than observations to run lake models for both current and future climate scenarios (Hostetler and Giorgi 1995; Blenckner *et al.* 2002; Malmaeus *et al.* 2005). However, interactions between the lake and the overlying atmosphere have not been taken into consideration in most investigations. Thus, studies that focus on the effects of climate on

lakes, are generally confined to stand-alone experiments, *i.e.*, that lake models are forced with a prescribed atmosphere. The inclusion of a lake model, rather than prescribed surface conditions, may also better reproduce processes involved in the energy and radiation budgets, impacting air mass stability and cloud formation. The lack of literature dealing with such coupled models was recently highlighted by MacKay *et al.* (2009), and pointed to the need to better understand the role of lakes and reservoirs in the climate system.

For weather prediction applications, the fully interactive coupling of a lake model with an atmospheric model, such as the FLake model in the COSMO model (Mironov et al. 2010), is already possible, however this is mainly due to the fact that only short-term simulations, which are less computationally demanding, have been run. Two-way coupling of lake and atmospheric models for climate simulations is still in the very early stage. It is usually done using complex Global Climate Models (GCM) or Regional Climate Models (RCM), but lake models are still rather simple and simulations are run over short periods of time (Hostetler et al. 1993; 1994; Hostetler and Small. 1999; Small et al. 1999; Song et al. 2004). The first successful implementation included a mixed-layer-model (Goyette et al. 2000) and an eddydiffusivity model in the Canadian Regional Climate Model (Martynov et al. 2010). More complex models such as 3D lake models, can currently only interact with the atmosphere in a stand-alone mode for coupling and regionalization issues (Swayne et al. 2005). The high computational costs and the large amount of data required to calibrate, validate and run these 3 D models (Leon et al. 2007) restrict their use for climatological applications. Single Column Models (SCMs) with their lower computational costs represent a useful trade-off to study the effect of the climate on lakes at a particular location over a long time period. SCMs and 1D lake models are both less computationally-demanding than RCMs or 3D lake models, allow a good representation of vertical processes and may thus be used in the present context for long term simulations.

Here we describe a procedure to calibrate the lake model parameters using a 6-year test period. The optimal parameters were determined by minimizing the error to observed thermal profiles and were then used to run the coupled model under the influence of 1 x CO_2 and 2 x CO_2 climates. Lake warming caused by a doubling of the CO_2 concentration in the atmosphere was quantified by comparing the water column thermal profiles for both climate conditions. A description of changes at the air-water interface is made in terms of surface fluxes and other atmospheric variables. Epilimnic and hypolimnic water temperature obtained using this coupled model are compared to water temperatures from an uncoupled, one way-driven lake model.

4.2 The coupled model

The FIZC-SIMSTRAT coupled model used in this study is a two-way computational method where feedbacks between the lake and the atmosphere are allowed in the vertical dimension. In this section, an overview of the approach is provided and the readers are referred to the paper of Goyette and Perroud (2010) for a broader description of the model. The climate change application described in this paper may be considered as a follow-up study of the work undertaken earlier by Perroud and Goyette (2010). In the former case, the one-way modelling methodology assumed that the lake model SIMSTRAT is driven initially by observations that were subsequently perturbed to emulate a climatic change in the atmosphere. The lake then responded to atmospheric perturbations that were considered as differences diagnosed on the basis of outputs from a Regional Climate Model (RCM) in the context of the EU 5th Framework project "PRUDENCE" over the period 2071-2100 (Christensen *et al.* 2002).

A few changes have been made to the column model of the atmosphere described in Goyette and Perroud (2010). These changes, described below, include the implementation of an improved parameterization of the contributions to the dynamic tendencies, addition of an option to improve shortwave radiation by means of observed monthly mean stratospheric ozone profiles compiled from measurements made at the Payerne climate station (46.8N; 6.94E; 490 m a.s.l.) instead of the zonally-averaged concentrations used by GCMii (McFarlane *et al.* 1992), and the addition of the option to scale the driving specific humidity profiles.

The atmospheric model is a SCM, termed FIZC, which can be considered as an atmospheric column from the second generation of the Canadian General Circulation Model, or GCMii, taken in isolation from the rest of the GCMii, and applied at a particular location. GCMii has computational grid of 96 x 48 points in the horizontal and 10 levels in the vertical. It employs a semi-prognostic technique whereby the temporal evolution of the prognostic variables $\Psi = [u, v, T, q]$ in the column, where u and v represent the horizontal components of the wind velocity, T, the air temperature and q, the specific humidity, are described schematically as follows:

$$\frac{\partial \Psi}{\partial t} = D_{\Psi}^{\star} + P_{\Psi}^{\star} \tag{1}$$

As shown in Eq. (1), Ψ evolves in time following two main chains of processes, functions of the horizontal and vertical spatial dimensions, and of time. First, the contributions to the dynamic tendencies, also termed "the dynamics" D_{Ψ} , include the resolved processes of the flow fields operating mainly in the horizontal such as the pressure gradient, the advection, and the Coriolis terms. Second, the contributions to the physics tendencies, also termed "the physics" P_{Ψ} , include the parameterised effects of the unresolved processes of the flow fields operating mainly in the vertical, such as the solar and infrared radiation, cloud and precipitation processes, vertical diffusion of momentum, sensible and latent heat, convection, surface-atmosphere exchanges (momentum, heat, and moisture over either land or water surfaces) including dependencies on surface and subsurface processes.

While the contributions to the physics tendencies can be recomputed at each time step within the atmospheric column using the GCMii physics parameterization module, the contributions to the dynamics tendencies are *a priori* unknowns and must therefore be inferred and then prescribed to FIZC. During the course of GCMii simulations, the atmospheric profiles values of Ψ were archived at 12-hourly time intervals and the contributions to the physics tendencies, symbolized by \overline{P}_{Ψ} , were cumulated and archived at 24-hourly intervals. Consequently, the mean contributions to the Dynamics can be determined as follows:

$$\overline{D}_{\Psi} = \frac{\partial \Psi}{\partial t} - \overline{P}_{\Psi} \tag{2}$$

The large-scale dynamics, function of space and time, was then used to prescribe FIZC contributions to the dynamics in the atmospheric column:

$$D_{\Psi}^{\star} = (1 + R_{\Psi})\overline{D}_{\Psi} \tag{3}$$

The parameterization described in Eq. (3) is slightly different from the one described in Goyette and Perroud (2010) and shows better behaviour in time thus warranting a more realistic day-to-day variability in Ψ . Equation (3) represents the prescribed dynamics computed on the basis of GCMii archives in the column, \overline{D}_{Ψ} , which is superimposed on white noise, $R_{\Psi} = S_{\Psi} R^*$, with S_{Ψ} , a scaling parameter allowed to vary in the vertical for each prognostic variable and R^* , a random number ranging from -1 to +1. Consequently, this parameterized dynamics, combined with the computations of the physics, P_{Ψ} , serves to compute the evolution of atmospheric profiles of Ψ in the column at each time step.

The contributions to the dynamic tendencies employ a simple stochastic parameterization to represent the effects of unresolved processes. However, this parameterization may not cover the range of variability that is required to reproduce the unresolved scales of the flow and may result in model biases. In order to allow the FIZC computed atmospheric profiles to develop their intrinsic variability but at the same time avoid too much drift from the GCMii ones, a nudging option which allows relaxing FIZC prognostic variables Ψ toward those of the GCMii archives was implemented as follows:

$$\Psi_{m,\ell} = \mathcal{N}_{\Psi,\ell} \ \Psi_{GCMii,m,\ell} + (1 - \mathcal{N}_{\Psi,\ell}) \ \Psi_{FIZC,m,\ell} \tag{4}$$

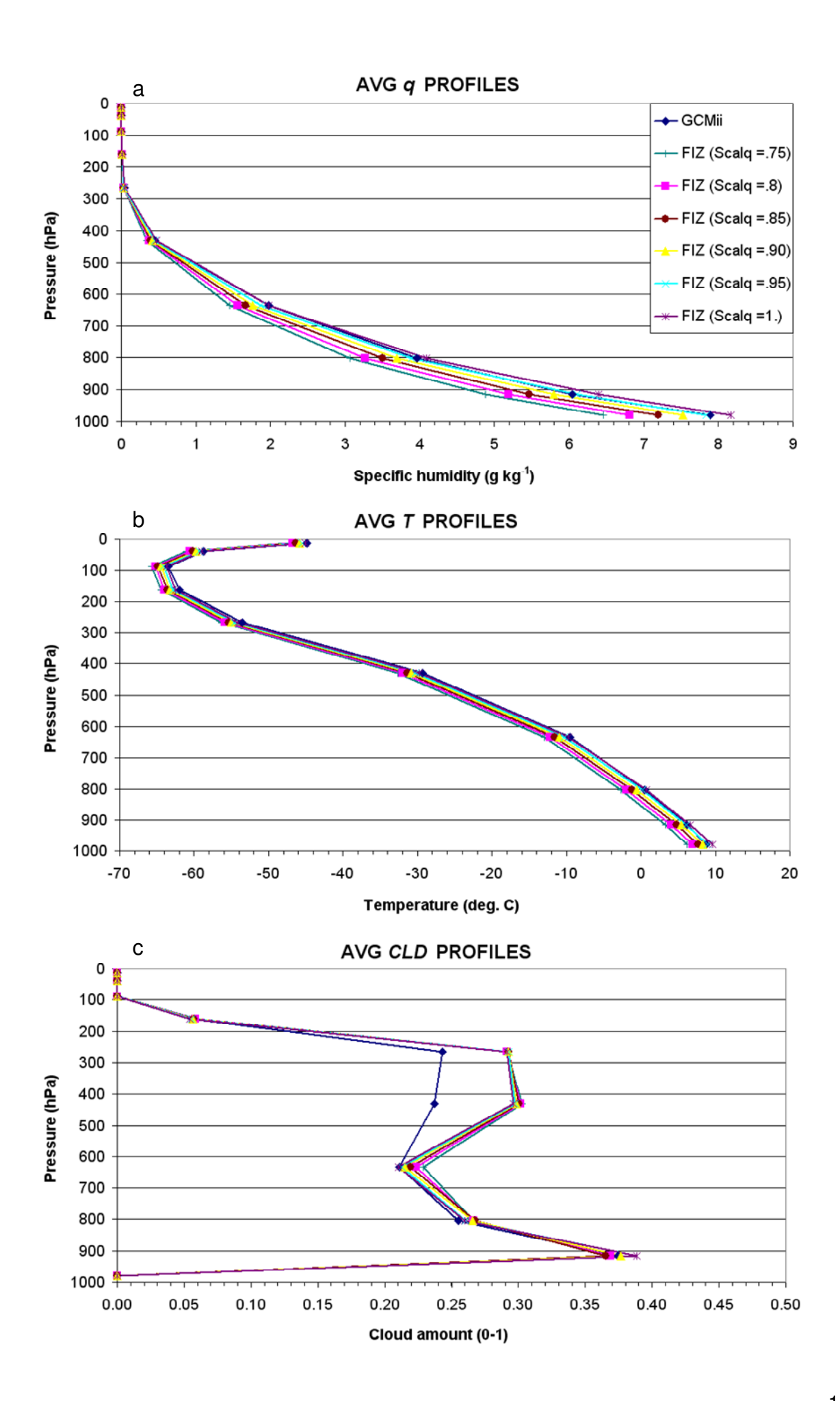
where the values of $\Psi_{m,\ell}$ at discrete step m and at level ℓ is a combination of the computed FIZC and the GCMii archived values controlled by $N_{\Psi,t}$, the nudging parameters, whose value is 1 for a complete nudging to GCMii archives and 0 for no nudging. The nudging scheme described by Eq. (4) may be viewed as a data assimilation technique. In Eq. (4), m is an integer defining the GCMii archive intervals such that $t_A = m \Delta t_A$, where Δt_A is 12 hours, the latter being larger than the model timestep. Variables are thus evolving in time according to a discretized version of Eq. (1) using the parameterized contributions to the dynamic tendencies depicted by Eq. (3) interpolated at each time step, and the contributions to the physics tendencies are recomputed at each time step. Then, the prognostic variables are allowed to be nudged independently of each other at all levels at each 12-hourly intervals according to Eq. (4) (where m > 0). An additional option has been developed in the current version allowing the atmospheric profiles to dry-cool in conjunction with the nudging procedure: the scaling is done through a parameter s_q , such that the GCMii specific humidity profiles are nudged as $s_q N_{q,\ell} q_{GCMii,m,\ell}$, where the scaling value $s_q \le 1$. This parameterization is implemented to better reproduce the moisture vertical profiles shown in Fig. 4.1. It is based on the conservation of the relative humidity so that the temperature profiles are modified according to the Clausius-Clapeyron equation. These changes are intended to better handle the simulated atmospheric profiles of T and q, impacting directly on the surface radiation and energy budget components relevant to the computation of soil surface temperature and the lake heat budget.

The lake model is the numerical one-dimensionnal SIMSTRAT model (Goudsmit *et al.* 2002), a buoyancy-extended k- ε model (Rodi 1980; Burchard *et al.* 1998) that has been updated to include the effects of internal seiches on the production of turbulent kinetic energy. To study thermal evolution in Lake Geneva with sufficient vertical resolution, 390 layers have been used. The coupling between the two models is achieved though the energy and momentum budget components at the air-water interface (Goyette and Perroud 2010). Downward solar and longwave radiation fluxes at the surface, S_{sfc}^{\downarrow} and L_{sfc}^{\downarrow} respectively, as well as the anemometer-level windspeed components [u_{10m} , v_{10m}] diagnosed at 10 m above the lake surface, are passed to the lake model. These can be further scaled as [$s_u u_{10m}$, $s_v v_{10m}$] with parameters s_u and s_v . These parameters are a model-option devised as a mean to reduce the model surface windspeed bias if needed. The reflected solar and emitted longwave fluxes, S_{sfc}^{\uparrow} and L_{sfc}^{\uparrow} respectively, are then computed as a function of the varying lake albedo

and surface water temperature. The atmospheric model computes the sensible and latent heat fluxes, $Q_{\rm H}$ and $Q_{\rm E}$, that can supply or extract energy to or from the lake, depending on the conditions at the air-water interface. In these runs, the surface drag coefficient has been kept at a constant value of $c_{\rm D}$ = 1.3 x 10 $^{-3}$.

4.3 Comparison of FIZC and GCMii simulated variables over land

Prior to running the coupled FIZC-SIMTSTRAT model, we ensured that FIZC run with the native land surface scheme was able to reproduce the atmospheric profiles as well as surface variables first simulated by the GCMii. This experiment also allowed for the assessment of the sensitivity of FIZC output variables to a number of user-defined parameters, i.e., $N_{\Psi \ell}$, S_{Ψ} , s_{q} , s_{u} , and s_{v} . Output variables produced by FIZC at the grid point located over Switzerland (46.5°N; 6.5°E) were compared to those of the GCMii when input parameters for soil and vegetation types, neutral drag coefficient, background albedo, as well as the initial conditions of the atmospheric and surface prognostic variables were the same as those used in the former GCMii experiments. The assessment was carried out over an arbitrary one year period where the comparison of annual average, standard deviation and linear correlation coefficients for variables archived on a 12-hourly basis, as originally devised in the GCMii simulations, were considered. The nudging parameters, N_{Ψ} , were fixed to 0.2 implying that the FIZC atmospheric profiles were allowed to deviate from these of the GCMii; the scaling values of S_{Ψ} were fixed at 1. Figure 4.1 compares six atmospheric profiles of air temperature, air moisture, horizontal wind speed, and cloud amounts simulated by the FIZC model using different values of the scaling parameter, s_a , for the specific humidity with those of the driving GCMii. The overall shapes of the annual-mean profiles are in a general agreement with those of the GCMii. On the vertical average and in relative terms, scaling the specific humidity from 1 to 0.75 impacted the atmospheric moisture content (-11%), the clouds (9.3%), and the windspeed below 300 hPa (6.8%), more than the air temperature (-0.6%). If this scaling varied from 1 (i.e., no scaling applied) to 0.75 (i.e., moisture is reduced by 25% in each layer) as can be seen in Fig. 4.1a, atmospheric moisture decreased throughout the atmospheric column in a linear fashion, differences ranged from 0.10 g kg⁻¹ to 0.49 g kg⁻¹ on the vertical average. A better correspondence with the GCMii annual profile is achieved with $s_q = 0.95$. At the same time, air temperature (Fig. 4.1b) decreased throughout the atmospheric column in a quasi-linear fashion, differences ranged from 0.95 °C to 2.65 °C, on the vertical average. Wind speed was more difficult to reproduce, especially above the 300 hPa level (i.e., above the 6th sigma level from the surface). While the differences were generally below 1 m s⁻¹ on the annual average, they reach 6 m s⁻¹ on average above that level (Fig. 4.1c). Cloud cover was generally well reproduced, and differences were below 3.5% on the annual average; however, on the 5th and 6th sigma level above the surface, the difference was about 23% as shown in Fig. 4.1d.



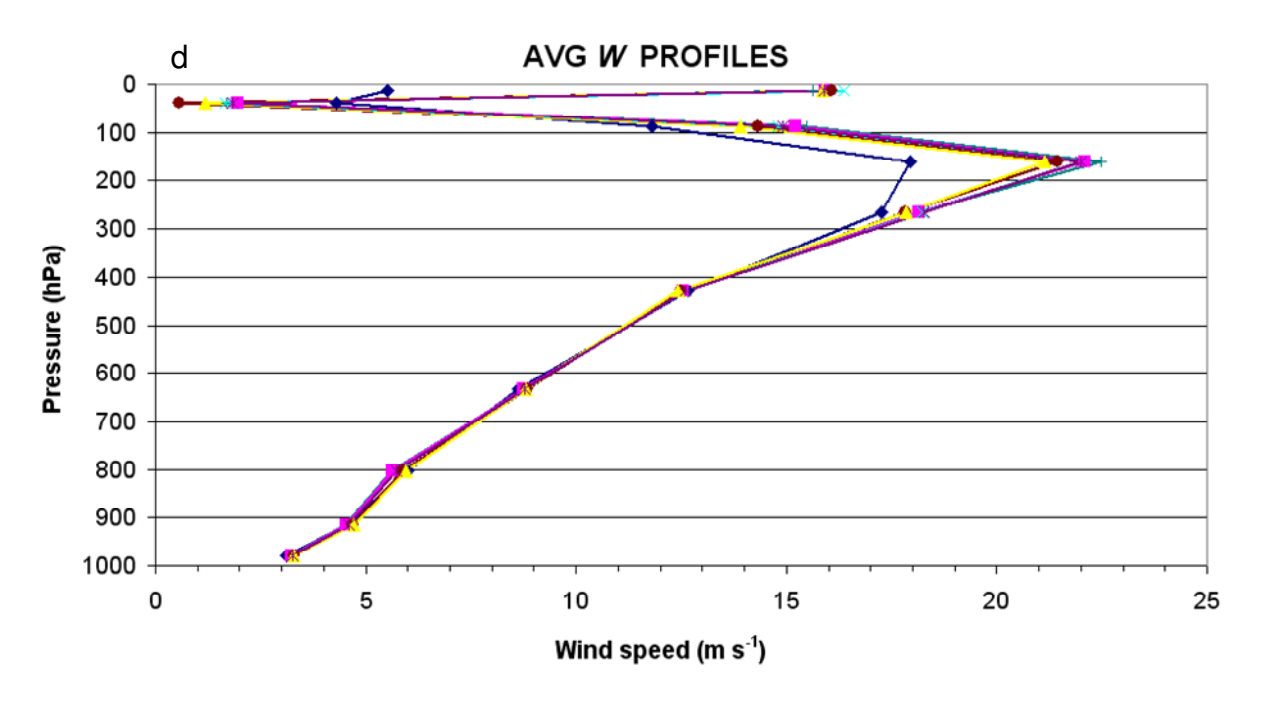


Figure 4.1. Annual mean atmospheric profiles of (a) specific humidity, q, in g kg⁻¹, (b) temperature, T, in °C, (c) horizontal windspeed, W, in m s⁻¹, and (c) cloud amount, CLD. Vertical dimension is sigma*1000, where sigma = $p p_s^{-1}$, with p the layer pressure and p_s the surface pressure.

The influence of s_q on a number of surface variables is shown in Table 4.1, together with a comparison with corresponding GCMii annual means and standard deviations. Linear correlation coefficients for the time series simulated by FIZC with those from corresponding GCMii series are also shown. The time evolution of the surface variables simulated by FIZC was well correlated with the GCMii ones as r = 0.85 on average, with a maximum of r = 0.95for $T_{\rm sfc}$, and a minimum of r = 0.67 for L_{atm}^* . The variability of the surface variables and fluxes is quasi-independent from the value of s_q and is less than the corresponding GCMii values; -8.6% on average in relative terms, with a maximum of -20.9% for L_{stc}^{\downarrow} , and a minimum of -2.7% for $Q_{\rm F}$. The annual means of the surface variables and energy fluxes were on average comparable to their corresponding GCMii values when $s_q = 0.95$. When the scaling factor s_q was reduced from 1 to 0.75, the annual average surface energy budget, \tilde{Q} , remained fairly close to 0, from -1.12 W m⁻² for s_q = 1 to -0.75 W m⁻² for s_q = 0.75. However, $T_{\rm sfc}$ decreased from 10.47 °C to 7.37 °C. The absorbed solar flux at the surface, $\kappa_{s/c}$, and the sensible heat flux, $Q_{\rm H}$ increased from 106.11 W m⁻² to 111.12 W m⁻², and 3.45 W m⁻² to 8.08 W m⁻² respectively, but, the latent heat flux, Q_{E} , and the downward longwave flux, L_{sfc}^{\downarrow} , decreased from 68.3 W m⁻² to 66.8 W m⁻², and 330.78 W m⁻² to 313.95 W m⁻², respectively. The absorbed solar, K_{atm}^* , and thermal infrared, L_{atm}^* , atmospheric fluxes also decreased as s_q decreased, from 51.36 W m⁻² to 48.25 W m⁻², and from -157.66 W m⁻² to -150.16 W m⁻² respectively.

It should be emphasized here that the optimal parameter values for the "land" experiment, even though they reproduced the GCMii variables accurately, may not be optimal for the "lake" experiment. This is because in coupled models, feedbacks arising from the interactions between the water and the atmosphere are allowed to take place, greatly modifying the surface fluxes of energy and momentum. The resulting simulated atmospheric profiles may thus be different, thereby subsequently influencing the lake water temperatures.

Table 4.1. Impact of the scaling parameter value, $s_{\rm q}$, on the vertical humidity profile for the annual average of surface temperature, $T_{\rm sfc}$ in °C, absorbed solar radiation at the surface, $K_{\rm sfc}^{\star}$ in W m⁻², sensible and latent heat fluxes, $Q_{\rm H}$ and $Q_{\rm E}$ respectively in W m⁻², total cloudiness, C, downward longwave radiation at the surface, $L_{\rm sfc}^{\downarrow}$ in W m⁻², solar radiation absorbed by the atmosphere, $K_{\rm atm}^{\star}$ in W m⁻², longwave radiation absorbed by the atmosphere, $L_{\rm atm}^{\star}$ in W m⁻², and on the energy budget at the surface defined as $\tilde{Q} = K_{\rm sfc}^{\star} + L_{\rm sfc}^{\downarrow} - \sigma (T_{\rm sfc} + 273.15)^4 - Q_{\rm H} - Q_{\rm E}$, computed with mean values, σ being the Stefan Boltzmann constant. Also shown are the standard deviations, std, of the annual time series and the linear correlation coefficients, r, with corresponding GCMii values.

s_{q}	$T_{ m sfc}$	$oldsymbol{\mathcal{K}}_{\mathit{sfc}}^{^{\star}}$	Q_{H}	Q_{E}	С	L_{sfc}^{\downarrow}	$oldsymbol{K}_{atm}^{^{\star}}$	$L_{atm}^{^{\star}}$	Q	V anem
GCMii :										
mean	9.48	118.44	4.95	71.1	0.66	315.24	54.08	-166.04	-4.7	1.70
std	6.3	83.0	27.4	55.5	0.4	55.3	30.4	42.1		1.0
$S_q =$										
0.75										
mean	7.37	111.12	8.08	66.8	0.71	313.95	48.25	-150.16		2.98
std	5.5	80.1	26.0	54.5	0.3	41.1	27.6	42.1		1.4
r	0.94	0.87	0.84	0.95	0.77	0.81	0.94	0.67	-0.75	0.86
$S_{q} =$										
0.80										
mean	8.09	110.49	7.05	67.3	0.71	317.48	48.87	-151.63		2.97
std	5.5	79.5	24.9	54.3	0.3	41.8	28.0	42.8		1.4
r	0.94	0.87	0.85	0.96	0.78	0.81	0.94	0.67	-0.95	0.85
<i>S</i> _q =										
0.85										
mean	8.78	110.75	5.89	67.6	0.70	319.92	49.37	-152.02		2.98
std	5.6	80.0	23.8	54.0	0.4	43.9	28.3	43.0		1.4
r	0.95	0.86	0.87	0.96	0.78	0.82	0.95	0.67	-0.94	0.85
$s_q =$										
0.90										
mean	9.39	109.49	4.99	68.0	0.70	323.73	50.11	-153.98		2.98
std	5.6	78.4	23.2	53.7	0.4	44.8	28.8	44.0		1.4
r	0.94	0.87	0.87	0.96	0.79	0.83	0.95	0.68	-0.94	0.84
$s_q =$										
0.95										
mean	9.94	107.98	4.34	68.1	0.71	327.52	50.78	-155.95		2.97
std	5.6	76.6	22.6	53.5	0.4	45.3	29.3	44.4		1.4
r	0.94	0.87	0.86	0.96	0.81	0.83	0.95	0.68	-1.00	0.84
$s_{\rm q} = 1.0$										
mean	10.47	106.63	3.45	68.3	0.71	330.78	51.36	-157.66		2.96
std	5.6	75.7	22.2	54.0	0.3	45.5	29.6	45.6		1.4
r	0.94	0.75	0.85	0.95	0.81	0.84	0.95	0.68	-1.12	0.85

4.4 Application of the coupled FIZC-SIMSTRAT to the deep Lake Geneva

4.4.1 Calibration

In the following experiments, the land surface scheme has been replaced by the SIMSTRAT lake model in the modelling system. In the previous model version, the sensitivity of the water temperatures in Lake Geneva to calibration parameters was assessed (Goyette and Perroud 2010). The water thermal profiles were reproduced with a root mean square error, RMSE, averaged over winter (DJF), spring (MAM), summer (JJA) and autumn (SON), of 0.75C° from the surface down to a depth of 10 m (Group of Depths No.1 or GD1), 0.38C° from 10 to 50 m (GD2), 0.24C° from 50 m to 200 m (GD3) and 0.15C° from 200 m to 309 m (GD4). Due to the sensitivity of the water temperatures to the computed atmosphere, the calibration parameters of this coupled version of FIZC-SIMSTRAT needed further optimisation.

A reference simulation, referred to as Sim_{ref}, was run for a 6-year period and served to assess the ability of the model to reproduce observed seasonal thermal profiles in Lake Geneva from 1978 to 1983 (Database INRA of Thonon-Les-Bains, Data CIPEL). Sim_{ref} used the mean observed profiles recorded between December 1980 and January 1981 as initial conditions. The simulated anemometer windspeed was scaled $[s_u u, s_v v]_s$ to fit observed meteorological data $[u, v]_{s,obs}$ over the lake, as recalcutated statistically from data taken at the inland station Changins, part of the Automatic Network (ANETZ) of the Federal Office of Meteorology and Climatology, MeteoSwiss (Bantle 1989). During these simulations the atmospheric profiles of Ψ were not strongly nudged towards the GCMii archived profiles $(N_{\Psi} = [0.1, 0.1, 0.1])$ and a weak scaling of the contributions to the Dynamics tendencies $(S_{\Psi} = [1, 1, 1])$ induced intraday variability on the order of \overline{D}_{Ψ} , fluctuations had a zero mean value. Subsequent simulations were then performed to reduce possible biases in the observed profiles by varying the parameters as follows: $S_{!!} = [1, 2, 3], s_q = [0.90, 0.95, 0.98],$ and $N_{\Psi} = [0.1, 0.2, 0.5, 1]$. The anemometer-level windspeed, the screen-level air temperature and specific humidity were also evaluated with respect to GCMii values, $\Psi_{s,GCMii}$ = $\{q_{s,GCMii}, T_{s,GCMii}, [u, v]_{s,GCMii}\}$ and for consistency with Changins observed meteorological data $\Psi_{s,obs} = \{q_s, T_s, [u, v]_{s,obs}\}$; an assessment was done with observed incoming surface solar and longwave radiative fluxes.

In order to compare the observed and simulated seasonal-mean profiles, lake soundings recorded 1 to 2 times a month at discrete depths (to a maximum of 20 depths) were interpolated and seasonally averaged. Values over the period lie within $5.21\,^{\circ}\mathrm{C}$ (spring) and $5.32\,^{\circ}\mathrm{C}$ (autumn) at the bottom and within $6.54\,^{\circ}\mathrm{C}$ (winter) and $19.4\,^{\circ}\mathrm{C}$ (summer) at the surface.

Sim_{ref} showed that seasonal water temperature profiles increased continuously over the 6 years at all depths and a positive bias to the observed profiles appeared. At the depths of smallest intra-annual variability (depths below 100 m), the mean seasonal warming went from 0.5° C to 0.9° C. A bias was noticed in the upper most layers and particularly at the surface where the maximal bias reached 1.85° C in winter, 1.5° C in spring and 0.04° C in autumn. However, in summer, temperatures were underestimated from the surface down to 25 m (-1.68 $^{\circ}$ C). Looking at the annual evolution of bottom water temperatures during the winter season, the warming changed at a mean rate of 0.057° C/year. At the end of the 6-year calibration period, the lake had not reached equilibrium and at the end of 14 years, the overall lake warming rate was still 0.049° C/year.

Water temperature profiles resulting from the multiple calibration runs were then compared to Sim_{ref} , with the hope that an optimal calibration would prevent the continuous warming of the simulated lake water temperature profiles. Changing values of S_{Ψ} produced seasonal variations throughought the profiles of less than 0.13 °C. As well, changes due to variations in

 $s_{\rm q}$ were small, particularly at depths below 150 m where they did not exceed 0.06 °C. Above 150 m, a low value of $s_{\rm q}$ decreased the water temperature, reducing the bias in observations in winter and spring but increasing the bias in summer and autumn. The Lake response was the opposite with higher $s_{\rm q}$. Sensitivity of the Lake to changes in $N_{\rm P}$ was significant. Compared to ${\rm Sim_{ref}}$, cooler water temperature profiles were simulated, reducing the seasonal error, throughout the profile in winter and spring and below 100 m during summer and autumn. However, changes remained lower than 0.05 °C from 200 m to the bottom, except when both $N_{\rm q}$ and $N_{\rm T}$ =1, in which case variations of 0.15 °C to 0.3 °C (below 200 m) indicate a significantly different behaviour of the profiles. Increasing the value of $N_{\rm u,v}$ caused a reduction in wind speed, decreasing the penetration of heat to deeper portions of the lake and reduced the error in the simulated profiles below 100 m. However, higher values of $N_{\rm u,v}$ were not optimal as at the same time that deeper waters cooled, surface waters warmed causing significant errors in the upper layers (e.g. an error increase of 0.5 °C in spring for $N_{\rm u,v}$ = 1).

Cross calibration of parameters indicated similar trends, with water temperature profiles only being significantly affected by the value given for the nudging parameters. Simulations obtained by varying s_q and S_Ψ , with N_q and N_T =1, caused small changes throughout the profiles but did not result in significant improvement. For example, while s_q = 0.90 lowered the bias in the observed deep-layer temperatures, it increases the bias in the upper layers (Table 4.2).

Compared to Sim_{ref} which produced a positive bias with respect to the observed volume-weighted temperatures in the epilimnion, T_{epi} , from January to July and in the hypolimnion, T_{hyp} , at any time, the simulations with N_T and $N_q = 1$ substantially reduced those errors (Fig. 4.2). Under these conditions, the lake reached a steady-state (*i.e.*, no significant trend in the mean-values) more rapidly and bottom water temperatures no longer varied. The annual rate of change in the bottom water temperatures in winter was between -0.05°C and 0.05°C for the 6-year simulation, and the range was only slightly wider for a 20 years simulation, (between 0.19°C and 0.06°C). Simulation with $N_T = 1$ and $N_q = 1$ produced mean winter surface water temperature that varied by less than 0.2°C over the 6-year simulation, far smaller than the 1.1°C increase found for Sim_{ref} .

Table 4.2. Mean of the seasonal root mean square error per group of depths determined for simulations with $N_{\Psi} = [1, 1, 0.1]$ but various s_q compared to the observations.

	$s_{q} = 0.90$	$s_{q} = 0.95$	$S_{q} = 0.98$
GD1	0.77	0.71	0.72
GD2	0.76	0.70	0.70
GD3	0.16	0.19	0.23
GD4	0.37	0.46	0.51

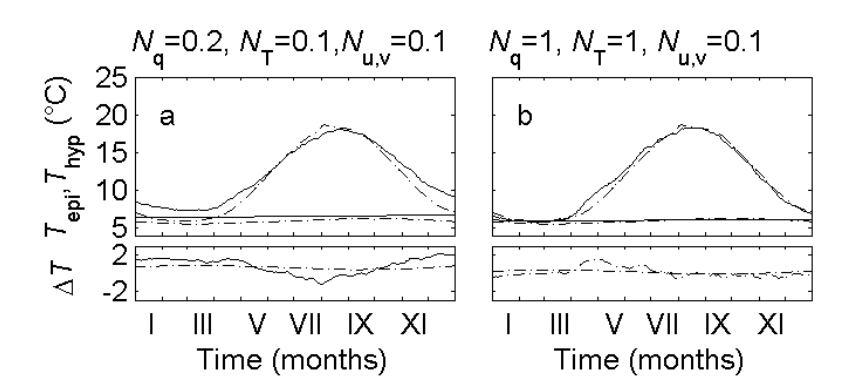


Figure 4.2. Observed (dotted line) and simulated (solid line) daily volume-weighted temperatures in the epilimnion $T_{\rm epi}$ (upper curves) and in the hypolimnion $T_{\rm hyp}$ (lower curves), averaged over the 6-year calibration period for (a) weak? and (b) strong nudging of the air temperature and specific humidity. Differences between simulated and observed daily $T_{\rm epi}$ (solid line) and $T_{\rm hpy}$ (dotted line) are given in the panels below (a) and (b).

Annual mean q_s , T_s and $[u, v]_s$ obtained using the set of calibration parameters, were systematically overestimated (Table 4.3) with respect to both the observations and the GCMii values. Annual mean $[u, v]_s$, was stronger than $[u, v]_{s,GCMii}$ and $[u, v]_{s,obs}$, but this was a consequence of using a lower value for the roughness height (z_0) of the water surface. Indeed, the lower frictional drag imposed on the flow at the lake boundary (here, 3.5 time lower) gave rise to a smoother decrease in the horizontal wind speed. The scaling applied to the simulated anemometer-level wind-speed ensured the right transfer of momentum to the lake. The overestimation of q_s and T_s was mainly related to surface water temperature and specific humidity over the lake surface. However, q_s and T_s simulated with $N_T = 1$ and $N_q = 1$ compared better with the observed values and thus diverged significantly from those resulting from the other calibrations, revealing again the need to apply the highest nudging to $q_{\rm s}$ and $T_{\rm s}$. This simulation produced lower $q_{\rm s}$ and colder $T_{\rm s}$ than Sim_{ref} in winter (bias of 0.78 g kg⁻¹ and 2.24 °C respectively) and autumn (0.73 g kg⁻¹ and 1.37 °C respectively), higher q_s and T_s in summer (1.06 °C and 1.08 g kg⁻¹ respectively) and similar values in spring. The effect of this strong nudging was noticed on the simulated screen-level temperature and specific humidity from the beginning of the simulation (as shown during the first 10 days of the simulation in Figure 4.3). A strong nudging value resulted in systematic cooling of T_s in winter and an effective variation of q_s at archived time intervals. Compared to Sim_{ref} , the benefit of such a simulation with strong nudging was to cool the uppermost layers of the epilimnion (Fig. 4.3), and to prevent unexpected warming of the water profiles. If the substitution of a low nudging value for a complete nudging of T and q induced seasonal changes in radiative forcing that were less than 10% during the first year, the sensible and latent heat flux diverged significantly. A cooler and drier atmosphere (i.e., when $N_{\Psi} = [1., 1., 0.1]$) caused a loss of energy in the lake by latent heat on average 3 times higher in winter, by sensible heat 3 times larger in autumn and a loss instead of a supply of heat by sensible heat in winter. This resulted in a negative energy budget for the lake, \tilde{Q} (see Table 4.1 for definitions), in winter and autumn less significant for N_{Ψ} = [0.1, 0.1, 0.1] than for N_{Ψ} = [1., 1., 0.1], so that the former winter and autumn, \tilde{Q} = -1.27 MJ day⁻¹ m⁻² and -4.44 MJ day⁻¹ m⁻² respectively, instead of -3.23 MJ day⁻¹ m⁻² and -7.30 MJ day⁻¹ m⁻² respectively. Nudging the prognostic variables T and q is thus required to prevent an excess of heat from diffusing downward with time. Consequently, the net heat storage in the lake averaged over the 6 year simulation period differed widely according to the nudging values. While $N_{\rm H}=$ [1., 1., 0.1] produced a fairly low annual net heat storage, $\tilde{Q}=0.04\pm0.12\,{\rm MJ\,day^{-1}~m^{-2}}$ for $s_{\rm q}=0.90,~\tilde{Q}=0.07\pm0.16\,{\rm MJ\,day^{-1}~m^{-2}}$ for $s_{\rm q}=0.95,$ $\tilde{Q} = 0.071 \pm 0.18 \, \mathrm{MJ \, day^{-1} \, m^{-2}}$ for $s_{\mathrm{q}} = 0.98$, this storage was however positive in $\mathrm{Sim}_{\mathrm{ref}}$ due

to the amount of heat accumulated in deep layers (0.41 \pm 0.34 MJ day⁻¹ m⁻²). Since a decrease in the nudging value caused a warmer and wetter atmosphere, that then resulted in the positive growth of the annual net heat storage, N_{Ψ} other than 1 is currently not acceptable in these coupled lake-atmosphere experiments.

Table 4.3. Mean values of the prognostic variables simulated over the 6-year calibration period for a set of calibration parameters.

	Prognostic variables			
	T (°C)	q (g kg ⁻¹)	ν (ms ⁻¹)	
Observations	10.8	6.6	2.90	
$N_{\Psi} = [0.1 \ 0.1 \ 0.1], \ S_{\Psi} = [1 \ 1 \ 1], \ S_{q} = 0.95$	12.7	8.5	2.91	
$N_{\Psi} = [0.1 \ 0.1 \ 0.1], \ S_{\Psi} = [3 \ 3 \ 3], \ s_{q} = 0.95$	12.6	8.4	2.92	
$N_{\Psi} = [0.1 \ 0.1 \ 0.1], \ S_{\Psi} = [1 \ 1 \ 1], \ S_{q} = 0.90$	11.8	7.8	2.91	
$N_{\Psi} = [0.1 \ 0.1 \ 0.1], \ S_{\Psi} = [1 \ 1 \ 1], \ S_{q} = 0.98$	13.0	9.1	2.91	
$N_{\Psi} = [1 \ 1 \ 0.1], \ S_{\Psi} = [1 \ 1 \ 1], \ s_q = 0.95$	12.0	8.5	2.90	

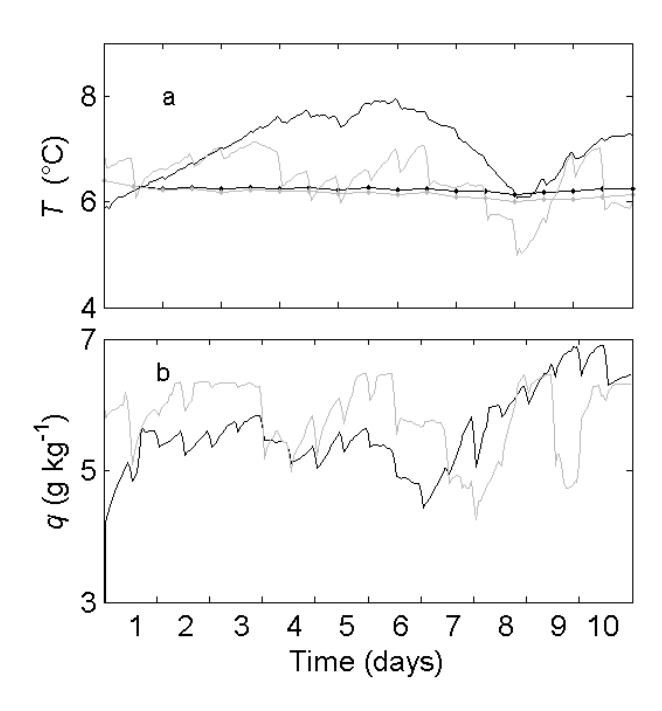


Figure 4.3. Hourly values of screen-level (a) air temperature and (b) specific humidity from the first 10 days of a 6-year simulation, using the nudgings $N_{\Psi} = [0.1,0.1,0.1]$ (black line) and $N_{\Psi} = [1,1,0.1]$ (grey line). The days were chosen to illustrate the strong influence of the nudging on their intra-daily evolution. Simulated lake surface water temperatures, resulting from the two nudgings (circle-line), are plotted at 12 hours intervals in panel (a).

Comparison of the observed incoming solar radiation flux, S_{sfc}^{\downarrow} , and the incoming longwave diagnosed on the basis of the observed cloudiness at the Changins station L_{sfc}^{\downarrow} was done with respect to radiation fluxes simulated by FIZC using $N_{\psi}=[1.,\,1.,\,0.1]$, with $s_{\rm q}$ varying over the range of 0.90 to 0.98. Even though different values of $s_{\rm q}$ did not improve the simulated

water temperature profiles, they may yet change the moisture content of the atmosphere. The annual mean fluxes of S_{sfc}^{\downarrow} and L_{sfc}^{\downarrow} were overestimated when $s_q = 0.95$ (Table 4.4), but compared well to the GCMii values, such as from the land experiment. Cloudiness (+ 20%) following an increase in s_q to 0.98 had a positive effect on the bias of S_{sfc}^{\downarrow} , but a negative effect on the bias of L_{sfc}^{\downarrow} . Conversely, the reduction of the cloudiness (- 35 %) when $s_q = 0.90$ produced a higher S_{sfc}^{\downarrow} but a smaller L_{sfc}^{\downarrow} bias.

Table 4.4. Mean surface downward radiative flux (MJ m⁻² day⁻¹) calculated over the 6-year calibration period, determined from observed values, GCMii values and simulated values using $N_{\Psi} = [1,1,0.1]$ and $s_q = 0.90, 0.95$ and 0.98.

	Observations	GCMii	$s_{q} = 0.90$	$s_{q} = 0.95$	$s_{q} = 0.98$
S_{sfc}^{\downarrow} (MJ m ⁻² day ⁻¹)	11.97	13.05	14.36	13.14	12.57
L_{sfc}^{\downarrow} (MJ m ⁻² day ⁻¹)	24.93	27.11	26.60	27.37	27.76

Sensible and latent heat flux, $Q_{\rm H}$ and $Q_{\rm E}$ have not been measured at the lake interface and thus it was not possible to undertake any comparisons. However, a seasonal analysis of surface prognostic variables suggests some bias in the convective fluxes. Even though mean air temperature was correctly reproduced with respect to the observations, variability was lower than the observations. For instance, the observed air temperature was 18.5 ± 4.7 °C while the simulated value was 18.4 ± 1.9 °C when $s_{\rm q} = 0.95$ in summer.

4.4.2 Simulated lake water thermal profiles under a 1 X CO₂ climate

A simulation with the FIZC-SIMSTRAT coupled model under the 1 x CO₂ climate condition, termed Sim_{1XCO2}, was investigated to assess the model performance in reproducing Lake Geneva water temperatures over the period 1961-1990. The model was run with the calibration parameter, that minimized the error of simulated water temperature profiles with observed water soundings and reproduced the observed fluxes more accurately (*i.e.* $N_T = 1$, $N_q = 1$, $N_{u,v} = 0.1$, $s_q = 0.95$, $s_{\Psi} = 1$). The simulation started using the mean water thermal profile of the 1st of January of each year from 1960 to 1990. A spinup period was required to allow the lake to reach its equilibrium state. Fields generated by the GCMii allowed this coupled model to run over a 20-year period.

Two runs of 20 years were necessary to spin up the water temperature profiles. Differences in daily profiles between the first and the last 20-year reduced rapidly with time. Less than 1% of daily records over the profile experienced differences higher than 0.1 °C after the 4th year of simulation. This was significant since these differences were up to 0.3 °C at the surface, 0.5 °C at 100 m and 0.22 °C at the bottom during the first year.

The onset of stratification may be diagnosed when a 1 $^{\circ}$ C difference appears between the 100 m and 2 m layer (Jacquet *et al.* 2005) and the stability of the water column may be given by the Brunt-Väisälä frequency N^2 at the depth with the highest vertical temperature gradient.

The simulated daily water temperature profiles in Sim_{1XCO2} were averaged over the last 20 years and compared to observed values (Fig. 4.4). Simulated profiles agreed well with the observations on a seasonal basis. Seasonal biases in the observation lay within $0.4^{\circ}C$ and $0.7^{\circ}C$ from 150 m downward. Above 150 m, the seasonal biases were in general on the same order, *i.e.*, lower than $0.2^{\circ}C$ in winter and lower than $0.7^{\circ}C$ otherwise. However, a positive bias of $0.7^{\circ}C$ to $1^{\circ}C$ was noticed in the first meters below the surface in spring. Conversely, lower simulated water temperatures may occur at the water surface but mainly at depths of 10 m to 50 m in summer and from the surface to 50 m in autumn, with maxima

of $1.9\,^\circ$ C and $1.8\,^\circ$ C at 20 m respectively. These biases resulted from a slightly too strong stability simulated in the metalimnion in spring that then prevented heat from penetrating deeper. The position of the thermocline was correctly simulated during the stratified months. Volume-weighted temperature in the epilimnion, $T_{\rm epi}$, and in the hypolimnion, $T_{\rm hyp}$, were also well simulated. The mean error was $0.26\,^\circ$ C $\pm 0.27\,^\circ$ C in $T_{\rm epi}$ and was $0.31\,^\circ$ C $\pm 0.14\,^\circ$ C in $T_{\rm hyp}$. The largest differences, were found from April to mid-June, and corroborate the lower location of the simulated thermocline. These model biases were not detrimental to model performance since they were related to small shifts in the thermocline locations which affected only a small slab of water within the profile.

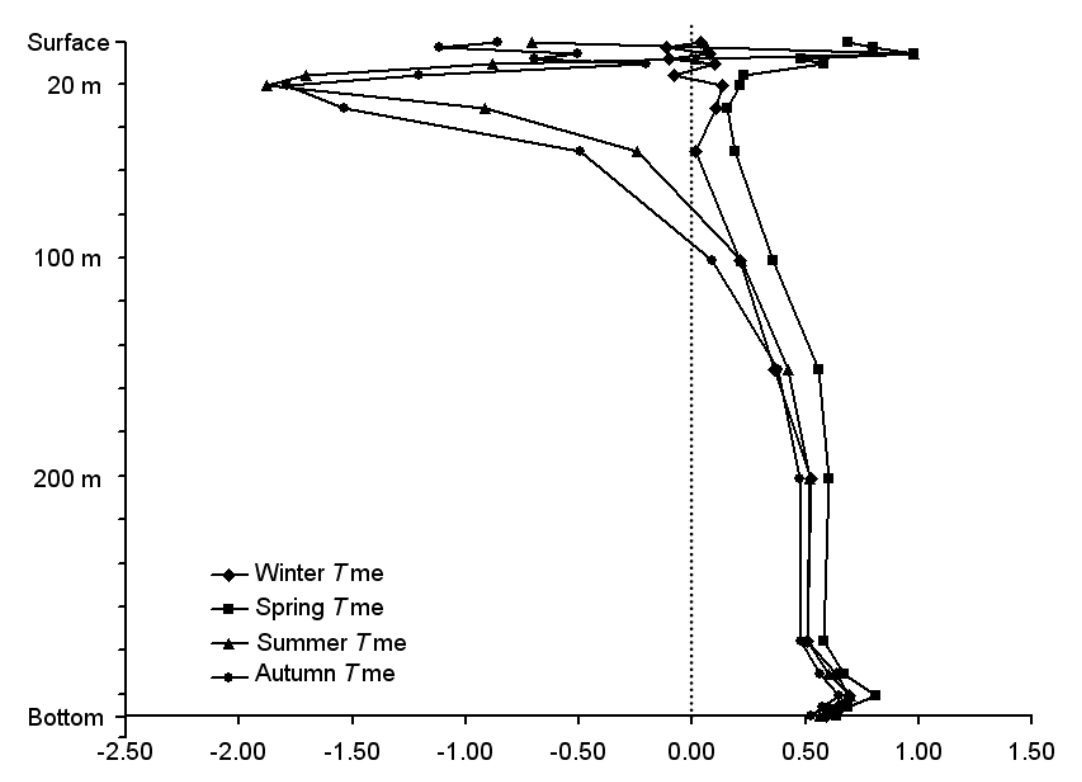


Figure 4.4. Seasonal mean error between simulated (Sim_{1XCO2} averaged over the last 20 years of the simulation) and observed (1961 - 1990) water temperatures profiles.

Figure 4.5 shows the monthly energy budget components of the lake averaged over the last 20 years of the simulation. Net radiation was positive from February to October, reached a maximum in June, and was the source of heat for the Lake. In contrast, the sensible and latent heat fluxes were negative on a monthly average and were energy sinks. The evolution of net heat storage in the lake was strongly correlated with net radiation, storing heat from March to August, with a maximum in June. Periods of lowest correlation were initiated by variations in the latent heat flux, and only to a minor extent by the sensible heat flux as the latter remained nearly constant. Net heat storage thus increased proportionally less from April to May and then dropped off significantly less from September to October than the net radiation. The cooling by latent heat flux was the lowest from December to April (-36 to -51 Wm⁻²) and was roughly twice those amounts in July, August and September. Latent heat flux was always at least 3 times higher, in absolute values, than the sensible heat flux.

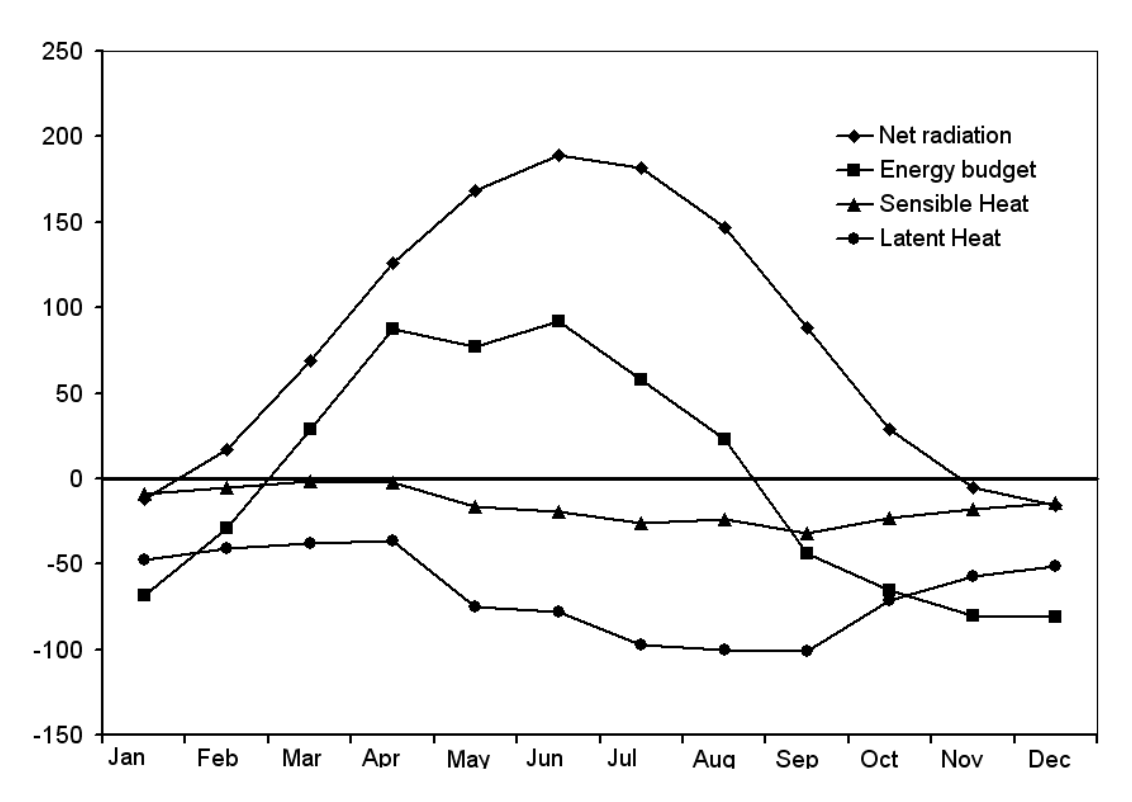


Figure 4.5. Monthly-averaged energy amounts are given for net radiation, sensible and latent heat fluxes, as well as for the energy budget.

4.4.3 Simulated lake thermal profiles under a 2 X CO₂ climate warming scenario

Changes in Lake Geneva water temperature profiles in response to global warming following a doubling of the atmospheric CO_2 concentration were simulated and then compared to the "control" 1 x CO_2 simulation outputs. In this simulation, the time to stabilize the warming through the whole column was longer than in Sim_{1XCO_2} due to a "cold start" procedure. Three 20-year spinups were required to produce temperature variations lesser than 0.1 °C at the bottom (temperatures reach equilibrium after 37 years). Profiles generated during the third 20-year series thus served to assess the expected changes in temperature, as well as in stability, duration and evolution of the thermocline in the lake waters.

Daily water temperature profiles produced by Sim_{1XCO2} and Sim_{2XCO2} were both averaged over a 20-year period. Differences between daily means of both periods, shown in Figure 4.6, were used to assess expected monthly mean changes in lake temperature profiles. Interannual variability of lake thermal profiles between both simulations was not considered in this study. An annual mean temperature increase of 2.1 °C to 3.3 °C was expected from the bottom up to the surface. Even though the water warms more in the upper layers, a zone of lower increase was noticed in the lower metalimnion with a minimum of 2.1 ℃ at 20 m. The main daily increase in temperature was in the epilimnion and upper metalimnion. Temperatures may warm up to 4°C in the first 7 m below the surface from mid-June to mid-August. At the surface, the increase exceeded 4.5 °C during 2 weeks in late July and early August, with a maximum of 4.8 ℃. In Sim_{2XCO2}, the stability of the metalimnion was expected to strengthen, hampering the penetration of summer heat to deeper layers in the future. As a result, the lower metalimnion warms less during stratified periods. These layers of lower increase moved with dynamic deepening of the thermocline. Warming of less than 2°C was simulated between 13 m and 18 m in mid-June, 14 m and 28 m in mid-August, and 16 m and 32 m in mid-October. Increases in hypolimnion temperature were between 2°C and 2.5°C after the onset of the stratification, and between 2°C and 3°C during the weakly stratified period, *i.e.*, from the bottom up to the surface.

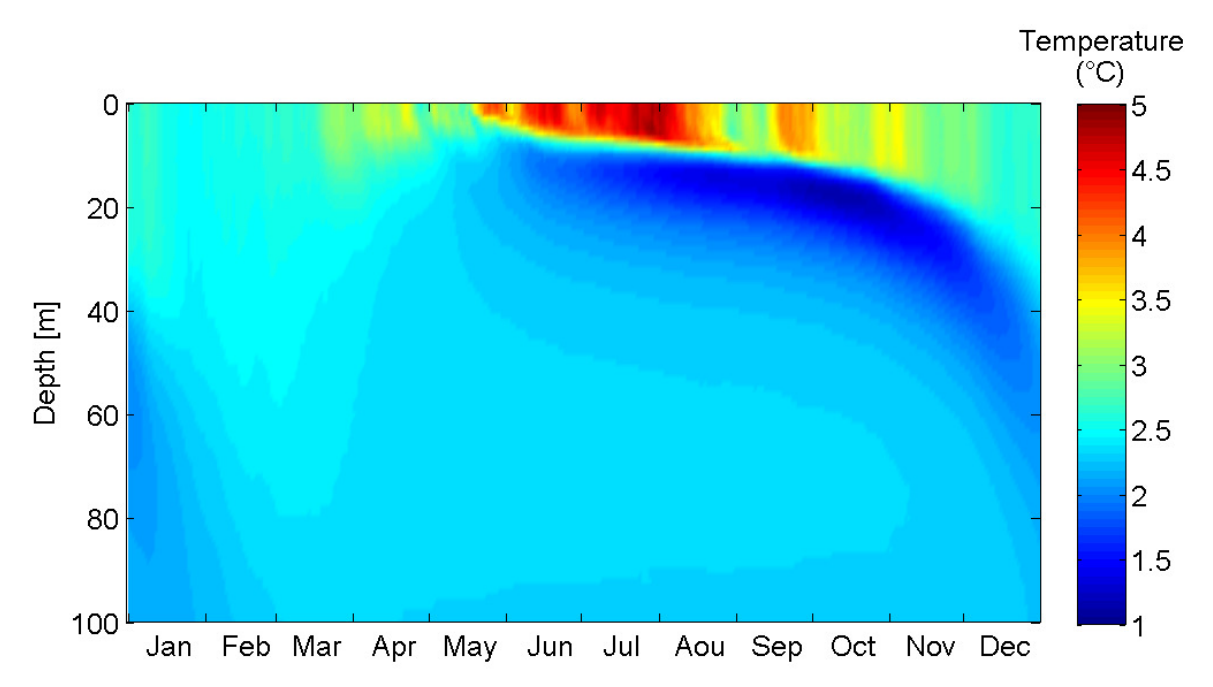


Figure 4.6. Contour plots of mean daily temperature differences in the first 100 m below the surface between simulated profiles under a $2 \times CO_2$ and $1 \times CO_2$ climate.

Changes in monthly-mean water temperature were investigated using $T_{\rm epi}$ and $T_{\rm hyp}$ (Fig. 4.7). The increases in $T_{\rm epi}$ varied between 2.6 °C (January-February) and 4.2 °C (July). $T_{\rm hyp}$ rose between 2.2 °C (January) and 2.3 °C (March). While $T_{\rm epi}$ was equal or slightly higher than $T_{\rm hyp}$ (< 0.3 °C) in Sim_{1XCO2} from January to March, such values were simulated only in February for Sim_{2XCO2} .

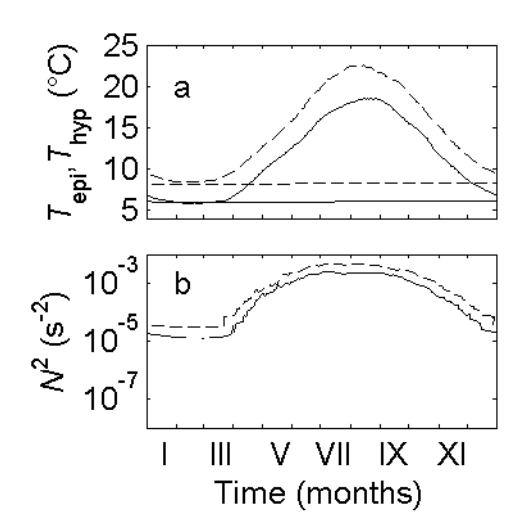


Figure 4.7. Mean daily volume-weighted temperatures in the epilimnion $T_{\rm epi}$ and in the hypolimnion $T_{\rm hyp}$, under a 1 x CO₂ (solid line) and 2 x CO₂ (dotted line) climate (a). Daily values of water column stability, N^2 are shown for similar periods (b).

Warmer conditions also impacted the lake metalimnic characteristics. Lake stability was 2 times stronger in Sim_{2XCO2} than in Sim_{1XCO2} during spring, summer and autumn (Fig. 4.7). Moreover, differences between $T_{\rm epi}$ and $T_{\rm hyp}$ increased by 12 % to 20 % during the stratified months, and by more than 30% during the coldest months, confirming the stronger stability of the water column. The stronger stability of the lake water and systematically higher $T_{\rm epi}$ than $T_{\rm hyp}$ (Fig. 4.7), may indicate a severe reduction in the frequency of complete overturns (which

currently occur less than once per decade). Changes in wind speed (currently of $3.10\,^{\circ}\text{ms}^{-2} \pm 1.20$, it is expected to be of $3.10\,^{\circ}\text{ms}^{-2} \pm 1.10$) were unsignificant and thus did not moderate the decrease in convective mixing depth. In summer, the depth of the thermocline was similar for both simulations, but slight changes were expected in autumn. Due to stabler conditions, the thermocline should resist colder conditions longer and the decay of the stratification should be delayed. The thermocline remained closer to the surface during a longer period and its mean depth was 2-3 m shallower in autumn. As a result, the duration of the stratification period lasted 2 weeks more. Since the lake was also expected to stratify earlier in Sim_{2XCO2} , the length of the stratification period lengthens by more than 3 weeks.

Change in radiative forcing was initially due to increased concentrations of CO_2 in the atmosphere. The temperature and specific humidity profiles were then modified accordingly having an impact on the energy budget, namely on the downward solar, $S_{s/c}^{\downarrow}$, due to the change in cloudiness, the sensible heat due to changes in air temperatures and the latent heat due to changes in both air temperature and saturation state of the atmosphere.

Differences were diagnosed in the downward (+ 1.39 MJ day⁻¹ m⁻²) and emitted (+ 1.40 MJ day⁻¹ m⁻²) longwave radiation fluxes at the surface, L_{sfc}^{\downarrow} and L_{sfc}^{\uparrow} respectively, due to warmer air temperature, modified cloudiness and lake surface temperature (Fig. 4.8). If the net longwave budget was positive early in the 2 x CO₂ climate simulation, it balanced out at equilibrium (Table 4.5) once the surface temperatures stabilized.

Table 4.5. Total daily energy amount of K_{sfc}^* , solar radiation, L_{sfc}^* , infrared radiation, Q_E , latent heat flux, Q_H , sensible heat flux and energy budget \tilde{Q} in W m⁻² under 1 x CO₂ and 2 x CO₂ climates.

	Radiation budget	(MJ m ⁻² day ⁻¹)		Convection budget (MJ m ⁻² day ⁻¹)		
	1 X CO ₂	2 X CO ₂		1 X CO ₂	2 X CO ₂	
$oldsymbol{\mathcal{K}}_{ extit{sfc}}^{^{\star}}$	12.44	12.92	Q_{H}	-1.36	-1.10	
$L_{ m sfc}^{*}$	-5.31	-5.32	Q_{E}	-5.78	-6.44	
$oldsymbol{Q}^{^{\star}}$	17.75	18.24	Q	-0.016	0.07	

As shown in Figure 4.8, an increase in the incident shortwave radiation at the surface S_{sc}^{\downarrow} was simulated in spring (+ 0.68 MJ day⁻¹ m⁻²) and summer (+ 1.89 MJ day⁻¹ m⁻²), resulting from a reduction in cloud cover during both seasons. In fact, even though an increase in the specific humidity at the screen-level was simulated on average (+ 1.2g kg⁻¹ in winter and 3.8 g kg⁻¹ in summer), a higher increase in air temperatures at the screen-level was simulated in summer than in winter (+2.8 °C in winter and +4.2 °C in summer) which amplified the dew point depression during warm months. This produced drier atmospheric profiles in summer and a reduction in cloudiness. The stronger increase in the surface air temperature compared to the one in the lake water in winter and autumn reduced the thermal gradient and less heat was extracted from the lake by sensible heat flux (Fig. 4.8), where reductions were 0.48 MJ day 1 m⁻² and 0.56 MJ day 1 m⁻² respectively. A decrease in the latent heat flux was particularly important in summer (Fig. 4.8), while it was likely that a slight shift would be observed in spring and autumn. In fact, even though air and lake surface water vapour pressure both increased in the future, the water vapour deficit became larger. A summer increase of this deficit caused an additional loss of heat through evaporation of 1.95 MJ day m⁻². The seasonal changes in the energy budget components simulated in the 2 x CO₂ experiment, implied monthly variations in the lake heat storage. As climate warms, the January to March period exhibited a stronger gain in heat due to the warming effects of sensible heat. Conversely, an earlier onset of evaporative cooling processes implied a stronger loss of heat during April. While simulations indicated that there would be larger net radiation from May to August in the future, the cooling by latent heat had a compensatory

effect. Net heat storage thus remained similar to current values during that period, and may even decrease in August. Despite the cumulative changes in the fluxes, the effective annual energy budget of the lake reached equilibrium in both simulations (Table 4.5). Only 6 years of a 60 years of simulation were needed to reach equilibrium. This agreed with the time required to stabilize surface temperatures. Note that, as was mentioned earlier, the lake takes more than 8 times longer to reach a steady-state.

Variations in the hourly-mean latent and sensible heat fluxes in winter and autumn were particularly pronounced. These were due to the high nudging values applied to the atmospheric profiles (Fig. 4.8). Since fluxes were computed on the basis of the air temperature and specific humidity differences between the surface and the lower atmosphere, the effect of the nudging on energy budget components was indeed expected.

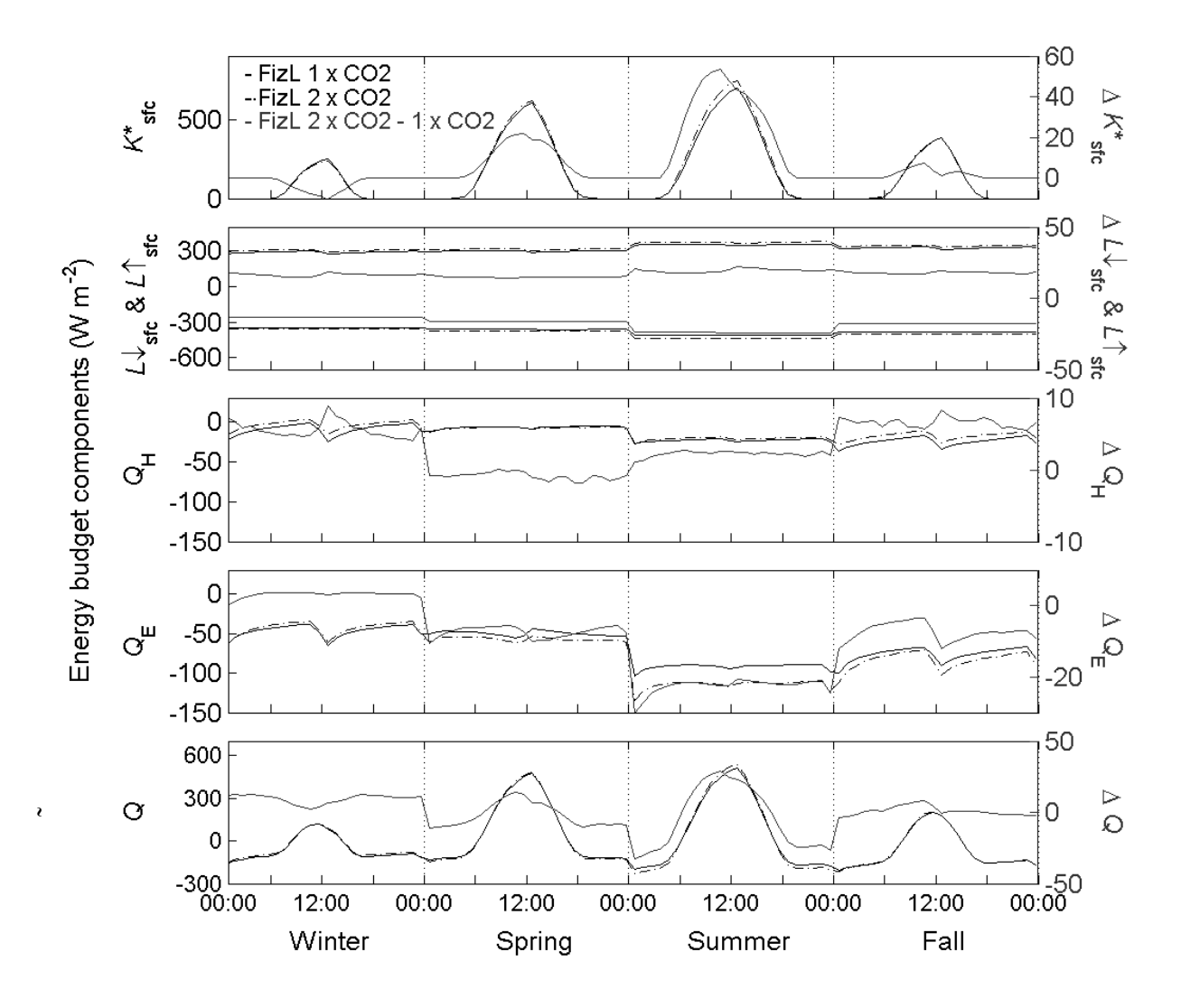


Figure 4.8. Hourly energy amount for each season for \mathcal{K}_{sfc} , solar radiation, $\mathcal{L}_{sfc}^{\downarrow}$ and $\mathcal{L}_{sfc}^{\uparrow}$, downward and upward infrared radiation, Q_{E} , latent heat flux, Q_{H} , sensible heat flux and energy budget \tilde{Q} in W m⁻² under a 1 x CO₂ (solid line in black) and 2 x CO₂ (dotted line in black) climate. Differences between 2 x CO₂ and 1 x CO₂ hourly energy amount are superimposed in red on plots of each of the components of the energy budget.

4.5 Discussion

The coupled FIZC-SIMSTRAT lake-atmosphere model used in this study was applied to the Swiss Lake Geneva for current and future climate conditions, and directly follows the earlier work of Perroud and Goyette (2010) and Goyette and Perroud (2010).

As a first step, numerical experiments were carried out over land with FIZC using the native GCMii land-surface scheme and produced results that compared well with those of GCMii over the grid point located in Switzerland. Annual-mean surface variables and fluxes, as well as the mean atmospheric profiles, simulated by FIZC could have diverged from those of GCMii, but no significant drifts were noticed despite the weak relaxation towards the GCMii profiles. The rather good linear correlations between FIZC and GCMii simulated variables were partly due to the implementation of an improved parameterization of the contributions to the Dynamics tendencies (Eq. 3). However, the variability was slightly less than for the corresponding GCMii values, and this could be attributed in part to the low value of the scaling factors to the contributions to the dynamics tendencies, S_{Ψ} . The nudging parameter values, N_{Ψ} , as well as those of S_{Ψ} might be changed to better correspond to the GCMii simulated variables and profiles; however, devising optimal values is not the main aim here as in the "lake" experiments these may be different. The option to scale the driving humidity allowed to "cool" and to "dry" the atmospheric profiles without significantly modifying the windspeed profiles. This impacted on the surface radiation and energy fluxes where an enhanced downward solar flux, together with a decreased atmospheric downward longwave flux at the surface were simulated with a decrease in s_q . The solar and longwave fluxes absorbed by the atmosphere also decreased due to the strong influence exerted by the water vapour in the air. This was of particular interest for the "lake" experiment where interactions and feedbacks between the lake and the atmosphere were stronger than in the "land" case. The reproduction of all the individual fluxes of solar, atmospheric longwave, in addition to the sensible and latent heat fluxes were important for accurately reproducing the evolution of water temperature profiles. The option to run FIZC with monthly-averaged ozone profiles measured at a particular observing station (i.e., Payerne, Switzerland) did not have a significant impact on the surface energy budget nor on the annual mean atmospheric profiles [less than 0.1 W m⁻² on the annual average, (not shown)]. However, this option was kept for later use, particularly if the study area was to be located in a place where the local ozone concentrations were different from the zonal averages used by GCMii.

In the second step, the lake experiment showed that the annual mean surface energy budget took several years to reach equilibrium, depending on the calibration parameter values. This contrasts with the land simulation where a "close-to-zero" net energy budget was rapidly attained. This can be explained by the large thermal capacity of the lake compared to the land surface, to the large amount of heat that can be stored in the deep Lake Geneva and to the time lag for heat to reach the lake bottom. However, our experiments have shown that steady state conditions can still be reached if the specific humidity and air temperature were more strongly nudged toward the GCMii profiles (*i.e.*, N_q and N_T close to 1). This results in increased energy loss by sensible and latent heat at the surface during winters and autumns. Therefore reductions of surface available heat to greater depths by convective overturning and wind mixing prevents unrealistic warming of the deep hypolimnion over the year and helps to close the annual energy budget in less than a decade.

Lake thermal profiles were less sensitive to variations in the other calibration parameters (*i.e.*, S_{Ψ} , s_{q} , etc.) than to variations in the nudging parameters. Variations of s_{q} may improve simulated water profiles, helping to close the annual lake surface energy balance. As for the land experiment, lower values of s_{q} caused an increase in S_{sfc}^{\downarrow} and a decrease in L_{sfc}^{\downarrow} . However, while the simulated total cloud cover did not significantly vary during the land experiment for s_{q} ranging from 0.90 to 0.98, the values were nearly doubled over the lake surface. The optimal value of s_{q} for reproducing the water thermal profiles was 0.95. This

value allows for a better reproduction of the observed downward solar and longwave infrared fluxes; values however were still overestimated, similarly to those of the GCMii. The optimal value of s_q was thus a useful compromise to obtain realistic downward radiative fluxes, rather than an ad hoc parameter to modify the cloudiness over the lake.

Seasonal variations in the surface energy budget components simulated during the control experiment (1 x CO₂) were similar to those of other studies for northern temperate lakes (Winter *et al.* 2003; Lenters *et al.* 2005). While net radiation was the main source of heat for lakes, sensible and latent heat fluxes were heat sinks. As in Lenters *et al.* (2005) which studied variations in lake evaporation rates, the cooling by latent heat began increasing in spring, reached a maximum in late summer, more than a month after the maxima of net radiation, and decreased in autumn. However, the sensible heat flux used in the 1 x CO₂ experiment may differ in the details from that of other studies. In the autumn, the sensible heat had a lower cooling effect than in summer. Unlike Lenters *et al.* (2005), the sensible and latent heat fluxes could thus not reach similar values in early November.

Analysis of the sensible and latent heat fluxes simulated by FIZC with respect to observations was not possible as they were not available over the lake. Thus, a comparison was done with seasonal trends reported in the literature. In Vercauteren et al. (2008), an experiment carried out during the summer over Lake Geneva indicated negative values for latent heat flux, but hourly averaged sensible heat flux, either negative (loss of heat) or positive (gain of heat), in the range -40 W m⁻² to 15 W m⁻². If the negative seasonal latent heat flux agrees with our study in summer, the simulated sensible heat flux produce a permanent loss of heat at the lake surface. Presumably, the lack of seasonal variability was due to the lack of variability in simulated atmospheric components. Over Lake Geneva, simulated air temperatures rarely exceeded the water temperature in summer and lead to an underestimation of positive values of sensible heat flux. The sensible heat fluxes may also be affected during other periods. In winter for instance, it is likely that the loss of heat by sensible heat flux (due to low air temperature compared to the water surface) may be underestimated. This could be an issue for determining the complete mixing of the water column. Despite these biases, the coupled FIZC-SIMSTRAT model reproduced the annualmean value of the lake energy budget. Even though slight differences compared to observed fluxes were noticed, the overall energy budget was much more important than the values of the individual fluxes.

Once calibrated, the third step involved a simulation with the concentration of atmospheric carbon dioxide doubled (2 x CO₂) and a comparison with the control experiment (1 x CO₂). Water was warmed throughout the column, with significant monthly variations in the epilimnion only. Monthly $T_{\rm hyp}$ variations were lower than 0.07 °C for a maximum increase in water temperature of 2.25 °C at the time of lowest stratification. Changes in $T_{\rm epi}$ were between 2.56 °C and 4.2 °C, with minima and maxima synchronized with lower and higher screen level air temperature increases (January-February and July respectively).

The sensitivity of the Lake to increases in greenhouses gas concentrations leads to conclusions that agree well with other studies. Not only was the warming of the epilimnion closely linked to increases in air temperature (Hondzo and Stefan 1993; Stefan *et al.* 1993; DeStasio *et al.* 1996; Peeters *et al.* 2002; 2007), epilimnic warming was only slightly lower than the projected increase in air temperature (Robertson and Ragotkie 1990; DeStasio *et al.* 1996). Studies by Peeters *et al.* (2002; 2007) investigated changes in several perialpine lakes of analogous geographic elevation and latitude due to a fixed 4°C atmospheric warming and found similar increases in upper layer water temperatures. In our study, the monthly maximum increase in epilimnic temperatures occured during summers (July). This was not entirely consistent with other studies (Huttula *et al.* 1998; Peeters *et al.* 2007; Saloranta *et al.* 2009). The lower evaporation simulated in this scenario likely did not dampen, as discussed in the conclusions of Perroud and Goyette (2010), the warming produced by air temperature increases in summer. It may also be argued that the more intense stratification in the simulation under current conditions than was observed lead to the

warm bias simulated in April and May which, in turn, may have caused the increase in water temperatures in spring. Unlike surface water temperature, changes in the monthly hypolimnic temperature are not significantly related to atmospheric forcings (Robertson and Ragotzkie 1990; Fang and Stefan 2009) and thus a warming of deeper layers may or may not be detected in lake simulations (Hondzo and Stefan 1993; Hostetler and Giorgi 1995; Stefan *et al.* 1998; Lehman 2002; Komatsu *et al.* 2007; Fang et Stefan 2009). In many stratified lakes, the increase in bottom temperatures was related to the sensitivity of lakes to conditions prevailing prior to the onset of summer stratification and after its breakdown (Robertson and Ragotzkie 1990; DeStasio *et al.* 1996). Indeed, when complete mixing occurs, the water column is homogeneized and hypolimnetic temperatures increase in accordance with the trend observed in the epilimnion during the coldest period (Fang *et al.* 1997; Peeters *et al.* 2002; Perroud and Goyette 2010). In Lake Geneva, the potential occurence of overturns (as epilimnic and hypolimnic temperatures are similar during February and March) suggests that the increase in bottow water temperatures may also be related to winter surface water conditions.

Since a stronger warming of the upper layers compared with the lower layers of the water column were noticed in most investigations of the effects of climate change on lakes (Hondzo and Stefan 1991, 1993; Gaedke *et al.* 1998; Fang and Stefan 2009), a strengthening of the stratification was expected for Lake Geneva. However, changes in the duration of the stratification remained unknown. In this numerical investigation of Lake Geneva's response to climate change, the response tended towards an earlier onset of stratification and a delay in its decay at the end of summer, leading to a mean increase in the period of stratification of 3 weeks. Other studies that examined the increase in the number of days during which a lake was stratified reached similar conclusions, though the predicted increase in the current study was near the lower end of the range predicted by other studies with similar climatic scenario (Boyce *et al.* 1993; Stefan *et al.* 1993; Lehman 2002).

Matzinger *et al.* (2007) studied the effects of various rates of atmospheric warming on vertical mixing and stratification in a deep lake and showed that the increases in bottom temperature and the stability of the stratification were not linear. Assessing the impact of climate change on Lake Geneva with a 2 x CO₂ climate rather than a transient climate could thus amplify the stratification, rapidly decoupling deep water from the upper layers, suggesting that bottom temperatures are underestimated. The FIZC-SIMSTRAT coupled model does not currently allow us to verify this hypothesis as the GCMii provides archives under current and doubled CO₂ concentrations only. However, Perroud and Goyette (2010) give us confidence in the conclusions of this work. They showed that water temperature profiles as well as energy budgets produced from two 120-year simulations compared well during the last decade whether an absolute temperature change or an increase in atmospheric warming rate was applied to atmospheric data driving the lake model. The only condition, fulfilled here, was that the absolute temperature change method be run over a period sufficiently long to allow the lake to reach a steady-state (more than four decades).

Compared to the one-way driven experiment (Perroud and Goyette 2010), the main challenge of this method was related to controling the feedbacks between the lake surface and the atmosphere that has shown a sensitivity to the moisture variations in the atmospheric column, and to cloud formation which influences both the downward solar and longwave radiative fluxes. However, optimal parameter values for the "lake" experiment to reproduce the observed lake thermal behaviour suggest that a strong nudging of T and q should be applied. This can thus be interpreted as a model limitation where vertical transfer of heat and moisture should be done in close association with the horizontal transfer of these quantities, i.e., that the parameterization of the contributions to the dynamics tendencies of T and q should be carefully designed.

Compared to the one-way method described in Perroud and Goyette (2010) the simulated changes in cloud amounts in summer modulate radiation fluxes. The reduction of the water

vapour diffusion in the atmospheric column decreased the development of clouds, increased downward solar radiation and decreased longwave radiation at the surface. Changes in the annual mean screen-level air temperatures simulated in the coupled compared to the uncoupled experiments (3.3 °C and 3.9 °C respectively) also caused a lower annual mean change in L_{sfc}^{\downarrow} . Increases in air temperature in turn modified the partition of the sensible and latent heat fluxes in both experiments, resulting in a higher energy budget at the surface and more heat being diffused throughout the atmosphere. However, in the uncoupled experiment, the larger monthly mean screen-level air temperature, coupled with lower dew point temperatures, caused a decrease in relative humidity during summer. The atmosphere became drier and more heat was lost by the lake than in the coupled experiment. Even though the coupled FIZC-SIMSTRAT model predicted a smaller increase in air temperature. the total energetic gains were higher, 3.71 MJ day⁻¹ m⁻² compared to 3 MJ day⁻¹ m⁻², for the coupled and the uncoupled experiments respectively. This comparison highlights the importance of the humidity component on the lake response. For instance, while a 6.9 °C increase in mean screen-level air temperature is predicted by the HIRHAM RCM (PRUDENCE, Christensen et al. 1998) in August, versus a 3.34℃ increase by the FIZC-SIMSTRAT coupled model, the simulated $T_{\rm epi}$ is higher in the coupled experiment. In addition, due to the change in atmospheric humidity, the increase in air and water temperature were not similarly correlated using both methods; the increase in $T_{
m epi}$ represented 55 to 98% vs 90 to 99% of the monthly mean increase in air temperature in the uncoupled and in the coupled method respectively. Despite the differences in the monthly values of the energy budget components, monthly differences in change of $T_{\rm epi}$ (less than 0.2°C, except in March and July) and Thyp (less than 0.1°C) were small and the increase of 3 weeks in the duration of the stratification was consistent. Finally, minimum and maximum $T_{\rm epi}$ corresponded to lower and higher increases in air temperature in both studies, with the maximum occurring one month earlier in the coupled experiment.

4.6 Conclusion

This study was the first attempt at using a coupled lake-atmosphere model to investigate thermal evolution of Lake Geneva Switzerland, under warmer global climatic conditions caused by a doubling of carbon dioxide concentrations in the atmosphere. The FIZC-SIMSTRAT model was first used to reproduce mean daily water temperature profiles for Lake Geneva over the years 1960 to 1990 using a control experiment, called 1 x CO_2 climate. During that experiment, optimal parameter values were determined for running the coupled model. These values were then used in the 2 x CO_2 experiment in order to evaluate the impacts of climate change on the lake thermal structure.

Fluxes computed by the SCM for a 1 x $\rm CO_2$ global climate were consistent with those archived by the GCMii model for the land and lake experiment. Feedbacks from the Lake on the atmosphere were hindered by the strong nudging toward the GCMii that had been applied in order to allow the Lake to reach a realistic equilibrium. With the help of calibration, the coupled FIZC-SIMSTRAT model demonstrated genuine skills in reproducing observed water temperature profiles recorded prior to the intense warming over a 20 year period (RMSE < $0.71\,^{\circ}$ C).

The entire water column of Lake Geneva responded to the 2 x CO₂ global warming scenario, with the lowest temperature increase in the hypolimnion, and the epilimnion as well, during the weakly stratified period. In the epilimnion, seasonal variability was strong, with the largest increases in temperature occurring during summers. Water column stratification is expected to be stronger as climate warms, causing the decay of the thermocline to be delayed during autumn. These projections agreed with changes that have been observed in water

temperature monitoring records for Lake Geneva over the past 5 decades (Lazzarotto *et al.* 2004; Dokulil *et al.* 2006). Few studies have correlated observed changes in lacustrine ecosystems to the effects of warmer air temperatures (Anneville *et al.* 2005; Jacquet *et al.* 2005; Molinero *et al.* 2007). These studies provide insight into how changes in bio-chemical mechanisms and other biological activities (such as those related to population and phenology) may be altered if global temperatures continues to rise. Gillet and Quétin (2006) demonstrated the effects of changes in temperature on the reproduction cycle of the roach. A recent study by Tadonléké (2010) showed long-term seasonal variations in the sensitivity of phytoplankton productivity to observed warming trends in water temperature. He also showed that increases in phytoplanktonic productivity rates were stronger when phosphorus availability was higher. This last assessement suggests that an evaluation of the impacts of climate on a freshwater ecosystem requires, at the same time, investigations into future lake nutrient loads.

Although this coupled model showed realistic results in reproducing current climate conditions (*i.e.*, 1 x CO₂), some improvements to the numerical formulation are needed for future studies. The first concerns the lack of variability simulated in the meteorological variables, especially at the lake surface. It is likely that the diurnal cycle of the sensible and latent heat fluxes, as well as convection in the lake may be better reproduced, if the daily variability of atmospheric components were higher. In the calibration section, it was shown that underestimation of maximum air temperatures in summer prevented intra-day episodes of lake warming by sensible heat flux.

If this was not detrimental to the annual energy budget surface, the overestimation in minimum air temperatures had consequences on the performance of the coupled model by using a low nudging value, especially in winter. The option to strongly nudge atmospheric profiles prevented an unrealistic accumulation of heat in the lake. However, should a number of feedbacks between the lake and the atmosphere take place, some freedom needs to be allowed for the FIZC to generate its own internal variability rather than precisely reproducing GCMii profiles by using high nudging values. The improvement of the parameterization of the contributions to the dynamics tendencies, a higher archival frequency in the dynamical tendencies, and model higher resolution simulations (*i.e.*, using a RCM) would also help to recover intra-day variability.

It would also be useful to assess the sensitivity of water temperature of Lake Geneva to climate change by testing other warming scenarios. Multi-model ensemble experiments would better test the robustness of the simulated thermal profiles and reduce and quantify the uncertainty in the representation of the lake warming in the future.

The coupled model used in this study provides an economical framework for assessing the sensitivity of water temperature profiles to current and perturbed climatic conditions. This study demonstrated some of the difficulties related to processes occurring at an air-water interface compared to an air-land interface, and provides explanations to understand some of these drifts. It is hoped that these results may be useful for modelers developing full three-dimensional lake-atmosphere coupling in RCMs, since the computational load of such experiments is often too large to reach the conclusions drawn in this paper.

4.7 Acknowledgments

The authors would like to thank Martin Beniston for providing helpful comments and Aaron Adamack for proof-reading the manuscript. We are thankful to the Canadian Centre for Climate modelling and analysis (CCCma) for providing access to the GCMii outputs.

4.8 References

- Abegg, B, S. Agrawala, F. Crick, and A. de Montfalcon. 2007. Climate change impacts and adaptation in winter tourism, in Climate Change in the European Alps, edited by S. Agrawala, pp. 25–60, OECD, Paris, France.
- Alcamo, J., J. M. Moreno, B. Nováky, M. Bindi, R. Corobov, R. J. N. Devoy, C. Giannakopoulos, E. Martin, J. E. Olesen, and A. Shvidenko. 2007. Europe, in Climate Change 2007: Impacts, Adaptation and Vulnerability. Contribution of Working Group II to the Fourth Assessment Report of the Intergovernmental Panel on Climate Change, edited by M.L. Parry *et al.*, pp. 541-580, Cambridge Univ, Press, Cambridge.
- Anneville, O., S. Gammeter, and D. Straile. 2005. Phosphorus decrease and climate variability: mediators of synchrony in phytoplankton changes among European perialpine lakes. Freshw. Biol. 50: 1731-1746.
- Bantle, H. 1989. Programmdokumentation Klima-Datenbank am RZ-ETH Zürich, MeteoSwiss Publication, Zürich.
- Beniston, M. 1997. Variations of snow depth and duration in the Swiss Alps over the last 50 years: links to changes in large-scale climatic forcings. Climatic Change. 36: 281-300.
- Beniston, M., B. Uhlmann, S. Goyette, and J. I. Lopez-Moreno. 2010. Will snow-abundant winters exist in the Swiss Alps in an enhanced greenhous climate? Int. J. Climatol. [in press.]. DOI: 10.1002/joc.2151.
- Blenckner, T., A. Omst, and M. Rummukainen. 2002. A Swedish case study of contemporary and possible future consequences of climate change on lake function. Aquat. Sci. 64: 171-184.
- Boyce, F.M., P. F. Hamblin, L. D. Harvey, W. M. Schertzer, and R. C. McCrimmon. 1993. Response of the thermal structure of Lake Ontario to deep cooling water withdrawals and to global warming. J. Great Lakes Res. 19: 603-616.
- Burchard, H., O. Petersen, and T. P. Rippeth.1998. Comparing the performance of the Mellor-Yamada and the κ - ϵ two-equation turbulence models. J. Geophys. Res. 103: 10543-10554.
- Christensen, J. H., B. Hewitson, A. Busuioc, A. Chen, X. Gao, I. Held, R. Jones, R. K. Kolli, W.-T. Kwon, R. Laprise, V. Magaña Rueda, L. Mearns, C. G. Menéndez, J. Räisänen, A. Rinke, A. Sarr, and P. Whetton. 2007. Regional Climate Projections, in Climate Change 2007: The Physical Science Basis. Contribution of Working Group I to the Fourth Assessment Report of the Intergovernmental Panel on Climate Change, edited by S. Solomon *et al.*, pp. 847-940, Cambridge Univ. Press, Cambridge and New York.
- Christensen, J.H., T. Carter, and F. Giorgi. 2002. PRUDENCE employs new methods to assess European climate change. EOS 82,147.
- Christensen, O. B., J. H. Christensen, B. Machenhauer, and M. Botzet. 1998. Very high-resolution regional climate simulations over Scandinavia Present climate. J. Climate. 11: 3204-3229.

- De Bono, A., P. Peduzzi, S. Klaser and G. Giuliani .2004. Impacts of Summer 2003 Heat Wave, Environment Alert Bulletin, 4 p., United Nations Environment Programme, DEWA / GRID-Europe.
- De Stasio B. T., D. K. Hill, J. M. Kleinhans, N. P. Nibbelink and J. J. Magnuson. 1996. Potential effects of global climate change on small north-temperate lakes: Physics, fish and plankton. Limnol. Oceanogr. 41: 1136-1149.
- Della-Marta, P. M., M. R. Haylock, J. Luterbacher, H. Wanner H. 2007. Doubled length of western European summer heat waves since 1880. J. Geophys. Res. 112: D15103. doi:10.1029/2007JD008510.
- Dokulil, M. T., A. Jagsch, G. D. George, O. Anneville, T. Jankowski, B. Wahl, B. Lenhart, T. Blenckner, and K. Teubner. 2006. Twenty years of spatially coherent deepwater warming in lakes across Europe related to the North Atlantic Oscillation. Limnol. Oceanogr. 51: 2787-2793.
- Fang, X., and H. G. Stefan. 2009. Simulations of climate effects on water temperature, dissolved oxygen, and ice and snow covers in lakes of the contiguous U.S. under past and future climate scenarios. Limnol. Oceanogr. 54 (6, part 2): 2359–2370.
- Fang, X., R. Psapula, and H. G. Stefan. 1997. Projections of potential climate change effectson water temperature, dissolved oxygen and associated fish habitat of small lakes in the contiguous U.S., Vol. II Effects of projected future climate conditions. Project Report 403, pp. 234, St. Anthony Falls Laboratory, University of Minnesota, Minneapolis, MN
- Gaedke U., D. Ollinger, P. Kirner, E. Bauerle. 1998. The influence of weather conditions on the seasonal plankton development in a large and deep lake (L. Constance) III: The impact of water column stability on spring algal The impact of irradiance, air temperature and wind on the algal spring development an analysis based on long-term measurements, in Management of Lakes and Reservoirs during Global Climate Change, edited by D. G. George *et al.*, pp. 39-55, Kluwer Academic Publishers, Netherlands.
- Gillet, C., and P. Quétin. 2006. Effect of temperature changes on the reproductive cycle of roach in Lake Geneva from 1983 to 2001. J. Fish. Biol. 69: 518-534.
- Goudsmit, G.-H., H. Burchard, F. Peeters, and A. Wüest. 2002. Application of k-ε turbulence models to enclosed basins: The role of internal seiches. J. Geophys. Res. 107: 3230-3243. doi:10.1029/2001JC000954.
- Goyette, S., N. McFarlane, and G. Flato. 2000. Application of the Canadian Regional Climate Model to the Laurentian Great Lakes: Implementation of a lake model. Atmos.-Ocean. 38: 481–503.
- Goyette, S., and M. Perroud. 2010. Interfacing a one-dimensional lake model with a single-column atmospheric model: Application to the deep Lake Geneva, Switzerland. Submitted to Ecol. Model.
- Hondzo, M., and H. G. Stefan. 1991. Three case studies of lake temperature and stratification response to warmer climate. Water Resour. Res. 27: 1837-1846.
- Hondzo, M., and H. G. Stefan. 1993. Regional water temperature characteristics of lakes subjected to climate change. Clim. Change 24: 187-211.

- Hostetler, S. W., and F. Giorgi. 1995. Effects of a 2 3 CO2 climate on two large lake systems: Pyramid Lake, Nevada, and Yellowstone Lake, Wyoming. Global Planet. Change 10: 43–54.
- Hostetler, S. W., F. Giorgi, G. Bates. 1994. Lake-atmosphere feedbacks associated with paleolakes Bonneville and Lahontan. Science 263: 665-668.
- Hostetler, S. W., and E. E. Small. 1999. Response of North American freshwater lakes to simulated future climates. Journal of the American Water Resources Association. 35: 1625-1638.
- Hostetler, S. W., G. T. Bates and F. Giorgi. 1993. Interactive coupling of a lake thermal model with a regional climate model. J. Geophys. Res. 98: 5045-5057.
- Huttula, E. T., A. Peltonen, and J. Virta. 1998. The effects of climate change on the temperature conditions of lakes. Boreal Environ. Res. 3: 137-150.
- Jacquet, S., J.F Briand, C. Leboulanger, L. Oberhaus, G. Paolini, J.C. Druart, O. Anneville, and J. F. Humbert. 2005. The proliferation of the toxic cyanobacterium Planktothrix rubescens following restoration of the largest natural French lake (Lake Bourget). Harmful Algae. 4: 651-672.
- Jones, P. D., and A. Moberg. 2003. Hemispheric and large scale surface air temperature variations: an extensive revision and an update to 2001. J. Clim. 16: 206-223.
- King, J. R., B. J. Shuter, and A. P. Zimmerman. 1997. The response of the thermal stratification of South Bay (Lake Huron) to climatic variability. Can. J. Fish. Aquat. Sci. 54: 1873-1882.
- Komatsu, E., T. Fukushima, and H. Harasawa. 2007. A modeling approach to forecast the effect of long-term climate change on lake water quality. Ecol. Model. 209: 351–366.
- Lazzarotto, J., F. Rapin, and C. Corvi. 2004. Physical—chemical changes and tests for metals and various micropollutants in the waters of Lake Geneva, in Rapp. Comm. Int. prot. Eaux Léman contre pollut., Campagne 2003, pp. 31-58, CIPEL.
- Lehmann, J. T. 2002. Mixing patterns and plankton biomass of the St. Lawrence Great Lakes under climate change scenarios. J. Great Lakes Res. 28: 583-596.
- Lenters J. D., T. K. Kratz, and C. J. Bowser. 2005. Effects of climate variability on lake evaporation: results from a long-term energy budget study of Sparkling Lake, northern Wisconsin (USA). J. Hydrol. 308: 168-195.
- Leon, L. F., D. C. L. Lam, W. M. Schertzer, D. A. Swayne, and J. Imberger. 2007. Towards coupling a 3D hydrodynamic lake model with the Canadian regional climate model: Simulation on Great Slave Lake. Env. Modeling and Software. 22: 787-796.
- Livingstone, D. M. 2003. Impact of secular climate change on the thermal structure of a large temperate central European lake. Clim. Change. 57: 205-225.
- Luterbacher, J., D. Dietrich, E. Xoplaki, M. Grosjean and H. Wanner. 2004. European seasonal and annual temperature variability, trends, and extremes since 1500. Science. 303: 1499-1503.

- MacKay, M. D., P. J. Neale, C. D. Arp, L. N. De Senerpont Domis, X. Fang, G. Gal, K. D. Jöhnk, G. Kirillin, J. D. Lenters, E. Litchman, S. MacIntyre, P. Marsh, J. Melack, W. M. Mooij, F. Peeters, A. Quesada, S. G. Schladow, M. Schmid, C. Spence, and S. L. Stokes. 2009. Modeling lakes and reservoirs in the climate system. Limnol. Oceanogr. 54 (6, part 2): 2315-2329.
- Malmaeus, J. M., T. Blenckner, H. Markensten and I. Persson. 2005. Lake phosphorus dynamics and climate warming: A mechanistic model approach. Ecol. Model. 190: 1-14.
- Martynov, A., L. Sushama, and R. Laprise. 2010. Simulation of temperate freezing lakes by one-dimensional lake models: performance assessment for interactive coupling with regional climate models. Boreal Env. Res. 15: 143-164.
- Matzinger, A., M. Schmid, E. Veljanoska-Sarafiloska, S. D. Patceva, B. Guseska, B. Wagner, M. Müller, A. Sturm, A. Wüest. 2007. Eutrophication of ancient Lake Ohrid: Global warming amplifies detrimental effects of increased nutrient inputs. Limnol. Oceanogr. 52(1): 338-353.
- McCormick, M. J., and G. L. Fahnenstiel. 1999. Recent climatic trends in nearshore water temperatures in the St. Lawrence Great Lakes. Limnol. Oceanogr. 44: 530-540.
- McFarlane, N. A., G. J. Boer, J.-P. Blanchet, and M. Lazare. 1992. The Canadian climate centre second generation general circulation model and its equilibrium climate, J. Climate. 5: 1013-1044.
- Mironov, D., E. Heise, E. Kourzeneva, B. Ritter, N. Schneider, and A. Terzhevik. 2010. Implementation of the lake parameterisation scheme FLake into the numerical weather prediction model COSMO. Boreal Env. Res.15: 218-230.
- Molinero, J. C., O. Anneville, S. Souissi, L. Laine, and D. Gerdeaux. 2007. Decadal changes in water temperature and ecological time series in Lake Geneva, Europe-relationship to Atlantic climate variability. Clim. Res. 34: 15-23. doi:10.3354/cr034015.
- Nakicenovic, N., J. Alcamo, G. Davis, D. de Vries, J. Fenhann, S. Gaffin, K. Gregory, A. Grübler, T. Y. Jung, T. Kram, E. L. La Rovere, L. Michaelis, S. Mori, T. Morita, W. Pepper, H. Pitcher, L. Price, K. Riahi, A. Roehrl, H.-H. Rogner, A. Sankovski, M. Schlesinger, P. Shukla, S. Smith, R. Swart, S. van Rooijen, N. Victor and Z. Dadi. 2000. Special Report on Emissions Scenarios, Working Group III, Intergovernmental Panel on Climate Change (IPCC). Cambridge Univ. Press, Cambridge.
- OcCC, (2008), Le climat change que faire? Le nouveau rapport des Nations Unies sur le climat (GIEC 2007) et ses principaux résultats dans l'optique de la Suisse. Rapport Annuel, 47 pp., OcCC Organe consultatif sur les changements climatiques, Berne.
- Paul, F, A. Kaab, M. Maisch, T. Kellenberger, W. Haeberli. 2004. Rapid disintegration of Alpine glaciers observed with satellite data. Geophys Res Lett. 31: L21402
- Perroud, M. and S. Goyette. 2010. Impact of warmer climate on Lake Geneva water-temperature profiles. Boreal Env. Res. 15: 255-278.
- Peeters, F., D. M. Livingstone, G.-H. Goudsmit, R. Kipfer, and R. Forster. 2002. Modeling 50 years of historical temperature profiles in a large central European lake. Limnol. Oceanogr. 47: 186-197.

- Peeters, F., D. Straile, A. Lorke, and D. M. Livingstone. 2007. Earlier onset of the spring phytoplankton bloom in lakes of the temperate zone in a warmer climate. Glob. Change Biol. 13: 1898-1909.
- Robertson, D. M., and R. A. Ragotzkie. 1990. Changes in the thermal structure of moderate to large sized lakes in response to changes in air temperature. Aqu. Sci. 52: 360-380.
- Rodi, W. 1984. Turbulence models and their application in hydrodynamics A state of the art review. 2nd ed. Int. Assoc. Hydraul. Res.
- Saloranta, T. M., M. Forsius, M. Järvinen, and L. Arvola. 2009. Impacts of projected climate change on the thermodynamics of a shallow and a deep lake in Finland: model simulations and Bayesian uncertainty analysis. Hydrol. Res. 40: 234-248. doi:10.2166/nh.2009.030
- Schindler, D. W., S. E. Bayley, and B. R. Parker. 1996. The effect of climatic warming on the properties of boreal lakes and streams at the experimental lakes area, Northwestern Ontario. Limnol. Oceanogr. 41: 1004-1017.
- Schmidli, J., C. Schmutz, C. Frei, H. Wanner, and C. Schär. 2002. Mesoscale precipitation variability in the region of the European Alps during the 20th century. Int. J. of Clim. 22: 1049-1074.
- Small, E., L.C. Sloan, S. Hostetler, and F. Giorgi. 1999. Simulating the water balance of the Aral Sea with a coupled regional climate-lake model. J. Geophys. Res. Atmospheres. 104: 6583–6602.
- Song, Y., H. F. M. Semazzi, L. Xie, and L. J. Ogallo. 2004. A coupled regional climate model for the Lake Victoria basin of East Africa. Int. J. Climatol. 24: 57-75
- Stefan, H. G., M. Hondzo, and X. Fang. 1993. Lake water quality modeling for projected future climate scenarios. J. Environ. Qual. 22: 417-431.
- Stefan, H. G., X. Fang, and M. Hondzo. 1998. Simulated climate changes effects on year-round water temperatures in temperate zone lakes. Clim. Change. 40: 547-576.
- Swayne, D., D. Lam, M. MacKay, W. Rouse, and W. Schertzer. 2005. Assessment of the interaction between the Canadian Regional Climate Model and lake thermal hydrodynamic models. Env. Modelling and Software 20: 1505-1513.
- Tadonléké, R. D. 2010. Evidence of warming effects on phytoplankton productivity rates and their dependence on eutrophication status. Limnol. Oceanogr. 55: 973-982. doi: 10.4319/lo.2010.55.3.0973
- Theurillat, J-P., and A. Guisan. 2001. Potential impact of climate change on vegetation in the European Alps: A review. Climatic change. 50: 77-109.
- Uhlmann, B., S. Goyette, and M. Beniston. 2009. Sensitivity analysis of snow patterns in Swiss ski resorts to shifts in temperature precipitation and humidity under condition of climate change. Int. J. of Clim. 29: 1048-1055.
- Vercauteren, N., E. Bou-Zeid, M. B. Parlange, U. Lemmin, H. Huwald, J. Selker, and C. Meneveau. 2008. Subgrid-scale dynamics of water vapour, heat, and momentum over a lake, Bound.-Layer Meteorol. 128: 205–228. doi:10.1007/s10546-008-9287-9.

- Voigt, T., J. van Minnen, M. Erhard, M. Zebisch, D. Viner, R. Koelemeijer. 2004. Impacts of Europe's changing climate. An indicator-based assessment, EEA Report No2/2004, Office for Official Publications of the European Communities, Luxembourg.
- Winter, T.C., D. C. Buso, D. O. Rosenberry, G. E. Likens, A. M. Sturrock, and D. P. Mau. 2003. Evaporation determined by the energy-budget method for Mirror Lake, New Hampshire. Limnol. Oceanogr. 48: 995-1009.

Conclusion

This thesis has developed a more comprehensive understanding which lake models may be used to simulate the thermal profiles of large lakes. It has also achieved a better comprehension of the sensitivity of the water temperature profiles to warmer climatic conditions through a specific numerical investigation of the response in Lake Geneva, Switzerland, from enhanced atmospheric carbon dioxide concentrations, utilising both oneway and coupled experiments.

The ability of a lake model to simulate the thermal characteristics of Lake Geneva in a current climate, and the assessment of the expected change in its thermal properties are presented in the conclusions of each chapter. Here, I would like to give an overview of the main issues discussed in the previous chapters, provide a final discussion on these findings, and suggest further work that could arise from this work.

- The suitability of the four 1D models for simulating daily outputs at the deepest point of Lake Geneva (SHL2) over a 10-year period was tested. We have shown that some models, after slight calibration and with no significant changes to model formulations, are able to predict seasonal evolution of water temperature profiles with reasonable accuracy. If all models simulate surface temperatures well, the location and the slope of the seasonal thermocline are reproduced accuratelyby two of them solely, namely DYRESM and SIMSTRAT. In addition, it so happens that these 2 models include the seiching parameterization to generate turbulent mixing. However, SIMSTRAT is the only model to significantly account for summer-autumn deepening of the thermocline and seasonal deep hypolimnion temperature variations. SIMSTRAT has thus been chosen for further climatic purpose.
- To assess the climate change impacts on Lake Geneva water temperature profiles in the one-way experiment, changes diagnosed in the outputs of the HIRHAM RCM for a future and current climate under the IPCC A2 scenario served to perturb observed atmospheric variables driving the lake model. With regards to the differences determined for input variables driving the lake model, only the air temperature and relative humidity at screen level are sensitive to future modifications. Lake response to temperature changes only has the effect of maximizing climate change impacts and thus highlights the importance of including moisture components. Indeed, the decrease in relative humidity further enhanced the cooling of water through evaporation in summer, reducing the effects of increasing air temperature on the lake.
- In the second experiment, the coupled FIZC-SIMSTRAT model was employed to simulate changes in thermal characteristics of Lake Geneva using a doubling of CO₂ compared to a "control" simulation (1 X CO₂). Prior to performing the climatic application, sensitivity analysis showed that the mean and the variability of seasonal water thermal profiles, the screen-level temperature and humidity, the anemometer-level windspeed and downward radiative fluxes can be reproduced realistically by devising a set of adjustable parameters. Compared to the one-way method, coupling allows strong feedbacks between the lake surface and the atmosphere, producing variations in atmospheric moisture and cloud cover.

- In both experiments, changes in atmospheric CO₂ concentrations produced significant changes in the components of the energy budget. Due mainly to the increase in air and surface water temperature, higher values of downward infrared and upward radiation were diagnosed, resulting in a positive balance for the lake. Additionally, changes in sensible heat flux had a warming effect on the lake. While on the contrary, a combined increase in air temperature and decrease in relative humidity enhanced the water vapour deficit at the air-water interface, inducing a cooling effect in the lake. Unlike the one-way experiment, the coupled experiment, developed to include feedbacks between the lake surface and the atmosphere, showed sensitivity to the moisture variations in the atmospheric column, and to cloud formation which had an influence both on the downward solar as well as on longwave radiative fluxes. The reduction of the water vapour diffusion in the atmospheric column thus decreased the development of clouds and increased the values of the downward solar radiation in the coupled experiment solely. Even though slight differences appeared in the value of each individual flux between each experiment. the total energy budget gained by the lake when it has reached a steady state in a future climate is similar.
- The lake sensitivity analysis to changes in greenhouses gases showed a warming of the whole column, of a maximum of 3.83°C (August) and 4.20°C (July) in the epilimnion and of 2.33 °C (March) and 2.25 °C (March) in the hypolimnion, for each experiments respectively. The evolution of monthly epilimnic temperatures correlate with that of the air temperatures, without any delay in the timing of maxima and minima water temperatures. Due to a higher warming in in the upper layers compared to the lower layers of the water column, the metalimnion proved to be more strongly stratified. Epi-hypolimnic heat exchanges are thus reduced compared to today's regime. Furthermore, the stronger stability of the water column reduces mixing caused by wind stress at the end of summer and hence delays the stratification decay. A 3 week increase in the period of stratification was also simulated in both experiments, with changes almost as equally due to an earlier onset as to a longer duration of the statification. The shorter duration of the weakly stratified period should reduce the frequency of complete mixing. However, a similar increase in water temperatures through the whole column in both February and March or February only (method dependant) suggests that overturns might still occur occasionally.
- This study has confirmed the necessity to run simulations over a long time period in order to assess the warming trend in a body of water as deep as 300 m. When the lake model is driven by atmospheric fluxes in response to a a doubling or tripling of CO2 concentration, over 4 decades are required for the lake to reach a steady-state. In chapter 2, the effects on the lake of progressive changes in atmospheric data over a century time-scale were compared to those of an abrupt change. These experiments produced similar resulting water temperature profiles and energy budgets once the lake has evolved towards a mean steady state.

Although the one-way and the coupled experiments produced similar conclusions on Lake Geneva's response to global warming, heat fluxes driving the lake model proved to diverge, particularly in summer. These differences may be due to lake feedback mechanisms as well as to the climate models and modelling assumptions used to provide the future climate (Hingray *et al.* 2007). Indeed, feedbacks between the lake surface and the atmosphere in the coupled experiment produced variations in atmospheric moisture and cloud cover that modified the downward radiation, which could not be captured in the one-way experiment. Variations in lake surface fluxes could also have been inherited from the results of GCM used to drive HIRHAM as well as those used to drive the SCM in the second. Räisänen (2001; 2002) highlighted the different climate evolutions, for the same emissions scenario, to be a result of the numerical algorithms, the spatial resolutions, the configuration of model

grids, and the sub grid-scale parameterizations encoded in the GCMs. The emissions scenario used in each experiment may finally explain variations in climate response and in simulated energy exchanges. Even though the lake responded similarly to global warming in both experiments, it is recognised that this study is not exhaustive. It would be valuable to increase the confidence level in the results by taking more emission scenarios into account as well as outputs from several GCMs as driver for RCM and SCM. In order to better take local effects into account in the coupled experiment, impacts on the lake should also be assessed using a higher resolution GCM or even a RCM. However, we believe that this research proposes a few ideas on the extent to which global warming may affect Lake Geneva response.

Lakes can also influence regional climatology. Because the FIZC-SIMSTRAT model simulates heat exchanges at the air-water interface, we may find an opportunity to investigate the role of the lake as a moderator of local climate in the current and future climate. It is possible that the lake is able to store part of the heat in excess, thus damping impacts of climate change in a region. Solving such an issue is also the goal of many research centers that have or intend to couple a lake models to RCMs. However, the technique used in this study to interface a lake model with an atmospheric model is less demanding computationally than any other coupled experiments, and thus represent an economical framework for assessing the future local climate.

Methods presented in this study allow an evaluation of the potential climate change impacts on Lake Geneva. The conclusions drawn would suggest that these approaches could be applied to other lakes. However, further work designed to investigate lake response to a future climate should consider the validation of SIMSTRAT in other aquatic environment. Since SIMSTRAT performed well in deep lakes that require a long time to reach a steady-state and have processes as complex as seiching, we have confidence in the application of this model to shallower peri-alpine lakes. In lakes strongly affected by the inflow of a river, it is however likely that issues may appear and should be addressed in future work. Additionally, it may be required to include new routines that parameterize processes which are presently not accounted for in the current version. The large number of dimictic lakes located in the peri-alpine area necessitates the inclusion and the validation of an ice module. An experiment led on Sparkling Lake (max depth of 20 m) for instance showed that a cold bias is simulated at the bottom if the ice formation is negelected (Stepanenko 2010). Ice is an important element to consider as it insulates the lake from the atmosphere and so reduces both momentum and heat fluxes.

This thesis served to quantify predicted changes in thermal characteristics in a deep lake. It thus constitutes a first step in a broader project to assess the potential impacts of climate change on cyanobacteria blooms and their potential effects on water quality and healthrelated risks. An earlier onset of stratification, less frequent complete winter overturns, a stronger stability of the water column, and an overall warming of the entire water column expected in the coming decade suggests that there is an increasing threat of harmful cyanobacteria on this perialpine lake. However, it is still premature to conclude that water characteristic changes will necessarily lead to growth of cyanobacteria. To assess the impacts of climate change on this specific phytoplankton group, the freshwater ecosystem as a whole should be studied. Indeed, other environmental factors such as phenology changes and nutrient concentrations could also have a significant impact on cyanobacteria abundance. Our first conclusions show there is room for further studies involving coupled physical and biological models. Such coupled model experiments will help understand changes in biogeochemical processes under shifting conditions of lake temperature and stratification, and assess their effects on the proliferation of toxic algae and other aquatic pathogens.

References

- Alcamo, J., J.M. Moreno, B. Nováky, M. Bindi, R. Corobov, R.J.N. Devoy, C. Giannakopoulos, E. Martin, J.E. Olesen, and A. Shvidenko. 2007. Europe, p. 541-580. *In* M.L. Parry, O.F. Canziani, J.P. Palutikof, P.J. van der Linden and C.E. Hanson [eds], Climate Change 2007: Impacts, Adaptation and Vulnerability. Contribution of Working Group II to the Fourth Assessment Report of the Intergovernmental Panel on Climate Change. Cambridge University Press, Cambridge.
- Bechtold, P., and al.. 2000. A GCSS model intercomparison for a tropical squall line observed during TOGA-COARE. II: Intercomparison of single-column models and a cloud-resolving model. Quart. J. Roy. Meteor. Soc. 126: 865–888.
- Benson, L., and F. Paillet. 2002. 2002. HIBAL: a hydrologic-isotopic-balance model for application to paleolake systems. Quat. Sci. Rev. 21: 1521-1539.
- Betts, A. K, and M. J. Miller. 1986. A new convective adjustment scheme. Part II: Single column tests using GATE wave, BOMEX, ATEX and arctic air-mass data sets. Quart. J. Roy. Meteor. Soc. 112: 693-709.
- Bohle-Carbonell, M. 1986. Currents in Lake Geneva. Limnol. Oceanogr. 31: 1255-1266.
- Boyce, F. M., P. F. Hamblin, L. D. Harvey, W. M. Schertzer, and R. C. McCrimmon. 1993. Response of the thermal structure of Lake Ontario to deep cooling water withdrawals and to global warming. Journal of Great Lakes Research 19: 603-616.
- Bührer, H., and H. Ambühl. 2001. Lake Lucerne, Switzerland, a long term study of 1961-1992. Aquatic Sci. 63: 432-456.
- Burchard, H., and H. Baumert. 1995. On the performance of a mixed layer model based on the k-e turbulence closure. J. Geophys. Res. 100: 8523-8540.
- Carmichael, W.W. 2001. Health effects of toxin producing cyanobacteria: the 'CyanoHABS'. Hum Ecol Risk Assess 7: 1393–1407.
- Caya, D., R. Laprise, M. Giguère, G. Bergeron, J. P. Blanchet, B. J. Stocks, G. J. Boer, and N. A. McFarlane. 1995. Description of the Canadian regional climate model. Water, Air and Soil Pol. 82: 477-482.
- Bader, D.C., C. Covey, W.J. Gutowski Jr., I.M. Held, K.E. Kunkel, R.L. Miller, R.T. Tokmakian, and M.H. Zhang. 2008: Climate Models: An Assessment of Strengths and Limitations. A Report by the U.S. Climate Change Science Program and the Subcommittee on Global Change Research. Department of Energy, Office of Biological and Environmental Research, Washington, D.C., USA.
- Chorus, I. 2001. Cyanotoxins: Occurrence, Causes, Consequences. Springer-Verlag, Berlin.
- Christensen, J.H., O.B. Christensen, P. Lopez, E. Van Meijgaard, and M. Botzet. 1996. The HIRHAM4 Regional Atmospheric Climate Model. Scientific Report 96-4. DMI, Copenhagen.
- Christensen, O. B., J. H. Christensen, B. Machenhauer, and M. Botzet. 1998. Very high resolution regional climate simulations over Scandinavia Present climate. J. Climate 11: 3204-3229.

- Christensen, J.H., T. Carter, and F. Giorgi. 2002. PRUDENCE employs new methods to assess European climate change. EOS 82,147.
- Christensen, J.H., B. Hewitson, A. Busuioc, A. Chen, X. Gao, I. Held, R. Jones, R.K. Kolli, W.-T. Kwon, R. Laprise, V. Magaña Rueda, L. Mearns, C.G. Menéndez, J. Räisänen, A. Rinke, A. Sarr, and P. Whetton. 2007. Regional Climate Projections. *In S. Solomon*, D. Qin, M. Manning, Z. Chen, M. Marquis, K.B. Averyt, M. Tignor, and H.L. Miller [eds.], Climate Change 2007: The Physical Science Basis. Contribution of Working Group I to the Fourth Assessment Report of the Intergovernmental Panel on Climate Change. Cambridge University Press, Cambridge, United Kingdom and New York.
- Clayson, C. A., and A. Chen. 2002. Sensitivity of a coupled single-column model in the tropics to treatment of the interfacial parameterizations. J. Climate 15: 1805-1831.
- Codd, G.A. 1995. Cyanobacterial toxins: occurrence, properties and biological significance. Water Sci Technol 32: 149–156.
- Copetti, D. 2005. Modelling the effects of nutrients loads and hydrodynamic regime on the phytoplankton and zooplankton populations in lacustrine environment. Ph.D. thesis. University of Milan.
- Cox, P.A., S.A Banack., and S. J. Murch. 2003. Biomagnification of cyanobacterial neurotoxins and neurodegenerative disease among the Chamorro people of Guam. Proc. Natl. Acad. Sci. USA 100: 13380-13383.
- Cullen, M.J.P. 1993. The Unified Forecast/Climate Model. Meteor. Mag. 122: 81-94.
- Dake, J. M. K., and D. R. F. Harleman. 1969. Thermal stratification in lakes analytical and laboratory studies. Water Resour. Res. 5: 484-495.
- Danis, P.A. 2003. Modélisation du fonctionnement thermique, hydrologique et isotopique des amélioration des reconstructions paléoclimatiques. Ph.D. thesis. University of Savoie.
- DeStasio, B. T., D. K. Hill, J. M. Kleinhans, N. P. Nibbelink, and J. J. Magnuson. 1996. Potential effects of global climate change on small north-temperate lakes: Physics, fish and plankton. Limnol. Oceanogr. 41: 1136-1149.
- Dickinson, R.E., A. Henderson-Sellers, P. J. Kennedy, and M. F. Wilson. 1986. Biosphere Atmosphere Transfer Scheme (BATS) for the NCAR Community Climate Model, NCAR Technical Note, NCAR, TN275+STR.
- Dickinson, R.E., R.M. Errico, F. Giorgi, and G.T. Bates. 1989. A regional climate model for the western United States. Clim. Change 15:383-422.
- Dickinson, R. E., A. Henderson-Sellers, and P. J. Kennedy. 1993. Biosphere Atmosphere Transfer Scheme (BATS) Version le as Coupled to the NCAR Community Climate Model, NCAR Technical Note, NCAR.
- Dill, W.A. 1993. Inland fisheries of Europe. EIFAC Technical Paper No. 52. Rome, FAO, 1990.
- Fernald, S.H., N.F. Caraco, and J.J. Cole. 2007. Changes in cyanobacterial dominance following the invasion of the zebra mussel Dreissena polymorpha: long-term results from the Hudson River Estuary. Estuaries Coasts 30: 163–170.

- Ford, D.E., and L.S. Johnson. 1986. An assessment of reservoir mixing processes. E-86-7. US Army Engineers Waterways Experiment Station, Vicksburg, MS.
- Frei, C, R. Schöll, J. Schmidli, S. Fukutome, and P.L. Vidale. 2006. Future change of precipitation extremes in Europe: an intercomparison of scenarios from regional climate models. J. Geophys. Res. 111: D06105. doi:10.1029/2005JD005965
- Ghan, S. J., D. Randall, K. Xu, R. Cederwall, D. Cripe, J. Hack, S. Iacobellis, S. Klein, S. Krueger, U. Lohmann, J. Pedretti, A. Robock, L. Rotstayn, R. Somerville, G. Strenchikov, Y. Sud, G. Walker, S. Xie, J. Yio, and M. Zhang. 2000. A comparison of single-column model simulations of Summertime midlatitude continental convection. J. Geophysi. Res. 105: 2091-2124.
- Giorgi, F. 1990. Simulation of regional climate using a limited area model nested in a general circulation model. J. Clim. 3: 941-963.
- Giorgi, F. 2006. Regional climate modeling: status and perspectives. Journal de Physique IV, 139: 101-118.
- Giorgi, F., and L. O. Mearns. 1999. Introduction to special section: Regional climate modeling revisited. J. Geophys. Res. 104: 6335-6352.
- Giorgi, F., B. Hewitson, J. Christensen, M. Hulme, H. Von Storch, P. Whetton, R. Jones, L. Mearns, and C. Fu. 2001. Regional climate information: Evaluation and projections (Chapter 10), p. 739-768. *In* J.T. Houghton, Y. Ding, D.J. Griggs, M. Noguer, P.J. van der Linden, X. Dai, K. Maskell, and C.A. Johnson [eds], Climate Change 2001: The Scientific Basis, Contribution of Working Group I to the Third Assessment Report of the IPCC. Cambridge University Press, Cambridge.
- Goudsmit, G.-H., H. Burchard, F. Peeters, and A. Wüest. 2002. Application of k-€ turbulence models to enclosed basins: The role of internal seiches. J. Geophys. Res. 107: 3230-3243. doi:10.1029/2001JC000954.
- Goyette, S., N. A. McFarlane, and G. M. Flato. 2000. Application of the Canadian Regional Climate Model to the Laurentian Great Lakes region: Implementation of a lake model. Atmos.-Ocean 38: 481-503.
- Grell, G., Y. Kuo, and R.J. Pasch. 1991. Semi-prognostic tests of of cumulus parameterization schemes in the middle latitudes. Mon. Wea. Rew. 119: 5-31.
- GWA (Global Warming Art). 2007. (http://www.globalwarmingart.com).
- Henderson-Sellers, B., M. J. McCormick, and D. Scavia. 1983. A comparison of the formulation for eddy diffusion in two one-dimensional stratification models. Appl. Math. Model. 7: 212-215.
- Hendricks Franssen, H.-J., and S. C. Scherrer. 2008. Freezing of lakes on the Swiss Plateau in the period 1901-2006. Int. J. of Clim. 28: 421-433. doi:10.1002/joc.1553.
- Hewitt, C.D., and D. Griggs. 2004. Ensembles-based Predictions of Climate Changes and their Impacts. EOS 85: 566.

- Hingray, B., N. Mouhous, A. Mezghani, K. Bogner, B. Schaefli, and A. Musy. 2007. Accounting for global-mean warming and scaling uncertainties in climate change impact studies: application to a regulated lake system. Hydrology and Earth System Sciences 11: 1207-1226.
- Hodges, B., J. Imberger, A. Saggio, and K.B. Winters. 2000. Modeling basin-scale internal waves in a stratified lake. J. Limnol .Oceanogr. 45: 1603-1620.
- Hostetler, S. W., and P. J. Bartlein. 1990. Simulation of lake evaporation with application to modelling lake-level variations at Harney-Malheur Lake, Oregon. Water Resour. Res. 26: 2603-2612.
- Hostetler, S. W., and E. E. Small. 1999. Response of North American freshwater lakes to simulated future climates. Journal of the American Water Resources Association 35: 1625-1638.
- Hostetler, S. W., G. T. Bates, and F. Giorgi. 1993. Interactive coupling of a lake thermal model with a regional climate model. J. Geophys. Res. 98: 5045-5057.
- Huisman, J., R. R. Jonker, C. Zonneveld, and F. J. Weissing. 1999. Competition for light between phytoplankton species: experimental tests of mechanistic theory. Ecology 80:211-222.
- Huisman, J.M., H.C.P. Matthijs, and P.M. Visser. 2005. Harmful Cyanobacteria. Springer Aquatic Ecology Series 3. Springer, Dordrecht, the Netherlands.
- Imberger, J., J. C. Patterson, B. Hebbert, and I. Loh. 1978. Dynamics of reservoir of medium size. J. Fluid Mech. 78: 489-512.
- IPCC. 1990. Climate Change: The IPCC Assessmenmt. Cambridge University Press, New York.
- IPCC. 2001. The scientific basis. *In* J.T. Houghton, D.J. Ding, D.J. Griggs, M. Noguer, P.J. van der Linden, D. Xiasou [eds], Climate change 2001. Cambridge University Press, Cambridge and New York.
- Jacob, D., and R. Podzun. 1997. Sensitivity studies with the regional climate model REMO. Meteorology and Atmospheric Physics 63: 119–129.
- lacobellis, S.F., and R.C.J. Somerville 1991. Diagnostic modeling of the Indian monsoon onset, part I, Model description and validation. J. Atmos. Sci. 48: 1948-1959.
- Jacquet, S., J. F. Briand, C. Leboulanger, L. Oberhaus, G. Paolini, J. C. Druart, O. Anneville, and J. F. Humbert. 2005. The proliferation of the toxic cyanobacterium Planktothrix rubescens following restoration of the largest natural French lake (Lake Bourget). Harmful Algae 4: 651-672.
- Jöhnk, K.D., J. Huisman, J. Sharples, B. Sommeijer, P.M. Visser, and J.M. Stroom. 2008. Summer heatwaves promote blooms of harmful cyanobacteria. Glob Change Biol 14: 495-512.
- Johns, T.C., J.M. Gregory, W.J. Ingram, C.E. Johnson, A. Jones, J.A. Lowe, J.F.B. Mitchell, D.L. Roberts, D.M.H. Sexton, D.S. Stevenson, S.F.B. Tett, and M.J. Woodage. 2003. Anthropogenic climate change for 1860 to 2100 simulated with the HadCM3 model under updated emissions scenarios. Climate Dynamics 20: 583–612.

- Jones, P.D., and A. Moberg. 2003. Hemispheric and large scale surface air temperature variations: an extensive revision and an update to 2001. J. Clim. 16: 206-223.
- Jones, R.G., J.M. Murphy, and M. Noguer. 1995. Simulation of climate change over Europe using a nested regional-climate model. I: Assessment of control climate, including sensitivity to location of lateral boundaries. Quart. J. Roy. Meteor. Soc. 121: 1413-1449.
- Jungo, P., and M. Beniston. 2001. Changes in the anomalies of extreme temperature anomalies in the 20th Century at Swiss climatological stations located at different latitudes and altitudes. Theor. and Appl. Clim. 69: 1-12.
- Kraus, E. B., and J. S. Turner. 1967. A one dimensional model of the seasonal thermocline: II. The general theory of its consequences. Tellus 19: 98-106.
- Laprise R. 2006. Regional climate modelling. J. Comput. Phys.doi:10.1016/j.jcp.2006.10.024.
- Lazzarotto, J., P. Nirel, and F. Rapin. 2006. Physical-chemical changes in the waters of Lake Geneva, p. 31-63. *In* CIPEL [eds.], Report of the international commission for the protection of the waters of lake Geneva against pollution, Campaign 2005. (written in French)
- Legnani, E., D. Copetti., A. Oggioni, G. Tartari., M. T. Palumbo, and G. Morabito. 2005. Planktothrix rubescens'seasonal dynamics and vertical distribution in Lake Pusiano (North Italy). J. Limnol. 64: 61-73.
- Leon, L.F., D.C.L. Lam, W. M. Schertzer, D.A. Swayne, and J. Imberger. 2007. Towards coupling a 3D hydrodynamic lake model with the Canadian regional climate model: Simulation on Great Slave Lake. Env. Modeling and Software 22: 787-796.
- Leung, L.R., and S.J. Ghan. 1999. Pacific Northwest climate sensitivity simulated by a regional climate model driven by a GCM. Part II: 2xCO2 simulations. J. Climate 12: 2031-2053
- Maeda, H., A. Kawai, and M.M. Tilzer. 1992. The water bloom of cyanobacterial picoplankton in Lake Biwa, Japan. Hydrobiologia 248: 93-103.
- Marchetto, A. and S. Musazzi. 2001. Comparison between sedimentary and living diatoms in Lago Maggiore (N. Italy): implications of using transfer functions. Journal of Limnology 60: 19-26.
- Marinucci, M. R., F. Giorgi, M. Beniston, M. Wild, P. Tschuck, and A. Bernasconi. 1995. High resolution simulations of january and july climate over the western alpine region with a nested regional modeling system. Theor. and Appl. Clim. 51: 119-138.
- Markofsky, M. and D.R.F. Harleman. 1973. Prediction of water quality in stratified reservoirs. ASCE. Journal of the Hydraulics Division 99, 5: 729-745.
- McFarlane, N. A., G. J. Boer, J.-P. Blanchet, and M. Lazare. 1992. The Canadian climate centre second generation general circulation model and its equilibrium climate. J. Climate 5: 1013-1044.
- McGregor GR. 1999. Basic meteorology, p. 21-49. *In S.T. Holgate et al.* [eds.], Air Pollution and Health. London Academic, San Diego.

- Meehl, G.A., T.F. Stocker, W.D. Collins, P. Friedlingstein, A.T. Gaye, J.M. Gregory, A. Kitoh, R. Knutti, J.M. Murphy, A. Noda, S.C.B. Raper, I.G. Watterson, A.J. Weaver, and Z.-C. Zhao. 2007. Global Climate Projections. *In* S. Solomon, D. Qin, M. Manning, Z. Chen, M. Marquis, K.B. Averyt, M. Tignor and H.L. Miller [eds.], Climate Change 2007: The Physical Science Basis. Contribution of Working Group I to the Fourth Assessment Report of the Intergovernmental Panel on Climate Change. Cambridge University Press, Cambridge and New York.
- Mironov, D. V. 2008. Parameterization of lakes in numerical weather prediction. Description of a lake model. COSMO Technical Report, No. 11, Deutscher Wetterdienst, Offenbach am Main, Germany.
- Mironov, D., E. Heise, E. Kourzeneva, B. Ritter, N. Schneider, and A. Terzhevik. 2009. Implementation of the lake parameterisation scheme FLake into numerical weather prediction model COSMO. Boreal Env. Res. 15: 218-230.
- Nakicenovic, N., J. Alcamo, G. Davis, D. de Vries, J. Fenhann, S. Gaffin, K. Gregory, A. Grübler, T. Y. Jung, T. Kram, E. L. La Rovere, L. Michaelis, S. Mori, T. Morita, W. Pepper, H. Pitcher, L. Price, K. Riahi, A. Roehrl, H.-H. Rogner, A. Sankovski, M. Schlesinger, P. Shukla, S. Smith, R. Swart, S. van Rooijen, N. Victor, and Z. Dadi. 2000. Special Report on Emissions Scenarios, Working Group III, Intergovernmental Panel on Climate Change (IPCC). Cambridge Univ. Press, Cambridge.
- Nõges, P., K. Kangur, T. Nõges, A. Reinart, H. Simola, and M. Viljanen. 2008. Highlights of large lake research and management in Europe. Hydrobiologia 599:1, 259-276.
- Noilhan, J., and S. Planton. 1989. A simple parameterization of land surface processes for meteorological models. Mon Weather Rev. 117:536-549.
- Noilhan, J, and J.F. Mahfouf. 1996. The ISBA land surface parametrization scheme. Global Planet Change 13:145-159.
- OcCC. 2002. Le climat change En Suisse aussi. OcCC Organe consultatif sur les changements climatiques, Berne. ISBN: 3-907630-21-1.
- OcCC. 2008. Le climat change que faire? Le nouveau rapport des Nations Unies sur le climat (GIEC 2007) et ses principaux résultats dans l'optique de la Suisse. OcCC Organe consultatif sur les changements climatiques, Berne. ISBN: 978-3-907630-34-1.
- Orlob, G. T., and L. G. Selna. 1970. Temperature variations in deep reservoirs. J. Hydraul. Div. Proc. 96: 393-410.
- Paerl, H.W. 1988. Nuisance phytoplankton blooms in coastal, estuarine, and inland waters. Limnol. Oceanogr. 33: 823–847.
- Paerl, H.W., and J. Huisman. 2008. Blooms like it hot. Science 320: 57–58.
- Paerl, H.W., and J. Huisman. 2009. Climate change: a catalyst for global expansion of harmful cyanobacterial blooms. Environ. Microb. Reports 1: 27-37.
- Peeters, F., D. M. Livingstone, G. Goudsmit, R. Kipfer, and R. Forster. 2002. Modeling 50 years of historical temperature profiles in a large central European lake. Limnol. Oceanogr. 47: 186-197.

- Peeters, F., D. Straile, A. Lorke, and D. M. Livingstone. 2007. Earlier onset of the spring phytoplankton bloom in lakes of the temperate zone in a warmer climate. Glob. Change Biol. 13: 1898-1909.
- Pesquero, J.F., S.C. Chou, C.A. Nobre, and J.A. Marengo. 2010. Climate downscaling over South America for 1961-1970 using the Eta Model. Theor. Appl. Climatol. 99: 75-93. DOI 10.1007/s00704-009-0123-z.
- Pitman, A. J. 1994. Assessing the sensitivity of a land-surface scheme to the parameter values using a single column model. J. Climate. 7: 1856-1869.
- Pope, V.D., M.L. Gallani, P.R. Rowntree, and R.A. Stratton. 2000. The impact of new physical parametrizations in the Hadley Centre climate model Had AM3. Clim. Dyn. 16:123-146.
- Räisänen, J., 2001. CO2-induced climate change in CMIP2 experiments: Quantification of agreement and role of internal variability. J. Climate 14: 2088-2104.
- Räisänen, J., 2002. CO2-induced climate changes in interannual temperature and precipitation variability in 19 CMIP2 experiments. J. Climate 15: 2395-2311.
- Räisänen J., U. Hansson, A. Ullerstig, R. Döscher, L.P. Graham, C. Jones, H.E.M. Meier, P. Samuelsson, and U. Willén. 2004. European climate in the late twenty-first century: regional simulations with two driving global models and two forcing scenarios. Clim. Dyn. 22: 13-31.
- Randall, D. A., K.-M. Xu, R. J. C. Somerville, and S. Iacobellis. 1996. Single column models and cloud ensemble models as links between observations and climate models. J. Climate 9: 1683-1697.
- Randall, D.A., R.A. Wood, S. Bony, R. Colman, T. Fichefet, J. Fyfe, V. Kattsov, A. Pitman, J. Shukla, J. Srinivasan, R.J. Stouffer, A. Sumi, and K.E. Taylor, 2007: Cilmate Models and Their Evaluation. *In* S. Solomon, S., D. Qin, M. Manning, Z. Chen, M. Marquis, K.B. Averyt, M.Tignor and H.L. Miller [eds.]. Climate Change 2007: The Physical Science Basis. Contribution of Working Group I to the Fourth Assessment Report of the Intergovernmental Panel on Climate Change. Cambridge University Press, Cambridge and New York.
- Reynolds, C.S. 1987. Cyanobacterial water blooms. Adv. Bot. Res. 13: 67-143.
- Rinke, A., K. Dethloff, J. Cassano, J.H. Christensen, J.A. Curry, P. Du, E. Girard, J.E. Haugen, D. Jacob, C. Jones, M. Koltzow, R. Laprise, A.H. Lynch, S. Pfeifer, M.C. Serreze, M.J. Shaw, M. Tjernstrom, K. Wyser, and M. Zagar. 2006. Evaluation of an ensemble of Arctic regional climate models: Spatial patterns and height profiles. Clim. Dyn. 27: 433-435. doi: 10.1007/s00382-005-0095-3.
- Rinta-Kanto, J.M., A.J.A. Ouellette, G.L. Boyer, M.R. Twiss, T.B. Bridgeman, and S.W. Wilhelm. 2005. Quantification of toxic Microcystis spp. during the 2003 and 2004 blooms in western Lake Erie using quantitative real-time PCR. Environ. Sci. Technol. 39: 4198-4205.
- Rotach, M., M. Wild, P. Tschuck, M. Beniston, M.R. Marinucci. 1996. A double CO2 experiment over the Alpine region with a nested GCM-LAM modeling approach. Theor. Appl. Climatol. 57: 209-227.

- Ryan, E.F., D.P. Hamilton, and G.E. Barnes. 2003. Recent occurrence of Cylindrospermopsis raciborskii in Waikato lakes of New Zealand. NZ. J. Mar. Freshwater Res. 37: 829-836.
- Saucier, F. J., S. Senneville, S. Prinsenberg, F. Roy, G. Smith, P. Gachon, D. Caya, and R. Laprise. 2004. Modelling the sea ice—ocean seasonal cycle in Hudson Bay, Foxe Basin and Hudson Strait, Canada. Climate Dynamics 23:303–326.
- Schär, C., P.L. Vidale, D. Lüthi, C. Frei, Häberli, M. Liniger, and C. Appenzeller. 2004. The role of increasing temperature variability in European summer heatwaves. Nature 427: 332-336.
- Schmidli, J., and C. Frei. 2005. Trends of heavy precipitation and wet and dry spells in Switzerland during the 20th century, Int. J. Climatol. 25, 753–771
- Schmidli, J., C. Schmutz, C. Frei, H. Wanner, and C. Schär. 2002. Mesoscale precipitation variability in the region of the European Alps during the 20th century. Int. J. Climatol. 22:
- 1049-1074
- Simon, T.J. 1973. Development of three-dimensional numerical models of the Great Lakes, Scientific Series 12, Canada Centre for Inland Waters, Burlington.
- Small, E., L.C. Sloan, S. Hostetler, and F. Giorgi. 1999. Simulating the water balance of the Aral Sea with a coupled regional climate-lake model. J. Geophys. Res. Atmospheres 104: 6583–6602.
- Song, Y., H. F. M. Semazzi, L. Xie, and L. J. Ogallo. 2004. A coupled regional climate model for the Lake Victoria basin of East Africa. Int. J. Climatol. 24: 57-75.
- Stefan, H. G., and X. Fang. 1994. Dissolved oxygen model for regional lake analysis. Ecol. Model. 71: 37-68.
- Stepanenko, V. M., and V. N. Lykosov. 2005. Numerical modelling of heat and moisture transfer processes in the system "water reservoir soil". Russian Journal of Meteorology and
- Hydrology 3: 95-104.
- Stepanenko, V. M., S. Goyette, A. Martynov, M. Perroud, X. Fang, and D. Mironov. 2010. First steps of a Lake Model Intercomparison Project: LakeMIP. Boreal Env. Res. 15. In press.
- Stewart, K.M., and R.K. Haugen. 1990. Influence of lake morphometry on ice dates. Int. Ver. Theor. Angew. Limnol. Verb. 24: 122-127.
- Swayne, D., D. Lam, M. MacKay, W. Rouse, and W. Schertzer. 2005. Assessment of the interaction between the Canadian Regional Climate Model and lake thermal hydrodynamic models. Env. Modelling and Software. 20: 1505-1513.
- Tans P. 2009. NOAA/ESRL: www.esrl.noaa.gov/gmd/ccgg/trends.
- Vassiljev, J., S.P. Harrison, S. Hostetler, and P.J. Bartlein. 1994. Simulation of long-term thermal characteristics of three Estonian lakes. J. Hydrol. 163: 107-123.

- Verschuren D., T.C. Johnson, H.J. Kling, D.N. Edgington, P.R. Leavitt, E.T. Brown, M.R. Talbot, and R.E. Hecky. 2002. History and timing of human impact on Lake Victoria, east Africa. Proceedings of the Royal Society of London 269: 289-294.
- Verseghy, D.L. 1991. Class-a Canadian land surface scheme for GCMs I. Soil model. Int. J. Climatol. 11: 111-133.
- Verseghy, D.L., N.A. McFarlane, and M. Lazare. 1993. Class-a Canadian land surface scheme for GCMs, II. Vegetation model and coupled runs. Int. J. Climatol. 13: 347-370.
- Voigt, T., J. Van Minnen, M. Erhard, M. Zebisch, D. Viner, and R. Koelemeijer. 2005. Impacts of Europe's changing climate. An indicator-based assessment. Luxembourg: Office for Official Publications of the European Communities, 2004. EEA Report No2/2004. ISBN 92-9167-692-6.
- Walsby, A.E. 2007. Cyanobacterial heterocysts: terminal pores proposed as sites of gas exchange. Trends Microbiol. 15: 340-348.
- Walsby, A. E., and F. Schanz. 2002. Light-dependent growth rate determines changes in the population of Planktothrix rubescens over the annual cycle in Lake Zürich, Switzerland. New Phytol. 154: 671-687.
- Wang, Y., L.R. Leung, J.L. McGregor, D.-K. Lee, W.-C. Wang, Y. Ding, and F. Kimura. Regional climate modelling: progress, challenges, and prospects. J. Meteorol. Soc. Jpn. 82: 1599-1628.
- Wetzel, R.G. 2001. Limnology. Lake and River Ecosystems. 3rd ed. Academic Press, San Diego.
- Wiedner, C., J. Rücker, R. Brüggemann, and B. Nixdorf. 2007. Climate change affects timing and size of populations of an invasive cyanobacterium in temperate regions. Oecologia 152: 473-484.
- Zhang, G. J., and N. A. McFarlane. 1995. Sensitivity of climate simulations to the parameterization of cumulus convection in the Canadian Climate Centre general circulation model. Atmos. Ocean 33, 407-446.